PROCEEDINGS OF THE FIRST AUSTRALIA-NEW ZEALAND CONFERENCE ON GEOMECHANICS

MELBOURNE 1971

VOLUME I

TONKIN & TAYLOR
CONSULTING ENGINEERS
P.O. BOX 5271
AUCKLAND.

Australian Geomechanics Society

Proceedings of the First Australia-New Zealand Conference on Geomechanics

Melbourne, 9-13 August, 1971

Volume 1

Sponsored by
The Institution of Engineers, Australia
The Australasian Institute of Mining and Metallurgy
The New Zealand Institution of Engineers
The New Zealand National Society of Soil Mechanics and Foundation Engineering

Preface

Beginning in 1952, five Australia-New Zealand Conferences on Soil Mechanics and Foundation Engineering have been held. The First Australia-New Zealand Conference on Geomechanics continues the series, but its scope has been extended to include both soil and rock mechanics. It is sponsored by the Australian Geomechanics Society which was formed in January, 1970, as a Technical Unit of The Institution of Engineers, Australia, in association with The Australasian Institute of Mining and Metallurgy. The New Zealand Institution of Engineers and The New Zealand National Society of Soil Mechanics and Foundation Engineering are also sponsors. This volume contains the papers presented at the Technical Sessions of the Conference. Volume 2 of the Proceedings will contain the General Reporters' reviews of the papers, the discussion on the papers, the Conference Keynote Address and the addresses to the Symposium on " Geomechanics—a Tool in National Development ".

Edited and published by the Secretary of The Institution of Engineers, Australia,
Science House, 157 Gloucester Street, Sydney.

Registered at the G.P.O. Sydney, for transmission through the post as a book.

Printed by Simmons Limited, 32 Parramatta Road, Glebe, Sydney.

CONTENTS

Residual Strength Determination in Direct Shear

By

R. M. Cullen, B.E., Ph.D. (Nott.)

(Lecturer in Civil Engineering, Monash University)

AND

I. B. Donald, B.C.E., M.Eng.Sc. (Melb.), D.I.C., Ph.D. (Lond.), M.I.E.Aust.

(Associate Professor of Civil Engineering, Monash University)

SUMMARY. - Current concepts on residual strength are outlined, and test results obtained from a large displacement fully automatic reversing direct shear apparatus are reported. The maximum travel between reversals and the rate of shearing were varied. Strength envelopes were obtained from sets of samples and from stage tests on single samples. The time-saving benefit of applying a large initial deformation at high speed was also investigated. Typical load displacement curves and strength envelopes are given. For some soils the travel available in the standard shear box is insufficient for an adequate determination of residual strength. A suggested procedure is given although the precise test technique is not important provided deformation rates are adequately low. In general, stage testing with fast initial shearing is recommended. Two common causes of abnormal load deflection curves are noted. Brittleness Indices up to 0.75 at 30 p.s.i. normal stress, and ϕ_r' values down to 10^o were obtained.

I INTRODUCTION

The concept of a residual shear strength has appeared in soil mechanics literature since 1937, but it was largely the work of Skempton (Ref. 1) which highlighted it as an important factor to be considered in long term stability analyses of natural slopes and cuts in certain soils, notably overconsolidated clays and clay shales.

Laboratory shear tests are frequently stopped once peak strength has been passed, but it is now accepted that, for soils with brittle strength characteristics, progressive failure in the field can lead to average mobilised shear strengths much lower than peak values and the complete stress-strain curve must then be taken into account.

A simplified picture of large strain behaviour of soils is given in Figure 1. The effective stress shear parameters c' and ϕ' are deduced from peak strength values, and the residual shear parameters c_r' and ϕ_r' from values of τ and σ at large strains, when the shear strength has reached a constant or near constant value. The difference between peak and residual strengths depends on soil type and stress history, and is most marked for heavily overconsolidated clay soils. This strength drop can be represented

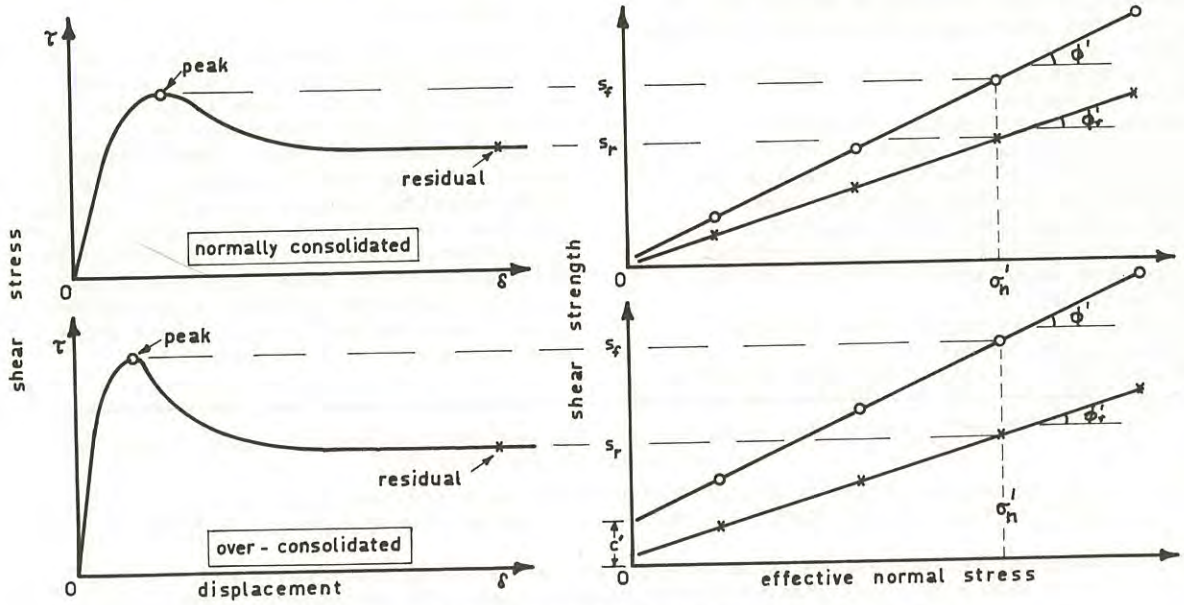

FIG. 1 Simplified Shear Strength Properties of Clay
(after Skempton and Hutchinson, Ref. 2)

by the Brittleness Index I_B[1], which is not a soil constant but decreases with increasing normal stress.

As the residual strength sets the lower limit of progressive strength reduction, to design for this value under all conditions would be unnecessarily conservative. However evidence shows that for brittle soils, under some circumstances, the field strength is likely to approach this minimum.

Skempton and Skempton & Petley (Refs. 1 and 4) have shown that the residual strength as determined in the reversing shear box correlates closely with the average mobilised strength calculated for a number of field failures in overconsolidated clays where movement has occurred along existing slip surfaces. Further, Bjerrum (Ref. 5) has concluded that for some overconsolidated plastic clays and clay shales the average shear strength along first time failure surfaces is likely to be close to residual. It also seems likely that for natural slopes in clay the ultimate or very long term stability is controlled by the residual strength. (Ref. 1)

Laboratory determination of residual shear strength is therefore necessary in relation to the analysis of long term stability of slopes, both natural and man-made. Residual strength is also of interest as a fundamental property of the soil, being largely related to the mineral composition of the clay on the failure surface (Kenney, Ref. 6) and more or less independent of the initial moisture content of the sample.

II CHOICE OF TEST TYPE

Residual strength is generally determined from one or more of three types of test:-

(a) Reversing direct shear
(b) Triaxial compression
(c) Ring shear

Most residual strength testing to date has been done in 6 cm. square direct shear boxes, modified to permit reversal of the direction of shear (Ref. 1). This test has many advantages for residual strength determination, viz:-

(i) Thin samples with reasonably rapid drainage times can be used;
(ii) Specimens can be readily oriented in the correct direction of sliding - this is valuable when testing defects such as faults, fissures and pre-existing slip planes;
(iii) Large deformations can be obtained by continuous reversing of shear direction;
(iv) Reasonably large areas of failure surface can be tested;
(v) Specimens can be readily wire cut after consolidation, if desired;
(vi) The apparatus is widely available and needs only minor modification.

The triaxial test has also been used by a number of investigators.[2] Published data shows that, in general, comparable values of $\emptyset'_r$ are obtained from direct shear and triaxial tests, whether on intact samples or preformed slip surfaces, and the simplicity of the shear box therefore makes if preferable.

The ring shear apparatus has also been used to investigate residual strength behaviour (de Beer, Ref. 9; Sembenelli and Ramirez, Ref. 10). This test, in which an annular[3] specimen is subjected to torsional shear, is the only test in which very large uniform deformations can be applied in the laboratory. Although Skempton and Hutchinson (Ref. 2) have recently claimed that such large deformations, of the order of one metre or more, could be required to reach the residual state for some clays, and that the values of $\emptyset'_r$ so obtained by ring shear are appreciably lower that those otherwise obtained, this contradicts the observations of de Beer (Ref. 9) who found lower values of $\emptyset'_r$ from the direct shear test. The ring shear apparatus has a number of disadvantages, but the greatest one at this point in time seems to be that there is so far no direct field evidence to substantiate the applicability of residual strengths measured in this way.

Such direct evidence does exist for a number of soils tested in direct shear, as already mentioned. A further factor which tends to confirm the validity of direct shear testing for obtaining residual strengths is the observation of Skempton and Petley (Ref. 4) that in reversing shear tests performed on initially unsheared material the results were in good agreement with both shear box and triaxial tests on natural (i.e. existing) slip surfaces.

Because of the above considerations the reversing direct shear test seems to be preferable for current studies of residual shear strength.

III EXPERIMENTAL PROGRAMME

(a) Background

Despite the apparently wide use of direct shear testing for determining residual strength, little has been published on the exact techniques used or the effect of different techniques on the strength parameters obtained. For example there does not appear to be any information on:- the effect of distance travelled between reversals, and whether or not this has a minimum acceptable value; the possibility of obtaining multiple data from single specimens; or the possibility of using high strain rates to achieve large displacements quickly, with subsequent low strain rates for much shorter times while drained equilibrium is being established.

---

1 $I_B = \frac{s_f - s_r}{s_f}$, Where s_f and s_r are, respectively, the peak and residual strengths in any one test (suggested by Bishop, Ref. 3)

2 Techniques and/or results obtained using normal triaxial equipment have been described by Chandler (Ref. 7) Webb (Ref. 8), and Skempton & Petley (Ref. 4). There are a number of difficulties of which the most important are:-

(i) That of obtaining accurate estimates of strength at low confining pressures (Webb, loc cit), and
(ii) The likelihood with many clays that sufficient movement cannot be obtained to achieve the residual stage on other than existing discontinuities or precut planes (cf. Webb, Fig. 12).

3 Or, rarely, disc shaped as in the work of Sembenelli and Ramirez; Ref. 10

Information such as this can be of great assistance to the investigator in increasing both the productivity of his testing programme and the confidence which he places in his results. The object of this experimental programme has been to provide such information, and subsequently to define as well as possible the simplest acceptable procedure for reversing-direct-shear determination of residual strength.

(b) Series A

Series A test results were obtained on a decomposed Silurian clay which outcrops extensively around Melbourne. It is normally a yellow-brown stiff fissured clay with a stress-strain behaviour indicating that it is quite highly overconsolidated. The clay is Kaolinitic, and for the samples tested the PI has been around 35%. The peak drained strength of samples tested has generally been between 20 and 30 lb/sq.in. and the ratio of peak to residual strength between 2 and 3, with a maximum of 4.

Thirty four test results are available for study. For simplicity in presentation the tests have been grouped in "sets" of results within the Series. All samples within each set were taken immediately adjacent to one another, and the whole series has been conducted on soil from one block sample. Twenty four test results have been obtained at the same normal stress (30 lb/sq.in.) in order to determine the effects of strain rate, length of travel, and different reversing techniques. Other samples have been used to investigate handwinding and stage testing effects.

(c) Series B and C

These results are selected from many obtained on samples made available in the course of commercial testing.

The Series B soil was a stiff grey over - consolidated silty clay. This material is from the clay layer underlying the coal seam presently being mined by the State Electricity Commission, Victoria, at Morwell. It is Kaolinitic, with a PI around 20-25%, varying somewhat with clay content.

The most important information presented from these tests relates to the validity of multiple normal stress stage testing of individual samples. Data was also obtained as to the effect of handwinding - the use of high speed (undrained) initial deformations (2 ins. per minute) - on the subsequent drained deformation required to define the residual strength.

Series C tests were conducted on remoulded samples of a fault zone infill - a white clay with high fines content, exceptionally talcy when dry, with a low mica content and a PI of 22%. The mineral composition of the sample is not known. These results are presented as an illustration of the low residual shear strength and the formation of well-developed slickensides which have been observed in remoulded soils.

(d) Series D

Remoulded Kaolin samples were used to determine whether the procedures of pre-cutting the failure plane or rapid initial shearing affected measured residual strength. These tests also provide a basis for comparison with the results of other investigators.

IV APPARATUS

(a) All the results reported in this paper have been obtained from direct shear tests. For one set of tests a standard Wykeham Farrance Reversing Shear Box Apparatus was used, but the remainder have been carried out on an extensively modified version of the same manufacturer's basic non-reversing machine.

(b) The relevant modifications which have been adopted to produce the Monash automatic reversing, automatic recording, large displacement shear box are as follows:-

(i) Replacement of the standard upper and lower halves of the shear box which, because of partially relieved contact faces,[1] can only be used for shear in the forward direction.

(ii) Provision of a roller connexion between the shear box and the proving ring. This connexion is designed to transmit horizontal tension and compression loads with negligible end float, without restraining free vertical movement of the upper half of the shear box.

(iii) Provision of a screwed connexion between the motor drive and the reservoir to give push pull control, again with negligible end float.

(iv) Provision of a universal ball joint at the fixed end of the proving ring, and calibration of the ring in tension as well as compression.

(v) Accurate realignment of the whole apparatus to prevent extraneous forces from being developed as a result of the rigid and semi-rigid connexions.

(vi) Various minor modifications in order to increase the maximum possible box displacement to $\pm 1\frac{1}{2}$ in. from the central position.

(vii) Control of the motor drive is achieved with a 12 volt relay switching system. Direction control utilizes one micro switch at each end of the travel range.

(viii) The recording of force and displacement was achieved initially by the use of two LVDT displacement transducers - one measuring deflection of the proving ring, and the other measuring the relative displacement of the two halves of the shear box. Output from the LVDT's was fed directly into an X-Y recorder giving a printout such as that in Figure 2.

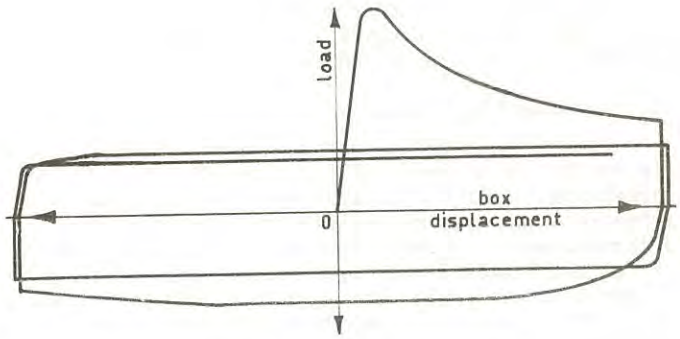

FIG. 2 X-Y Recorder Printout

[1] This relief is presumably to reduce the area of metal to metal contact which occurs if the upper half of the box settles onto the lower half.

An alternative arrangement has employed an X-T recorder. Using this recorder the transducer measuring box displacement has been eliminated. If required, box displacement at any time can be calculated knowing the chart speed, the actual (not the nominal) machine speed, and the ring compression or extension. However, as the later results show, it is seldom necessary to know this value precisely.

V EXPERIMENTAL TECHNIQUES

(a) General

All tests have been on 6 cm. square by one inch thick samples which have been set up under the required normal stress and allowed to consolidate overnight. Deformation rates are discussed in Section VI. Testing has been conducted under controlled temperature and humidity conditions.

(b) Standard Technique

It seems likely that the test procedure outlined in the Wykeham Farrance Reversing Shear Box booklet is fairly widely used and it will therefore be described as standard. Other techniques investigated have been prompted by the economic desirability of:-

(i) Reducing machine time to a minimum consistent with obtaining genuine values for the residual shear strength, and

(ii) Obtaining as much information as possible from each sample.

In the standard technique, the initial shearing procedure is the same as for regular non-reversing tests. At the end of normal forward travel (presumably about 0.25-0.30 in.) the proving ring load is first released by adjusting the tail stock and the motor then manually reversed. The shear box is then driven back to a zero displacement position with the ring in tension, and the load in the ring is again released before the motor is reverted to forward travel. This procedure is repeated as often as required to obtain the residual shear strength.

(c) Automatic Reversing

In this variation, when the box reaches the limit of its forward travel the motor is automatically reversed and the stress release process occurs at a slow rate, controlled by the motor. This is repeated at each direction reversal, and eliminates the need for an operator. Periodic readings of the dial gauges are taken to provide a check of the values obtained from the record chart.

(d) Increased Box Travel

In nature, residual shear strength conditions are reached as a result of large uni-directional deformations. In the standard shear box large deformations can only be achieved by cumulative small deformations in opposite directions. In particular, use of the standard technique requires quite a number of reversals to achieve the required conditions, and it is not known what effect these reversals have on the ultimate strength behaviour of the sample.

To investigate this effect in the 6 cm. shear box, the box was modified to allow a maximum travel of 1 in. between reversals, and tests were conducted with maximum displacements of ± 1/8 in., ± ¼ in., and ± ½ in. from the central position.

When box displacements are large a problem arises as to the necessity of applying area corrections. An important advantage of the ± deflexion shear box is that the shear stress can be measured at the position of zero displacement both for the forward and reverse directions of travel, and consequently the question of area correction need not arise. Furthermore, study of the variation of shear load with box displacement makes possible some conclusions as to the necessity of these corrections.

(e) Stage Testing

Because of their potential for time saving, multiple normal stress stage tests have been investigated.

Once residual strength conditions have been established at the initial normal stress, the shearing is stopped and the normal stress increased. In some cases the sample has been left to consolidate overnight before shearing is recommenced. The residual strength envelopes obtained this way have been compared with the envelopes determined from individual samples.

(f) Speed Variations

The question of speed effects in relation to measured residual strength is a complex one, and a wide range of speeds and combinations of speeds has been investigated. Two concepts in particular have seemed important. Firstly, it appears that a significant factor in the drop-off of strength to the residual value is the orientation of domains of clay particles (Ref. 4). This orientation process might be independent of the speed of shearing, and if this were so a satisfactory technique would be to apply large deformations (with consequent substantial particle orientation) at high speed and to then slow down the test to let drained conditions establish before the residual strength is determined. A novel version of this technique which has been tried is that of applying the initial deformation by handwinding at about 2 ins. per minute, before completing the test at the normal slow rate.

Secondly, there is the question of pore pressure equilibrium in relatively fast tests. Since even for these tests the time to completion can be large, there is a possibility that the pore pressure equilibrium established during that time is an adequate one as far as the determination of residual shear strength is concerned. To investigate this possibility the effect of testing at rates above those normally accepted for drained testing has been examined.

VI EXPERIMENTAL RESULTS

(a) Typical Load-displacement Curves

Figure 3 shows two sections of a typical load-displacement curve for a soil with large reversal peaks. Each of the numbered shear stages represents a change of shear direction. The curve shows the brittle peak characteristic of overconsolidated soils. This is followed by the usual continuous drop in load after peak strength (usually for ½-1 in.), and a tendency for the load to drop a little *at each later reversal* until the residual state is reached. Note however that the load frequently remains approximately constant between direction changes.

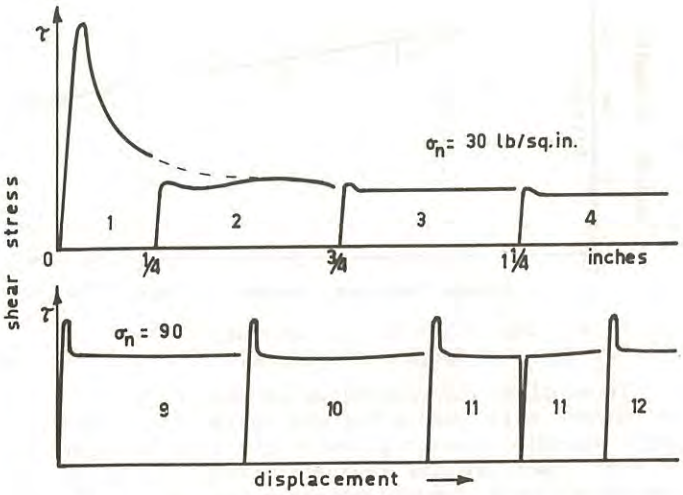

FIG. 3 Typical Load-displacement Curve

It follows that it is not necessarily sufficient to test the sample until a sensibly constant load value is obtained over a small displacement, but it is generally advisable to test until two consecutive reversals have the same failure loads. The practice of the authors has been to continue the test until two consecutive compression or tension runs are the same, because of the fact that tension and compression loads seldom correspond exactly. The variation is usually of the order of ± 5% at residual. It is possible that some of this difference is accumulation of apparatus errors despite the fact that great care has been taken with factors such as ring calibrations to reduce these errors as much as possible. That there are other factors involved is shown by the fact that in some tests consistent residual strength behaviour has varied by as much as 13% from the tension to the compression runs. In this case the lower value has always been accepted.

With some soils it has been found that the strength is consistently lower in the first forward direction (differences of the order of 10%), and this has occurred with many of the Series B samples. A similar effect is apparent in some of Kenney's results (Fig. 1, Ref. 6) and seems likely to be associated with a lack of perfect particle re-orientation on reversal.

The effects of reversal on the stress-strain curve vary significantly from sample to sample. Some samples show marked reversal peaks while other apparently identical samples show none at all.

Figure 3 shows the result (in reversal number 11) of reducing the shear load to zero and then re-commencing shear without reversing direction. In contrast to the sharp reversal peaks, the curve in this case does not peak at all. Kenney (loc cit) noted the same behaviour for shear tests on 1 mm. thick samples sheared between porous discs, and attributed the effect to a relocation of the shear plane at each reversal. In the direct shear box the zone within which the shear surface lies is usually much thicker than 1 mm., and quite large changes in the shear surface could occur between reversals. Some support for Kenney's explanation comes from the observation in some samples of dual failure surfaces separated by lenses of soil up to 3 mm. thick at the centre. It seems likely that the same phenomena could account for both the significant variation in reversal peaking between samples, and the apparently random variations between tension and compression strengths which so often occurs.

Although load curves frequently vary from the characteristic one shown, there are only two common significant variations which have evident causes. In tests which are conducted at speeds too great for drained conditions to be adequately established the load curve frequently rises over the full length of travel and never achieves a constant value: this behaviour no doubt arises as a result of the high strain rate giving inadequate time for pore pressure equilibrium in each cycle. In other tests it has sometimes been found that the load curve will behave as expected in one direction but each time rise gradually during at least part of the travel in the other direction. Figure 4 is a photograph of the shear plane in one such specimen and observation of test specimens indicates that inhomogeneities such as the one in this sample frequently contribute to this erratic type of load response.

(b) Typical Strength Envelopes

Figure 5 shows typical residual strength envelopes of three different soils. For the Series B samples the peak strength envelope is also shown.

For many of the soils tested the intercept c'_r for the stress range employed is non-zero. For other soils both zero intercept linear envelopes and curved

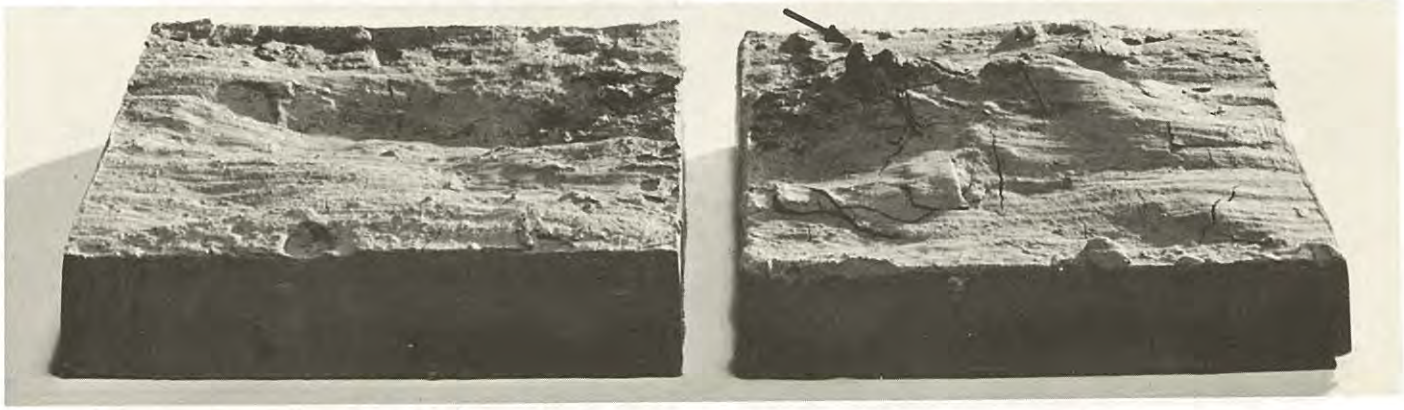

FIG. 4. Shear surface as affected by hard inclusion. (arrowed)

envelopes have been obtained, and the relatively high c'_r values which do occur are not considered to result from the test technique. Some investigators prefer to fit a curved envelope to test results in order to obtain $c'_r = 0$ (e.g. Skempton and Petley, Ref. 4). However, in cases where there is no evidence of envelope curvature over a wide stress range the authors consider that the use, in design, of c'_r values such as those given is reasonable.

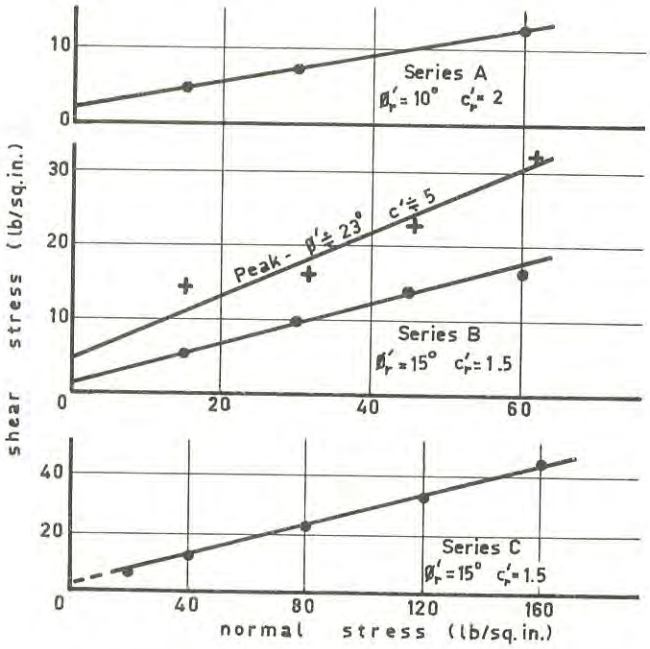

FIG. 5 Typical Strength Envelopes

(c) Effect of Moisture Content

Skempton (Ref. 1) demonstrated that the moisture content on the failure plane in a natural soil in the residual state can be significantly altered from the average moisture content of the adjacent soil. He suggests on the basis of this and other evidence (loc cit) that the stress history of a soil is not of any great significance in relation to the residual strength and that the angle ϕ'_r should therefore be a constant for any particular clay depending only on the nature of the particles. It follows that the moisture content on the failure plane and the residual shear strength should be much the same in all samples of a particular clay whatever the overall moisture content of the sample.

For the Series A tests which constitute the majority of the comparative testing the residual strengths at 30 lb/sq.in have been less consistent than might be expected from the above hypothesis. Figure 6 shows the residual shear strength plotted against sample moisture content at failure for 18 specimens all from the same block sample, and tested under the same conditions. There is clearly a variation of residual strength which correlates with sample moisture content although not necessarily arising from it. The significant factor in both variables could be the degree of weathering of the clay [1] although this has not as yet been investigated.

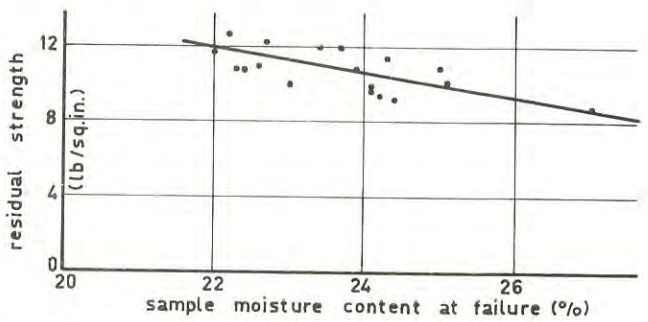

FIG. 6 Residual Strength vs. Moisture Content of Sample at Failure.

To simplify the comparison of results an approximate relationship between residual strength and sample moisture content given by the line in Figure 6 has been drawn, and the measured strengths have been "corrected" to a standard moisture content of 22%. All Series A results at 30 lb/sq.in (as corrected) are plotted on Figure 7.

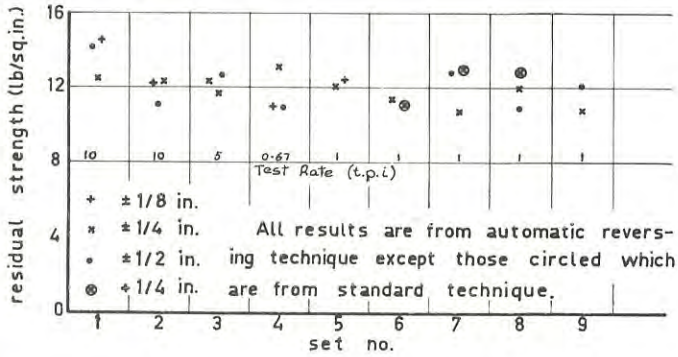

FIG. 7 Corrected Series A Results (30 lb/sq.in. tests)

(d) Area Corrections

Figure 2 is a reproduction of a typical load-displacement curve from an X-Y recorder (Load-vertical axis, relative box displacement-horizontal axis). After the first two reversals the load remains virtually constant over almost the entire 1 in. travel ($-\frac{1}{2}$ in. to $+\frac{1}{2}$ in.) for each subsequent reversal. It would seem from this that it is not valid to apply area corrections even when the relative displacement of the box halves is of the order of 20% of the sample length. (i.e. if one assumes that the normal load is distributed over the full area of the sample, then the shear load should also be assumed to act over the full sample area.).

On physical considerations this is rather difficult to justify unless one assumes that the coefficient of friction - soil to soil - equals the coefficient of friction - soil to brass. However this behaviour has been regularly observed on soils having ϕ'_r values from 13^o to 34^o

In most tests it has been possible to obtain the load reading with the box at the central position, and the question of area corrections does not arise. Where this has not been possible, as for example in tests using the standard technique, no area corrections

[1] Since this determines the nature and quantity of clay particles within the soil it would be significantly reflected in both the residual strength and the equilibrium moisture content of the sample.

have been applied.

(e) Effects of Slow Stress Release at Reversal

In the standard technique the ring load is manually released at the end of each travel thus giving an immediate stress release to the sample. Using an automatic reversing machine the stress release occurs at motor drive speed and is quite slow.

In Figure 7 sets 6 to 8 have results from the standard technique circled, and these may be compared with all other results in sets 5 to 10 which were run at the same speed. No difference in measured strength seems to result from this change in procedure.

(f) Effect of Maximum Displacement

Figure 7 also shows that there is no consistent effect of different maximum displacements. However, on some occasions it has been found that ¼ in. travel between reversals is insufficient to obtain a steady load-displacement curve, a saw-toothed result (Figure 8) being obtained instead. For a reasonable estimate of residual shear strength ¼ in. travel tests are therefore likely to be unsatisfactory for some soils.

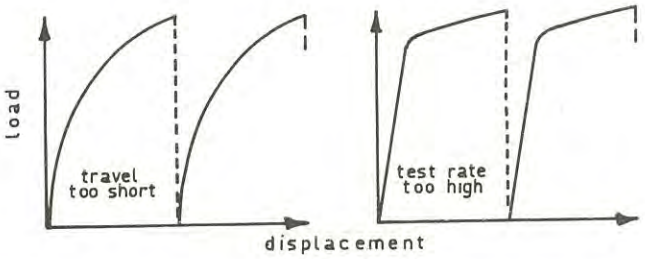

FIG. 8 Load-displacement Curve (Unsatisfactory test conditions)

This explains the difficulty noted by Skempton and Petley in interpreting stress-strain curves for some soils obtained from reversing shear tests in which the travel between reversals was only about 0.3 in. (Ref. 4).

Maximum displacement also affects the number of reversals necessary to reach the residual state. In the majority of tests on various soils, whatever the rate of testing (rapid handwinding excluded), the measured shear strength has become relatively steady after total shearing displacements of about 3 in. (extreme range 1¼-4 in.), and the number of reversals required to achieve the total displacement has not mattered.

(g) Effects of Handwinding, and Precutting Failure Planes

Handwinding at relatively high speed has been tried extensively, with the total travel before slow shear being varied from 3 in. to 10 in. Table I gives results from series B and D experiments.

Handwinding clearly does not produce the same extent of particle orientation as slow shearing, although the time to completion of the test using handwinding is generally somewhat reduced. A much more effective method of reducing the test time is that of pre-cutting a failure plane in the soil. This is not very feasible if the peak strength is required, but has been found satisfactory otherwise.

TABLE I

Series	Handwinding Travel (inches)	Further travel to residual after 16 hours consolidation (inches)
B	0	2 - 3
	3	1½
	7	2
	10	1½ - 2
D*	0	1
	5	3/4

* No time allowed for consolidation after handwinding

The (undrained) strength at the end of handwinding is frequently well below the residual strength. If handwound or pre-cut samples are sheared without further consolidation their strength tends to rise over the first reversal or two, presumably while drained equilibrium is being established.

The results on Kaolin showed the same residual strengths (within 1%) from tests using normal technique, handwinding, and pre-cut failure planes.

(h) Speed Effects

Investigations of residual shear strengths of a range of minerals and natural soils at speeds from very slow to creep rates (Kenney, Ref. 6) show insignificant speed effects in the range 70-10^6 mins/mm. using 1 mm. thick samples. However it is noticable from Kenney's results that Kaolin, a relatively permeable clay, shows some increase in measured strength between 80 and 8 mins/mm., i.e. somewhere between ½ and 5 thousandths of an inch per minute (t.p.m.).

In the present test, sample thickness was approximately 25 mm. and the rates of testing were from 0.64 to 10 t.p.m. (60-4 mins/mm.) i.e., making allowance for drainage conditions, the speed range used here could be considered an extension of that investigated by Kenney in the direction of greater rates of deformation.

Test rates are shown on Figure 7, and there is no apparent effect of increasing the speed from 2/3 to 5 t.p.m. However the results from set 1 (10 t.p.m.) are noticably higher than average while those from set 2 (also 10 t.p.m.) are not. It seems then that for this soil 10 t.p.m. is possibly a little too fast and that undesirable pore pressures may exist at this speed.

To investigate this further, a number of samples have been deformed at low speed (1 t.p.m.) until residual strength is reached, and the test rate has then been increased to 10 t.p.m. In other tests the high speed "residual" has been obtained, and then the rate of deformation has been decreased to 1 t.p.m. and the changes in shear strength observed.

Where residual conditions have been reached at slow speeds initially, increase in test rate has in some cases had no effect on shear strength. In the majority of cases however it has altered both the shape of the load-displacement curve, and the estimated shear strength. At the higher speeds it is frequently found that the load curve is something like that represented in Figure 8 and a positive interpretation of the test results is very difficult.

For these tests the shear strength calculated from the load at the zero relative displacement condition has generally been found to be 10-15% higher than the slow speed residual value.

Where steady values of shear strength have first been obtained at 10 t.p.m. and the machine speed subsequently reduced to 1 t.p.m., the residual strength has been from 0 to 15% lower than the steady state high speed value. Subsequent return to high speed shearing resulted generally in a return to the higher strength values.

It seems fairly clear from the above results that significantly erroneous values will be obtained for the residual shear strength if test rates increase beyond a certain level. For the soil used in these tests - a relatively impermeable clay with PI ≐ 35% - that level would seem to be about 5 t.p.m.

Where it is necessary to select a suitable speed without any previous experience as a guide it would probably be advisable to run two tests at different speeds (say 10 t.p.m. and 1 t.p.m.) until steady state conditions are reached, and then reduce speed by a factor of 10 in each test and observe the changes in measured strength. When interpreting the results the variability of natural samples should be considered. For those who want a simple guide, results on the Series A soil used here show that if speed effects (as determined above) alter the measured strength by 10-20% the test rate in question should be considered 10 times too high. Other soils may, however, have more critical rate effects.

In the majority of tests or parts of tests which have been run at the higher speed (10 t.p.m.) the load deflection graph has been of the form shown in Figure 8. If this form of curve is obtained the shearing speed may well be too high, and this should be investigated.

(i) Stage Testing

Figure 9 shows the results of four Series B tests in which each sample has been failed at a different initial normal stress, with subsequent increases in normal stress in each test. τ vs. σ graphs are presented firstly for each sample showing all stages, then for the collected first stage results, and finally for all results obtained from the four samples. The four samples were taken from adjacent locations.

Figure 9 also shows results from one Series A test in which the load has been varied a number of times both up and down. It is evident that the strength is not affected by the stress history of the sample within the range tested, and that later stages give values the same as those obtained from the early stages.

All these results indicate that stage testing is a valid extension of the normal technique. At the test rate used for these samples the machine time required to obtain each initial point is usually about 2½ days, whereas that for further points is about 1 day only. (These are minimum times and both are significantly dependent on the constraints of normal working hours). Furthermore up to four points on the strength envelope can be obtained from one sample and from one setting up operation, although the brittleness is only obtained at one stress level.

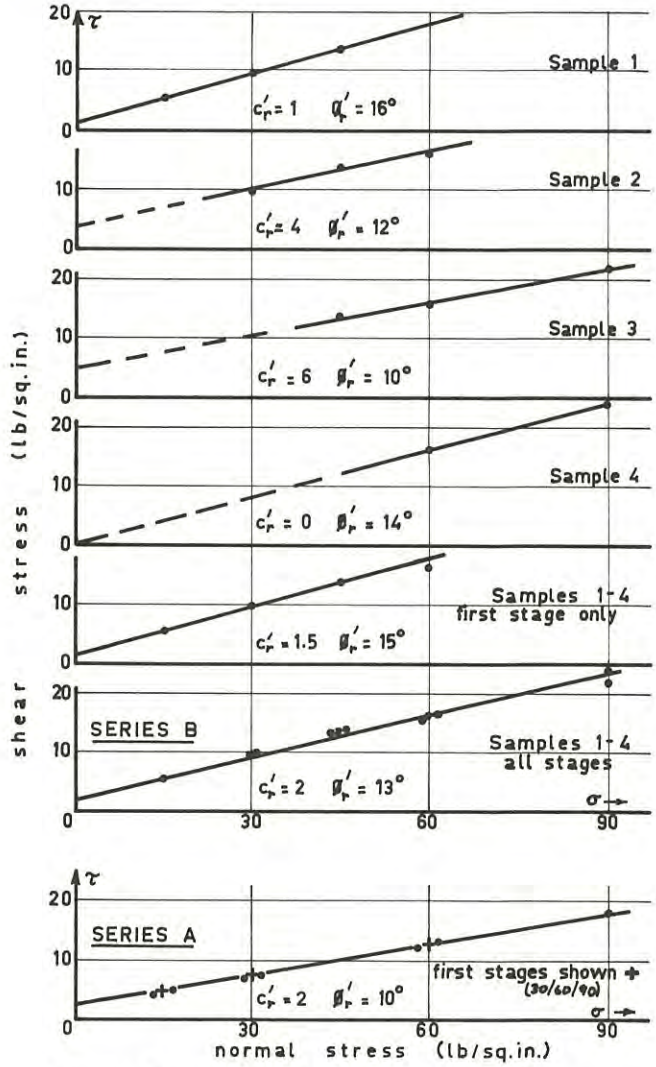

FIG. 9 Strength Envelopes from Stage Tests

It is found that the test is completed more quickly if shear is not interrupted when normal load increments are applied. Any further consolidation which then occurs does so as the test progresses.

(j) Sample Erosion

At high normal stresses some samples have been found to wear away fairly rapidly. No difference seems to exist between rates of erosion in the standard box using the standard technique and rates in the modified box using larger maximum displacements. Where stage testing is employed the sample will generally be subjected to very substantial cumulative shear displacements and it is advisable to have ½ in. thickness of sample above the shear plane for such tests. Thickness of all samples in the tests reported herein have been 1 in. with the failure plane approximately at midsample height at setup.

It should be recognized that the material being sheared at one reversal is not precisely the same as

that sheared at the next and in stage tests the results should be expected to reflect to some extent the small-scale variability of the natural materials.

(k) Remoulded Samples

Tests on remoulded samples in Series C and D were generally found to reach residual strengths more quickly than was the case for natural samples. Slickensides are formed in remoulded material as in natural samples, and a photograph of one such case is shown in Figure 10. (The sample separated readily). Total travel for this sample was 2 inches at 1 t.p.m. (40 min/mm) and normal stress was 20 lb/sq.in. The residual strength envelope for this material is shown in Figure 5. (four different samples.)

FIG. 10 Slickenside Formed in Remoulded Sample

(l) Kaolin

Results for the Kaolin were as follows:- for $c' = 0$, $\tan \phi_r' = 0.18$ ($\phi_r' = 10^o$), at normal stresses of both 30 and 60 lb/sq.in. This is somewhat lower than the value obtained by Kenney (Ref. 6) in his apparatus.

(m) Machine Modifications

The circled results on Figure 7 were obtained using not only the standard technique, but the standard Wykeham Farrance Reversing shear machine. As previously noted these results are not significantly different from those obtained on the extensively modified shear box. It follows that the results from the standard machine have not been affected noticably by the relatively large amounts of end play in the drive system, or the considerable amount of vertical restraint which can be afforded the top half of the shear box by its yoke system. Modifications (ii), (iii), and (v) (Section IV) can therefore be considered unnecessary.

VII CONCLUSIONS

(a) The reversing shear box is a convenient apparatus for measuring both peak and residual strengths of soils. The laboratory conditions under which these tests are made are quite different from those which exist in the field. It does not follow, however, that these differences necessarily lead to significant errors in the laboratory estimation of field residual strengths. A number of variables and variations of test technique have been isolated and examined to determine their effects on measured residual strength. In general the test results are insensitive to significant changes in the test procedure, deformation rate being the one exception.

On the basis of the tests analysed so far the following procedure would be recommended for a machine with minimum modification.[1]

(i) For a 6 cm. square box a 1 in. thick sample should be used.
(ii) Using unmodified shear box halves the travel limits should be set at about plus 0.4 ins., and minus nothing. (Unmodified boxes might not always allow sufficient travel for correct determination of residual strength.)
(iii) A deformation rate suitable for determining the drained strength parameters for the soil in question should be selected. A speed of 0.001 inches/min. is likely to be suitable for fissured overconsolidated clays.
(iv) The normal stress should be selected on the basis of the number of samples available. Both "positive" and "negative" staging give satisfactory results.
(v) Consolidation of the sample under the applied normal stress is only necessary where peak drained strengths are desired from the sample.
(vi) After the peak strength has been passed, rapid handwinding for 2-3 ins. travel can be used to hasten particle orientation.
(vii) The test should be continued until closely similar results are obtained on consecutive forward or consecutive reverse movements, and not stopped when the load appears to be steady within one movement. It will generally be found that about 2-2½ ins. total deformation is necessary, irrespective of the number of reversals involved.
(viii) When the residual state has been reached the normal stress may be varied in whatever stages are required by the investigation programme, a check being kept on sample erosion particularly when the normal stresses are high.

(b) Load-deformation curves which are difficult to interpret will often be found to result from heterogeneous specimens, or from too high deformation rates.

(c) With some soils uni-directional movements greater than 0.4 ins. might be necessary for correct determination of the residual strength. The standard 6 cm. square shear box would not give adequate travel for these soils.

---

[1] For a basic non-reversing shear box the minimum modification is:-
(i) Provision of push-pull connexions at motor drive and proving ring.
Desirable modifications are considered to include:-
(ii) Automatic reversing control.
(iii) Automatic load recording.
(iv) Modification of upper and lower box halves to give unrelieved faces allowing displacement in both directions.

(d) The value of c'_r is not necessarily zero even for relatively low stress ranges.

(e) The results for the Kaolin indicate that the method of conducting residual shear tests does affect the laboratory estimate of ϕ'_r.

(f) Some Australian soils show very high brittleness indices (up to 0.75 at 30 lbs/sq.in) and it is worth noting that it is for soils such as these that residual strengths are most likely to be of relevance.

VIII ACKNOWLEDGEMENTS

All tests reported in this paper were carried out in the Soils Engineering Laboratories of the Department of Civil Engineering, Monash University, Victoria. The effort of Mr. R. H. Stokes who carried out a major part of the laboratory work is gratefully acknowledged. Series B samples were provided by the State Electricity Commission, Victoria.

VIII REFERENCES

1. SKEMPTON, A.W. - Long-term stability of Clay Slopes. Fourth Rankine Lecture. Geotechnique, Vol. XIV, No. 2, June 1964, pp. 77-101.

2. SKEMPTON, A.W. and HUTCHINSON, J. - Stability of Natural Slopes and Embankment Foundations. State of the Art Report. Proc. Seventh Int. Conf. Soil Mech. and Found. Engg., Mexico, 1969, Supp. Vol., pp. 291-340.

3. BISHOP, A.W. - Progressive Failure with Special Reference to the Mechanism Causing it. Panel Discussion, Proc. Geotech. Conf., Oslo, 1967, Vol. 2, pp. 142-150.

4. SKEMPTON, A.W. and PETLEY, D.J. - The Strength Along Structural Discontinuities in Stiff Clays. Proc. Geotech. Conf., Oslo, 1967, Vol. 2, pp. 29-46.

5. BJERRUM, L. - Progressive Failure in Slopes in Over-consolidated Plastic Clays and Clay Shales. Third Terzaghi Lecture. Proc. ASCE (Journ. Soil Mech. and Found. Div.), Vol. 93, No. SM5, 1967, pp. 3-49.

6. KENNEY, T.C. - The Influence of Mineral Composition on the Residual Strength of Natural Soils. Proc. Geotech. Conf., Oslo, 1967, Vol. 1, pp. 123-130.

7. CHANDLER, R.J. - The Measurement of Residual Strength in Triaxial Compression. Geotechnique, Vol. XVI, No. 3, 1966, pp. 181-186.

8. WEBB, D.L. - Residual Strength in Conventional Triaxial Tests. Proc. Seventh Int. Conf. Soil Mech. and Found. Engg., Mexico, 1969, Vol. 1, pp. 433-441.

9. de BEER, E. - Shear Strength Characteristics of the "Boom Clay", Proc. Geotech. Conf., Oslo, 1967, Vol. 1, pp. 83-88.

10. SEMBENELLI, P. and RAMIREZ, L. - Measurement of Residual Strength of Clays with a Rotation Shear Machine. Specialty Session No.16, Proc. Seventh Int. Conf. Soil Mech. and Found. Engg., Mexico, 1969, Vol. 3, p. 528.

Undrained Shear Strengths in Clays

By
R. H. G. Parry, M.A., Ph.D., M.I.E.Aust.
(Lecturer in Engineering, Cambridge University)

SUMMARY - A theoretical relationship is developed between undrained shear strengths in saturated clays for triaxial compression, triaxial extension and plane strain. The basic assumptions made are that at critical state the clay obeys a strength criterion in effective stress space of the Mohr-Coulomb type and also that a unique relationship exists at critical state between voids ratio and mean effective stress. Using these assumptions, which are based on experimental observations, it is predicted that undrained shear strengths in extension will be less than in compression by up to 30% and plane strain values will be less than triaxial compression values by about 8% on average. A comparison of these theoretical differences with published experimental values shows promising agreement.

I. - INTRODUCTION

If a soil is subjected to continuous shear strain it eventually reaches a state when deformation will continue indefinitely at constant applied stress. No further change in volume or pore pressure will occur under this applied stress, and the soil has reached a critical state, which is equally valid for clays and sands.

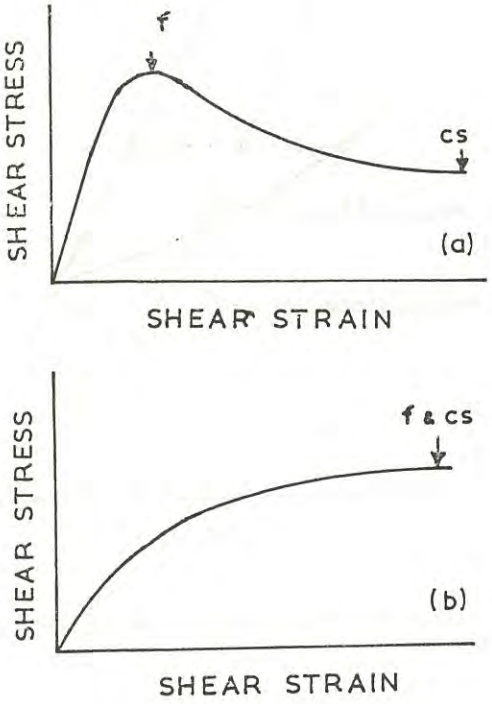

Fig.1 Typical stress-strain curves for soils.

Shear stress vs shear strain curves for soils are of the general form given by either Fig.1a or 1b. In Fig.1a the curve passes through a peak failure point (f) during which the soil is still showing strong dilatancy effects - i.e. volume changes or pore pressure changes are still occurring. Under continued shearing, however, a point will be reached where dilatancy effects are no longer present. Shear strains then continue without change in external or internal stress or volume change and the soil flows as a frictional fluid. This is critical state (cs).

The curve in Fig.1b does not show any peak: the failure condition and critical state are reached simultaneously, usually at high strains. This paper is concerned primarily with laboratory prepared saturated clay specimens, both normally consolidated and overconsolidated, which in each case generally show undrained stress-strain curves of type 1b, with failure and critical state coincident.

Critical state (then referred to as critical voids ratio) was predicted for clays by Roscoe, Schofield and Wroth (Ref.1) after studying the end points of a relatively small number of tests on sands and clays. Parry (Ref.2) predicted the critical state after studying the continuing volume change or pore pressure behaviour at the peak conditions. It was also shown that the rate of volume change or pore pressure change was proportional to the "distance" from the critical state, and that a unique relationship existed at critical state between voids ratio and mean effective stress, which was independent of the initial state of consolidation of the soil or the stress path followed to reach critical state.

Another phenomenon observed in carrying out shear tests on remoulded saturated clay, applying different stress paths, is that the undrained strength of the clay is stress path dependent. Referring to Fig.2, plots of deviator stress against axial strain are shown for undrained triaxial compression and extension tests on remoulded saturated Weald clay (w_L = 46 w_p = 20). The specimens in Fig.2a were both initially normally consolidated under an isotropic pressure of 410 kN/m^2. The specimens in Fig.2b were both overconsolidated under isotropic pressure, applying a maximum pressure of 825 kN/m^2 and allowed to rebound to 103 kN/m^2 before shearing. It can be seen that in Fig.2a the strength in undrained extension is 13% less than in undrained compression. In Fig.2b the strength in undrained extension is 16% less than in undrained compression.

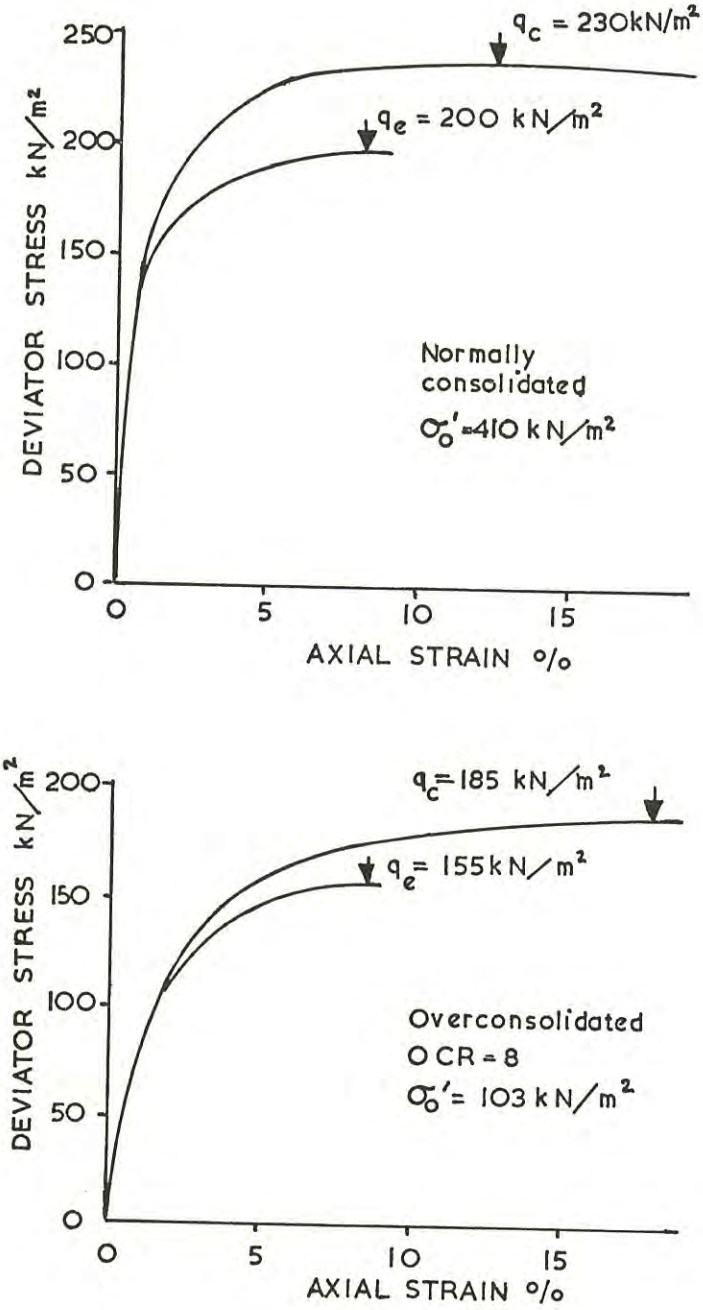

Fig.2. Undrained triaxial compression and extension tests on Weald clay.

The purpose of this paper is to use critical state theory to predict the relationship between undrained strengths in triaxial compression (q_c), triaxial extension (q_e) and plane strain (q_p), and compare those predictions with published evidence.

II. - PREDICTED RATIOS q_e/q_c AND q_p/q_c

The use of the critical state theory in this paper is confined to the simple concept that, under continuing shear, a soil regardless of its initial condition will reach a point on a unique e-p line, the critical state line, as shown in Fig.3, where e is voids ratio and p is mean effective stress, $\frac{1}{3}(\sigma_1'+\sigma_2'+\sigma_3')$. This is one of the basic principles of critical state theory.

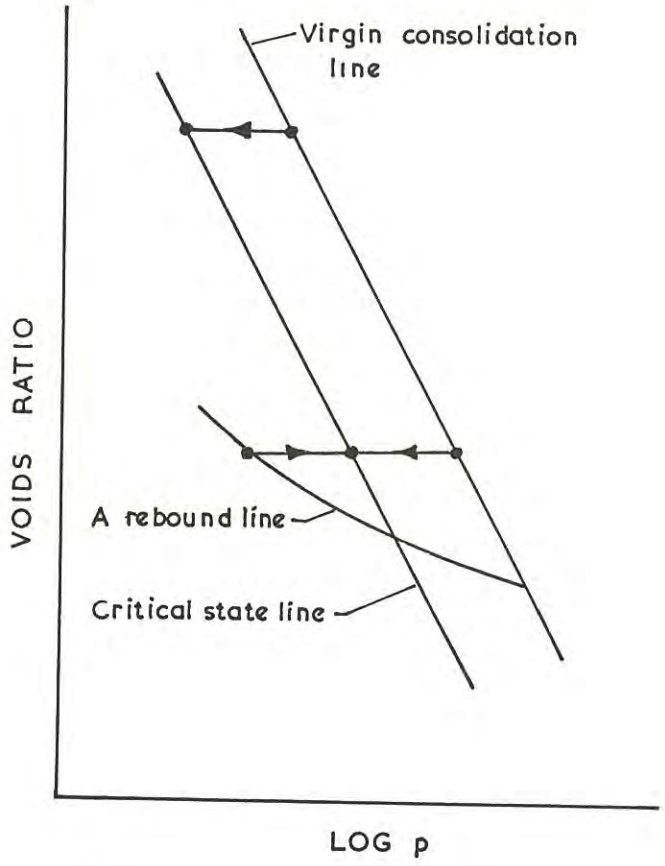

Fig.3. Undrained test paths on an e-log p plot.

Two other assumptions are also made in the paper as follows:

1. At the critical state the effective stress Mohr-Coulomb envelope for un-

drained shear tests on laboratory prepared saturated clay specimens has no zero stress intercept (i.e. no apparent cohesion c'). It is well known that the effective stress envelope for normally consolidated clays is usually a straight line passing through the origin, but it is less well known that the effective stress envelope for overconsolidated clay (laboratory prepared specimens) lies very close to the envelope for the normally consolidated clay. This has been shown for Weald clay and London clay by Parry (Ref.3)and the envelopes for undrained compression and extension tests on remoulded Weald clay are shown in Fig.4a to 4d.

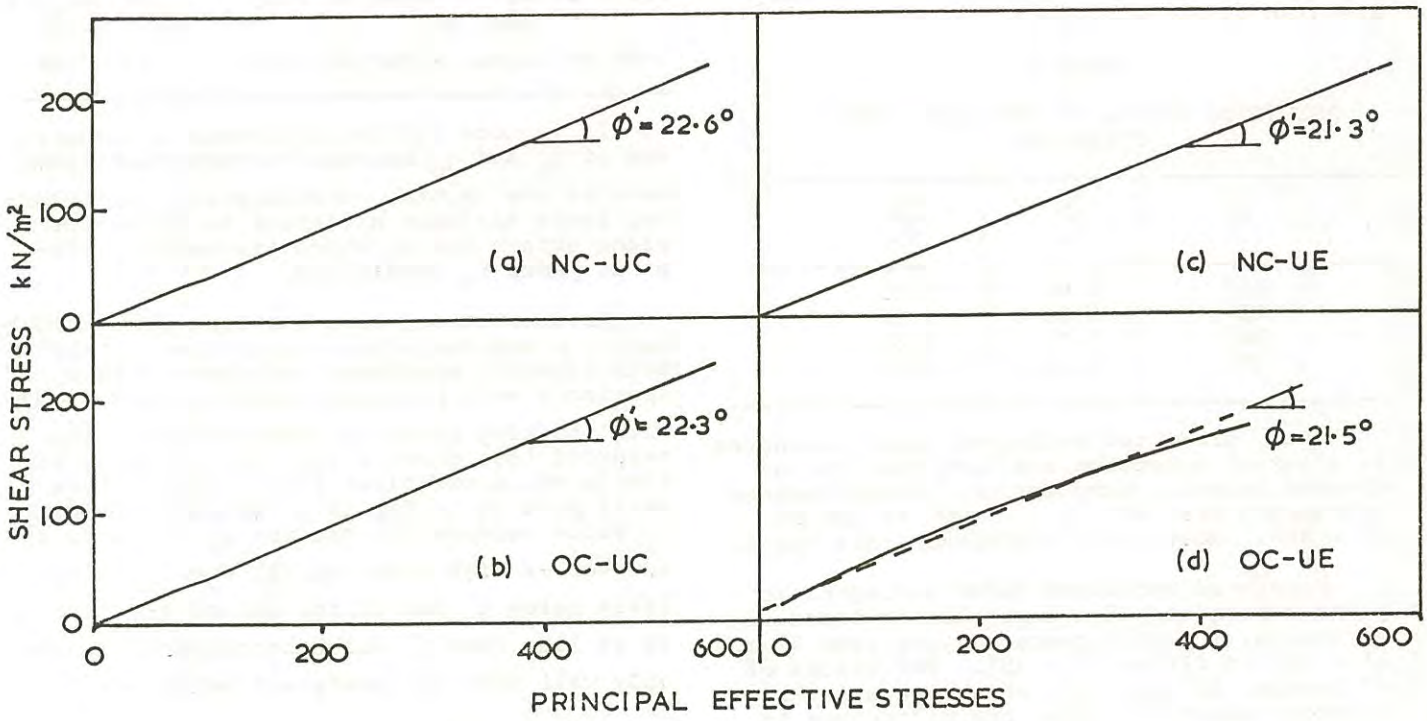

Fig.4. Effective stress Mohr-Coulomb envelope for Weald clay.

2. The value of ϕ' is assumed to be independent of stress path for clay. It can be seen in Fig.4 that the variation is in the range of 1^0 to 2^0 and this amount of variation is common for clays and is negligible for the purposes of this paper.

Using the assumption of a constant ϕ' the ratio of major to minor principal effective stress at critical state becomes

$$\frac{\sigma_1'}{\sigma_3'} = \frac{1+\sin\phi'}{1-\sin\phi'} \qquad (1)$$

where ϕ' is the critical state value, and also the failure value for most laboratory prepared specimens.

Putting $\sigma_1'-\sigma_3' = q$

and $p = \frac{1}{3}(\sigma_1'+2\sigma_3')$ for triaxial compression (2a)

$p = \frac{1}{3}(2\sigma_1'+\sigma_3')$ for triaxial extension (2b)

$p = \frac{1+m}{3}(\sigma_1'+\sigma_3')$ for plane strain (2c)

where $m = \frac{\sigma_2'}{(\sigma_1'+\sigma_3')}$

it can be shown from Eq.1 that, at critical state:

Compression $\left(\frac{q}{p}\right)_c = \frac{6\sin\phi'}{3-\sin\phi'}$ (3a)

Extension $\left(\frac{q}{p}\right)_e = \frac{6\sin\phi'}{3+\sin\phi'}$ (3b)

Plane strain $\left(\frac{q}{p}\right)_p = \frac{6\sin\phi'}{2(1+m)}$ (3c)

Thus: $\left(\frac{q}{p}\right)_e \Big/ \left(\frac{q}{p}\right)_c = \frac{3-\sin\phi'}{3+\sin\phi'}$ (4a)

$\left(\frac{q}{p}\right)_p \Big/ \left(\frac{q}{p}\right)_c = \frac{3-\sin\phi'}{2(1+m)}$ (4b)

Samples of saturated soil with identical initial conditions tested in undrained shear along different stress paths will, when they

reach the ultimate critical state, have identical p values according to the hypothesis made earlier in this paper. Undrained strength ratios from equations 4a and 4b at critical state will be given by:

$$\frac{q_e}{q_c} = \frac{3 - \sin \phi'}{3 + \sin \phi'} \qquad (5a)$$

$$\frac{q_p}{q_c} = \frac{3 - \sin \phi'}{2(1+m)} \qquad (5b)$$

Values of m for clays have been found to be about m = 0.4 for remoulded clays (Ref. 4, Ref. 5). Taking a value of 0.4 gives the values of $\frac{q_p}{q_c}$ shown in Table 1 for different values of ϕ'. Values of $\frac{q_e}{q_c}$ are also given in Table 1.

TABLE I

PREDICTED RATIOS OF UNDRAINED SHEAR STRENGTHS

ϕ'	$\frac{q_e}{q_c}$	$\frac{q_p}{q_c}$
20^0	0.80	0.95
25^0	0.75	0.92
30^0	0.71	0.89
35^0	0.68	0.87

Thus, predicted undrained shear strengths in triaxial extension are less than in undrained triaxial compression, the difference increasing from 20% at $\phi' = 20^0$ to 32% at $\phi' = 35^0$. Most clays lie within this range.

Predicted undrained shear strengths in plane strain are also less than in triaxial extension, the difference ranging from 5% at $\phi' = 20^0$ to 13% at $\phi' = 35^0$. For values of ϕ' between 20^0 and 25^0, which range includes a large number of clays, the difference is 8% or less, which is only just distinguishable in normal routine laboratory testing.

III. - COMPARISON OF PREDICTIONS WITH OBSERVED RESULTS

Strict comparison of observed q_e, q_p and q_c values can be made in the light of the above theory only at the critical state condition. Most published test results are for failure (i.e. peak deviator stress) in remoulded clays, but the stress strain curves for remoulded clays, both normally consolidated and overconsolidated, are usually of the type shown in Fig.1b. Thus the critical state and failure conditions are coincident and these results can be compared with the predictions.

All published information for undrained triaxial tests on saturated clays show shear strengths in extension to be less than shear strengths in compression by 14% to 30%, averaging 20%, and so in general there is good agreement between predicted and experimental results. Actual published results are given in Table II.

TABLE II

OBSERVED RATIOS OF q_e/q_c

Worker	Soil	ϕ'	q_e/q_c
Parry (Ref.3)	Rem.NC & OC clay	22^0	0.85
Hirshfield(Ref.6)	Und.NC clays	--	0.75 to 0.80
Wu et al (Ref.7)	Rem.NC clay	32^0	0.70
Broms et al (Ref.8)	Rem.NC clay	29^0	0.70 to 0.80
Ladd et al(Ref.9)	Rem.NC clay	33^0	0.86

It is more difficult to make a comparison of q_p and q_c because for most published results the initial consolidation for triaxial tests has been different to those for plane strain tests, which are usually prepared under K_o conditions.

An interesting case has been published by Henkel & Wade(Ref.4)for Weald clay ($\phi'=24^0$). Both triaxial specimens and plane strain specimens were prepared under K_o conditions with the clay normally consolidated. The triaxial test shows a flat top curve as in Fig.1b while the plane strain curve shows a small peak as in Fig.1a. Thus the maximum q_p value exceeds the maximum q_c value by 4%. However at high shear strain the q_p value falls below q_c and at the end of the test q_p is 4% less than q_c which corresponds reasonably well with the predicted behaviour.

Shibata and Karube(Ref.10) using equipment applying all three principal stresses independently show, for normally consolidated clay, similar behaviour to that shown by Henkel and Wade. Assuming their tests where m = 0.4 to correspond closely to plane strain conditions they show ultimate shear strengths for these tests about 4% less than compression values.

The q_p values of 4% less than q_c observed by Henkel and Wade (Ref.4) and Shibata and Karube(Ref.10) compare with predicted difference of 7%. However these predicted and observed differences vary only by 3% which is less than the experimental accuracy for this type of testing.

Where initial consolidation conditions for two samples of a clay are not identical, comparisons of the dimensionless terms $\left(\frac{q}{p}\right)_p$ and $\left(\frac{q}{p}\right)_c$ can be made against predictions

given by Eq.4a and 4b. The predicted ratios will be the same as given for q_{p/q_c} in Table I. On this basis of comparison plane strain values obtained by Thurairajah (1961) were 8% less than triaxial compression values for Spestone Kaolin ($\phi' = 24^0$). This agrees very well with the predicted relationships.

IV. - DISCUSSION

Conditions in practice rarely correspond closely to triaxial extension conditions but frequently correspond to plane strain conditions. Thus, according to the above theory, differences in ultimate strength for different stress paths in the field are not likely to be greater than about 13% for clays and should be more commonly in the range from 5% to 10%.

However, where interchange in the directions of the major and minor principal stresses occurs, stress-strain curves (i.e. q vs axial strain) can show quite different shapes to those where no interchange occurs. In these cases the theory above will not apply in making a comparison of maximum deviator stresses. In some soft clays in the field, however, this condition of principal stress interchange during shear may not be important. Most soft clay deposits are lightly overconsolidated, often through movements of ground water level (Ref. 12) , and the K_o value which is typically 0.6 for a clay normally consolidated in the laboratory rises to unity for overconsolidation ratios between 2 and 3. Thus, when the soil in the field has been lightly overconsolidated to this extent, the initial stress conditions will be almost isotropic and so principal stress interchange would not occur in the field.

V. - CONCLUSIONS

Using a simple critical state concept and the Mohr-Coulomb failure criterion,it has been predicted that undrained shear strengths for clays will be less in triaxial extension than in triaxial compression by amounts ranging typically from 20% to 32% and laboratory observations confirm this. It has also been predicted that undrained shear strengths in plane strain will be less than in triaxial compression by values ranging typically from 5% to 10%, and laboratory observations again confirm these lower values.

The large predicted and observed differences between extension and compression is of a limited interest practically because extension conditions are rarely encountered in the field. Plane strain conditions are common in the field and the results given in this paper will have some relevance in predicting relative undrained shear strengths, except where an interchange in the direction of maximum and minimum principal stresses occurs during shearing.

REFERENCES

1. ROSCOE K.H., SCHOFIELD A.N. and WROTH C.P. On the yielding of soils. Géotechnique Vol.8, No.1, March 1958, pp 22-53.

2. PARRY R.H.G. Discussion - "On the yielding of soils". Géotechnique Vol.8, No.4, Dec 1958, pp 183-186.

3. PARRY R.H.G. Strength and Deformation of Clay. Ph.D.Thesis, London, 1956.

4. HENKEL D.J. and WADE N.H. Plane strain tests on a saturated remoulded clay. A.S.C.E., J. SMFD Vol.92, No.SM6, Nov 1966, pp 67-80.

5. HAMBLY E.C. Plane Strain Behaviour of Soft Clay. Ph.D.Thesis, University of Cambridge, 1969.

6. HIRSHFIELD R.C. Factors Influencing the Constant Volume Strengths of Clay. Ph.D.Thesis, Howard University, 1958.

7. WU E.T., LOH A.K. and MALVERN L.E. Study of failure envelope of soils. ASCE, J. SMFD, Vol.89, No.SM1, Feb 1963, pp 145-181.

8. BROMS B.B. and CASBARIAN A.O. Effects of rotation of principal stress axes and of the intermediate principal stress on the shear strength. Proc. 6th Int.Conf.Soil Mech.Montreal 1965 Vol.1, pp 179-183.

9. LADD C.C. and VARALLYAY J. The influence of stress system on the behaviour of saturated clays during undrained shear. M.I.T.Report R.65-11, 1965.

10. SHIBATA T. and KARUBE D. Influence of the variation of the intermediate principal stress on the mechanical properties of normally consolidated clays. Proc.6th Int.Conf.Soil Mech. Montreal 1965, Vol.1, pp 359-363.

11. THURAIRAJAH A. Some Shear Properties of Kaolin and of Sand. Ph.D.Thesis, University of Cambridge, 1961.

12. PARRY R.H.G. Overconsolidation in soft clay deposits. Géotechnique Vol.20, No.4, Dec 1970, pp 442-446.

Effects of Salt Content on Thixotropic Behaviour of a Compacted Clay

By

Surachat Sambhandharaksa, M.Eng.

(Lecturer, Chulalongkorn University, Thailand)

and

Za-Chieh Moh, Sc.D.

(Professor of Geotechnical Engineering, Asian Institute of Technology, Thailand)

SUMMARY This paper presents some data on the effects of salt content on the thixotropic characteristics of a compacted clay. Both short range and long range interparticle forces are considered in the interpretation of test results. Various amounts of salt (sodium chloride) were added to the clay to study the effects of salt on compaction, strength and thixotropic characteristics of the clay. An increase in salt content in the compacted Bangkok Clay resulted in (1) an increase in dry unit weight on the dry side of optimum, (2) an insignificant change in dry unit weight on the wet side of optimum, and (3) a reduction in the compressive strength when compacted on the wet side of optimum. The effect of salt content on the thixotropic characteristics provided additional experimental evidence in support of Mitchell's hypothesis. The results indicated that the maximum thixotropic strength increase occurred at the maximum excess internal energy which resulted from the shear strains induced by the compaction process. The magnitudes of the shear strains were, in turn, dependent upon the soil structure.

From the test results it is postulated that the main factors which influence the soil structure are the applied external stresses, the interparticle contacts and the physical interference between the particles. The short range interparticle forces are necessarily to be considered along with the long range interparticle forces.

I. INTRODUCTION

The importance of the effect of soil structure on the behavior of fine-grained soils has been recognized for over fifteen years. A number of hypotheses have been proposed (for example Ref. 1) to explain soil behavior on the basis of colloidal theory by considering the long range interparticle forces. It has been shown by a number of investigators (Ref. 2, 3 and 4) that the double layer theory is quite satisfactory for clay-water systems with high moisture contents.

Olson and Mitronovas (Ref. 5), and Mitchell (Ref. 6) have shown that it is not sufficient just to consider the long range interparticle forces when a clay is at a low moisture content and is subjected to externally applied stresses. Mitchell (Ref. 7) postulated that, for engineering purpose, the strength properties are mainly controlled by the conditions of the particle contacts, and, thus, short range forces and physical interferences between the particles become of controlling importance.

This paper reports an investigation aimed at (1) the study of the effects of applied external stress and short range interparticle forces on soil structure and (2) the establishment of further understanding of the mechanisms of thixotropic behavior of compacted clays. Since salt concentration is one factor which can change the interparticle forces as well as the particle orientation of a soil mass, it was chosen as the primary variable in the study. The soil used was a clay which was originally deposited in a marine environment and was subsequently subjected to leaching by fresh water. The present concentration of salt in the pore fluid depends upon the distance of the deposit from the present shoreline. Since this soil, called "Bangkok Clay", covers a large area of the rapidly developing Chao Phraya Plain in Thailand, the effects of salt content on the engineering behavior of this clay are of considerable interest to both researchers and practicing engineers.

II. EXPERIMENTAL INVESTIGATION

(a). Treatment of Raw Soil Sample

The soil sample used was a dark gray, medium plastic clay containing thin layers of silt, and was taken from a ditch at a depth of about 3 m below the ground surface at the new AIT site at Rangsit 40 km north of Bangkok. The clay was cut into slices and air-dried in the laboratory. The air-dried soil was then ground and sieved through a U.S. Standard Sieve No. 12. About 10 per cent of the soil was retained on the sieve and was discarded. The index properties of the soil sample, both in the air-dried and natural conditions, are presented in Table I. A typical mineralogical composition of the Bangkok Clay is shown in Table II.

(b). Preparation of Specimens

Reagent grade sodium chloride was used as the "salt" to be added to the soil. The salt was first dissolved in distilled water and then mixed with the soil in solution form. Extreme care was undertaken to assure a uniform distribution of the added salt and water throughout the soil sample in order to achieve the desired salt concentration and moisture content. The allowable variation in the moisture content at compac-

TABLE I

INDEX PROPERTIES OF SOIL SAMPLE USED

Soil Property	Pretesting Condition	Results
Liquid Limit, %	Natural	80.0 ± 2.0
	Air-dried	62.0 ± 2.2
Plastic Limit, %	Natural	36.2 ± 2.3
	Air-dried	31.7 ± 1.3
Plasticity Index, %	Natural	43.8 ± 4.3
	Air-dried	25.8 ± 3.5
Specific Gravity	Natural	2.69 ± 0.05
Textural Composition, %		
Silt (0.002-0.074 m.m.)	Air-dried	75.0 ± 5.0
Clay (< 0.002 m.m.)	Air-dried	25.0 ± 5.0
pH	Air-dried	7.2 ± 0.1
Total Soluble Salt Content, % by Weight	Air-dried	0.33 ± 0.01

TABLE II

MINERAL COMPOSITION OF A TYPICAL BANGKOK CLAY*

Mineral	Per Cent by Weight**
Illite	35
Montmorillonite	30
Kaolinite	10
Quartz	15
Unidentified	10

*Data reported in (Ref. 8).

**Per cent based on clay fraction (< 2 micron)

tion was ± 0.5 per cent.

Soil specimens were prepared by dynamic compaction in a miniature mold, 3.56 cm (1.4 in.) in diameter and 7.63 cm (3.0 in.) high. The compaction energy was delivered by a hammer, 477 gm in weight, which dropped through a height of 30 cm. The specimens were compacted in three layers with 40 blows per layer. This compaction energy produced a compaction curve nearly the same as that obtained by the Standard Proctor Compaction (Ref. 9).

(c). Curing and Testing of Specimens

The specimens used for the study of the thixotropic characteristics required curing at constant temperature. Immediately after compaction, the specimens were tightly wrapped with plastic paper and aluminum foil. They were then placed in closed containers and stored in a constant temperature fog room (maintained at $70^{\circ} \pm 2^{\circ}$F) for various periods of time.

The specimens, either as compacted or after curing, were tested in unconfined compression to determine the stress-strain characteristics at a rate of strain of 1.5 per cent per minute until failure.

III. COMPACTION CHARACTERISTICS

Fig. 1a shows the compaction curves plotted in the conventional manner, i.e. dry unit weight versus moisture content by weight. A large portion of the increase in the dry unit weight of the specimens as salt content increased was actually due to the presence of salt in the solid phase. By replotting the

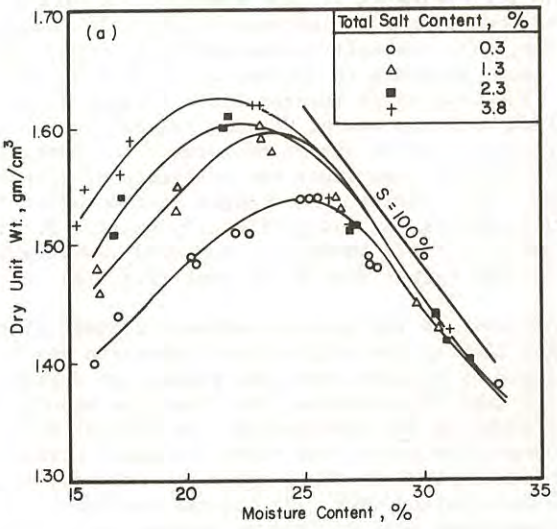

(a) Salt as part of solid.

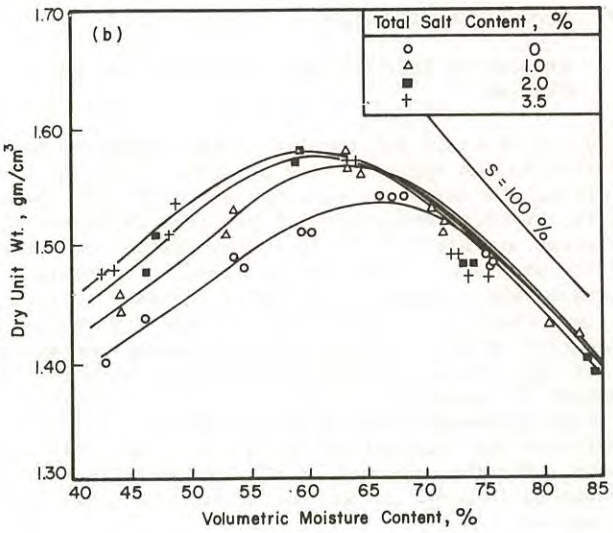

(b) Salt as part of pore fluid.

Fig. 1 - Effect of Salt Content on Compaction Characteristics.

results in terms of the volumetric moisture content, which was defined as the ratio of the volume of water and salt to the volume of dry soil, the effect of salt content on the compacted unit weight was greatly reduced (Fig. 1b). In both cases, the trends of the effect of salt content are similar. The effects of the addition of salt to the clay were (i) to increase the dry unit weight at low moisture contents, (ii) to reduce the optimum moisture content, and (iii) to

cause insignificant changes in the dry unit weight at moisture contents above the optimum.

At low moisture contents, soil structure before compaction tends to change from edge-to-face type of flocculation to face-to-face flocculation (or so called "salt flocculation") as the salt concentration increases (Ref. 10 and 11). Consequently, under the influence of dynamic compaction, the clay particles become more oriented and the compacted dry unit weight increases with increase in the salt content. However, when the salt concentration is high, there is a large increase in the net attractive forces (i.e. the long range interparticle forces) which, combined with the amount of ions present in the soil-water system, offer strong resistance for particles to move closer even under the influence of compaction forces. As a result, the changes in the compaction characteristics are insignificantly small. For the Bangkok Clay, this phenomenon occurred when the salt content was higher than 2 per cent (Fig. 1b).

The decrease in the optimum moisture content of the Bangkok Clay as the salt content increased may be explained by the fact that the higher the degree of face-to-face flocculation, the lower the amount of water required for lubrication. On the wet side of the compaction curve, the effect of shear strains, which are imposed by the compaction process, on particle orientation (Ref. 12) becomes dominant. The clay particles tend to form an oriented structure irrespective of the difference in salt content and this diminishes the effect of salt on the dry unit weight.

IV. COMPRESSIVE STRENGTH

(a) Effects of Salt Content on Stresses at Low Strains

Figure 2 presents the results of the effect of salt content on the stresses at 2 per cent strain by considering the salt as a part of the solid. An increase in the salt content to 2.3 per cent increases the stresses at this low strain for specimens compacted on the dry side of the optimum moisture content. However, the stresses decrease as the salt content is further increased. On the other hand, for specimens compacted on the wet side of the optimum, the stresses at this strain continuously decrease as the salt content is increased. Figure 2 further indicates that an increase in the molding moisture content decreases the strength of the soils at all salt contents. For the explanation of these results, it is necessary to refer to the compaction characteristics of the soil.

The decrease in strength at low strains with increase in the molding moisture content can be explained on the basis of the concepts proposed by Lambe (Ref. 1) and Mitchell et al (Ref. 13). At low moisture contents, the compacted soil has a random particle orientation but as the moisture content increases, the soil particles become more oriented. Since the number of interparticle contacts in a randomly oriented structure is more than in a soil with oriented structure (Ref. 7), the effective stresses and hence the strength in soils compacted at low moisture contents should be higher than those compacted at higher moisture contents (Ref. 13). The reduction in strength might be expected to be even more pronounced

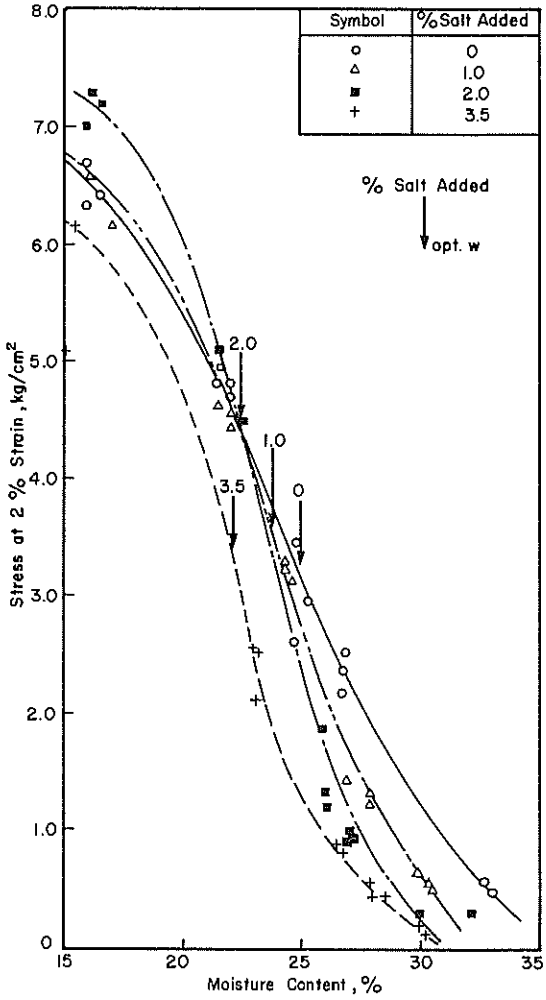

Fig. 2 - Relationship between Stress at 2 Per Cent Strain and Molding Moisture Content.

when the moisture content is above the optimum, since the degree of particle orientation will continue to improve due to the combined effects of high moisture content (Ref. 1) and shear strains caused by the compaction process (Ref. 12).

For consideration of the effect of salt content, it is necessary to consider in detail effects of salt content on the interparticle forces, in both short range and long range, as well as on the particle orientation in a soil-water mixture. An increase in the sodium chloride concentration in the pore fluid of a clay-water system has three effects. Firstly, it increases the net attractive forces between the soil particles (Ref. 1); secondly, it increases the short range adsorptive forces which are due to increases in the local ionic interactions and the hydration capacity from the sodium ions (Ref. 14); and thirdly, it increases the potential energy of the clay particles (Ref. 12). The second and third effects may be regarded as the short range forces, whilst the first effect is of a long range nature. Available data seems to indicate that the first and second effects control the soil behavior at low salt contents and the third effect controls the soil behavior at high salt contents.

Results obtained in the plasticity and compaction tests appear to indicate that, an increase in the salt content decreases the particle contacts and, interference between the particles. Compaction generally increases the interparticle contacts and interference (Ref. 13), and at the same time tends to improve the particle orientation. The latter effect is more pronounced than the former when the initial soil structure is in a dispersed condition (Ref. 1 and 12). An increase in particle contacts will depend upon the effective stresses in the soil prior to compaction. The lower the initial effective stresses in the soil, the higher will be the effect of the increase in particle contacts (Ref. 15). The above discussion attempts to point out that, at moisture contents below the optimum, the effect of compaction is more pronounced in increasing the particle contacts when the salt content is low, but the effect on particle orientation becomes more important when the salt content is high. At low salt contents, compaction induces an increase in both the particle contacts and the net interparticle attractive forces as the salt concentration increases. Thus, the stress at low strain increases as the salt concentration is increased. At a very high salt content, the high degree of particle orientation might offset the increase in the net attractive forces, which might consequently result in a reduction in the strength.

For molding moisture contents higher than the optimum, the effect of salt content on the optimum moisture content has to be considered. As discussed previously, an increase in salt content results in a decrease in the optimum moisture content. Thus, the effects of shear strains caused by compaction do not occur at the same moisture content. The higher the salt content in a compacted clay, the lower the water content at which the effects of shear strains will occur. Therefore, for consideration of the strengths of specimens compacted at the same water content, the effect of shear strains will be more pronounced in the soil containing a higher salt content. As pointed out by Seed & Chan (Ref. 12) and Mitchell (Ref. 7), the strength of a compacted clay at low strains is primarily dependent upon the particle contacts and, hence, the orientation of the particles, Therefore, the effect of the difference in the shear strains caused by the compaction process could offset the changes in the net attractive forces between the particles. As a result, a decrease in the strength is found as the salt content is increased.

(b) Effect of Salt Content on Peak Stress

As shown in Fig. 3, the trend of the effect of salt content on the peak compressive strength is similar to that of stress at low strain. At the peak, i.e. at failure, there are three components contributing to the shearing resistance of the soil; these are cohesion, dilatancy and friction (Ref. 16). The cohesion component has already been discussed in the previous section on stresses at low strains. It is now necessary to investigate the effect of salt content on the mobilization of strength resulting from dilatancy and friction. Since the unconfined compression test does not provide adequate information to separate the components of dilatancy and friction, only an indirect method can be used for their evaluation. This is based on the postulation that, if there is any effect of salt content on the mobilization of strength, the difference between the stresses

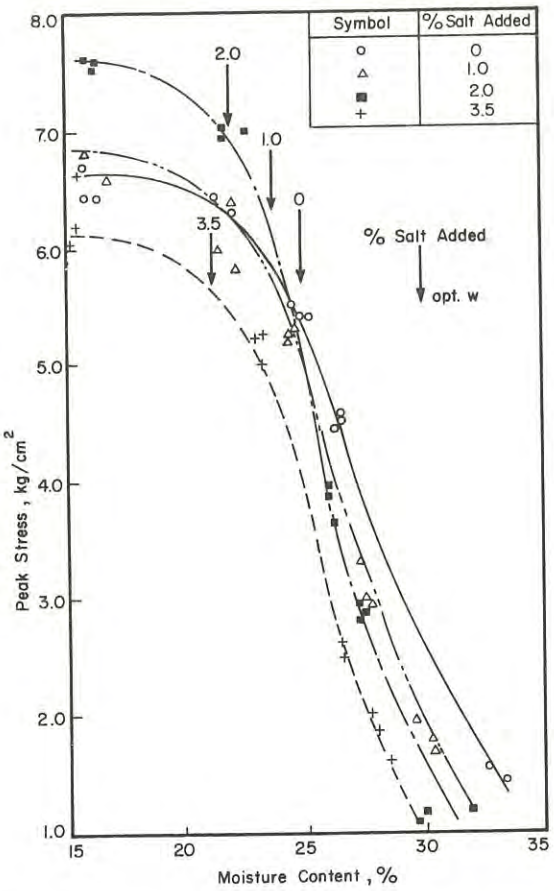

Fig. 3 - Relationship between Peak Stress and Molding Moisture Content.

at low and high strains for soils compacted at the same moisture content but with different salt contents should not be the same. Figure 4 shows the relationships between salt concentration and stresses at two particular strains, viz. 2 per cent and at failure, for soil specimens compacted at three moisture contents. The data indicate that the differences between the stresses at 2 per cent and failure strains are practically the same and are independent of salt concentration for soil compacted both above and below the optimum moisture content. There appears to be no significant effect of salt content on the mobilized peak strength resulting from the dilatancy and friction components. Therefore, it can be concluded that, for specimens compacted at the same moisture content, the change in the peak stress caused by a change in the salt content is primarily a result of a change in the cohesion component.

V. THIXOTROPIC CHARACTERISTICS

The significant effects of shear strains and long range interparticle forces on the thixotropic behavior of compacted clays have been studied by Mitchell (Ref. 17). The role of particle contacts and short range interparticles forces in influencing thixotropic behavior of compacted clays can be considered on the basis of the compaction characteristics and strength behavior of the soil under the influence of different salt concentrations. Previous studies have shown that thixotropic behavior is most pronounced when the soil is compacted on the wet side of optimum.

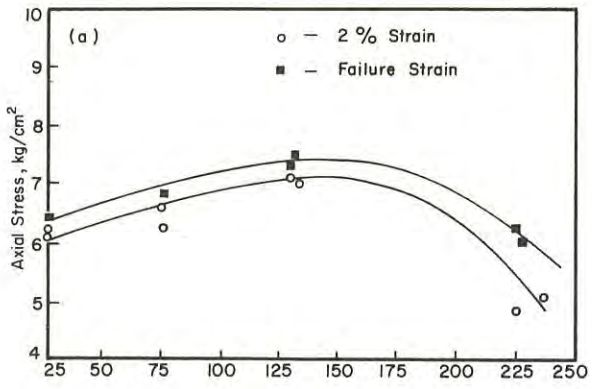

(a) Molding moisture content = 16 %

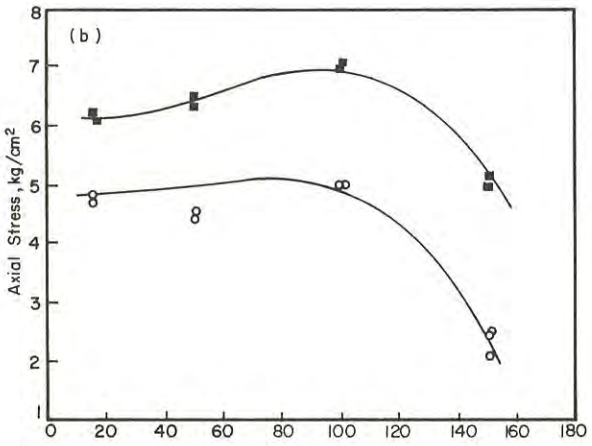

(b) Molding moisture content = 22 %

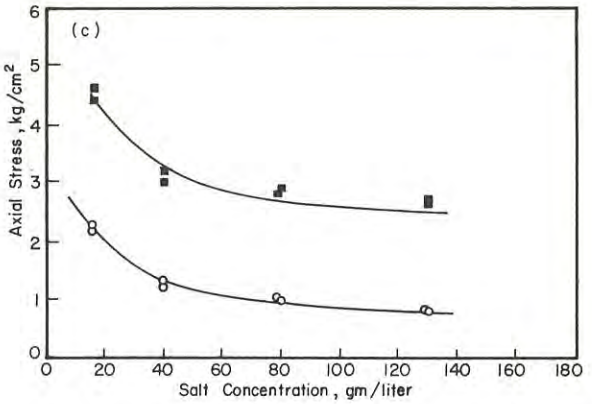

(c) Molding moisture content = 27 %

Fig. 4 - Effect of Salt Concentration on Stresses at Particular Strains.

In this investigation, two sets of specimens were prepared. In the first set, all the specimens were compacted at the same moisture content of 27.0 per cent (or 72.5 per cent volumetric water content); and the specimens in the second set were compacted at a moisture content of optimum plus 2 per cent.

The effect of thixotropic behavior on compacted clay can be measured in terms of the thixotropic strength increase at a particular strain; this is defined as:

$$\text{Thixotropic Strength Increase} = \frac{c_t - c_o}{c_o} \times 100 \text{ percent}$$

where c_o = strength at a certain strain tested immediately after compaction,

c_t = strength at the same strain tested after t days of curing.

(a) Effect of Salt Concentration on Thixotropic Strength Increase

Figures 5 and 6 present the relationships between salt concentration and thixotropic strength increase at two strains, for the two sets of tests. The strains selected for comparison are: (i) a low strain of 2 per cent which falls on the initial straight

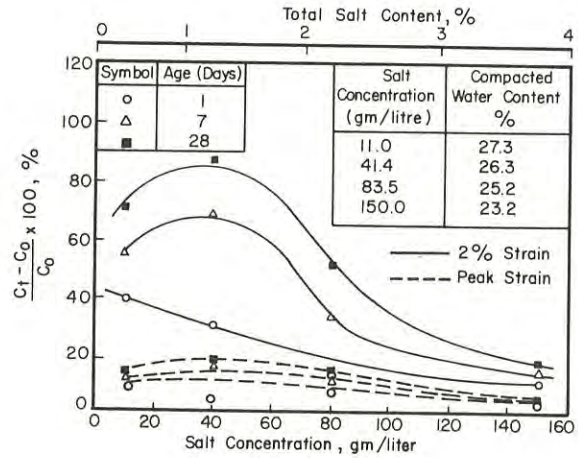

Fig. 5 - Effect of Salt Concentration on Thixotropic Strength Increase for Soil Compacted at Optimum Moisture Content Plus 2 Per Cent.

line portions of the stress-strain curves, and (ii) the strain at peak stress, which generally occurs between 8 to 10 per cent. The results clearly show that a pronounced effect of salt concentration occurs only at low strain. At the peak condition, the effect of salt concentration on the thixotropic characteristics is very small. The optimum salt concentration for a maximum thixotropic strength increase appears to be independent of curing time, with the exception of the case of the 1-day cured specimens compacted at optimum plus 2 per cent. The specimens compacted at the same moisture content exhibit higher thixotropic strength increases than those compacted at the optimum moisture content plus 2 per cent. The optimum salt concentration is also higher in the former case.

According to Mitchell (Ref. 17), the excess internal energy in a soil which is responsible for its thixotropic behavior is dependent upon the shear strains induced by compaction and the net interparticle forces (the long range interparticle forces). As discussed in the previous sections, the salt concentration influences the initial soil structure upon compaction. The magnitude of the shear strains induced in soils

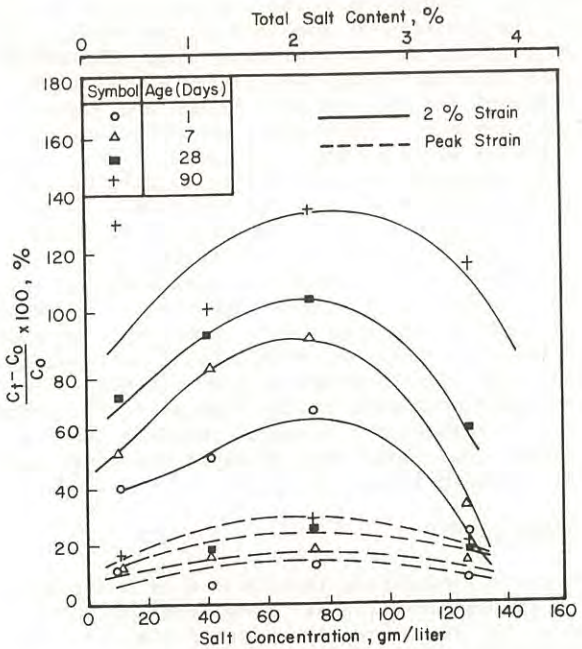

Fig. 6 - Effect of Salt Concentration on Thixotropic Strength Increase for Soil Compacted at 27 Per Cent Moisture Content.

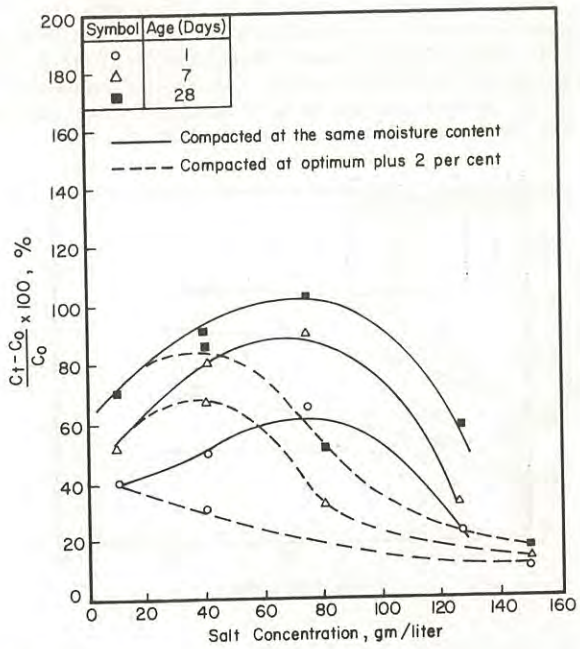

Fig. 7 - Effect of Difference in Shear Strains on Thixotropic Strength Increase.

compacted at the same position relative to the optimum moisture content (i.e. optimum plus 2 per cent) will be different. An increase in face-to-face type orientation due to an increase in salt concentration will decrease the shear strains induced by compaction. As a result, the amount of excess internal energy after compaction will decrease as the salt concentration increases. On the other hand, an increase in salt concentration will depress the double layer around the clay particles and will result in an increase in the net attractive forces between the particles and, hence, in an increase in the excess internal energy. The combination of these two opposite effects might result in an initial increase in the excess internal energy as the salt concentration increases. The net excess internal energy would then start to decrease after the maximum value is reached as the salt concentration is further increased. It was found in this study that the optimum salt concentration for a maximum per cent thixotropic strength increase for soils compacted at optimum plus 2 per cent was about 40 gm per liter (Fig. 5).

For specimens compacted at the same moisture content, i.e. 27 per cent, with different salt concentrations, the dry unit weights of the specimens were about the same. Under these conditions, the sources of excess internal energy will also be the same. However, specimens at different positions relative to the optimum moisture content will also sustain different shear strains due to compaction which will cause differences in the excess internal energy. It would, therefore, be reasonable to expect that the thixotropic strength increases, as well as the optimum salt concentration for thixotropy, would be higher for soils compacted at 27 per cent moisture content (way on the wet side for most of the mixtures) than those compacted at optimum plus 2 per cent. A replot of the data results in Fig. 7 compares the effect of salt concentration on the thixotropic strength increase at 2 per cent strain for the two sets of specimens. The difference between the two sets of results could be considered as the additional excess internal energy contributed by shear strains during compaction. The maximum effect of shear strains occur at a salt concentration of about 80 gm per liter, which is also the optimum salt concentration for the maximum thixotropic strength increase of soil compacted at 27 per cent moisture content. Thus, it could be further stated that the maximum thixotropic strength increase will always occur at the maximum excess internal energy.

(b) Effect of Salt Concentration on Rate of Thixotropic Strength Increase

According to Mitchell (Ref. 17), the rate of thixotropic strength increase is directly dependent upon the rate of dissipation of the excess internal energy. Therefore, it is related to the magnitude of the excess internal energy as well as to the mobility of the particles. The mobility of the particles is in turn dependent upon the mobility of the ions in the double layer and the number of interparticle contacts. The larger the number of particle contacts and the larger the interference between the ions in a soil-water mixture, the lower will be the rate of thixotropic strength increase.

In the early stages of curing, the movement of particles is probably more controlled by redistribution of ions in the double layers. In other words, the higher the salt concentration in the pore fluid, the less the particle movement that will occur. It is possible that the effect of ion concentration on mobility could offset the effect of excess internal energy at early stages of curing and, then, the latter takes over after longer curing time. In this investigation, for soils compacted at optimum moisture content plus

2 per cent, the rate of thixotropic strength increase decreased as the salt concentration increased during the early stage (1-day) and, then, the soil with the highest excess internal energy (at a salt concentration of 40 gm per liter) gained strength more rapidly than the other samples as shown in Fig. 8.

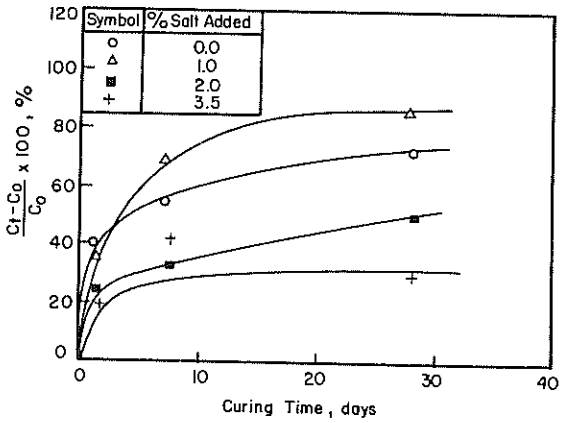

Fig. 8 - Thixotropic Strength Increase versus Curing Time for Soil Compacted at Optimum Moisture Content Plus 2 Per Cent.

For soils compacted at the same moisture content on the wet side, i.e. 27 per cent, the rate of thixotropic strength increase appeared to be directly dependent upon the amount of excess internal energy (Fig. 9). For this group of specimens, the excess internal

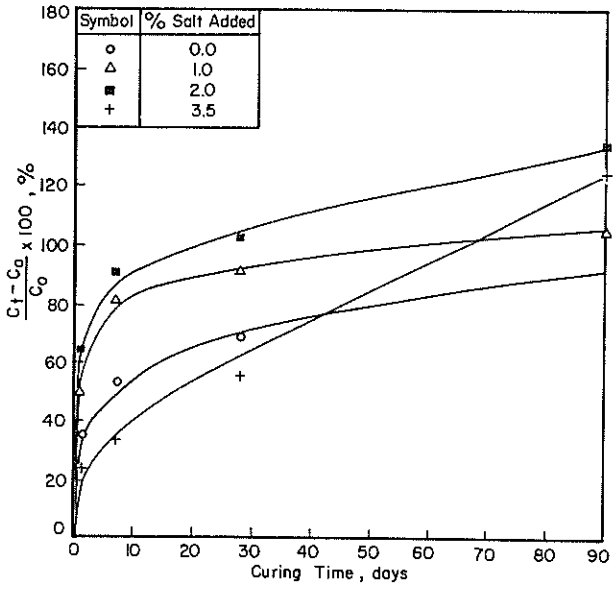

Fig. 9 - Thixotropic Strength Increase versus Curing Time for Soil Compacted at 27 Per Cent Moisture Content.

energy was higher than for the first group. It is likely that even during the early stage of curing, the effect of excess internal energy overshadowed the effect of ion concentrations on the ion mobility.

On the basis of the above data, it might be postulated that the main factors which control the rate of thixotropic strength increase are the excess internal energy, the mobility of the ions in the double layer and the rigidity of the soil structure. The effect of excess internal energy would then appear to be the most dominant and the rigidity of the soil structure the least dominant. The latter probably controls the soil behavior after a very long curing time. At that stage, the movement of soil particles will be relatively more pronounced, and the resistance to the movement will be due to the rigidity of the soil structure itself, which, in this investigation, appeared to decrease as the salt concentration increased. Thus, a soil with a higher salt concentration will offer less resistance to particle movement in the long term than one with a lower salt concentration. The results shown in Fig. 9 indicate that, for specimens compacted at the same moisture content, the rate of thixotropic strength increase after a long curing time (more than 28 days) increases with the salt concentration.

VI. CONCLUSIONS

The need for considering the effects of externally applied stress and the short range interparticle forces on the structure of compacted clay has been illustrated by experimental evidence.

The mechanism of the thixotropic characteristics of the clay studied in general follows the hypothesis proposed by Mitchell (Ref. 17). This hypothesis has been extended to postulate that the maximum thixotropic strength increase occurs at the maximum excess internal energy and that the rate of thixotropic strength increase is dependent upon the magnitude of the excess internal energy as well as the mobility of the soil particles. As far as the mobility of particles is concerned, the role of the short range interparticle forces seems to be of minor significance. On the other hand, the magnitude of the excess internal energy is primarily dependent upon the applied external stresses and upon the particle contacts, for which the short range interparticle forces are of great importance. However, the effects of the long and short range interparticle forces on the magnitude of the excess internal energy cannot be separated from each other at this time. This research should stimulate further studies on the importance of the effects of short range forces.

VII. REFERENCES

1. LAMBE, T.W. - The Structure of Compacted Clay. J. Soil Mech. Foundation Div. Am. So. Civ. Eng., Vol. 84, No. SM2, May 1958, pp. 1654/1-34.

2. WARKENTIN, B.P. - Measurement of Shear Strength, Plasticity, and Water Retention of Clay Related to Interparticle Forces. Proc. 16th Canadian Soil Mechanics Conf., 1962, pp. 43-58.

3. SEED, H.B., WOODWARD, R.J. and LUNDGREN, R. - Fundamental Aspects of the Atterberg Limits, J. Soil Mech. Foundation Div., Am. Soc. Civ. Eng., Vol. 90, No. SM6, 1964, pp. 75-105.

4. AZIZ, M.H. - The Influence of Exchangable Ions and Their Concentrations in the Pore Fluid on Plastic and Strength Properties of Cohesive Soil, Thesis (Ph.D.), Utah University, 1965.

5. OLSON, R.E. and MITRONOVAS, F. - Shear Strength and Consolidation Characteristics of Calcium and Magnesium Illite. Proc. 9th Nat. Conf. Clay and Clay Minerals, Pergeman Press, New York, 1962, pp. 185-209.

6. MITCHELL, J.K. - The Application of Colloidal Theory to the Compressibility of Clays. Proc. Seminar in Interparticle Forces in Clay-Water-Electrolyte System, C.S.I.R.O., 1960, pp. 2.92-2.97.

7. MITCHELL, J.K. - Shear Resistance of Soil as a Rate Process. J. Soil Mech. Foundation Div., Am. So. Civ. Eng., Vol. 90, No. SM1, 1964, pp. 29-63.

8. COX, J.B. - A Review of the Engineering Characteristics of Recent Marine Clays in South East Asia. Research Report No. 6, Asian Inst. of Tech., 1968, pp. 65-67.

9. THIRAWAT, S. - Thixotropic Characteristics of Compacted Bangkok Clay. Thesis (M. Eng.), Asian Inst. of Tech., Bangkok, 1968.

10. WARKENTIN, B.D. and YOUNG, R.N. - Introduction to Soil Behavior. Macmillan Company, New York, 1966,

11. VAN OLPHEN, H. - An Introduction to Clay Colloid Chemistry. Interscience Publishers, John Wiley & Sons, New York, 1963.

12. SEED, H.B. and CHAN, C.K. - Structure and Strength Characteristics of Compacted Clay. Trans, Am. So. Civ. Eng., Vol. 126, 1961, pp. 1344-1385.

13. MITCHELL, J.K., SINGH, A. and CAMPANELLA, R.G. - Bonding, Effective Stresses and Strength of Soils. J. Soil Mech. Foundation, Div., Am. So. Civ. Eng., Vol. 95, No. SM5, 1969, pp. 1219-1246.

14. MITCHELL, J.K. - Components of Pore Water Pressure and Their Engineering Significance. Proc. 9th Nat. Conf. on Clays and Clay Minerals, Pergeman Press, New York, 1962, pp. 162-184.

15. OLSON, R.E. - Effective Stress Theory of Soil Compaction. J. Soil Mech. Foundation Div., Am. So. Civ. Eng., Vol. 89, No. SM2, 1963, pp. 27-45.

16. LAMBE, T.W. - A Mechanistic Picture of the Shear Strength in Clays. Proc. Conf. on Shear Strength of Cohesive Soils, Am. So. Civ. Eng., Boulder, 1970, pp. 555-580.

17. MITCHELL, J.K. - Fundamental Aspect of Thixotropy in Soils, J. Soil Mech. Foundation Div., Am. So. Civ. Eng., Vol. 86, No. SM3, 1960, pp. 19-52.

The Deformation and Yield of Clays in Direct Simple Shear

By
L. K. Walker, Ph.D. (Cantab.), M.Eng.Sc., M.I.E.Aust.
(Senior Soils Engineer, Maunsell and Partners Pty. Ltd., Melbourne)

SUMMARY. - Simple shear tests on saturated kaolin have confirmed the existence of a unique state boundary surface enclosing all possible states of the clay. Stress paths lying on this surface result in volumetric yielding, while paths beneath the surface produce an elastic volumetric response. Angular strains associated with volumetric yielding are small in magnitude, with total angular strains being adequately represented by a strain contour pattern which is independent of stress path.

I. - INTRODUCTION

Over the past 15 years, an idealised model for clay (here-after referred to as Cam-Clay) has been developed at Cambridge and refined in the light of available experimental data. Cam-Clay is assumed to behave mechanically as an elasto-plastic, isotropic, non-viscous continuous medium, and has been analysed mathematically by Roscoe and Schofield (1963) and Roscoe, Schofield and Thurairajah (1963) for the case of triaxial compression tests. The parameters used in these analyses are simple derivatives of the stress and strain invariants applied to the case of the triaxial test, and are defined in detail in the above papers. In the following discussion, general reference is made to the volumetric strain v (directly related to void ratio e), shear strain ε, mean effective pressure p, and deviator stress q.

The Cam-Clay theory aims to predict the small strain increments caused in a soil element by the application of a probing stress increment. Plastic yielding of the material is assumed to satisfy the stability criterion of Drucker (1959), which is applied mathematically to an energy equation relating input energy to stored (elastic) and dissipated (plastic) energy. Central to the development of the theory is the assumption of a unique relationship between void ratio (e) and effective stresses (q, p) which defines a succession of "critical states" of the clay. It is postulated that all clay samples, regardless of stress history, will reach a point on this critical state line when deformed under continually increasing shear stresses.

A full development of the theory is presented by Schofield and Wroth (1968), and leads to the mathematical definition of a surface in e, p, q space which encloses all possible states of Cam-Clay, and which is referred to as the state boundary surface.

The primary purpose of this Paper is to investigate experimentally the nature of the state boundary surface under plane strain test conditions in the simple shear apparatus. After first describing the experimental procedure, the Paper discusses the significance of the state boundary surface as is understood in the development of the Cam-Clay theory. The region enclosed by this surface is then investigated using tests with a number of stress paths. The experimental data are presented in two sections, the first dealing with volumetric strains as a function of applied stresses (section IV), and the second analysing the observed angular strains (section V). Conclusions derived from both sections are then summarised.

II. - EXPERIMENTAL PROCEDURE

The experimental programme consisted of incremental stress-controlled shear tests on saturated kaolin. Samples were preconsolidated from a slurry which was initially mixed under vacuum at a moisture content of 160%, about twice the liquid limit. The shear tests were performed in a model of the simple shear apparatus (S. S. A) whose basic design and mode of operation has been described by Roscoe (1953). The apparatus was designed to test 6 cm x 6 cm x 2 cm samples of clay under conditions of plane strain, while ensuring that a uniform distribution of stress and strain through-out the sample is maintained. All tests were performed in a constant temperature room at 25°C ($\pm \frac{1}{2}$°C).

The vertical stress (σ_{yy}) was applied through the S.S.A. piston by means of a hanger and dead weights. The horizontal shear stress (τ_{xy}) was applied by means of a dead loading system of tanks, being transmitted to the top of the sample through the base of the piston. The shear stress was varied by pumping water from one tank to the other. This method of shear stress application minimizes

inertial loading effects which can occur with the sudden dead-loading of hangers.

Preliminary tests in the S. S. A. established the errors caused by friction in the shearing mechanism, and by vertical yield of the apparatus under load. Corrections were applied to the experimental data to account for these factors. The effect of side friction on the samples was considerably reduced by the presence of rubber (lubricated with silicone grease) between the sample and the enclosing walls of the apparatus. Volume change measurements were derived both from burette readings and from vertical dial gauge readings, thus minimising errors caused by water leakage through the membrane enclosing the sample. The angular strain during shear was determined from the ratio of horizontal displacement to sample height.

The stress and strain parameters used in the analysis of results are thus volumetric strain v (or void ratio e), angular strain γ_{xy}, effective vertical stress σ'_{yy} and shear stress τ_{xy}.

III. - THE STATE BOUNDARY SURFACE

(a) General

The experimental data will be discussed in the following section with reference to current concepts of the Cam-Clay model. As considerable use will be made of the properties of the state boundary surface, this surface will now be discussed in greater detail with reference to shear tests performed in the S. S. A.

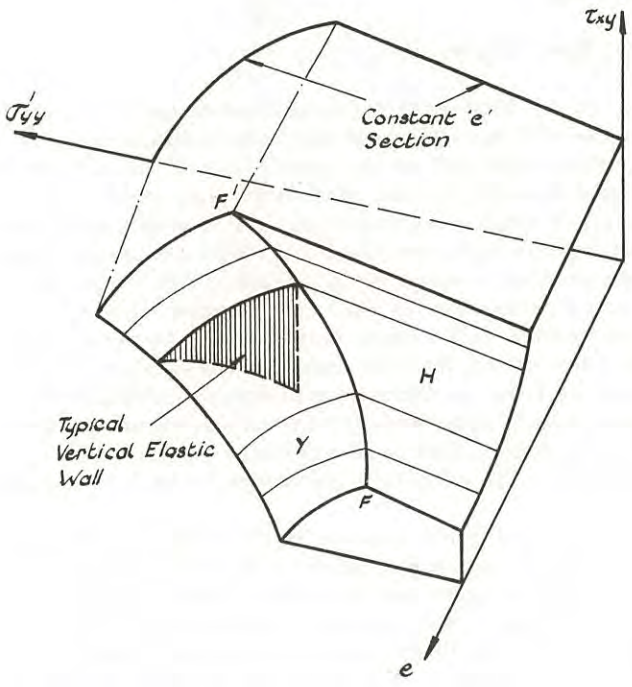

Fig. 1. The State Boundary Surface

The state boundary surface (shown diagrammatically in Figure 1) encloses all possible states of specimens tested in the simple shear apparatus, and is made up of two portions - the volumetric yield surface Y and the Hvorslev surface H (Roscoe et al 1958). The volumetric yield surface is bounded by the virgin consolidation line in the plane ($\tau_{xy} = 0$), and by the 'critical state' line FF', which represents the limiting equilibrium states attainable by normally consolidated specimens. The Hvorslev surface contains all possible states of failure (represented by peak shear stress ($\tau_{xy})_f$), and includes the 'critical state' line as one of its edges. In fact the critical state condition is not achieved in plane strain tests, due to the intervention of a Mohr-Coulomb rupture criterion (Henkel and Wade 1966). For this reason, the term 'n. c. rupture' line will be used in the remainder of this Paper to denote the failure state of all normally consolidated (n. c.) samples. Results to be presented confirm the assumption that a planar Hvorslev surface (including the n. c. rupture line) results from S. S. A. tests using a variety of stress paths.

The full state boundary surface can conveniently be represented by a two-dimensional plot (Burland 1965) involving the parameters τ_{xy}/σ_e and σ'_{yy}/σ_e, σ_e being the equivalent consolidation pressure defined by Hvorslev (1960). Such a plot is illustrated in Figure 2, the volumetric yield surface being represented by the portion AX, the Hvorslev surface by BX with the n. c. rupture line represented by the point X. The region beneath the surface can be divided into two sub-regions (termed "wet" and "dry") by the line XX' in Figure 2. Samples on the wet side of XX' ultimately fail on the n. c. rupture line at X, and if drained show a volume decrease under increasing shear stress. Samples on the dry side of XX' fail on attaining some point on the Hvorslev surface and increase in volume as the point X is approached.

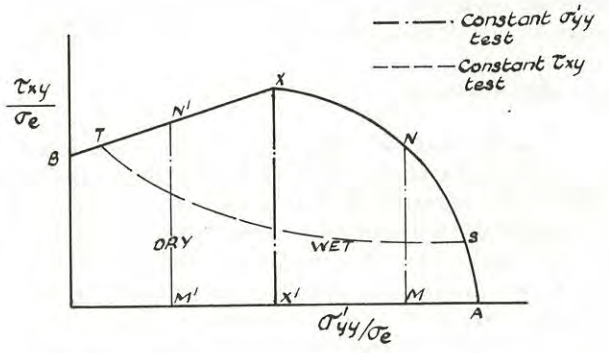

Fig. 2. Two-Dimensional Representation of the State Boundary Surface

(b) Volumetric Strains

The majority of S. S. A. tests performed by the author were drained tests, and therefore some consideration should be given to the general pattern of volumetric strains predicted by the Cam-Clay model. Irrecoverable (plastic) volumetric strains occur only when the sample state moves across the volumetric yield surface due to a change in the applied stresses. The magnitude of such strains is related directly to the magnitude and direction in stress space of the applied stress increment.

If an applied stress increment is such that the sample state lies always beneath the state boundary surface, then only recoverable (elastic) volumetric strains occur. In such a case, the strains are confined to a vertical elastic wall whose projection on the e - log p plane is parallel to an elastic swelling line. A typical elastic wall has been represented in Figure 1. Each of the many possible elastic walls is defined by the combination of σ'_{yy} and τ_{xy} at which yielding last occurred. During elastic deformation, the void ratio is thus solely a function of the mean effective pressure, and is independent of possible variations in the applied shear stress.

Specific illustrations of the above are provided by two types of test used in the experimental programme. The first is a "constant σ'_{yy} " test, i. e. a drained shear test during which the vertical applied load is held constant. Such tests can be performed with various initial over-consolidation ratios as represented on Figure 2 by idealised paths such as MN and M'N'. The second test, a "constant τ_{xy} " test involves three stages. Consolidation to a value of σ'_{yy} is carried out, followed by an increase of τ_{xy} from zero up to the selected value. Failure is then induced by a successive step-wise reduction in σ'_{yy} , with drained conditions at all stages. An idealised stress path for this type of test is given by AST in Figure 2.

A variety of tests can be selected using either constant σ'_{yy} or constant τ_{xy} stress paths and these provide evidence against which the basic assumptions of the Cam-Clay model can be assessed.

(c) Shear Strains

The theoretical Cam-Clay model presented thus far associates shear strains only with irrecoverable volumetric strains; this is a logical extension of the application of Drucker's stability criterion. All shear strains (angular strains in the S. S. A. test) therefore occur as a result of movement of the sample state across the volumetric yield surface. Thus a stress increment which involves sample states lying wholly beneath the state boundary surface should cause no shear strains.

This idealised specification of shear strains in the Cam-Clay model is incomplete as (for example) it has been established that significant shear strains occur during triaxial tests on overconsolidated samples (Bishop and Henkel 1962). Attempts have been made recently (Wroth and Loudon 1967, Roscoe and Burland 1968) to include into the framework of the Cam-Clay theory additional shear strains which overcome the obvious objections to the simplified model. This has been done essentially by considering shear strains as being of two types - the first being a function of plastic volumetric strains as discussed above and a second involving shear strains which are independent of yielding on the state boundary surface.

The second category of shear strain is the subject of current interpretation. On a two-dimensional representation of the state - boundary surface, Wroth and Loudon (1967) presented contours of equal shear strain for standard undrained triaxial compression tests on overconsolidated clay speciments, including one normally consolidated sample. They showed that the use of these contours enable an accurate prediction to be made of the total shear strains occurring in a drained overconsolidated test.

The author has used this strain contour concept to present results from a number of tests involving different stress paths. While this approach is empirical in its nature, some more fundamental basis for its use is contained in the work by Roscoe and Burland (1968). For the present, the empirical approach does enable a significant assessment to be made of one area in which the overall theory is deficient.

(d) Time Effects

Time-dependent deformations of the idealised clay model have thus far not been considered. It has been assumed in the past (Roscoe, Schofield and Thurairajah 1963) that such deformations are the result of a diffusion process, and that the effective soil structure is non-viscous. This assumption has been studied in some detail (Walker 1969), as the viscous properties of real clays prove to be of significance under some conditions. In essence it has been shown that the mean stress-strain curve obtained from an incremental stress-controlled shear test is independent of the increment duration time, provided that pore pressure equalization throughout the sample is achieved in each increment.

The stress increments in the author's drained S. S. A. tests were permitted to act for the 100% consolidation time defined during preliminary consolidation of the sample. This time varied between 20 and 90 minutes for different samples. For the few undrained tests reported herein, an increment time of 10 minutes was generally used.

In this way, pore pressure equalization was achieved during all increments, and secondary deformations were kept to a minimum. Only the 'equilibrium' data at the end of each increment are presented below.

IV. - EXPERIMENTAL DATA - VOLUMETRIC STRAINS

In this section, the experimental data obtained from various S. S. A. tests will be presented with the intention of studying the volumetric yielding of one particular clay, and its relation to the idealized behaviour discussed in the preceding section. Presentation of the angular strain data from some of these tests will be made in the following section.

(a) Compression Curve

The compression curve from a typical one-dimensional consolidation test performed in the S. S. A. is shown in Figure 3. The particular sample for this test was consolidated in increments to 5.5kg/cm^2, unloaded to a vertical stress of 0.3kg/cm^2, and reconsolidated to 5.5 kg/cm^2. The virgin compression curve is linear on the log. pressure plot, while the unloading curve is markedly non-linear at low stresses. The swell-back and reconsolidation curves together define a significant hysteresis loop. The assumptions of the Cam-Clay theory are thus approximations when large cyclic stress changes are involved. The important assumption of a straight virgin consolidation line is, however, justified by the data.

(b) Normally Consolidated Shear Tests

A series of standard drained and undrained S. S. A. tests on normally consolidated samples was carried out to establish the shape of the volumetric yield surface. Samples were consolidated to various vertical pressures (σ'_{yy}) and tested by increasing the horizontal shear stress (τ_{xy}) in steps until failure occurred.

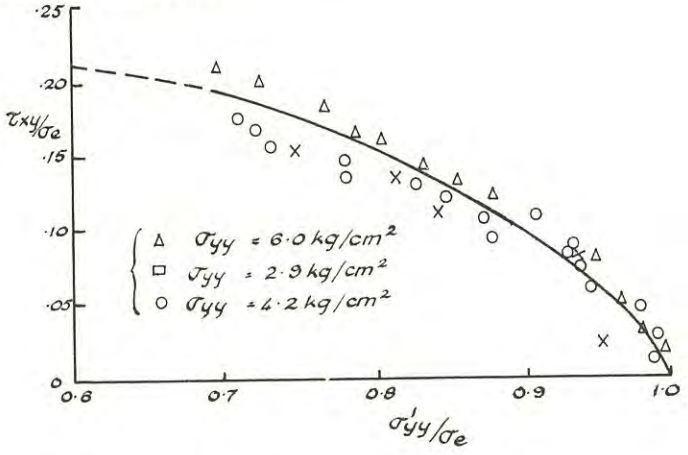

Fig. 4. Drained Volumetric Yield Surface

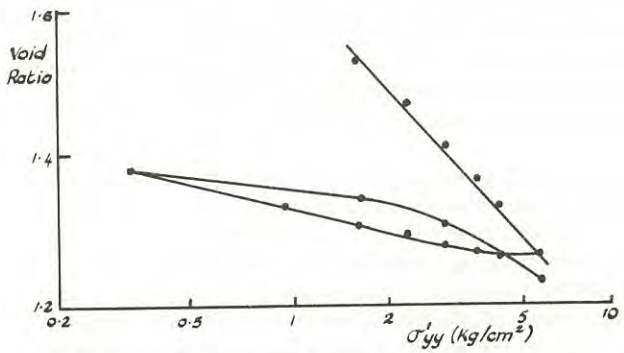

Fig. 3. Compression Curve ($\tau_{xy} = 0$)

Two-dimensional plots of the yield surface are shown both for drained tests (Figure 4) and for undrained tests (Figure 5). The mean line from the drained tests has been transferred onto the undrained test results as a broken line. Taken together the Figures show that the volumetric yield surface is reasonably independent both of consolidation pressure and type of test. Normally consolidated drained and undrained tests in the S. S. A. thus define a unique yield surface, a conclusion which was reported by Roscoe and Thurairajah (1966) for strain-controlled tests in the S. S. A.

Failure states in stress-controlled shear tests are difficult to define precisely; the failure stress ratio obtained from Figures 4 and 5 is approximately

$$\tau_{xy} / \sigma'_{yy} = 0.38 \ (\pm 0.02)$$

Now in their application of the Mohr-Coulomb rupture criterion to plane strain tests, Roscoe and Burland (1968) predicted that, for S. S. A. tests on normally consolidated speciments, the failure stress ratio is given by

$$\tau_{xy} / \sigma'_{yy} = \frac{\sqrt{4\eta_r^2 - \left(\frac{M^2}{3} - \eta_r^2\right)^2}}{2 + M^2/3 - \eta_r^2}$$

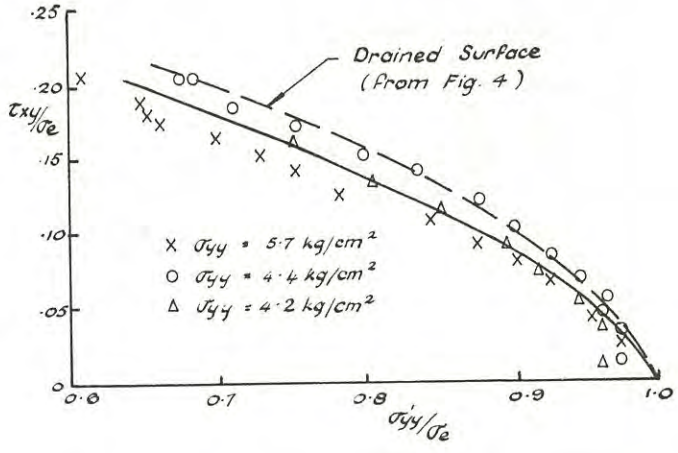

Fig. 5. Undrained Volumetric Yield Surface

where $\eta_r = \frac{3M}{6+M}$, and M is the critical state strength defined by triaxial compression tests. Using Roscoe and Burland's value of M = 0.9 for remoulded kaolin gives a predicted S.S.A. stress ratio at failure of 0.37 i.e. in good agreement with observation, thus confirming the validity of the Mohr-Coulomb rupture criterion.

The end points of each of the tests shown in Figures 4 and 5 have been plotted in an e vs log σ'_{yy} diagram in Figure 6. The results from two long-term (one day increment) undrained tests have been added to broaden the spread of the data. The initial points of all samples have been corrected in void ratio to lie on the virgin consolidation line of Figure 3, and the final void ratios corrected by a similar amount. A line can be drawn bounding the points in Figure 6, being approximately parallel to the normal consolidation line. This n.c. rupture line, which plots as a point on the state boundary surface (X in Figure 2) defines the states at which normally consolidated samples reach a peak shear stress.

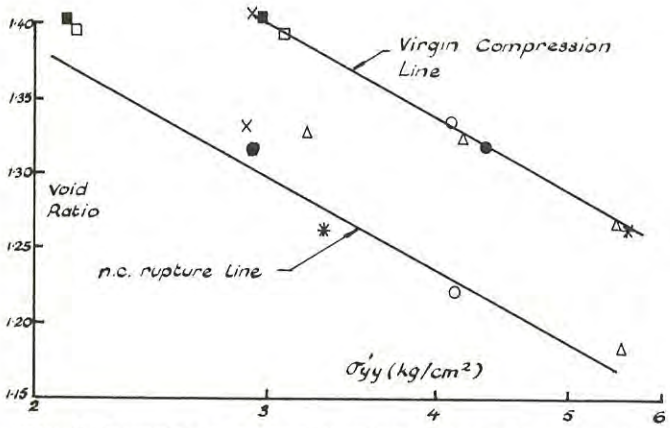

Fig. 6 Compression and Rupture Lines for n.c. tests

(c) Constant σ'_{yy} Tests

A series of drained S.S.A. tests on over-consolidated samples was carried out as a first step in the investigation of the region beneath the state boundary surface. Over-consolidation ratios of 1.3, 1.9, 3.5, 8.3 and 19.2 were used with a constant preconsolidation pressure of 5.96 kg/cm^2. Volumetric strains occurring in these tests have been interpreted in terms of a two-dimensional plot of the state boundary surface.

The experimental data are presented in Figure 7, the volumetric yield surface (AX) in this figure being the mean curve of the drained tests plotted in Figure 4. Beneath the state boundary surface, all over-consolidated state paths are closely vertical, thus confirming the idealised behaviour shown in Figure 2. The lightly overconsolidated specimen (test No. 6.6) undergoes significant volumetric strains once the yield surface is reached, and shows a state path close to the idealised path MNX shown in Figure 2; the yield surface is reached by a gradual curve rather than at the ideal discontinuity N. All initially dry samples undergo very little volume change before failing (cf. M'N' in Figure 2). Despite the difficulty of determining failure stresses accurately in the S.S.A. tests, a reasonable straight line (BX) can be drawn through all failure points. This line defines the Hvorslev surface, and completes the experimental definition of the state boundary surface AXB.

(d) Constant τ_{xy} Shear Tests

A series of drained constant τ_{xy} tests was carried out on normally consolidated samples. Four of the tests (Nos. 5.3-5.6) were initially consolidated under the same vertical stress (4.1 kg/cm^2) but with values of τ_{xy} varying from 0.11 kg/cm^2 to 0.69 kg/cm^2. Experimental data from the tests are presented in two figures. The state paths are plotted on the state boundary surface representation in Figure 8, and on the e vs log σ'_{yy} diagram in Figure 9.

The state boundary surface drawn in Figure 8 has been taken from Figure 7. For each test represented in Figure 8, the first point (labelled by

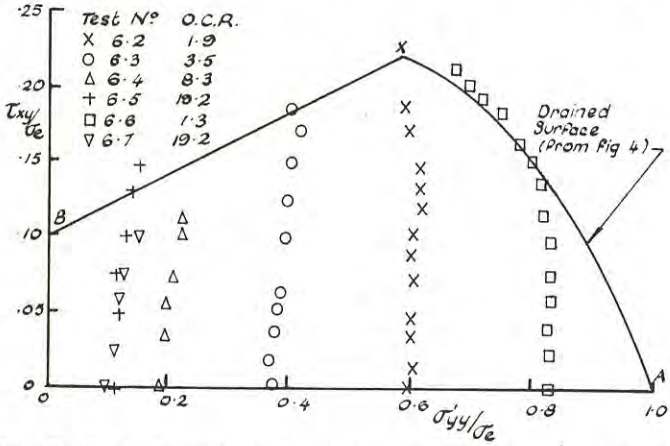

Fig.7. State Boundary Surface - Constant σ'_{yy} Tests

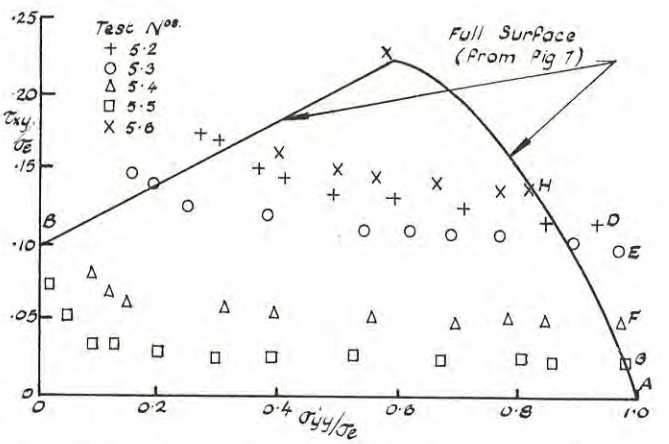

Fig. 8. State Boundary Surface - Constant τ_{xy} Tests

letters D to H) represents the equilibrium state under the constant value of τ_{xy} . The final point represents the final equilibrium state before failure occurred. To a fair approximation, the same line BX governs the failure conditions for both constant σ'_{yy} and constant τ_{xy} tests. In addition state paths follow the general shape given by the idealised curve ST in Figure 2.

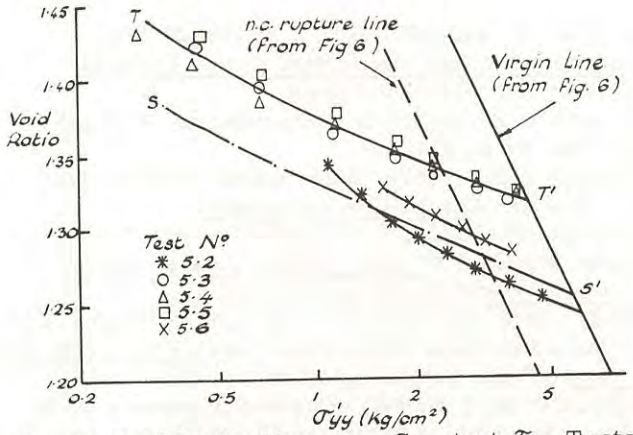

Fig. 9 Void Ratio Changes - Constant τ_{xy} Tests

The changes in void ratio accompanying the reduction of vertical stress in the constant τ_{xy} tests are shown in detail in Figure 9. The broken line (SS') in this Figure is the rebound line taken from Figure 3. The line TT' has been drawn parallel to SS' and closely represents the average of tests No. 5. 3, 5. 4 and 5. 5 which commence at approximately the same point on the volumetric yield surface. The results indicate that the state paths for the three tests have almost the same projection on the e log σ'_{yy} plot despite the significant differences in τ_{xy} values, i.e. the three state paths lie approximately in the same vertical elastic wall, whose projection is parallel to that established for the consolidation test. This behaviour is in accord with the theoretical model.

Data from the remaining tests (5. 2 and 5. 6) produce lines which deviate in slope from SS' as σ'_{yy} approaches its failure value. These two tests were performed with higher values of τ_{xy} , and it might therefore be concluded that, as failure on the Hvorslev surface is approached, volumetric strains exceed those to be expected from elastic behaviour, i.e. small plastic volumetric strains occur as the state boundary surface is approached.

V. - EXPERIMENTAL DATA - ANGULAR STRAINS

Angular strain data have been interpreted using the strain contour concept introduced by Wroth and Loudon (1967). Their geometric contour pattern consists of a set of radial lines on the dry side of XX' (Figure 2) connecting to a set of horizontal lines for wet clays. It can be shown (Walker 1967) that the full contour pattern for both normally and over-consolidated samples can be usefully represented by

$$(\tau_{xy}/\sigma_e)/(\tau_{xy}/\sigma_e)_f = F(\gamma_{xy})$$

For a point represented by co-ordinates τ_{xy}/σ_e , σ'_{yy}/σ_e the value of $(\tau_{xy}/\sigma_e)_f$ is obtained by projecting the value of σ'_{yy}/σ_e onto the Hvorslev surface.

Data from drained over-consolidated tests are presented in Figure 10. This figure shows a plot of $(\tau_{xy}/\sigma_e)/(\tau_{xy}/\sigma_e)_f$ against angular strain, with overconsolidation ratios varying from 1 to 19. Of the six tests shown, only two provide stress paths which reach the volumetric yield surface before failure is achieved. Test No. 6. 1 is a normally consolidated test, while Test No. 6. 6, by reference to Figure 7, undergoes a limited amount of volumetric yielding before failure.

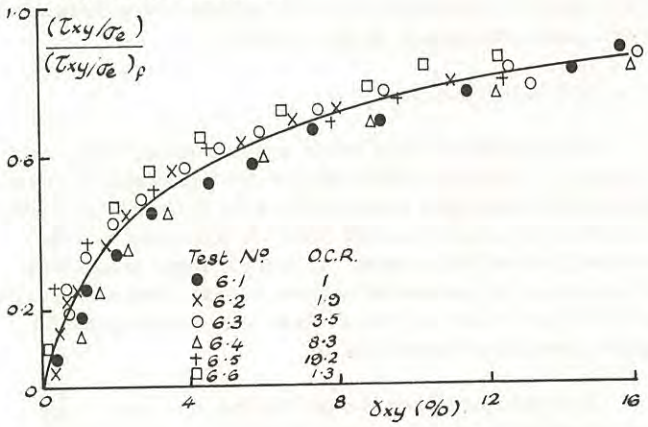

Fig. 10 Angular Strains - Constant σ'_{yy} Tests.

Within experimental scatter, the six tests define a curve which supports a unique pattern of strain contours independent of overconsolidation ratio. In general, the lightly overconsolidated test results lie above the mean line, while the heavily overconsolidated tests give points below the mean line. The exception to this pattern is the normally consolidated test result which lies below the mean curve. This variation is, however, of secondary significance despite the fact that volumetric yielding occurs throughout the n. c. test. It must therefore be concluded that angular strains in all constant σ'_{yy} tests in the S. S. A. are predominantly of the second type discussed in section 111 above, i. e. strains not associated with volumetric yielding.

An analysis of angular strain data from undrained and constant τ_{xy} tests has also been made, using a similar approach to that outlined above. These additional results are closely represented by the mean curve of Figure 10 and thus confirm that a unique strain contour pattern exists for S. S. A. tests regardless of the stress path adopted. In no S. S. A. test have angular strains associated with volumetric yielding been shown to be a significant proportion of the total.

This latter conclusion is in marked contrast to the deformation characteristics of the same clay in the triaxial compression test. Published data show conclusively that shear strains in drained triaxial shear tests on normally consolidated clays are largely associated with volumetric yielding of the clay. As a consequence, shear strain prediction using the Cam-Clay theory is quite accurate (Burland 1965). Roscoe and Burland (1968) have discussed the stress probes possible in plane strain shear tests, and the S.S.A. test in particular, and have justified the small shear strains observed in such tests.

It is apparent from the test results presented above that the mathematical Cam-Clay theory as presently constituted is deficient to the extent that shear strains which are not associated with volumetric yielding can dominate under certain stress conditions. Such strains cannot as yet be quantitatively assessed within the framework of the theory.

VI. - CONCLUSIONS

Experimental data from simple shear tests with a variety of stress paths have been analysed in terms of current concepts associated with Cam-Clay model. The stress paths involved both an increase and decrease in vertical stress, although at no stage was a reduction in horizontal shear stress applied, hence conclusions must be restricted only to those paths which have been investigated.

The data confirm the existence in τ_{xy} , σ'_{yy} , e space of a unique state boundary surface which, together with the co-ordinate axes, enclose all possible states of the clay studied. The surface is composed of two parts - the volumetric yield surface and the Hvorslev surface - which are joined by a line which contains all possible failure states of normally consolidated samples. The yield surface defines the surface on which irrecoverable volumetric strains may occur, while the Hvorslev surface contains all possible failure states of the clay. Within the limitations of the experimental programme, the state boundary surface as a whole was found to be independent of the stress path chosen.

Void ratio changes beneath the surface are essentially recoverable and are confined to a series of vertical elastic walls, whose projections on the e vs. $\log \sigma'_{yy}$ plane are parallel to the swelling curve obtained from one dimensional consolidation tests. Angular strains associated with stress paths beneath the state boundary surface define a family of strain contours which appear to be independent of the chosen stress path. The test data indicate that angular strains associated with volumetric yielding are relatively small, and consequently the determination of a strain contour pattern is of considerable importance in the interpretation of plane strain test results.

VII. - ACKNOWLEDGEMENTS

The experimental work reported above was performed in the Engineering Laboratories at Cambridge University under the direction of the late Prof. K.H. Roscoe.

REFERENCES

BISHOP, A.W. and HENKEL, D.J. (1962) "The Measurement of Soil Properties in the Triaxial Test". 2nd. ed. Edward Arnold.

BURLAND. J.B. (1965) Correspondence. Geotechnique Vol. 15 pp 211-214.

BURLAND, J.B. (1967) "Deformation of Soft Clay" Ph.D. Thesis, Cambridge University.

DRUCKER, D.C. (1959) "A Definition of a Stable Inelastic Material" J.App. Mech, Trans. Amer. Soc. Mech. Eng. Vol. 26 pp 101-106.

HENKEL, D.J. and WADE, N.H. (1966) "Plane Strain Tests on a Saturated Remoulded Clay" Proc. Am. Soc. Civ. Eng., Vol. 92 SM6 pp 67-80

HVORSLEV, M.J. (1960) "Physical Components of the Shear Strength of Saturated Clays" Proc. Am. Soc. Civ. Eng., Res. Conf. at Boulder, Colorado pp169-273

ROSCOE, K.H. (1953) "An Apparatus for the Application of Simple Shear to Soil Samples" Proc. 3rd Int. Conf. S.M. and F.E. Vol. 1 pp 186-191

ROSCOE, K.H. and BURLAND, J.B. (1968)"The Generalized Stress-Strain Behaviour of Wet Clay" Symp. on Eng. Plasticity, Cambridge University.

ROSCOE, K.H. and SCHOFIELD, A.N. (1963) "Mechanical Behaviour of an Idealized Wet Clay" Proc. Europ. Conf. Soil Mech. Wiesbaden Vol. 1pp47-54.

ROSCOE, K.H. SCHOFIELD, A.N. and THURAIRAJAH, A(1963) "Yielding of Clays in States Wetter than Critical" Geotechnique Vol. 13 pp 211-240.

ROSCOE, K.H., SCHOFIELD, A.N. and WROTH, C.P. (1958)-"On the Yielding of Soils". Geotechnique Vol. 9 pp 72-83.

ROSCOE, K.H. and THURAIRAJAH, A. (1966)"On the Uniqueness of Yield Surfaces for Wet Clays" IUTAM Symp. on Rheology and Soil Mech. Grenoble Springer-Verlag, Berlin pp 364-384

SCHOFIELD, A.N. and WROTH, C.P. (1968) "Critical State Soil Mechanics" McGraw-Hill

WALKER, L.K. (1967) "The Deformation of Clay as a Time-Dependent Process." Ph.D. Thesis, Cambridge University.

WALKER L.K. (1969) "Secondary Compression in the Shear of Clays" Proc. Am. Soc. Civ. Eng. Vol. 95 SM1 pp 167-188

WROTH, C.P. and LOUDON, P.A. (1967)"The Correlation of Strains within a Family of Triaxial Tests on Over-consolidated Samples of Kaolin". Proc. of Conf. on Shear Strength Properties of Natural Soils and Rocks, Oslo Vol. 1 pp 159-163.

Brittle Fracture of Rock at Low Confining Pressures

By
E. T. Brown, B.E., M.Eng.Sc., Ph.D., M.I.E.Aust., A.M.Aus.I.M.M.
(Senior Lecturer in Engineering, James Cook University of North Queensland)

SUMMARY.- Recent investigations into the controlled compressive fracture of rock are summarized and four types of fracture and stress-strain behaviour identified. No failure theory in current use is applicable to all types of rock behaviour. In at least one of the four behavioural classes identified failure in the field will always be catastrophic; in other cases it may be controlled.

I.- INTRODUCTION

The study of the mechanism of brittle fracture in rock is a most vital area of geomechanics research. Clearly, it is not possible to prevent fracture and subsequent failure (in foundations or around underground openings), or cause fracture (in drilling, blasting and comminution) with maximum efficiency if the mechanism by which this fracture occurs is not fully understood.

Although engineers have tested rock in uniaxial compression since the 1840's and in triaxial compression since around 1900, it is only in very recent years that an understanding of the mechanism of brittle fracture has begun to emerge. Perhaps the factor which has hindered development of this subject more than any other, is the explosive nature of the failure resulting when rock is tested in uniaxial compression or at low confining pressures in conventional testing machines. This violent failure is caused by the sudden release of stored strain energy from the testing machine into the specimen soon after the peak load-bearing capability of the specimen has been reached. If these strain energy releases can be prevented, failure of the rock can be controlled, and detailed studies of the structural disintegration process and the associated complete stress-strain curve can be made.

In the present paper, recently developed methods of achieving this control are outlined and results obtained using these techniques are discussed. The remarks made pertain to brittle rather than to ductile behaviour, and relate to confining pressures in the range from zero to less than half the brittle-ductile transition pressure. The term fracture is used throughout to describe the process in which new surfaces in the form of cracks are formed within the material. Failure on the other hand, is a more general term which refers to failure of the rock to fulfil its prescribed engineering function. Most often this takes the form of strength failure.

II.- LABORATORY METHODS OF CONTROLLING ROCK FRACTURE

The primary approach to this problem has been to attempt to reduce the energy stored in the loading system by increasing its longitudinal rigidity. The stiffness of conventional hydraulic testing machines likely to be used in rock mechanics laboratories varies from around 0.5×10^6 lb./in. for 50 ton machines 5×10^6 lb./in. for 500 ton machines. These stiffnesses may be most readily increased by reducing the volume of oil in the machine's hydraulic system (Ref. 1) or by increasing the stiffness of the tie bars. In practice, it has often proven more convenient to simply load steel columns or rings in parallel with the specimen (Refs.2-4). The effective stiffnesses of 50 and 100 ton machines have been increased to around 10×10^6 lb./in. using this method. A more complicated method developed for concrete but which has proven unsuitable for rock, is to use an hydraulic "stiffness compensator" in which system strain energy is stored in parallel springs so that the machine deflection is controlled during loading (Ref.5).

Cook and Hojem (Ref.6) developed an ingenious system in which the final compression of the specimen is achieved by thermal contraction of short, heavy columns connected to the machine cross-heads. Wawersik (Refs.7-10) has used an improved version of this machine to obtain complete stress-strain curves for a wide variety of rocks. In Wawersik's method, great skill is required of the operator in that the specimen must be unloaded manually when the load registered on an X-Y plot of axial load against displacement begins to drop. Load is then reapplied, the specimen weakened further, and the load again quickly removed manually. The envelope of the loading-unloading cycles so produced gives a smooth curve in the post-peak region. Using this technique, Wawersik was able to control the failure of rocks which fail explosively in even the stiffest of stiff testing machines. He classified rocks as either Class I or Class II according to the shape of the load-deflection (or stress-strain) curve produced in uniaxial compression. The unloading curve for Class I rocks lies to the left of the vertical line ACD in Fig.1, while for the most part, the curve for Class II rocks lies to the right of ACD. In an infinitely stiff machine which stores no strain energy, Class I rocks will only fail by continued movement of the machine platens together, whereas Class II rocks will fail explosively even in an infinitely stiff machine. Failure

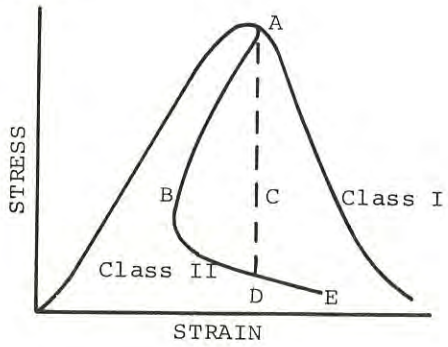

Fig. 1.

can only be controlled in Class II rocks by withdrawing energy from the system so that the platens follow path ABDE rather than ACDE. Wawersik achieved this by manually unloading the specimen when the situation appeared "dangerous".

A more sophisticated and reliable method of achieving the same end has been recently developed at the University of Minnesota (Refs.11-14). This method uses a closed-loop servo-controlled hydraulic loading system, the operation of which is shown schematically in Fig.2. The system is programmed for a desired function of some test variable which could be the lateral or axial deflection of the specimen, for example. The programmed value of this variable, p, is continuously electronically compared with a feedback signal from the experiment, f. If the program and feedback signals differ by more than a predetermined small amount, a servo-valve adjusts the load applied to the specimen until the feedback and program signals co-incide. The electronic comparison of the two signals is made at intervals of 10^{-4} seconds, and the net response time of the entire test system varies between 10×10^{-3} and 15×10^{-3} seconds.

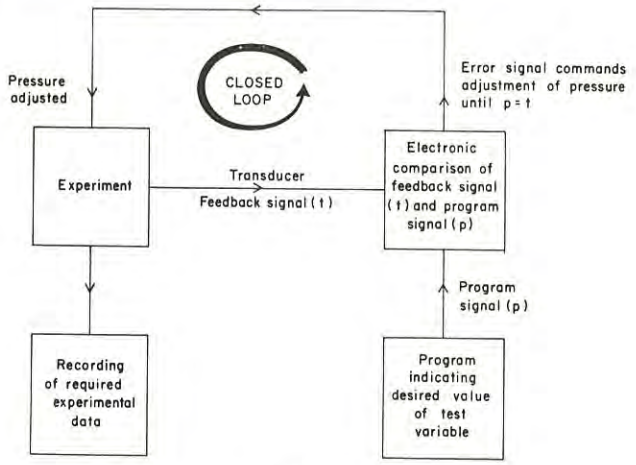

Fig. 2.

Rummel and Fairhurst (Ref.11) successfully servo-controlled the failure of a Class I rock, pink Tennessee marble, in uniaxial and triaxial compression tests using the axial displacement of the specimen as the feedback signal with a constant displacement rate being programmed. Since the negative slope of the complete stress-strain curve can be locally very high, it was found that if the programmed displacement rate was too great, explosive failure would occur because the system response time was not sufficiently rapid. At a sufficiently low rate of deformation, the complete stress-strain curve for Class I rocks can be obtained, provided the axial strain increases monotonically.

With Class II rocks, however, the complete stress-strain curves cannot be obtained in a servo-controlled machine by programming a constant axial strain rate, since the machine will follow the path ACDE in Fig.1. The curves can be obtained only if lateral displacement is used as a control. It has been found that for both Class I and II rocks, the lateral or circumferential displacement increases monotonically even though the axial displacement may not. Curves for a number of rock types have been obtained by wrapping a large gauge length strain gauge (forming one arm of a Wheatstone bridge) around the specimen at mid-height and using the bridge signal as a feedback. The axial deflection of the specimen is independently monitored (Refs.12,13).

III.- EXPERIMENTAL OBSERVATIONS

Experimental observations made in recent years would indicate that the manner in which fractures develop and the shape of the complete stress-strain curve obtained in laboratory compression tests at low confining pressures vary with rock type. At least three distinctive types of behaviour may be recognized.

(a) In highly porous, clastic, sedimentary rocks (e.g. many sandstones, some limestones) and in weathered rocks having a similar porous, granular texture (e.g. weathered granite), the only observable "fracture" feature in the region of the peak of the stress-strain curve is a collapse of the pore structure (Ref.15). Macro-fracture surfaces appear near the specimen ends only after the load-bearing capability has been reduced to 50-80% of its peak value (Refs.8,12,16). As the porosity decreases, microscopic sub-axial cracks appear in the region of the peak of the stress-strain curve. Such materials are characterized by low deformation moduli in the loading range and flat, Class I unloading curves. Failure can be controlled in any reasonably stiff testing system, and in many cases in a conventional hydraulic testing machine.

(b) In crystalline rocks other than those with ultrafine grains (i.e. in the majority of igneous and metamorphic rocks), the structural break-down process is a gradual one in which the formation of a number of inter- and intra-granular sub-axial cracks is the predominant feature (Refs.7-13). Here again, it is not until the load bearing capability of the specimen has been considerably reduced that macro-fracture surfaces appear. It is important to note that similar fracture patterns featuring large numbers of short cracks are obtained in a conventional testing machine if the test is stopped before explosive failure occurs (Ref.13). A section of white Tennessee marble tested in this way by the author is shown in Fig.3. The form of the complete stress-strain curve for these materials is shown in Fig.4. In region A, grain boundary cracks and pores close up and elastic compression of the material follows in zone B. Local fracturing begins in region C and continues into

region D. Internal and boundary faults appear in region E, extend in region F, and become inter-connected in region G to form a conjugate set of open shear fractures. Note that this view of fracture development differs in many respects from that put forward by Bieniawski (Refs.17,18).

Curves may be either Class I or Class II according to the nature of the rock. Considerable evidence exists regarding the influence of grain size on the strength of rocks (Refs.19,20). It is now suggested that for rocks of similar composition, grain size is an important determinant of the shape of the complete stress-strain curve. The limited evidence available suggests that as average grain size decreases, the unloading portion of the stress-strain curve is more likely to be Class II (see Table I).

Fig. 3.

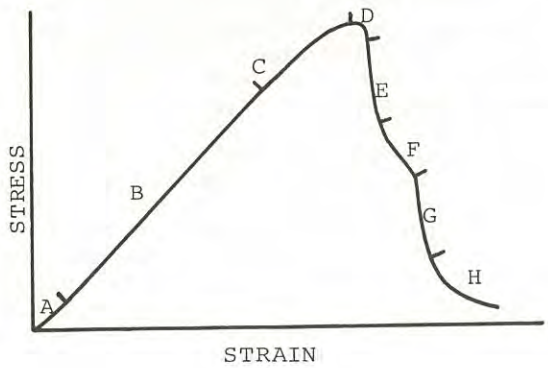

Fig. 4.

(c) In dense, ultra-fine grained rocks (e.g. Solenhofen limestone) attempts to control failure have thus far been unsuccessful. Apparently, this is because the structural break-down process is an almost instantaneous rather than a gradual or progressive one. Although the mechanism involved has not been defined experimentally it would appear that the homogeneity of the specimen ensures that local stress concentrations and hence local fracturing will not occur at pre-peak loads. It is considered quite likely that in such materials fracture initiation and propagation occur at the peak of the stress-strain curve. If violent fracture is to be prevented, large amounts of energy must be extracted from the specimen very quickly and this has not been achieved to date. The servo-control technique has not been successful in this regard because it relies upon the detection of an accelerating rate of lateral expansion of the specimen for its operation. This does not occur in this type of rock early enough for the servo-control system to be able to unload the specimen and prevent uncontrolled failure. Obviously, although no complete stress-strain curves for these materials have been obtained, they are very much Class II rocks.

The essential features of these broad categories of rock behaviour are summarized in Table I. For practical purposes it is necessary to distinguish between the Class I and Class II rocks in category (b). Thus the porous, granular rocks of category (a) are described as being Class Ia, the Class I rocks of category (b) as Class Ib, the Class II rocks of category (b) as Class IIa, and the very brittle rocks of category (c) as Class IIb. It should be emphasized that this is only a broad qualitative classification based on fracture morphology and stress-strain behaviour. It is incomplete in that data for certain important types of rock (e.g. shale) are completely lacking, but nevertheless it is considered instructive for practical purposes to attempt to classify the behaviour of rocks in this way.

IV.- FAILURE CRITERIA

The experimental studies referred to above, if nothing else, point to the inapplicability of certain well known failure criteria to the brittle fracture of rock. It is completely erroneous to attempt to use the Mohr-Coulomb theory as a fundamental criterion, assuming as it does that failure will take place by shear on a plane inclined at a certain angle to the specimen axis. The evidence is overwhelming that this is not the fracture pattern associated with the attainment of peak strength in the vast majority of rocks. The "shear" planes customarily observed in the laboratory are generally secondary features developed in the post-peak release of system strain energy. Perhaps slightly less obvious on the basis of the experimental evidence is the inapplicability of the Griffith concept of fracture to rock despite the attention it has received in recent years (Refs. 22,23). As noted by Wawersik and Brace (Ref.10), only very few Griffith crack configurations (i.e. inclined parent cracks with branch cracks emanating from the crack tip regions curving into the direction of greatest compression) can be found in fractured rock specimens.

Although it is apparent that fracture morphology varies with rock type, a reasonably clear picture of the process occurring in Class Ib and IIa rocks has

Class	Description	Known examples	Shape of compressive stress-strain curve.	Method required to control fracture
Ia	Soft, highly porous, granular sedimentary or weathered rocks.	Indiana limestone (Refs. 7-9,12), some sandstones (Refs.12,16), weathered granodiorite (author's unpublished data).	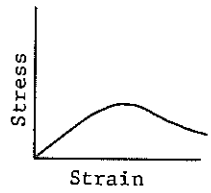	Conventional machine in some cases, stiffened machine in others.
Ib	Crystalline igneous and metamorphic rocks of low porosity with average grain size generally not less than 0.75 mm. Sedimentary rocks of medium low porosity.	Pink Tennessee marble (Refs.7-9,11) South African norite (Ref.16), South African quartzite (Refs.16,21), Charcoal Gray Granite (Ref.8,9).	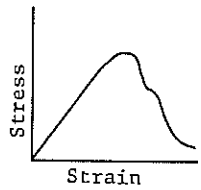	Thermal stiff machine or servo-control. Very stiff conventional machine in some cases.
IIa	Fine grained igneous and metamorphic rocks of low porosity.	White Tennessee marble (Ref.13), Westerley granite (Ref.10), Frederick diabase (Ref. 10), basalt (Refs.8,9).	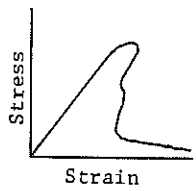	Thermal stiff machine possible but servo-control more convenient.
IIb	Dense, ultra-fine grained homogeneous rocks.	Solenhofen limestone (Refs.8,9).	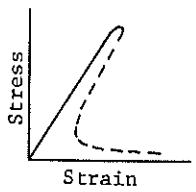	Failure generally uncontrollable.

TABLE I

now emerged. Short inter- and intra-granular sub-axial cracks of one or two grain diameters in length appear well before peak strength is reached and increase in numbers as deformation continues. There is no evidence of shear movement along these cracks and this, together with their orientation, would indicate that they are tensile fractures. The fact that this tensile cracking is a local phenomenon in most rocks tested in uniaxial compression is explained by the heterogeniety and anisotropy of the rocks resulting in a non-uniform distribution of stresses within the specimens.

The only currently available failure theory predicting this tensile mode of fracture is the effective tensile stress theory (Refs.24,25) in which it is postulated that when a specimen is loaded axially in compression, inter-particle bonds will be extended laterally and will eventually fail in tension. Development of the theory to date has been in terms of a particulate model of a linear, homogeneous material. In its present form the theory would appear to be ideally suited to Class IIb materials in which the stress-strain curve is closely linear up to its peak. The situation is not so straightforward with Class Ib and IIa materials in which the point of fracture initiation and the peak of the stress-strain curve do not so nearly coincide.

V.- PRACTICAL IMPLICATIONS

Following the development of techniques for the determination of complete stress-strain curves for rock, it was soon recognized that use of such data is an invaluable aid to the study of the stability of underground openings. Consider the simple example of a room and pillar mining system in which a given pillar has the load-deformation characteristic OAB in Fig.5, and the surrounding mine system has a local stiffness of -K. If the pillar is replaced with a jack, and the jack is slowly retracted, the roof will sag and some floor uplift will occur as the load decreases. Provided the roof remains intact, the curve relating the force on the jack to the convergence between the roof and floor will be an approximate straight line with a slope of -K. If this mine-stiffness characteristic is similar to that represented by AHE (Fig.5a), failure of the pillar will be catastrophic. This is because at any post-peak deformation, δ, an excess of energy equal to the area AHJ is available for accelerating the pillar into rapid collapse. If, on the other hand, the mine-stiffness characteristic takes the form of ALG in Fig.5b, the roof is unable to supply the force necessary to deform the pillar beyond the peak load so that the situation is stable, and controlled failure occurs.

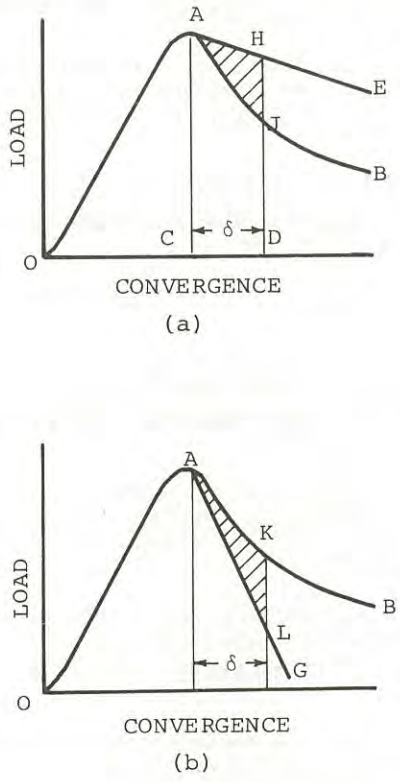

Fig. 5.

Problems of this type have been analysed in detail elsewhere (Refs.26-28). However, certain aspects of the phenomena involved are not yet fully understood, and the solution of practical problems is not as simple as the approach outlined above might suggest. The local mine-stiffness K is quite difficult to determine, depending as it does on the mechanical properties of the roof and floor, and the detailed geometry of the mine openings. If the pillar is composed of Class II rock, violent failure cannot be prevented unless some means of rapidly extracting energy from the system can be devised. Salamon (Ref. 28) determined the mathematical conditions under which pillar workings will be stable but completely overlooked the possibility of Class II behaviour. In such cases, pillars (or walls of abutments) are likely to collapse by a brittle buckling mechanism (Refs. 29,30).

Perhaps the greatest difficulty involved is that of applying laboratory data to the field situation. In addition to the well documented influence of geomechanical discontinuities on rock mass behaviour, the influence of specimen size on the mechanical behaviour of rock must be considered. Recent servo-controlled tests carried out at the University of Minnesota on a Class Ib rock suggest that the unloading portion of the stress-strain curve steepens with increasing specimen size. It is possible, therefore, that a mass of rock which, on the basis of laboratory tests, might appear to be stable in a given situation, will, in fact, be unstable in the field. A further unknown in this regard is the influence of time on the fracture process. Limited experimental evidence obtained by Bieniawski (Ref.31) suggests that the unloading curve for rock becomes flatter as the strain rate decreases. Despite difficulties such as these, it is considered important that the complete stress-strain curves of rocks involved in engineering structures be investigated so that some guide to their likely behaviour can be obtained.

The experimental results described above have great significance in the interpretation of the results of model studies of the behaviour of rock structures. The conditions for similitude of model and prototype behaviour in terms of peak strength and deformation properties up to the peak of the stress-strain curve are well developed (Ref.32), but it is now apparent that if the behaviour of the prototype is to be accurately and completely modelled, the model material should show the same mode of fracture development and post-peak stress-strain characteristics as the real rock. Since most model materials are soft and reasonably porous (Ref.33) their behaviour is likely to be Class Ia in which case they cannot be expected to adequately represent the post-peak behaviour of many rocks.

VI.- CONCLUSIONS

Recent advances in the experimental study of the mechanism of brittle fracture in rock have been made possible by the development of techniques for preventing uncontrolled fracture of laboratory specimens thus enabling their complete stress-strain curves to be determined. The pattern of fracture development and the shape of the associated complete stress-strain curve varies with rock type. Four broad behavioural types have been distinguished, the major determinants of behaviour in this regard being porosity and grain size. The primary feature of the fracture pattern in many rocks is the progressive development of large numbers of small, sub-axial, tensile cracks. Mohr-Coulomb and Griffith crack failure theories are inapplicable to brittle fracture in rock because they assume incorrect fracture mechanisms. Complete understanding of the behaviour of rock structures, particularly underground openings, cannot be obtained unless the post-peak behaviour of the rocks concerned is investigated.

VII.- ACKNOWLEDGMENTS

The original experimental work described herein was carried out in the Department of Civil and Mineral Engineering, University of Minnesota while the author was on study leave from the James Cook University of North Queensland. Most of the ideas presented were also developed during this period and owe much to the many valuable discussions held with Professor C. Fairhurst, Dr. J.A. Hudson, Dr. F. Rummel and Mr. M.P. Hardy.

REFERENCES

1. TURNER, P.W. and BARNARD, P.R. - Stiff Constant Strain Rate Testing Machine. The Engineer, Vol. 214, July 27, 1962, pp. 146-148.

2. COOK, N.G.W. - The Failure of Rock. Int.Jour. Rock Mech.Min.Sci., Vol.2, No.4, Dec., 1965, pp. 389-403.

3. PAULDING, B.W. - Techniques used in Studying Fracture Mechanics of Rocks. In Testing Tech-

niques for Rock Mechanics, ASTM STP 402, Am.Soc. Testing Mats., 1966, pp. 73-86.

4. BIENIAWSKI, Z.T. - Determination of Rock Properties. Council Sci.Ind.Res., Rept. MEG 518, Pretoria, South Africa, Jan., 1967.

5. HINDE, P.B. - Testing Machine Stiffness Problem. The Engineer, Vol.216, June 26, 1964, pp. 1124-1127.

6. COOK, N.G.W. and HOJEM, J.P.M. - A Rigid 50 ton Compression and Tension Machine. Sth.Afr.Mech. Engr., Vol.16, No.4, Nov., 1966, pp. 89-92.

7. WAWERSIK, W.R. - Discussion on the brittle fracture of rocks. In Failure and Breakage of Rock, C. Fairhurst (ed.), New York, AIME, 1967, p. 158.

8. WAWERSIK, W.R. - Detailed Analysis of Rock Failure in Laboratory Compression Tests. Thesis (Ph. D), Univ. of Minnesota, 1968.

9. WAWERSIK, W.R. and FAIRHURST, C. - A Study of Brittle Rock Fracture in Laboratory Compression Experiments. Int.Jour.Rock Mech.Min.Sci., Vol.7, No.5, Sept., 1970, pp. 561-575.

10. WAWERSIK, W.R. and BRACE, W.F. - Post-failure Behaviour of a Granite and Diabase. Rock Mech., (to be published).

11. RUMMEL, F. and FAIRHURST, C. - Determination of the Post-failure Behaviour of Brittle Rock using a Servo-controlled Testing Machine. Univ. of Minnesota, Min.Resources Res.Centre, Prog.Rept. No.21, July, 1970, pp. 1-20. (Submitted to Rock Mech.).

12. HUDSON, J.A., BROWN, E.T. and FAIRHURST, C. - A Method of Optimizing the Control of Rock Failure in Servo-controlled Laboratory Tests. Univ. of Minnesota, Min.Resources Res.Centre, Prog.Rept. No.21, July, 1970, pp. 78-91. (Submitted to Rock Mech.).

13. BROWN, E.T., HUDSON, J.A., HARDY, M.P. and FAIRHURST, C. - Controlled Failure of Hollow Rock Cylinders in Uniaxial Compression. Univ. of Minnesota, Min.Resources Res.Centre, Prog.Rept. No. 22, Nov., 1970, pp. 1-32. (Submitted to Rock Mech.).

14. HUDSON, J.A. - A Critical Examination of Indirect Tensile Strength Tests for Brittle Rocks. Thesis (Ph.D.), Univ. of Minnesota, 1970.

15. MOGI, K. - Pressure Dependence of Rock Strength and Transition from Brittle Fracture to Ductile Flow. Bull.Earthquake Res.Inst., Tokyo Univ., Vol.44, 1966, pp. 215-232.

16. CROUCH, S.L. - Experimental Determination of Volumetric Strains in Failed Rock. Int.Jour.Rock Mech.Min.Sci., Vol.7, No.6, Nov., 1970, pp. 589-603.

17. BIENIAWSKI, Z.T. - Mechanism of Brittle Fracture of Rock. Council Sci.Ind.Res., Rept. MEG 520, Pretoria, South Africa, Jan., 1967.

18. BIENIAWSKI, Z.T. - Stability Concept of Brittle Fracture Propagation in Rocks. Engg.Geol., Vol.3, No.2, Dec., 1967, pp. 149-162.

19. HOUPERT, R. - La résistance à la rupture des granite en fonction de la dimension de leurs minéraux. C.R.Acad.Sci.Paris, Vol.265, 1967, pp. 583-586.

20. BRACE, W.F. - Micromechanics in Rock Systems. Int.Conf.Struct.Solid Mech.Civ.Engg.Des., Southampton, 1969, Paper 18.

21. DENKHAUS, H.G. - Discussion. Rock Mech., Suppl. 1, 1970, pp. 130-134.

22. McCLINTOCK, F.A. and WALSH, J.B. - Friction on Griffith Cracks in Rock under Pressure. Proc. Fourth U.S. Nat.Congr.Appl.Mech., Berkeley, 1962, Vol.2, pp. 1015-1021.

23. HOEK, E. - Brittle Failure of Rock. In Rock Mechanics in Engineering Practice, K.G. Stagg and O.C. Zienkiewicz (eds.), London, John Wiley, 1968, pp. 99-124.

24. BROWN, E.T. and TROLLOPE, D.H. - The Failure of Linear Brittle Materials under Effective Tensile Stress. Rock Mech.Engg.Geol., Vol.5, No.4, 1967, pp. 229-241.

25. TROLLOPE, D.H. - The Mechanics of Discontinua or Clastic Mechanics in Rock Problems. In Rock Mechanics in Engineering Practice, K.G. Stagg and O.C. Zienkiewicz (eds.), London, John Wiley, 1968, pp. 275-320.

26. STARFIELD, A.M. and FAIRHURST, C. - How High-speed Computers Advance Design of Practical Mine Pillar Systems. Engg.Min.Jour., Vol.169, No.5, May, 1968, pp. 78-84.

27. STARFIELD, A.M. and WAWERSIK, W.R. - Pillars as Structural Components in Room and Pillar Mine Design. Proc.Tenth Symp.Rock Mech., Univ. of Texas, 1968.

28. SALAMON, M.D.G. - Stability, Instability and Design of Pillar Workings. Int.Jour.Rock Mech.Min. Sci., Vol.7, No.6, Nov., 1970, pp. 613-631.

29. FAIRHURST, C. and COOK, N.G.W. - The Phenomenon of Rock Splitting Parallel to the Direction of Maximum Compression in the Neighbourhood of a Surface. Proc.First Congr.Int.Soc.Rock Mech., Lisbon, 1966, Vol.1, pp. 687-692.

30. TROLLOPE, D.H. - The Stability of Deep Circular Shafts in Hard Rock. Proc.Second Congr.Int.Soc. Rock Mech., Belgrade, 1970, Vol.2, Paper 4-29.

31. BIENIAWSKI, Z.T. - Time-dependent Behaviour of Fractured Rock. Rock Mech., Vol.2, No.3, Sept., 1970, pp. 123-137.

32. OBERT, L. and DUVALL, W.I. - Rock Mechanics and the Design of Structures in Rock. New York, John Wiley, 1967, 650 pp.

33. STIMPSON, B. - Modelling Materials for Engineering Rock Mechanics. Int.Jour.Rock Mech.Min.Sci., Vol.7, No.1, Jan., 1970, pp. 77-121.

The Prediction and Measurement of the Long-Term Strength of Rock

By
D. P. Singh, Ph.D.
(Lecturer in Mining Engineering, Banaras Hindu University, India)
AND
W. E. Bamford, B.E., A.M.Aus.I.M.M.
(Senior Lecturer in Rock Mechanics, University of Melbourne)

SUMMARY.- The strength and deformation behaviour of rocks are time-dependent; the design of rock structures should be based on the long-term strengths rather than the strengths determined by short-term laboratory tests. As a direct method of determining the long-term strength of a rock is tedious and time consuming, short-term methods of indirectly predicting long-term strengths of rock should be developed. Some preliminary work to this end is reported, and a method based on observation of change in loading rate during a compression test conducted at a constant rate of axial deformation is suggested to be a simple, convenient, yet valid predictor of long-term strength of rock.

I.- INTRODUCTION

The strength of rock is difficult to define as it depends on many variables. Strengths of rocks from tests with high loading rates, such as impact tests, where failure occurs a fraction of a second after the onset of loading, may be several times the strength as determined when a load is slowly applied to the rock, and failure occurs hours or days after the onset of loading.

The time taken for a sustained load to cause fracture decreases with increasing stress and there is a particular stress below which the rock will not fail, no matter how long the force is applied. This stress has variously been called "fundamental strength", "true strength", "time safe stress", "sustained load strength" or "long-term strength" (Ref.1). It will be referred to as long-term strength in this work.

There are many practical difficulties associated with the study of strength-time behaviour of rocks and very few investigations have been made on this subject. Extremely homogeneous rocks are required, so that the strength values are consistent under similar sets of test conditions. Sometimes a very small variation of strength from the mean causes serious error. To develop a relationship between strength and time for a particular rock, many tests, run for long periods of time, are required.

II. - METHODS OF DETERMINING LONG-TERM STRENGTH

Methods of determining long-term strength of rock can be broadly classified into two groups, (1) direct methods and (2) indirect methods. The indirect methods can be further classified as (a) creep test method, (b) volumetric strain method, (c) log stress-log-strain method, (d) stress-strain rate method, and (e) sonic method.

In the direct method rock specimens are subjected to different sustained loads and the highest value of the load, under which no failure takes place even after a long time, is the long-term strength of the rock. It is usually expressed as the percentage of the ultimate strength determined by short-term tests in the laboratory.

In the indirect methods the long-term strength is determined by methods other than the application of sustained loads. Indirect methods require much shorter time than direct methods and therefore they are very useful to rock engineers for quick evaluation of long-term strengths of rocks.

Determination of long-term strength by the direct method does not require understanding of the mechanism of creep but this becomes a necessity in order to evolve indirect methods of determining long-term strength of rocks.

III.- MICROFRACTURING DURING CREEP

Though the creep curves of metals and rocks have similar features, the creep of brittle rocks has certain characteristics which do not occur in the case of plastic metals. Several workers have found that in creep tests near the fracture stress of the specimen, transverse creep strain (perpendicular to the direction of applied stress) is larger than longitudinal creep strain, (Refs. 2, 3, 4).
It was also observed that the transverse creep rate increased more rapidly than the longitudinal creep rate. These results suggest that the volume of the rock increases during creep. Robertson (Ref. 5) found that the density of Solenhofen limestone decreased during creep tests. The increase in volume contrary to elastic theory is known as dilatancy and is due to cracking (or microfracturing) that takes place in the specimen under sustained load.

Watanabe (Ref. 6) found that for granite under compression, the creep strain rate is directly proportional to the rate of detection of elastic shocks, attributed to microfracturing. Scholz (Ref. 7) suggested that creep in brittle rocks at low temperature and pressure is due to time-dependent microfracturing.

It seems certain that microfracturing in brittle rock is associated with a form of creep instability. It is observed that the appearance of the fracture surfaces formed in short-term compression tests, where the failure mechanism is thought to be microfracturing, is very similar to those formed after long-term loading tests, in which significant amounts of creep were observed prior to failure. This can be taken as evidence that microfracturing is important in the mechanism of creep, as well as that of rapid elastic deformation leading to brittle fracture.

Dilatancy has also been observed just before fracture in short-term compressive strength tests (Refs. 8, 9, 10). Bieniawski (Ref. 11) has made detailed investigations on this subject and postulated a theory of brittle fracture of rocks on the basis of microfractures developing during compression of rocks.

Fig. 1 is a schematic diagram of Bieniawski's postulated mechanism of brittle fracture of rocks under compression, with induced pore pressure effects (Ref. 12). The microcracks initially present in the intact rock first close, then elastic deformation of the specimen takes place for a limited stress range. At higher stresses the process becomes nonelastic, the strain is nonrecoverable and fracture propagation starts.

Bieniawski distinguished two phases of fracture propagation: stable and unstable. In stable fracture propagation, the failure process is a function of the loading and can be controlled accordingly but in unstable fracture propagation extensive microfracturing starts, the specimen dilates, and fractures propagate uncontrollably. It is in fact the stress at the onset of unstable fracture propagation which indicates the long-term strength of the rock. The stress at which unstable fracture starts is given by the point on the stress versus volumetric curve, above which the volumetric strain starts increasing rather than decreasing according to elastic behaviour, or where the stress versus axial strain curve departs from linearity.

The pore pressure curve shows initial curvature due to closure of inherent cracks and voids and then becomes linear as the rock acts elastically. Later the rate of increase of pore pressure starts decreasing, illustrating the phenomenon of fracture initiation. The pore pressure attains peak value when the volumetric strain becomes minimum. Beyond this point the pore pressure decreases and indicates the onset of unstable fracture propagation. The pore pressure goes below its initial value when the specimen starts dilating beyond the initial volume.

It is implied from the work of the above investigators that a rock specimen will not be able to sustain, for an indefinite length of time, a load higher than that required for unstable fracture propagation. The structural break-down of the specimen has already been initiated at this stage and the final rupture is just a matter of time.

IV.- THE VOLUMETRIC STRAIN METHOD

The success of the volumetric strain method for long-term strength determination depends on how accurately the point at which reversal of volumetric strain takes place can be established. The reversal of the volumetric strain curve usually takes place shortly before the fracture of a specimen and it is hard to accurately locate it unless a continuous recording system is used. The estimation of volumetric strain includes transverse strain of the specimen, which is difficult to record accurately. The volumetric strain is calculated from the equation

$$\varepsilon_v = \varepsilon_A + 2\varepsilon_T$$

where ε_v = volumetric strain,
ε_A = axial strain, and
ε_T = transverse strain.

Wiid (Ref. 13) has used the volumetric technique for determining the long-term strength of dolerite and found it quite close to the value that he obtained from direct tests. This technique has been also successfully used in concrete (Refs. 14 and 15).

V.- OBJECT OF EXPERIMENTAL INVESTIGATION

The object was to investigate short-term methods of finding the long-term strengths of rocks and to establish the validity of these methods by determining

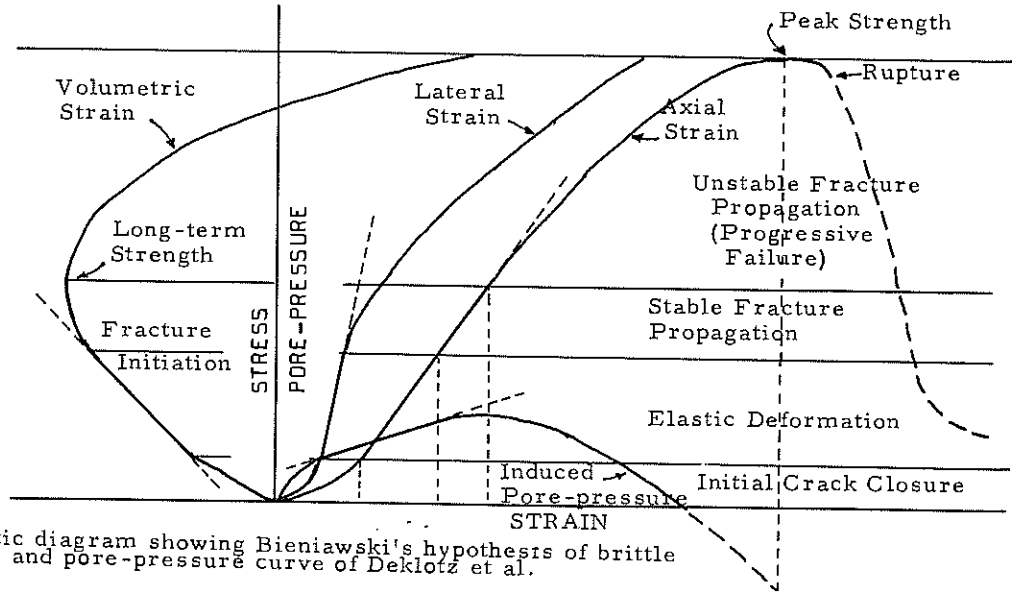

Fig. 1. Schematic diagram showing Bieniawski's hypothesis of brittle fracture and pore-pressure curve of Deklotz et al.

the long-term strengths of a few selected rocks by the direct method. It was also proposed to make a survey of some rocks from Australian mines, to find out whether their strengths are time-dependent.

The short-term methods proposed for predicting the long-term strengths of rocks were based on Bieniawski's hypothesis. This required the determination of stress and corresponding axial and lateral strain of a specimen in the usual compression strength tests in the laboratory. The direct method of finding the long-term strength of rocks involved loading of the specimens to various percentages of their ultimate strength and recording the time to failure.

The time-strain characteristics are important in many rocks for determining the life of existing mine workings and in planning future mines. Therefore it was decided to study the creep (time-strain) characteristics of some rocks subjected to sustained load.

Some rock specimens dilate near their fracture stress during short-term compression tests in the laboratory; to investigate whether this phenomenon occurs in the fracture of rocks in the creep tests, the axial as well as the lateral strains (strains parallel and perpendicular to applied load respectively) were measured on the specimens subjected to a sustained load.

Various other physical properties such as hardness, density, type and angle of fracture etc. were studied during the preparation and testing of the specimens.

VI.- SHORT TERM TESTS

Specimens were supplied by the mines sponsoring this project through the Australian Mineral Industries Research Association (AMIRA). These rock samples were mostly cores obtained during diamond drilling. Two other rocks, Wombeyan marble and Sicilian marble, were selected for detailed analysis. These rocks have uniform structures and were known to exhibit time-dependent properties so blocks of them were obtained from monumental stone merchants, and two inch diameter cores were obtained by drilling with a thin-walled diamond core barrel on a laboratory drilling lathe.

The specimens were cut by diamond saw to a length-diameter ratio of 3:1. This was considered to be a suitable ratio to minimise end effects and at the same time prevent buckling. The ends of the specimens were prepared on a surface grinder, which produced smooth parallel ends within the limits suggested in Ref. 16.

The short-term uniaxial compression tests were performed in an Avery compression testing machine of 400,000 lb. capacity. It had a spherically seated upper platen and a fixed lower one. The rate of loading could be approximately adjusted to a predetermined value.

Two Schaevitz Linear Variable Differential Transformers (LVDT's) of ± 0.10 in. range were used for measuring the axial deformation and four of ± 0.02 in. range were used to measure radial deformation of a specimen along two diameters at right angles.

An annular steel disc was placed concentric to the lower platen of the Avery machine, with six vertical steel posts, ½ in. dia., screwed into it to hold two axial and four lateral (radial) LVDT's. The cores of the axial LVDT's were screwed in a brass holder which was ultimately attached to a pot magnet. The transformers were carried in another holder whose vertical position on the post could be adjusted before each test. The pot magnets were attached to the upper platen and the transformers were made to slide over the core, thus measuring the movement of the upper platen, relative to the lower.

The transformer of each lateral LVDT was attached to a probe which was in normal contact with the side of the specimen. The core was attached to a micrometer head, which was used both for the calibration of the LVDT's and for establishing the null points, before each test. When the specimen expanded transversely, the transformer moved over the core.

A "Watanabe" multipen potentiometric recorder was used to continuously record the deformation of the specimen in the axial direction and in two lateral directions, together with load.

VII.- LONG-TERM LOADING APPARATUS

The long-term loading machine consisted of a gas-hydraulic system and a loading frame. Two such units were installed in a temperature controlled room.

An intensifier used compressed nitrogen at a maximum pressure of 1,000 lb/sq.in. to develop a fluid pressure of 10,000 lb/sq.in. The supply of gas to the intensifier was controlled by a regulator which at a particular setting supplied gas continuously and at a constant pressure. A small displacement of the ram caused virtually no change in the gas pressure and hence no change in the pressure of the fluid (Tellus 33 hydraulic oil) which acted on a 3 in. diameter ram which formed the lower platen of the loading frame. The upper platen was flat and rigid, and by means of adjustment nuts was fixed parallel to the lower platen, using dial gauges which could be read to .0001 in., both for checking parallelism of the platens and for measuring axial and lateral deformations of the loaded specimen. A maximum load of 70,000 lbs. could be applied by this system, and held almost indefinitely.

Fig. 2. Long-term Loading system - General View.

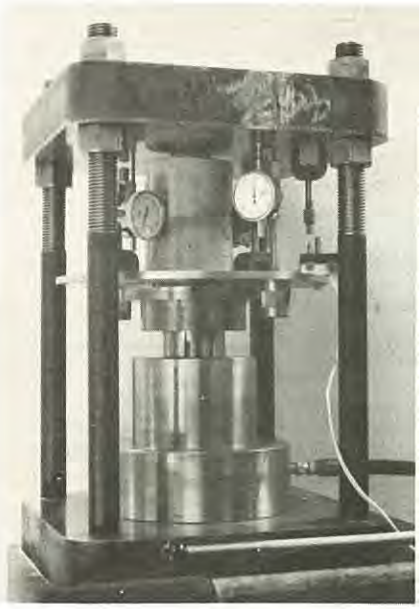

Fig. 3. Long-term Loading Frame

Specimens for long-term testing were prepared in the same way as for short-term tests, and were mounted centrally on the lower platen inside a steel cylinder guard. A hand priming pump was operated to bring the specimen in contact with the upper platen. The axial and lateral dial gauges were adjusted to measure the deformation of the specimen during loading and also during creep studies at constant load. The gas regulator valve was opened and adjusted until the desired load on the specimen was achieved.

Whenever it was desired to plot a stress-strain curve during loading, the specimen was loaded in steps, recording the dial gauge readings after each 500 lb/sq.in. increment. The specimen could be loaded quite quickly, depending on how fast the gas regulating valve was opened. Constant load could be maintained even during changing of the cylinders.

The deformation of the specimen with time and the time to fracture of the specimen at a particular stress were recorded in order to enable plotting of the strain-time and strength-time characteristics of the rock.

VIII.- PREDICTION OF LONG-TERM STRENGTHS

Following Bieniawski's hypothesis, during uniaxial compression tests the stress at which unstable fracture propagation starts in the specimens indicates the predicted long-term strength of the rock. It is expected that a specimen will be able to indefinitely sustain a stress below the long-term strength thus predicted.

The stress at which unstable fracture starts is characterised by an increase in the rate of microfracturing which results in gradual increase of axial strain rate with stress and also in dilatancy of the specimen indicating that transverse strain is increasing proportionately more rapidly than axial strain.

It is difficult to precisely determine the stress corresponding to the onset of unstable fracture propagation in a specimen. Methods variously suggested involve the plotting of applied stress versus axial strain or volumetric strain, or log stress versus log strain, etc.

IX.- THE LOADING RATE METHOD

The standard technique adopted at the Melbourne University Mining Dept. for determining the uniaxial compressive strengths and axial and lateral deformations in a specimen helped to evolve another method of determining the stress (or the load) initiating unstable fracture propagation in a specimen.

The load, axial deformation and lateral deformations along two diameters perpendicular to each other are continuously and simultaneously recorded during the uniaxial tests on the specimens. It is also possible to perform the tests at a constant deformation rate after the initial fluctuations due to closure of the cracks in the specimen, seating of the hemi-spherical head, compression of fluid in the hydraulic loading system etc. At the beginning of each test, the load valve is adjusted so as to load the specimens at 100 lb/sq.in./sec. After the initial adjustments, the rate of loading remains constant for a particular setting of the load valve and also the rate of travel of the lower platen of the compression testing machine and hence the axial deformation rate of the specimen is constant. This is inferrred from the load and axial deformation curves of the recorder chart.

The linear behaviour of the load and the axial deformation curves continue as long as the specimen deforms in an elastic manner. It is often observed that shortly before fracture the load curve starts deviating from linearity, indicating a lower rate of loading while the axial deformation curve continues to be linear until the specimen fractures (Fig. 4).

It is postulated that the decrease in the rate of loading indicates the start of unstable fracture propagation. In fact, the rate of work done by the machine continues to be the same but its ability to load the specimen decreases continuously as more and more energy is used up in creating more microfractures.

The load corresponding to the point from which the load curve starts deviating from linearity, while the axial deformation curve continues to be linear, was thought to coincide with the long-term load (from which long-term strength can be calculated) which the specimen can sustain indefinitely without fracturing. It is possible to precisely locate this point on the recorder chart by suitably presetting the recorder voltages and chart speeds at the beginning of each test. Since the curves are recorded continuously, the proposed method was considered to be more accurate than other methods in which the readings are taken at intervals.

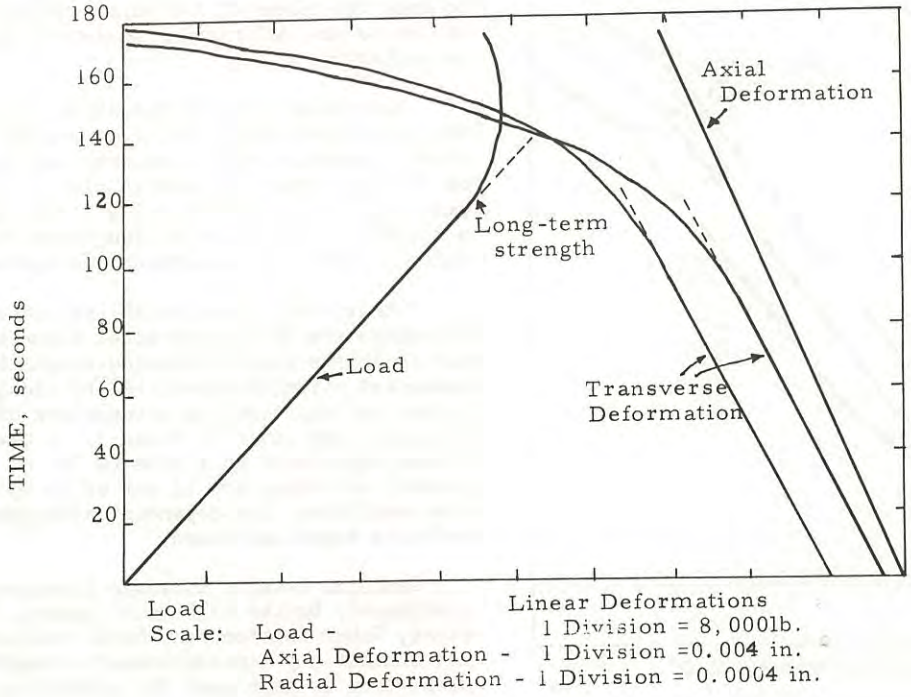

Fig. 4. Typical Chart Record of Load Axial Deformations and Two Perpendicular Radial Deformations. Sicilian Marble.

X.- COMPARISON OF PREDICTIONS BY DIFFERENT METHODS

The time-dependent strengths, expressed as percentages of maximum strengths, of Sicilian marble, Wombeyan marble, and North Broken Hill ore, predicted by the loading rate method, the volumetric strain method, the stress-axial strain method and log stress stress-log strain method are tabulated in Table 1. These three rocks were selected for comparison purposes as all the specimens of these rocks showed time-dependent strengths.

Long-term strength by the volumetric strain method was obtained from the point on the stress-volumetric strain curve from which volumetric strain starts increasing rather than decreasing. The predicted long-term strengths by this method are higher than those predicted by other methods.

Long-term strength predicted by the stress-strain method was obtained from the point on the stress-axial strain curves from which axial strain starts deviating from linearity. The values of predicted long-term strengths from the stress-strain method should have been the same as by the loading rate method. The variations between the two values are due to cumulative errors involved in the processes of taking the points from the recorder chart, calculating corresponding values of stress and strain, plotting the points, drawing the curves, and then estimating the point from which the curve starts deviating from linearity.

The log-log plot of stress-strain diagrams for concrete gives straight lines, and kinks represent changes in the internal structure of the specimen (Ref. 15). The stress-strain values of rock

TABLE 1

COMPARISONS OF PREDICTIONS OF LONG-TERM STRENGTH BY DIFFERENT SHORT-TERM METHODS

Rock Type	Number of Tests	Average Maximum strength lbs/sq.in.	Average Predicted long-term strength as Percentage of maximum strength			
			Loading-rate method	Volumetric strain method	Stress-strain method	Log-stress log strain method
Sicilian marble	24	13,200	88	94	89	85
Wombeyan marble	23	13,000	89	94	91	87
North Broken Hill ore	13	12,000	94	95	94	89
Bondi sandstone	5	7,200	91			
Coomalie Dolomite	8	27,700	89			
Mary-Kathleen Garnet-Diopside-Scapolite	10	22,400	95			

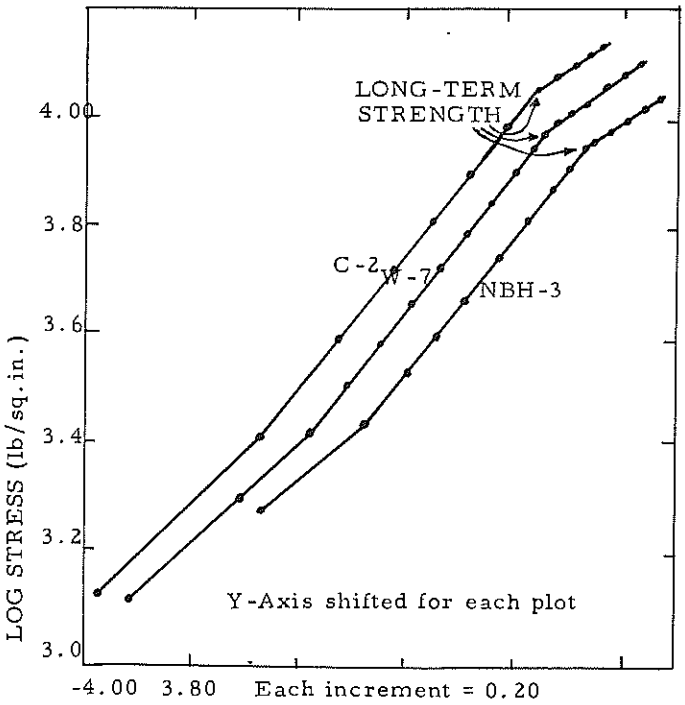

Fig.5. Log stress-log strain plots of Sicilian marble specimen (C-2), Wombeyan marble specimen (W-7) & North Broken Hill ore (NBH-3).

specimens tested in this programme were also plotted on log-log graphs. Two clear kinks were observed in the graphs for Sicilian marble, Wombeyan marble and North Broken Hill ore (Fig. 5). The second kink on log stress-log strain plots represents the point from which stress-axial strain curve deformation rate starts decreasing. Therefore, the stress corresponding to the second kink gives the long-term strength of the specimen. The long-term strength predicted by this method is the lowest of all the methods investigated in the present study.

The loading rate method was the quickest as the long-term load and hence the long-term strength could be predicted from the recorder chart as soon as the tests were over. The point at which the rate of loading starts decreasing could be easily found due to the sharp change in the gradient (Fig. 4). Since the processing and plotting of the data are not involved, the predicted long-term strengths by this method were considered to be more accurate than by other methods.

Where it is not possible to adopt the loading rate method due to lack of suitable equipment, log stress-log strain or simply stress-strain methods may be preferred due to their simplicity as compared to the volumetric strain method. The determination of lateral strain involved in volumetric strain is a tedious process and a completely correct representation of lateral deformation is possible only when it is measured at a number of places along the circumference and at a number of sections covering the entire height of the specimen. In fact the value of lateral strain measured perpendicular to the fracture surface is the most valid strain but it is difficult to know the plane of fracture before the test so as to locate the deformation measuring instruments accordingly.

Sometimes it is difficult to precisely locate the point from which the stress-axial strain curve starts deviating from linearity but the second kink in the log stress-log strain plot is obtained quite easily. The log stress - log strain method estimates a slightly lower value of long-term strength which is safer to adopt for designing underground structures.

Other rocks which exhibited time-dependent strengths are Bondi sandstone, Coomalie dolomite and Mary Kathleen garnet-diopside-scapolite. Their time-dependent strengths predicted by the loading rate method and expressed as percentages of maximum strengths are given in Table 1. A few specimens of Broken Hill South quartzite (3 out of 15 specimens tested) and Cobar ore (4 out of 33 specimens tested) also exhibited time-dependent strengths but no definite trend was found.

Kambalda basalt, Lilydale limestone (except 2 specimens), Broken Hill South gneiss, Mt. Isa greenstone, Cobar mudstone and Appin colliery shale did not exhibit any time-dependent strengths by the short-term methods used for predicting long-term strengths in this project. These rocks did not show any plastic deformation before fracture, which indicated that the strengths of these rocks are independent of time, at least to the limit of sensitivity of the measurements in the present investigation.

Kambalda basalt and Lilydale limestone mostly behaved in an elastic manner to the point of rupture, where the specimens failed suddenly in an explosive manner. A few specimens of Broken Hill South gneiss did show plastic behaviour but only after the stress reached its maximum value and there remained constant up to rupture while deformation continued at the same rate (Fig. 6).

Mt. Isa greenstone, Cobar mudstone and Appin colliery shale mostly failed along their pre-existing weakness planes and their stress-axial strain curves were linear up to rupture. In such rocks the weakness planes and their orientation to direction of loading play more important roles than the rock material itself.

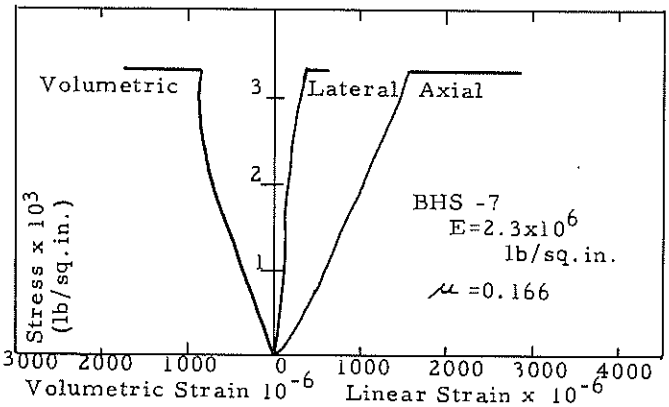

Fig. 6 Stress-strain curves for Broken Hill South Gneiss tested in uniaxial compression

XI.- TIME-DEPENDENT STRENGTHS

Wombeyan and Sicilian marbles were selected for the study of strength-time behaviour as they were found to have smaller variation in their strengths than other rocks tested in this programme. The coefficients of variation for strengths of Sicilian marble and Wombeyan marble were 0.036 and 0.085 respectively.

Table 2 shows the lengths of time passing before fracture occurred when sustained loads, equal to various fractions of the average short-term unconfined compressive strengths, were applied to the specimens in the long-term loading apparatus. Because of the effects of 2 natural variabilities, that of maximum strength, and that of the ratio of long-term strength to maximum strength, a large amount of scatter is evident when each point is plotted individually. To reduce this scatter, all results from tests carried out at tests of 3 consecutively lower sustained stress levels were grouped and averaged, to give each figure shown in Table 2. More emphasis in the testing was put on Sicilian marble, which has a lower coefficient of variation in strength than does Wombeyan marble; this, plus the higher number of test specimens, leads to more consistent results for the former rock.

The strength-time curve of Sicilian marble (Fig.7) shows a scatter of points but the general trend is that the curve is asymptotic at about 85 per cent of the average strength of the rock determined by short-term uniaxial tests. Therefore it is concluded that the long-term strength of Sicilian marble is about 85 per cent of its uniaxial compressive strength. This figure is quite close to the predicted percentage long-term strengths i.e. 87.8% by load rate method, 88.7% by stress-strain method and 84.9% by log stress-log strain method. Therefore it can be concluded that these proposed short term methods provide a quick estimation of long-term strengths of Sicilian marble and it is expected that these will be valid in other similar rocks also. The volumetric strain method, with the equipment used in the present investigations, predicts higher (94% of average compressive strength) time-dependent strength Therefore the time-dependent strength predicted by the volumetric strain method should be treated with reserve.

TABLE 2

RESULTS OF SUSTAINED LOADING TESTS

Rock Type	Sustained Stress Average Max. Strength	Time to Fracture (hours)
Wombeyan Marble	0.97	2.58
	0.90	23.31
	0.87	56.88
	0.81	52.84
Sicilian Marble	0.97	6.86
	0.94	2.66
	0.90	14.61
	0.87	253.1
	0.83	544.3

It is emphasised that these short-term methods of predicting the long-term strengths are based on Bieniawski's hypothesis which is for intact brittle rocks. It would be erroneous to assume that the long-term strength was 100% of the uniaxial short-term strength in those rocks which failed along weakness planes and exhibited linear stress-strain or load-deformation behaviour up to failure.

Mt. Isa greenstone and Appin colliery shale are understood to behave in a plastic manner in the field but the specimens of these rocks tested in uniaxial compression did not exhibit any predicted time-dependent strengths. This is probably due to the presence of weakness planes along which the specimens mostly failed. In pillars underground, failure along weakness planes might be inhibited due to end constraint.

It has also been reported that as the diameter-height ratio of the specimens increase in plastic materials, the tendency of the specimens to flow rather than to fracture increases (Ref. 17). This may be true for the observed flow underground where the ratios of the widths of the pillars to their heights are expected to be a lot higher than the one adopted in the present uniaxial tests. The flow observed in the pillars underground is due to failure of the rock material, as distinct from failure along weakness planes in the uniaxial tests.

XII.- CONCLUSIONS

The stress-axial strain curves of many rocks tested in the present investigation exhibited non-linear behaviour in the comparatively low-stress region, linear or quasi-linear behaviour in the middle region and again nonlinear behaviour near the failure stress.

Young's modulus and Poisson's ratio were found to be stress dependent. In most rocks tested in this program Young's modulus was found to be smaller at low stresses, constant in the middle stress region and again low near maximum failure stress. The Poisson's ratio was found to be smaller at low stresses, constant up to about 50% of failure stress and at higher stresses increased continuously.

The variability of strengths of rocks is a major problem in the study of strength-time behaviour, and may be why not much conclusive work has been done on it.

Microfracturing is an important mechanism of creep and dilatancy may be entirely attributed to this process. This suggests the basis of indirect methods of determining long term strengths. The short-term methods of predicting long-term strengths such as loading rate, stress-strain and log stress - log strain predicted the long-term strength of Sicilian marble quite close to the long-term strength determined by the direct method. The volumetric strain method predicted higher values of long-term strengths than those obtained by the direct method. With the present equipment, the loading rate method was found to be quicker and more accurate than the other short-term methods.

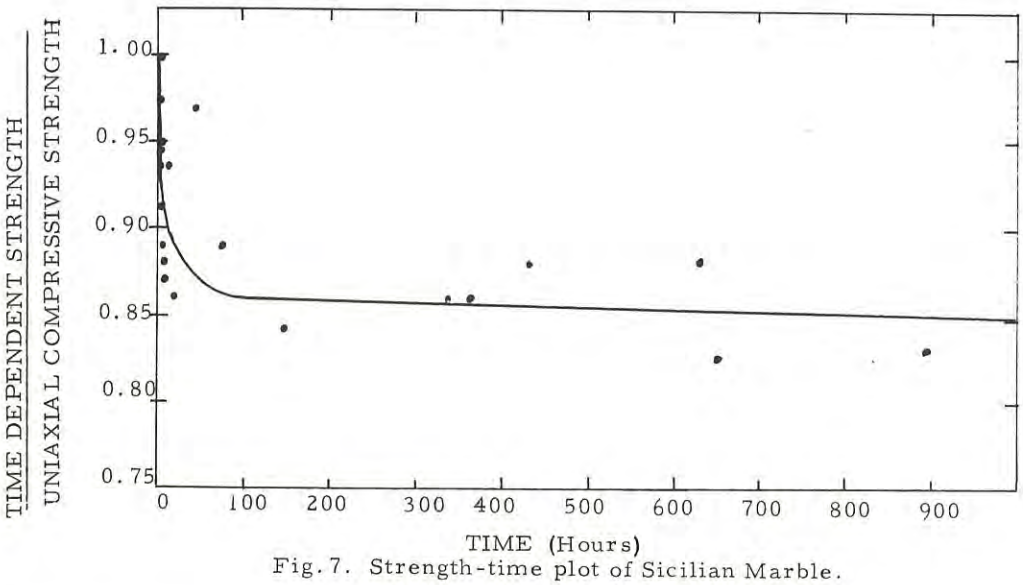

Fig. 7. Strength-time plot of Sicilian Marble.

The effect of moisture on long-term strength of rocks has not been investigated in detail. Wiid (Ref. 13) suggested that the long-term strength of a rock in wet conditions is inferred by the stress at which the volumetric strain curve starts deviating from linearity. The crack propagation in a long-term test is slow by comparison with the rate of moisture migration and therefore propagating cracks could be wetted easily. Since not much work has been done to establish this point, it will be worthwhile to do direct long-term tests in wet conditions and see if the strength thus found is close to the stress initiating stable fracture propagation in short-term compressive tests.

REFERENCES

1. PRICE, N.J. - Study of time-strain behaviour of coal measure rocks. Int. J. Rock Mech. Min. Sci. Vol. 1 1964, pp. 277-303.

2. EVANS, R.H., and WOOD, R.H. - Transverse elasticity of natural stones. Proc. Leeds Phil. Lit. Soc. Vol. 3, (5) 1937, pp. 340-352.

3. MATSUSHIMA, S. - On the flow and fracture of igneous rocks. Disaster Prevent. Res. Inst., Kyoto University Bull. Vol. 36 1960, pp. 1-9.

4. RUMMEL, F. - Studies of time-dependent deformation of some granite and eclogite rock samples under uniaxial, constant compressive stress and temperatures up to 400°C. Zeitschrift fur Geophysik, Vol. 35 1969, pp. 17-42.

5. ROBERTSON, E.C. - Creep of Solenhofen limestone under moderate hydrostatic pressure. In Rock Deformation Geo. Soc. Am. Mem. 79, 1960, pp. 227-244.

6. WATANABE, H. - The occurrence of elastic shocks during destruction of rocks and its relation to the sequence of earthquakes. Geophysical Papers Dedicated to Professor Kanso Sassa, 1963, pp. 653-658.

7. SCHOLZ, C.H. - Mechanism of creep in brittle rock. J. Geophys. Res. Vol. 73 (10) 1968, pp. 3295-3302.

8. BRIDGMAN, P.W. - Volume changes in the plastic stages of simple compression. J. Appl. Phys. Vol. 20 (12) 1949, pp. 1241-1251.

9. OROWAN, E. - Fracture and strength of solids. Rept. Progr. Phys., Vol. 12, 1948-49, pp. 185-232.

10. BRACE, W.F. - Brittle fracture of rocks, Int. Conf. State of Stress in the Earth's Crust, pp. 111-180. New York, Elsevier, 1964.

11. BIENIAWSKI, Z.T. - Mechanism of brittle fracture of rock. Int. J. Rock. Mech. Min. Sci. Vol. 4, 1967, pp. 395-430.

12. DEKLOTZ, E.J., HECK, W.J., and ALDRICH, M.J. - Development of equipment for studying pore pressure effects in rock, Tech. Rep. No. 3-68, Dept. Army, Missouri River Div. Omaha, 1968 pp. 52.

13. WILD, B.L. - The time-dependent behaviour of rock: consideration with regard to a research programme. Rept. S.A. Coun. Sci. Ind. Res. No. MEG 514, 1966.

14. RUSCH, H. - Physical problems in testing of concrete. Zement-Kalk-Gips. Vol. 12 (1) 1959, pp. 1-9.

15. DESAYI, P., and VISHWANATH, C.S. - True ultimate strength of plain concrete. RILEM Bull. No. 36 1967, pp. 163-173.

16. HOSKINS, J.R. and HORINO, F.G. - Effect of end conditions on determining compressive strength of rock samples. U.S. Bureau of Mines Rept. Inves. 7171, 1968.

17. OBERT, L. - Creep in model pillars. U.S. Bur. Min. Rept. Invest. No. 6703, 1965.

Liquefaction of Saturated Granular Soils

By

M. Kurzeme, B.E., M.Eng.Sc., Ph.D., Grad.I.E.Aust.

(Research Scientist, Division of Applied Geomechanics, C.S.I.R.O.)

SUMMARY.- The current status of published knowledge on the process of liquefaction in saturated granular soils is reviewed. Methods of determining material properties and initial conditions defining liquefaction response are investigated and their relevance to predictive methods examined. The importance of documenting observed cases of liquefaction under earthquake or other dynamic loading is stressed as being the only means of testing the validity of the investigation and prediction techniques.

I.- INTRODUCTION

Liquefaction is the phenomenon of the partial or total loss of strength and stability of saturated granular soils under the effect of dynamic loading. The source of the dynamic loading may be seismic events, blasting in mines and quarries, or machine foundations, and liquefaction can occur in filled land, embankments, dams, under building foundations and machine bases, and in hydraulically placed mine fill.

The shear strength τ_f of cohesionless granular soils under undrained conditions may be expressed as:

$$\tau_f = (\sigma - u_w) \tan \phi' \qquad \ldots(1)$$

where σ = total normal stress on the plane of failure,
u_w = pore water pressure, static plus dynamic,
ϕ' = effective angle of internal friction.

When such a soil is subjected to a suitably severe disturbance the pore water pressure u_w may rise to a value equal to the total normal stress σ, and the shear strength τ_f would drop to zero. In this condition the soil exhibits the properties of a viscous liquid and the phenomenon is known as liquefaction.

The process may be described qualitatively in the following sequence.

(i) Seismic energy from blasting or earthquake activity transmitted through the saturated soil mass causes a breakdown in the particle structure.
(ii) The structural breakdown, either sudden or progressive, accompanied by a re-orientation of the soil particles into a denser configuration, increases pore water pressures and reduces shear strength. This process results in some surface settlement of the soil mass.
(iii) When excess pore water pressure becomes equal to the confining pressure, the soil particles go into suspension and the soil mass liquefies. Superimposed structures begin to sink to attain hydrostatic equilibrium.
(iv) Dissipation of the excess pore water pressure is accompanied by a consolidation type process resulting in further surface settlement of the soil mass.
(v) The upward transport of water may maintain the liquefied state at the surface of the soil mass for a considerable period after the cessation of the seismic disturbance.

In consequence, structures which are founded on liquefying material settle as a result of recompaction and consolidation of the soil mass, and as a result of the failure and displacement of the liquefied material. Non-uniform structural and loading conditions, or non-homogeneous soil conditions, may modify the settlement and produce differential settlements or severe tilting of the structures (Ref. 1).

Buried structures (empty underground tanks, pipes and timber piles) experience severe hydrostatic upthrust and may rise to the surface during the liquefied condition (Ref. 2, 1). Embankments or slopes constructed of material that liquefies would spread and slump excessively, or fail by flowing downhill. The surface may exhibit large cracks as a result of lateral movement with corresponding distress to any superimposed structures (Ref. 3).

The dissipation of the excess pore water pressure, combined with general surface settlement, results in surface flooding (Ref. 2). The low permeability of silts and fine sands prevents rapid dissipation of the excess pore water pressure, and surface flooding, together with settlement of superimposed structures, may continue over a period of several minutes after the seismic shaking. If the soil deposits are non-homogeneous in permeability, the dissipation of excess pore water pressures may be concentrated at points of high permeability causing sand blows and sand volcanoes to eject considerable quantities of material (Ref. 4).

II.- RECENT EXAMPLES OF LIQUEFACTION

Damage to structures due to foundation material failure, and the collapse of slopes and embankments attributed to liquefaction, have been observed throughout history (Ref. 3). However, it is only recently that the available examples of liquefaction failure have received more than a general, dramatic description. Documented recent cases of widespread liquefaction failure resulted from seismic events in Chile 1960,

TABLE I

RECENT EXAMPLES OF LIQUEFACTION

Location	Chile	Alaska	Japan (Niigata)
Date	1960	1964	1964
Earthquake Magnitude	8.4	8.3	7.3
Maximum Modified Mercalli Intensities	XI	-	VIII
Epicentral Distances	160 - 400 km	60 - 150 km	60 km
Soil Conditions	Fluvial and glacial gravels, sands, silts, unconsolidated soil placed by dumping or hydraulically.	Sand layers and lenses in clay deposits; silts, sands and gravels.	Alluvial sands, filled land.
Phenomena Observed	Settlements and tilting of buildings and foundations, slumping of highway and railway embankments, overturning of bridge abutments and old walls. Mud pumping.	Coastal slope failures, slumping and cracking of beach and deltaic deposits.	Settlement and tilting of buildings, slumping and cracking of ground surface, slumping of embankments and sliding of slopes, surface inundation and sand boils.
References	Ref. 5, 3	Ref. 3	Ref. 6, 2

Alaska 1964, and Japan (Niigata) 1964 (Ref. 5, 3, 2, 6). A summary of data is given in Table I. In these cases severe damage to structures was caused by ground failure due to liquefaction rather than the direct effect of vibrations.

Examples of observed liquefaction response have defined areas susceptible to this type of failure. These areas include thick deposits of loose alluvial soils, saturated sand layers and lenses within otherwise stable soil masses, reclaimed land formed by hydraulic filling or dumping without compaction, and slopes and embankments of loose granular material. The problem is to predict the behaviour of any particular mass of granular soil when subjected to a dynamic disturbance. The duration of the disturbance can be short as from blasting, intermediate as from earthquakes, or continuous as caused by traffic or machine foundations. The volume of the soil mass involved is also dependent on the nature of the dynamic disturbance.

III.- REVIEW OF LIQUEFACTION RESEARCH

Liquefaction research has only developed during the last decade and has been directed primarily toward defining the soil properties and ambient conditions that control liquefaction response, and toward quantifying these parameters. Laboratory work has been restricted to the cyclic load testing of small, remoulded samples of soil in specially adapted triaxial loading apparatus or simple shear apparatus, and to the testing of bulk samples of remoulded soil subjected to cyclic or transient accelerations on a shaking table. The laboratory tests of liquefaction response are summarized in Table II.

The use of blasting methods in the field testing of granular soils to determine liquefaction response *in situ* has been pursued to a limited extent for evaluating limiting values of particle velocity to cause liquefaction (Ref. 7) and extending the range of laboratory results (Ref. 8).

Early research into liquefaction response pursued the concept of a critical acceleration. MOGAMI *et al.* (Ref. 9) applied the term liquefaction to the loss of strength in dry sand subjected to vertical acceleration. The shear strength was found to decrease with increasing vertical acceleration, reaching a value of approximately 20 per cent of the static shear strength at a vertical acceleration of 1g, thereafter decreasing slowly with further increase in vertical acceleration. The phenomenon was explained by KOLBUSZEWSKI *et al.* (Ref. 10) in terms of a decrease in effective stress on the potential horizontal failure plane with increasing vertical acceleration. Theoretically, the vertical effective stress would be zero at a vertical acceleration of 1g (the critical acceleration), with the strength dropping to zero. This condition occurs only over a small part of each cycle of acceleration which, together with the interlocking of the grains, provides some residual strength at accelerations greater than 1g. The mechanism of reducing the effective stress in this case is not dependent on the development of excess pore fluid pressure, so that neither the number of cycles of loading nor the frequency were controlling factors.

MASLOV (Ref. 11) considered the stability of submerged sandy foundations and structures under the effect of dynamic loading and developed a theory describing the total or partial loss of strength of the sand in such conditions. In the critical acceleration concept proposed, any phenomenon of a dynamic character was completely ruled out at accelerations below the critical value. The critical acceleration for any sand was determined experimentally and was found to depend on the properties of the sand (unspecified), its density (initial relative), the amplitude and frequency of acceleration, and the normal pressure imposed by the overburden and superimposed loads. The critical acceleration was therefore not uniform for the whole sand mass, but varied with depth. The

TABLE II

LABORATORY TESTS OF LIQUEFACTION RESPONSE

Investigator	Year	Sample Type	Sample Size	Type of loading simulated	Test Variables	Parameters Measured	Ref. No.
MASLOV	1957	Bulk Sample	Up to 25 ton	Vertical & Horizontal Vibrations	Porosity Acceleration Type of sand	Pore water pressure	11
FLORIN	1961	Bulk Sample	20cm thick	Impact and Vibration	Porosity	Pore water pressure Time of liquefaction	12
HUANG	1961	Triaxial		Vertical Vibration	Void ratio Confining pressure Acceleration	Pore water pressure	13
SEED	1966	Triaxial		Shear Waves	Void ratio Confining pressure Cyclic stress amplitude Cyclic strain amplitude	Axial strain Pore water pressure Cyclic stress Number of cycles	15
LEE	1967	Triaxial		Shear Waves	Void ratio Confining pressure Cyclic stress amplitude Failure criterion	Axial strain Pore water pressure Number of cycles Cyclic stress	16
SCHROEDER	1968	Triaxial		Compressional Waves	Void ratio Effective stress ratio Continuing pressure Initial pore pressure Cyclic stress amplitude	Axial deformation Pore water pressure Number of cycles	17 18
YOSHIMI	1967	Bulk Sample	50x25x27cm	Horizontal Vibration	Void ratio Surcharge pressure Acceleration Frequency	Pore water pressure Acceleration	19
TANIMOTO	1968	Bulk Sample	80x80x130cm	Horizontal Impact	Void ratio	Pore water pressure Acceleration Surface settlements	20 21
PEACOCK	1968	Simple Shear	6x6x2cm	Shear Waves	Void ratio Confining pressure Cyclic stress amplitude Frequency	Shear strain Pore water pressure Shear stress Number of cycles	22
PRAKASH	1970	Bulk Sample	105x60x25cm	Horizontal Vibration	Type of sand Void ratio Acceleration Surcharge pressure	Pore water pressure Number of cycles Surface settlements	8
FINN	1970	Triaxial Simple Shear	 5x5x2.8cm	Shear Waves)))) Shear Waves)	Void ratio Confining pressure Cyclic stress amplitude Strain history	Axial strain Shear strain Pore water pressure Applied stress Number of cycles	23

theoretical expressions were apparently adequately confirmed by experiment using small sample laboratory methods and large capacity (9 and 25 ton) field equipment.

FLORIN *et al.* (Ref. 12) defined the liquefaction conditions as the collapse of the structure of the sand, with the possibility of sand consolidation, and either partial or total saturation of the sand with water. The criteria of collapse proposed were intensity of disturbance, stress condition and weight of surcharge, and hydraulic gradient of water flow. The displacement of the soil surface and superimposed structures was then determined by the duration of the liquefied condition and the viscosity of the liquefied mass. This duration was found to depend on the thickness of the layer, the permeability, rate of change of volume of voids, intensity and location of drainage and duration of dynamic loading.

The change in porosity was observed experimentally

by changes in conductivity, pore pressure measurement using membrane type cells; the change in viscosity by the sinking of heavy bodies placed on the surface.

FLORIN found that under impact loading, a large sample of loose, saturated sand liquefied simultaneously over the entire depth of the responding stratum, and that increase of impulse intensity led to an increase in the depth of the liquefied zone, but not to an increase in the sand consolidation. The increased depth of the responding stratum appears to be consistent with MASLOV's critical acceleration concept. Consolidation took place from the bottom of the liquefied zone, with the surface layers remaining in the liquefied condition. Subsequent impact loads of the same intensity produced decreased depths of liquefaction.

Continuous vibration of a large sample produced liquefaction from the surface downwards. The surface layers liquefied first because of low overburden pressure, which in turn reduced the overburden pressure on the underlying layers and permitted them to liquefy. This description of the sequence of events masked the effect of the increased number of cycles of loading before liquefaction occurred in the lower layers. As soon as the entire stratum had liquefied consolidation occurred from the bottom up.

Based on laboratory experience, FLORIN concluded that all sufficiently loose, granular soils of any grain size may liquefy, as liquefaction is only an intermediate state between two stable states of compaction. The time, however, during which the liquefied state persists may vary greatly; for example, after the first impact of an impact test, a coarse sand remained liquefied for approximately 2 sec, while a fine sand remained liquefied for approximately 30 sec.

The presence of overburden required an increase in the intensity of the disturbance. FLORIN concluded, therefore, that at depths below the ground surface in excess of 10 to 15 m even very loose sands cannot be liquefied.

Using as an empirical indicator the surface settlement (in excess of 8 cm) at a radius of 5 m, FLORIN also proposed a 'standard' field blasting method (5 kg of explosives at 8-10 m deep) to determine susceptibility to liquefaction in the field.

HUANG (Ref. 13) investigated the liquefaction resistance of a remoulded silty sand sample under triaxial conditions as opposed to the anisotropic confining conditions experienced in bulk samples. The triaxial sample, with various values of vertical and lateral stress imposed, was subjected to vertical acceleration on a shaking table. The results showed that the developed pore water pressure decreased as the initial density, lateral and vertical stress increased, and acceleration decreased.

HUANG suggested that, using the results of the tests described, it was possible to determine the pore water pressure developed at any point in a given sand foundation under any dynamic loading. The key to the solution was to find the relationship between developed pore water pressure, intensity of dynamic action and state of stress in the sand mass. At that stage, the duration of the dynamic loading, implying progressive build-up of pore water pressure, was still not considered to be an important parameter.

Using dimensional analysis, BAZANT (Ref. 14) developed a concept of liquefaction acceleration which defines a critical value below which liquefaction cannot occur. The liquefaction acceleration was found to be a function of the soil density, the frequency of the vibration, the depth of the layer and the amplitude of the ground motion. The concept was developed from a consideration of dynamic stability of saturated sand. Stability was defined as the occurrence or non-occurrence of compaction under the action of a vertical acceleration. BAZANT assumed that earthquakes imparted predominantly vertical acceleration in the zones of interest; that is, longitudinal waves propagating vertically from the bedrock through the soil layers causing alternating compression and dilation within the soil. The presence of transverse waves was assumed to assist the compaction and increase the possibility of liquefaction and the loss of stability. BAZANT concluded that the measurement of profiles of soil density is one of the crucial points of examination in the investigation of the dynamic stability of an area.

The experimental studies of SEED *et al.* (Ref. 15) were the first to move away from the concept of critical acceleration and attempted to simulate the performance of soil elements within a soil mass subjected to an assumed seismic loading. The critical acceleration values, developed theoretically and experimentally previous to this time, were considered by SEED to be influenced by the frequency and duration of the shaking before liquefaction occurred and possibly also by the geometry and deformation of the container.

An element of soil within a soil mass is subjected to a complex system of loading, but SEED assumed that the major part of the soil deformation could be attributed to the upward propagation of shear waves from underlying layers. Therefore, each element of soil may be considered as being subjected to a series of cyclic shear stresses and strains. This condition, as imposed on a soil element under a level ground surface, could be approximately reproduced on a triaxial sample when tested in cyclic compression under undrained conditions.

Using this method, SEED established that under cyclic loading the pore water pressure gradually increased until it equalled the initial confining pressure. The deformation then increased suddenly and the soil was said to have liquefied. The number of cycles of loading required to cause liquefaction were found to depend on the initial void ratio, the initial confining pressure and the magnitude of cyclic stress. The authors concluded that the danger of liquefaction of a saturated sand as a result of cyclic loading was determined qualitatively by the following.

(i) The void ratio of the sand - the higher the void ratio the more easily liquefaction will occur.
(ii) The confining pressure acting on the sand - the lower the confining pressure the more easily liquefaction will develop.
(iii) The magnitude of the cyclic stress or strain - the larger the stress or strain the lower the number of cycles required to induce liquefaction.
(iv) The number of stress cycles to which the sand is subjected.

LEE *et al.* (Ref. 16) also used triaxial samples subjected to cyclic loading to quantify the qualitative

relationships established by SEED *et al.* (Ref. 15). LEE defined and used a number of failure criteria to study the susceptibility of sand to liquefaction and the development of large shear strains. The authors concluded that liquefaction resistance was determined by a complex, as yet undefined, relationship between the factors considered. However, over some ranges of the variables, approximately linear relationships existed, for example, between the relative density and the cyclic stress, and the confining pressure and the cyclic stress required to cause initial liquefaction in a given number of cycles of loading. These approximate relationships allow an estimate of the depth at which initial liquefaction takes place under any variation of cyclic stress with depth within the soil.

SCHROEDER *et al.* (Ref. 17, 18) also used a triaxial apparatus to investigate the liquefaction potential of sand samples under various conditions. Disregarding the effect of S waves (shear), SCHROEDER assumed that the primary cause of liquefaction was due to the arrival of P waves (longitudinal) at the site of interest, and tested the triaxial samples accordingly. The sudden onset of liquefaction was not observed, but a gradually increasing axial strain with increase in the number of cycles of loading was observed. The developed pore water pressures appeared to be asymptotic to a peak value which increased with increasing void ratio. It was found that the pore water pressure increased and hence liquefaction tendency increased with:

(i) decreasing initial effective stress ratios,
(ii) decreasing initial effective confining pressures,
(iii) increasing disturbance, and
(iv) increasing ratio of initial pore water pressure to initial intergranular pressure.

These findings were in general agreement with those of SEED *et al.* (Ref. 15) but the tests did not reproduce sudden liquefaction.

YOSHIMI (Ref. 19) conducted tests on large samples in a rigid box covered with an impervious membrane, with surcharge applied, and subjected to horizontal vibrations. The difference between this and other bulk sample tests (Ref. 12) was the presence of the impervious membrane and the disregard for the critical acceleration concept. YOSHIMI observed the pore water pressure increase at various depths within the sample (50 x 25 x 27 cm) and discovered that the process leading to complete liquefaction consisted of two distinct steps. The first was a period during which the pore water pressure at different depths increased uniformly and simultaneously while the sand remained stable, and the second was a very rapid rise in pore water pressure until it reached a value approximately equal to the total stress at that particular depth.

YOSHIMI idealized the pore water pressure-time curve into five distinct stages.

(i) Gradual increase in excess pore water pressure due to initial compaction process.
(ii) Sharp increase in pore pressure to a peak value, with sudden liquefaction.
(iii) Liquefied state with no change in pore water pressure.
(iv) Consolidation process proceeding from the bottom up with gradual decrease in pore water pressure.
(v) Stabilized state with excess pore water pressure at level of surcharge pressure in the constant volume apparatus.

These observations generally confirmed those of SEED *et al.* (Ref. 15), obtained by using the triaxial apparatus with considerably different boundary conditions and method of loading.

TANIMOTO (Ref. 20, 21) also observed distinct stages of development in the liquefaction process but in terms of surface settlement as well as excess pore water pressure development. TANIMOTO used an 80 cm square sand bin, 130 cm high, mounted on a vibration table and subjected to horizontal impact loading. The total surface settlement due to a single impact was found to consist of two components, one attributed to the temporary collapse of the granular structure of the sample leading to the development of excess pore water pressure, and the other to the dissipation of the excess pore water pressure accompanied by the squeezing out of the pore water. The latter phenomenon appeared to approximate general consolidation process. The magnitude of the two displacements appeared to be approximately equal, while the response times were in the approximate ratio of 1:100.

PEACOCK *et al.* (Ref. 22) developed and used a new sample testing technique which simulated the assumed ground conditions rather better than the triaxial test method, and it was claimed that this was the best possible means of evaluating quantitatively the stresses inducing liquefaction. The method applied a cyclic horizontal shear load to a small prismatic sample (6cm x 6cm x 2cm deep) of remoulded sand which was subjected to a vertical surcharge load. The general relationships between initial relative density, peak-pulsating shear stress, confining pressure and number of cycles of loading to produce liquefaction, were found to be substantially the same as those observed with triaxial samples. However, the value of the peak-pulsating shear stress to cause liquefaction in a given number of cycles in the simple shear apparatus was found to be approximately one third of that in the triaxial apparatus. The discrepancy could be partly attributed to the difficulty in preparing uniform samples in a sharp-cornered mould. Samples of non-uniform initial relative density appeared to have increased susceptibility to liquefaction. Special preparation of samples indicated that the value of the peak cyclic shearing stress, required to cause initial liquefaction under specified conditions, increased to approximately half of that in the triaxial tests. The discrepancy may also be attributed to differences in confining conditions found in the triaxial sample and the simple shear sample.

PRAKASH *et al.* (Ref. 8) used a vibration table and bulk sample to determine the liquefaction response of different sands. The sample size was 105cm x 60 cm x 25cm deep and a vertical surcharge could be applied. The general relationships between relative density, confining pressure, acceleration, and duration of loading were much the same as noted by other workers. One finding of interest was that, under an initial surcharge corresponding to an overburden of about 4m, the excess pore water pressure developed was negligible, and indicated that liquefaction may not occur below this depth in the sand tested.

FINN *et al.* (Ref. 23) extended the methods of triaxial and simple shear testing used by SEED *et al.* (Ref. 15) and PEACOCK *et al.* (Ref. 22) and developed a

procedure for comparing the results of simple shear and triaxial tests to show that they are equivalent and consistent with each other. The liquefaction resistance (number of cycles of loading to cause liquefaction) of a particular sand is uniquely defined by the initial effective confining pressure, the peak cyclic shear stress and the initial void ratio if the remoulded sand sample has not undergone any previous shear strain. For all other sand samples the liquefaction resistance appears to be predominantly controlled by the strain history of the sand.

FINN has indicated that a threshold value of the previous shear strain exists for a particular sand below which liquefaction resistance is increased, but above which liquefaction resistance is drastically decreased. All other controllable conditions are substantially identical. This change in liquefaction resistance has been attributed to the formation of a new soil structure which is particularly weak in resisting cyclic shear loads. The threshold value also depends on the number of times the particular shear strain has been cycled.

This work throws doubt on the validity of predictive techniques utilizing liquefaction response relationships observed on remoulded soil samples, and indicates the need to develop methods of *in situ* testing where the effects of the previous strain history of a soil mass are preserved. In any field situation, however, great difficulties are encountered in determining the material properties.

IV.-PREDICTION OF LIQUEFACTION RESPONSE

Research into liquefaction response has established that the resistance to liquefaction, expressed in the number of cycles of loading is defined by the confining pressure, the relative density, the magnitude of the cyclic stress and the strain history. No functional relationships linking the parameters involved, have been developed, and therefore no analytical solutions are available to predict the performance of a soil mass prone to liquefaction. However, various methods of conceptual, mathematical and physical modelling are available which can give an indication of the response under assumed loading conditions. In many cases the prediction may be restricted to defining whether liquefaction will or will not occur without indicating the extent or the duration.

For example the response of a soil mass with a horizontal surface may be investigated, and the depth at which initial liquefaction will occur predicted, using the results of laboratory investigations (Ref. 16). The confining stress in such a case increases linearly with depth of overburden. Laboratory tests indicate that the cyclic stress required to cause liquefaction in a specified number of cycles increases approximately linearly with confining pressure. The depth to initial liquefaction may then be defined for any variation of cyclic stress amplitude with depth. Liquefaction would first occur at the depth where the assumed cyclic stress variation corresponds with the least number of cycles required to cause liquefaction at a particular cyclic stress amplitude. Thus, if the assumed cyclic stress amplitude distribution is uniform with depth, liquefaction will be initiated at the surface and progress downwards with increasing number of cycles, assisted by the progressively reducing overburden pressure on the underlying soil as the surface layers liquefy. Alternatively, if the assumed cyclic stress amplitude increases uniformly with de the whole layer may be expected to liquefy simultaneously after the requisite number of cycles.

To predict response to impact loading, AMBRASEY *et al.* (Ref. 24) have proposed an alternative relati ship by defining a critical particle velocity, rela to the cyclic shear stress above which shear failur occurs. Liquefaction under cyclic loading conditio is initiated by progressive shear failure, but this will not take place until the critical particle vel ocity is exceeded. The relationship includes a por pressure parameter which depends on the time histor of the loading, but the form of this dependence has not been defined.

From the above considerations it follows that, initial liquefaction occurs within a soil mass at s point below the surface, the surface layers will be protected from further loading because the liquefie stratum cannot transmit shear stresses.

With structures of complex geometry, such as bu ing foundations, slopes, embankments and retaining walls, it is necessary to modify the previously described method because of the unknown distribution o confining stresses. One method, used in analysing the response of a dam founded on liquefaction-prone soil, has been described by SEED *et al.* (Ref. 25). The technique uses the finite element method of det mining the initial static stress distribution withi the soil mass. The base boundary is then subjected to an assumed seismic loading and the time history dynamic stressing of each soil element is inspected after an appropriate number of loading cycles. Laboratory cyclic loading tests, conducted under simpl shear conditions, are made to determine the equivalent uniform cyclic stress required to cause liquefaction in a given number of cycles of loading for range of initial confining pressures.

After each period of loading, the time histories of the complex dynamic shear stresses are equated t an equivalent number of cycles of uniform stresses. These values are compared to the stresses required t cause liquefaction under the appropriate confining stress conditions, the liquefied zone defined, and the stability of the structure investigated. Since the liquefied zone cannot sustain shear stresses, a new 'initial' stress distribution is defined for the next period of loading. The process is repeated until the end of the period of seismicity, and the increase in the extent of the liquefied zone can be followed progressively and the stability of the structure investigated at the end of each arbitrari chosen period of loading.

Another method of predicting the response of a complex structure is to use physical models. KRISHN *et al.* (Ref. 26, 27) used this means to investigate the possible liquefaction of foundation material under a dam. A scale model (1:200) of the dam and foundations was constructed and subjected to an approximately scaled periodic acceleration. The sand tested was found not to be prone to liquefaction und the anticipated ground motions at a relative density of 20 per cent. However, settlement due to compacti under the assumed ground motion would be of apprecia ble magnitude.

Field testing of liquefaction-prone material *in situ* is also a means of predicting whether liquefact

will occur under an assumed loading. KRISHNA and PRAKASH (Ref. 27) and PRAKASH *et al.* (Ref. 28) have described field blasting techniques used to obtain an indication whether liquefaction would occur in dam foundations of saturated sands.

V.- CONFIRMATION OF PREDICTIONS

In the development of any methods of predicting response, the most difficult step is the field observation of the response of the prototype structure to the design loadings. This step is necessary to determine the adequacy of the prediction technique and the relevance of the material properties and initial conditions used in the prediction. With liquefaction response the problem is compounded by the relatively infrequent occurrence of the design conditions and the difficulty in determining the margin of safety, if the prototype is subjected to the design loading and liquefaction failure has not actually taken place. Consequently, it is necessary to investigate any available examples of liquefaction failure.

The relatively recent development of an awareness of the factors defining liquefaction response has precluded the use of this knowledge in previous investigations of liquefaction-prone areas. While soil conditions after liquefaction may be studied in detail, the relevant soil conditions prior to the event are not usually known nor is the history of seismic shaking.

This problem was encountered by MARSAL (Ref. 29) in describing the effects of the Jaltipan (Mexico) Earthquake of 1959. No detailed information was available of the soil conditions existing prior to the earthquake, and the soil properties defined and tests used after the earthquake were not directly related to liquefaction response. The conclusions that structural damage resulted from soil liquefaction appear to have been drawn from the magnitude and nature of settlements and displacements rather than as a result of the subsequent soil exploration.

Notable exceptions to this problem occur when studying the response of man-made soil structures, such as dams or embankments, where detailed construction records have been kept, and in recently developed areas of cities where relevant material properties existing prior to the seismic event, may be deduced from the results of conventional site investigation procedures. The latter case occurred in Niigata (Ref. 30, 6) where in the course of development many borings and standard penetration tests had been carried out. It was possible to construct pre-earthquake soil profiles in terms of SPT N-values. As a result of ground failure through liquefaction, the area of the heaviest structural damage corresponded to the area of recent fluvial deposition and was also enclosed by the line defining the area of N = 20 or less at a depth of 5 m.

From the analysis of soil liquefaction at Niigata and other investigations it can be said that a saturated granular soil is prone to liquefaction under the effects of a moderate seismic loading (Modified Mercalli Intensities of VII-VIII), if the standard penetration test value N = 20 or less in the top 10 m. Standard penetration test results are usually available from conventional site investigations and require no specialized techniques to be developed. The test procedure imposes a standard intensity impact loading on the soil *in situ*. The resulting number of blows per unit displacement recorded depend in some complex manner on the relative density and confining pressure. The dynamic nature of the loading may cause liquefaction of a small volume of soil at the tip of the sampler thereby increasing the penetration per blow and reducing the N-value in liquefaction-prone soils.

In areas subjected to seismic activity, with structures founded on liquefaction-prone soil, it is desirable to investigate and measure the soil properties relevant to liquefaction response so that, if liquefaction occurs, the accuracy of methods of prediction can be confirmed. The soil parameters that require to be known are the relative density, the permeability, grain size distribution, particle orientation and soil fabric, stress-strain relationships, dynamic shear strength, and damping factors. This approach, however, would not be economical, and it may take a very long period of time before an adequate amount of useful information is accumulated.

Two approaches are available to overcome this problem. One method would be to establish a passive observational experiment in an area of known, high seismicity and suitable soil conditions. The soil conditions at the chosen site would be defined in terms relevant to liquefaction response and large concrete blocks of known weight and geometry constructed on the surface of the soil. Seismic accelerations would be monitored using appropriately located strong motion instruments, and the soil response monitored in terms of surface displacements, settlements of the concrete blocks and pore water pressure variations with time and depth. This would provide a means of obtaining relevant field observations over a reasonable period of time. Alternatively, if seismic events at a suitable site are not sufficiently frequent, explosives could be used to provide a seismic disturbance of desired duration and intensity.

VI.- SUMMARY AND CONCLUSIONS

Saturated granular soils, when subjected to seismic loading of sufficient duration and intensity, undergo a breakdown of the granular structure with attendant rise in pore water pressure. When the pore water pressure becomes equal to the total confining pressure, the effective intergranular stress becomes zero and the soil mass loses its strength. The soil now behaves as a viscous liquid and the phenomenon is termed liquefaction.

Laboratory methods have been developed that allow the material and environmental parameters controlling liquefaction response to be defined and general relationships to be established. This work has indicated that liquefaction resistance of a soil, expressed in terms of the number of cycles of loading necessary to cause liquefaction, is dependent on the initial relative density, the initial effective confining pressure, the magnitude of the cyclic shear stress, and the strain history of the soil. General trends have been established but no functional relationships are available defining the interrelationship between these parameters.

The results of laboratory investigations may be used to predict the response to seismic loading of liquefaction-prone soils. Prediction would in most cases be restricted to an indication of whether liquefaction would or would not occur, but no indication can be given of the extent of the liquefied zone or

the response of the system after liquefaction. Field tests using standardized blasting methods may also be used to predict whether liquefaction will occur under some assumed seismic loading.

Numerical methods are being developed which allow the development of the liquefied zone to be followed and the total stability of the soil mass and superimposed structures to be investigated progressively. These methods utilize the results of laboratory tests on small, remoulded soil samples, and difficulties may be encountered in predicting the performance of naturally occurring soil deposits where the strain history is unknown.

The most difficult step in developing a means of reliable liquefaction response prediction is the confirmation of the accuracy of the prediction. Analysis of observed liquefaction response is not very often helpful as the soil conditions prior to liquefaction are rarely available. This emphasizes the need for specially constructed field observation programs and the development of techniques of determining soil properties relevant to liquefaction response *in situ* so that the effects of the strain history are not destroyed.

REFERENCES

1. SEED, H.B. - Soil Stability Problems Caused by Earthquakes. Bituminous Materials Research Laboratory Rep., Dept. of Civil Engng, University of California, Berkeley, January 1967.

2. KAWASUMI, H. (Editor-in-Chief). - General Report on the Niigata Earthquake of 1964, Tokyo Electrical Engng College Press, 1968.

3. SEED, H.B. - Landslides During Earthquakes Due to Liquefaction. A.S.C.E. Journal of the Soil Mech. and Fdn Div., 1968, SM5, pp. 1055-1122.

4. HOUSNER, G.W. - The Mechanism of Sand Blows. Bull. Seismological Society of America, 1958, Vol. 48, pp. 155-161.

5. DUKE, C.M. and LEEDS, D.J. - Response of Soils, Foundations, and Earth Structures to the Chilean Earthquakes of 1960. Bull. Seismological Society of America, 1963, Vol. 53, No. 2, pp. 309-357.

6. SEED, H.B. and IDRISS, I.M. - Analysis of Soil Liquefaction Niigata Earthquake. A.S.C.E. Journal of the Soil Mech. and Fnd Div., 1967, SM3, pp. 83-108.

7. PUCHKOV, S.V. - Correlation between the Velocity of Seismic Oscillations of Particles and the Liquefaction Phenomenon of Water-Saturated Sands. Problems of Engineering Seismology. Consultant Bureau, New York, 1962, pp. 92-94.

8. PRAKASH, S. and GUPTA, M.K. - Liquefaction and Settlement Characteristics of Loose Sands under Vibration. Proc. Conf. on Dynamic Waves, University of Wales, Swansea, 1970, pp. 323-334.

9. MOGAMI, T. and KUBO, K. - The Behaviour of Soil during Vibration. Proc. 3rd Int. Conf. Soil Mech. and Fdn Engng, 1953, pp. 152-155.

10. KOLBUSZEWSKI, J. and ALYANAK, I. - Effects of Vibrations on the Shear Strength and Porosity of Sands. The Surveyor and Municipal Engineer, 1964, May 30 and June 6.

11. MASLOV, N.N. - Questions of Seismic Stability of Submerged Sandy Foundations and Structures. Proc. 4th Int. Conf. Soil Mech. and Fdn Engng, 1957, pp. 368-372.

12. FLORIN, V.A. and IVANOV, P.L. - Liquefaction of Saturated Sandy Soils. Proc. 5th Int. Conf. Soil Mech. and Fdn Engng, 1961, pp. 107-111.

13. HUANG, W. - Investigation on Stability of Saturated Sand Foundations and Slopes against Liquefaction. Proc. 5th Int. Conf. Soil Mech. and Fdn Engng, 1961, pp. 629-631.

14. BAZANT, Z. - Stability of Saturated Sand during Earthquakes. Proc. 3rd World Conf. on Earthquake Engng, 1965.

15. SEED, H.B. and LEE, K.L. - Liquefaction of Saturated Sands during Cyclic Loading, A.S.C.E. Journal of the Soil Mech. and Fdn Div., 1966, SM6, pp. 105-134.

16. LEE, K.L. and SEED, H.B. - Cyclic Stress Conditions Causing Liquefaction of Sand. A.S.C.E. Journal of Soil Mech. and Fdn Div., 1967, SM7, pp. 47-70.

17. SCHROEDER, W.L. and SCHUSTER, R.L. - Liquefaction Phenomena in Saturated Sands. 7th Annual Proc. Symp. on Engng Geol. and Soils Engng, University of Idaho, 1968.

18. SCHROEDER, W.L. and SCHUSTER, R.L. - Laboratory Simulation of Seismic Activity in Saturated Sands. Vibration Effects of Earthquakes on Soils and Foundations, ASTM, S.T.P. 450, 1969, pp. 57-70.

19. YOSHIMI, Y. - An Experimental Study of Liquefaction of Saturated Sands. Soil and Fdn, The Japanese Society of Soil Mech. and Fdn Engng, 1967. Vol. 7, No. 7, pp. 20-32.

20. TANIMOTO, K. - Liquefaction of Sand Layer Subjected to Shock and Vibratory Loads. Proc. 3rd Asian Reg. Conf. on Soil Mech. and Fdn Engng, 1967, Vol. 1, pp. 362-365.

21. TANIMOTO, K. - Study of Settlement Associated with Liquefaction of Sand Subjected to Impact Loads. Trans. of Japanese Society of Civ. Engrs, 1968, No. 152, pp. 39-44.

22. PEACOCK, W.M. and SEED, H.B. - Sand Liquefaction under Cyclic Loading, Simple Shear Conditions. A.S.C.E. Journal of the Soil Mech. and Fdn Div., 1968, SM3, pp. 689-708.

23. FINN, W.D.L., BRANSBY, P.L. and PICKERING, D.J. - Effect of Strain History on Liquefaction of Sands. A.S.C.E. Journal of Soil Mech. and Fdn. Div., 1970, SM6, pp. 1917-1934.

24. AMBRASEYS, N. and SARMA, S. - Liquefaction of Soils Induced by Earthquakes. Bull. Seismological Society of America, 1969, Vol. 59, No. 2, pp. 651-664.

25. SEED, H.B., LEE, K.L. and IDRISS, I.M. - Analysis of the Sheffield Dam Failure. A.S.C.E. Journal of the Soil Mech. and Fdn Div., 1969, SM6, pp. 1453-1490.

26. KRISHNA, J., PRAKASH, S., MATHUR, J.N. and GUPTA, M.K. - Study of Liquefaction of Obra Dam Sands. Journal I.E. (India), C.E. Division, 1968, Vol. 48, pp. 36-50.

27. KRISHNA, J. and PRAKASH, S. - Blast Tests at Obra Dam Site. Journal I.E. (India), C.E. Division, 1968, Vol. 48, pp. 1273-1284.

28. PRAKASH, S. and GUPTA, M.K. - Blast Tests at Tenughat Dam Site. Journal of South East Asian Society of Soil Engrs, 1970, Vol. 1, pp. 41-50.

29. MARSAL, R.J. - Behaviour of a Sandy Uniform Soil during the Jaltipan Earthquake, Mexico. Proc. 5th Int. Conf. Soil Mech. and Fdn Engng, 1961, pp. 229-233.

30. KISHIDA, H. - Damage to Reinforced Concrete Buildings in Niigata City with Special Reference to Foundation Engineering. Soil and Fdn, The Japanese Society of Soil Mech. and Fdn Engng, 1965, Vol. 6, No. 1, pp. 77-88.

The Collapse of Sands Upon Saturation

By
P. J. Moore, Sc.D., M.I.E.Aust.
(Senior Lecturer in Civil Engineering, University of Melbourne)
and
D. V. Millar, B.E.
(Graduate Student, Department of Civil Engineering, University of Melbourne)

SUMMARY. - The following possible mechanisms of collapse of sandy soils following saturation have been examined experimentally and theoretically:
(a) dissipation of initial capillary stresses,
(b) reduction in normal force at particle contact by increase in pore pressure,
(c) contact instability due to decrease in shearing resistance on saturation.
The magnitudes of the initial capillary stresses were estimated to be quite low and the influence of their dissipation upon collapse behaviour did not appear to be as marked as the decrease in shearing resistance following saturation. This decrease in resistance was quite significant particularly at void ratios which were large in comparison with the critical void ratio. It was at these high void ratios that the largest collapses were observed. The increase in pore air pressure during saturation was found to be negligible.

I.- INTRODUCTION

The principle of effective stress which states that:

(a) changes in volume and shearing resistance are due exclusively to changes in effective stress,

(b) effective stress is the difference between the total stress and pore water pressure

$$\sigma' = \sigma - u_w \qquad (1)$$

has been of fundamental importance in explaining the behaviour of saturated soils. For partially saturated soils Bishop (Ref. 1) proposed a modified form for the effective stress equation

$$\sigma' = \sigma - u_a + \chi\,(u_a - u_w) \qquad (2)$$

where the parameter χ varies between 0 and 1, and it was assumed that statement (a) remained valid.

In studies on the phenomena of volume decrease or collapse of partially saturated soils upon saturation some doubts have been raised about the validity of applying the principle of effective stress. Workers at M.I.T. (Ref. 2) showed that the collapse behaviour of partially saturated soils implied negative values of the χ parameter and they concluded that Bishops form of the effective stress equation was inadequate in explaining collapse. Jennings and Burland (Ref. 3) concluded from their studies on collapsing soils that statement (a) could not be validly applied to partially saturated soils because of the essential difference between the internal and external stresses involved. Both of these conclusions, however, are based upon the assumption that collapse is a result of the dissipation of initial capillary stresses. In this paper some other possible collapse mechanisms are considered through an examination of the causes of instability at particle contacts.

II.- NOTATION

σ	total stress
σ'	effective stress
u_w	pore water pressure
u_a	pore air pressure
χ	parameter in effective stress equation
N	normal force at particle contact
T	shear force at particle contact
ϕ_u	angle of friction at particle contact
ϕ_m	mobilized angle of friction
β	inclination of particle contact to vertical
H	horizontal force at particle contact
V	vertical force at particle contact
T_s	surface tension for water
w	water content

III.- CAUSES OF CONTACT INSTABILITY

From considerations of contact equilibrium (Fig. 1) three possible causes of instability could be considered:

(a) An increase in the shear force T without a corresponding increase in the normal force N. As it is difficult to visualise the process of saturation leading to an increase in T this possibility was not considered further.

(b) A decrease in N without a corresponding decrease in T. The force N could be decreased either by the dissipation of any initial capillary stress or by an increase in the pore pressure.

(c) A decrease in the angle of friction ϕ_u following soaking.

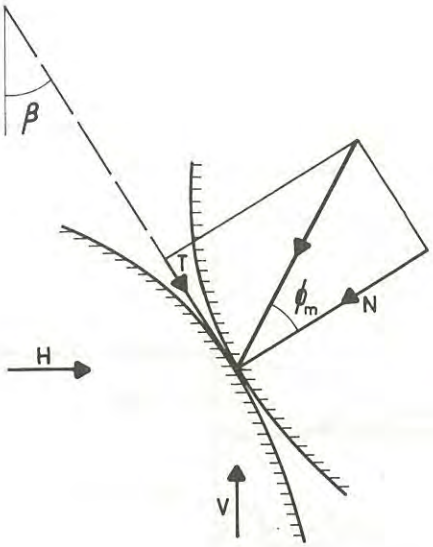

Fig. 1 Forces between Two Particles

V.- FORCES ACTING AT CONTACTS BETWEEN PARTICLES

The forces acting between two particles is represented in Fig. 1, in which ϕ_m is the mobilized angle of friction. By means of resolving forces it may be shown that

$$\frac{V}{H} = \tan(\beta + \phi_m) \qquad (3)$$

which reaches a maximum value for any contact when the friction has been fully mobilized, that is, when ϕ_m becomes ϕ_u. The relationship between $\frac{V}{H}$ and β for various values of ϕ_u when the friction has been fully mobilized is shown in Fig. 2. For contacts which are not on the point of instability the points would plot to the right or below these lines. In other words these lines represent envelopes, points to the right of which indicate stable contacts and points to the left indicate unstable contacts.

If contact instability is going to result from soaking the assemblage of particles in water then sliding will commence first at those contacts for which the friction is fully mobilized before soaking. That is the contacts of immediate interest will be those which plot on the lines in Fig. 2.

In order to examine the effect of soaking upon the stability of the assemblage the behaviour of one contact will be studied in detail. It will be assumed for purposes of discussion that ϕ_u is 20° (before soaking). Assume that point A in Fig. 2 represents a contact at the point of sliding before soaking. If the angle of friction ϕ_u is increased by, say 10° as a result of soaking then the limiting envelope will move from the 20°line to the 30° line in Fig. 2. This means that at contact A the particles will no longer be on the point of sliding. The assemblage would become more stable and no movement should result from soaking. On the other hand should soaking reduce the angle of friction ϕ_u by 10° the envelope will be moved from the 20° line to the 10° line. This means that contact A will be outside the envelope, the contact will be unstable and sliding will result. Some of the possible ways in which this sliding would occur are represented by the dotted lines in Fig. 2. This movement will cause a redistribution of forces and rearrangement of surrounding particles. Similarly all of the contacts which originally plotted between the 10° and 20° lines would become unstable and particle rearrangement would continue until all contacts plotted below the new 10° envelope.

On the basis of the foregoing model it is seen that the prerequisite for settlement or "collapse" of an assemblage of particles through soaking is that the angle of friction ϕ_u is decreased by the process of soaking. More generally, any effect of soaking that would induce contact instability could lead to sliding, particle rearrangement and a consequent compression of the sample.

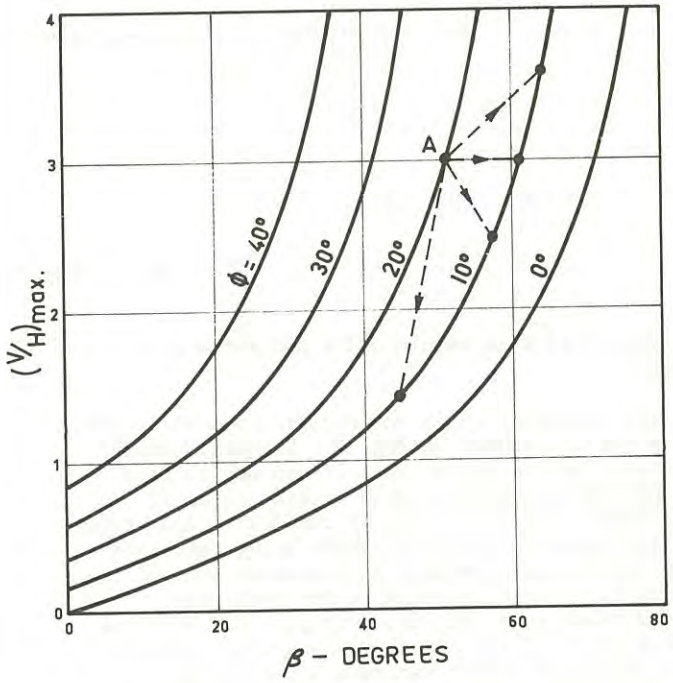

Fig. 2 Maximum Force Ratio at Particle Contacts

V.-COLLAPSE SIMMULATION IN OEDOMETER

In order to identify the causes of particle contact instability several series of laboratory tests were carried out. The first series consisted of the preparation of a variety of samples of sand-sized materials in an oedometer followed by

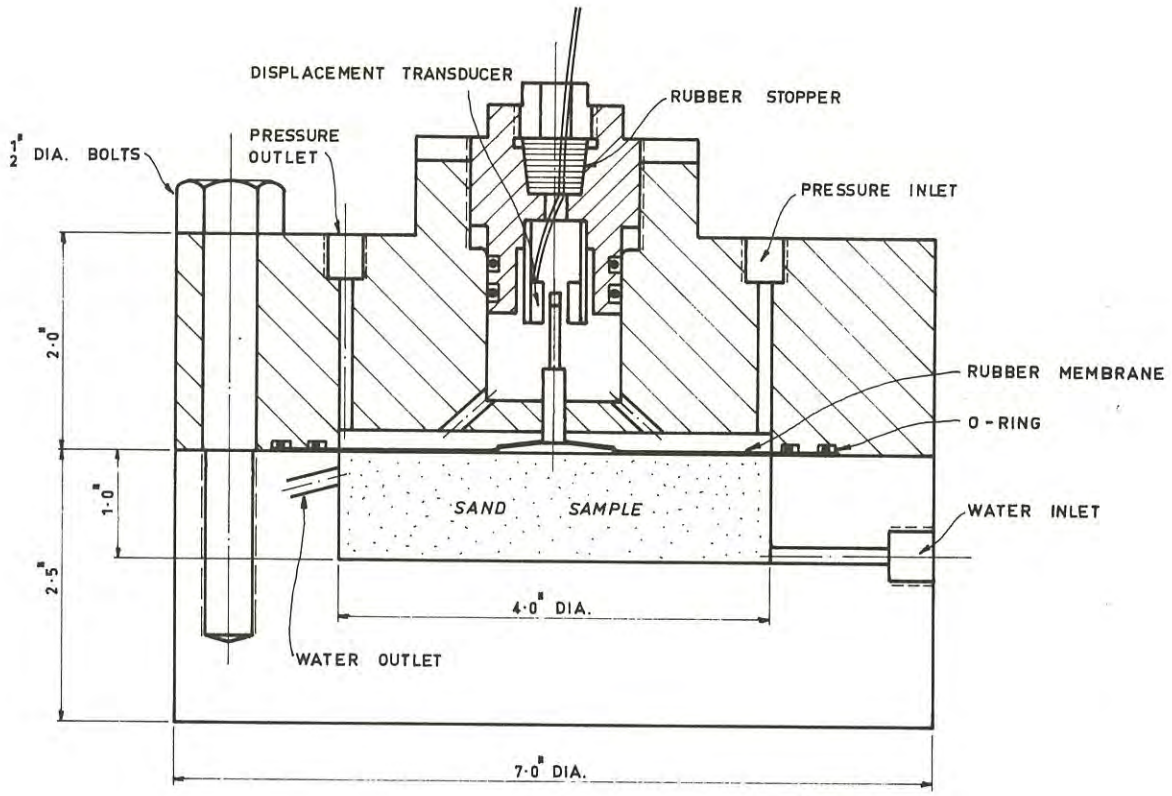

Fig. 3 Sketch of Oedometer

saturation of each sample while subjected to a stress.

The oedometer which was designed and built for these tests is shown in Fig. 3. The sand sample is placed in the bottom half of the device in a cylindrical chamber to which a water inlet is connected. The two halves of the device are firmly bolted together, the sand sample being separated from the pressure chamber in the upper half of the device by a rubber membrane which was sealed circumferentially with two O-rings. The vertical displacement of the sample was measured by means of a Schaevitz linear variable differential transformer (LVDT) which had a working range of ±0.030 in. The excitation for this displacement transducer was a voltage amplitude of 20 volts at a frequency of 20 kilo-hertz, which was provided by a model 200 CD Hewlett Packard oscillator, the output being displayed on the screen of a Tektronix 502A oscilloscope. The pressure was controlled by means of a pressure regulator the pressure being read on a Bourdon pressure gauge. This oedometer is similar in many respects to the one described by Moore (Ref. 4) but it possesses a major advantage over the earlier model, namely the LVDT can be reset to the null position while the sample is under

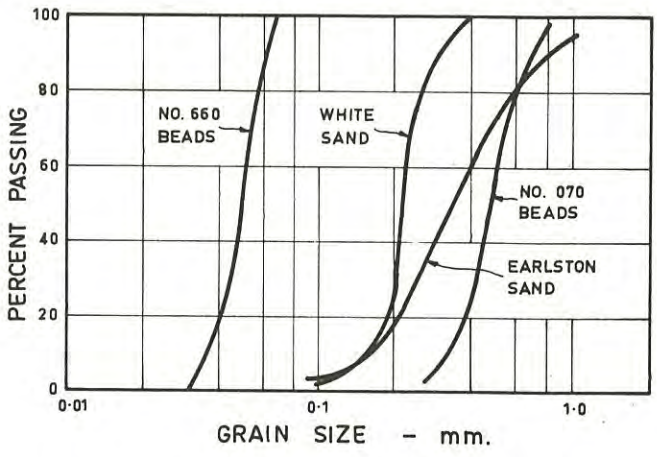

Fig. 4 Grain Size Distributions

pressure.

Tests in the oedometer were carried out on four samples - two quartz sands and coarse and fine samples of spherical glass beads. The grain size distributions of these four samples are shown in Fig. 4. The samples were prepared at 1% water content and in the oven dry state at various void ratios. The samples were spooned into the oedometer and levelled with a spatula. The pressure was increased to 10 lb/in^2 at a rate of approx. 1 lb./in^2/min. The sample was then inundated with water and any vertical compression was observed. The results of this series of tests are indicated in Fig. 5.

As expected the amount of collapse increases as the void ratio prior to saturation increases. For many of the dry samples little collapse was observed following saturation. Collapse was observed, however for some of the dry Earlston sand samples. As the results for the dry samples lie within the general scatter of results for the moist samples, this suggests that large collapse is not observed with the dry samples simply because of the difficulty of preparing these samples at higher void ratios. Larger collapses are observed with the moist samples because of the relative ease of preparing these samples in a looser condition. Since no initial capillary stresses were present with the dry samples, these foregoing observations suggest that particle contact instability due to dissipation of capillary stresses could not be the sole cause of collapse. Capillary effects may be a contributing factor in the collapse of initially moist samples but an examination of the capillary stresses in regular packings of spherical particles suggests that these stresses are quite small in magnitude.

Jennings and Knight (Ref. 6) have observed increasing amounts of collapse with increasing vertical overburden stress. Confirmation of this observation was not obtained with the present series of tests since the majority of the tests was carried out for one value only of the vertical stress.

VI.- CAPILLARY STRESSES IN REGULAR PACKINGS

Consider two equal spheres in contact at point A (Fig. 6) and connected by a film of water CADEABC. Since the mean curvature of the air-water interface is constant (Ref. 5) the pressure difference (u_a-u_w) across this interface may be found from the known mean curvature at point F.

$$u_a-u_w = T_s \left(\frac{1}{c} - \frac{1}{b}\right) \qquad (4)$$

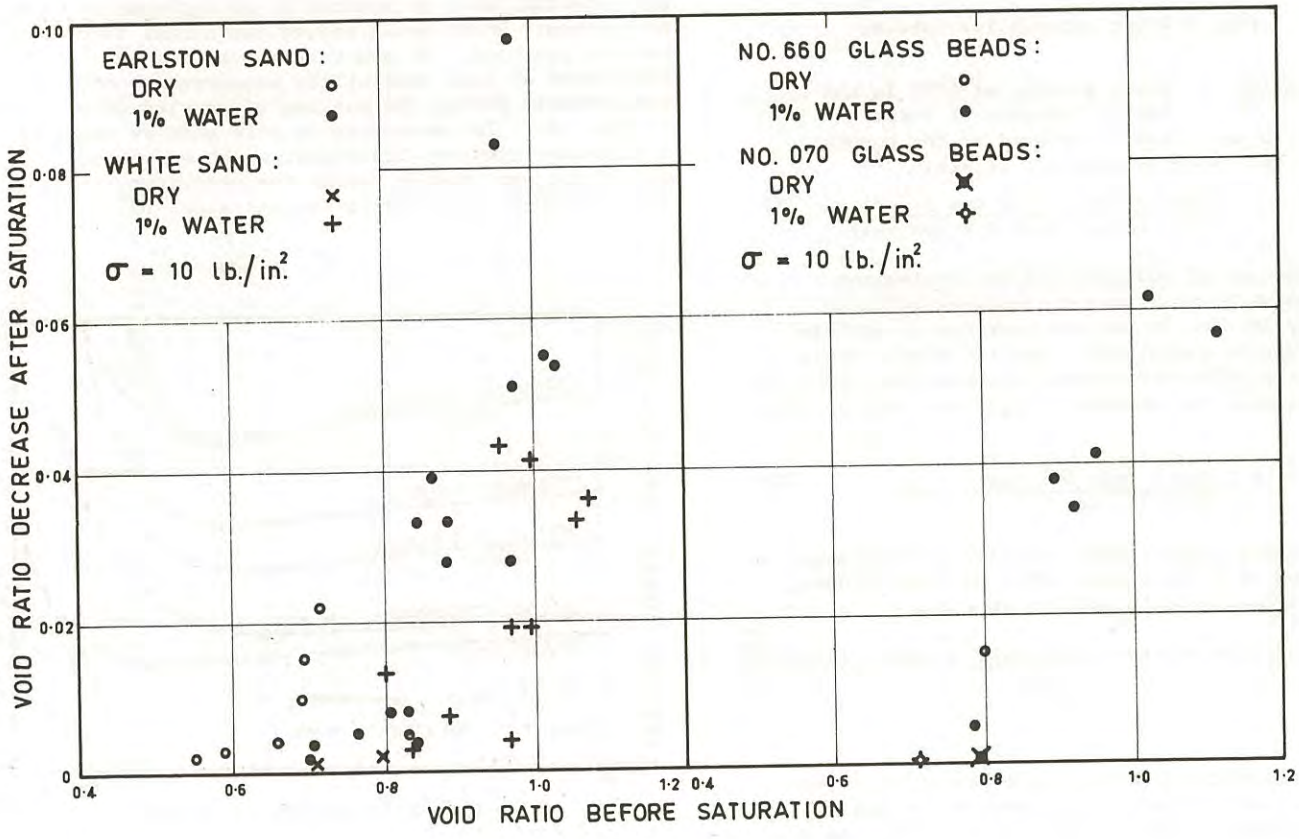

Fig. 5 Collapse of Sands Following Saturation

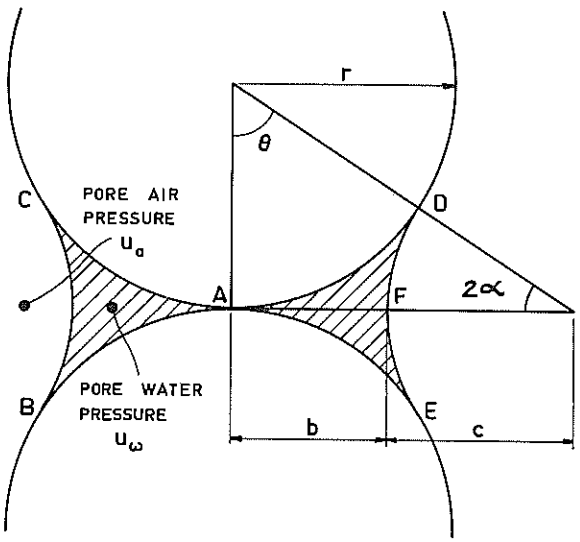

Fig. 6 Water between Two Spheres

where T_s = 0.005 lb./ft. at 67°F is the surface tension of water

The radii b and c may be related to the sphere radius r and subtended angle θ to yield

$$u_a - u_w = \frac{T \cos\theta\ (\sin\theta + 2\cos\theta - 2)}{r(1 - \cos\theta)\ (\sin\theta + \cos\theta - 1)} \qquad (5)$$

By the use of equation (5) the equivalent effective vertical stress σ' produced by these capillary effects in various packings of uniform spheres may be calculated. For the simple cubic packing the effective stress assuming that the u_a is identical with the ambient air pressure may be shown to be

$$\sigma' = \frac{\pi\ T \tan\theta\ (\sin\theta + \cos\theta - 1)}{4r\ (1 - \cos\theta)} \qquad (6)$$

The water content (w%) may also be determined as a function of θ for simple cubic packing assuming the specific gravity of solids as 2.65.

$$w(\%) = 113.2\left[\tfrac{1}{2}\tan^2\theta - 1 + \cos\theta - \frac{\alpha(1-\cos\theta)^2}{\cos^2\theta}\left\{3\tan\theta - \frac{(1-\cos\theta)}{\alpha}\right\}\right] \qquad (7)$$

The relationship between the effective stress and water content may be expressed as in Fig. 7. This relationship may be expected to change as the water content exceeds 6.25% (θ=45°) since the water films begin to merge at this point. At a water content of 19.55% air will be present only in the form of separated bubbles. If it is assumed that the pore air pressure is still equal to the atmospheric pressure the effective stress is as indicated in Fig. 7. For the water content to increase further to the saturation value of 34.3% the pore air pressure must be increased to permit the solution or escape of the bubbles.

Similarly the relationships between effective stress and water content may be determined for other regular packings of uniform spheres and these are also shown in Fig. 7. For these packings which cover a range of void ratios from 0.91 to 0.35 the effective stress is seen to decrease as the void ratio increases. This conclusion should also be applicable to irregular packings. For the Earlston and white sands that were used in the tests previously described the equivalent effective stress for the moist samples (1% water content) would be of the order of 0.2 to 0.3 lb/in^2. It appears that capillary effects are of importance only at relatively shallow depths in the field. For the oedometer tests previously described the dissipation of the capillary stress following soaking would reduce the effective stress and hence the normal force at particle contacts by roughly 3% or less. With this relatively small effect only those contacts near the point of sliding would be rendered unstable by soaking.

VII.- MEASUREMENT OF PORE AIR PRESSURE DURING COLLAPSE

As previously discussed contact instability upon soaking could be induced by an increase in pore air pressure which would reduce the normal force between contacts. In order to check upon the likelihood of this possibility measurements of pore air pressure during the soaking of samples were carried out. The measurements were made by means of a miniature pressure transducer which was placed within the sand sample inside the oedometer (Fig. 3). The transducer was a Micro-Systems model 1017

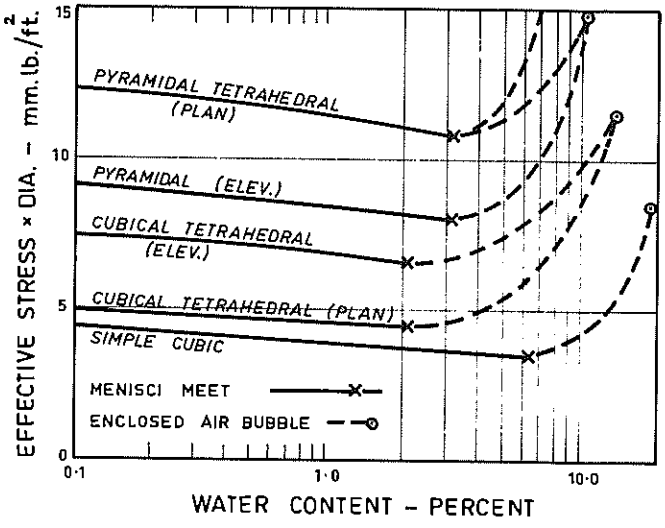

Fig. 7 Relation between Effective Stress and Water Content for Uniform Packing

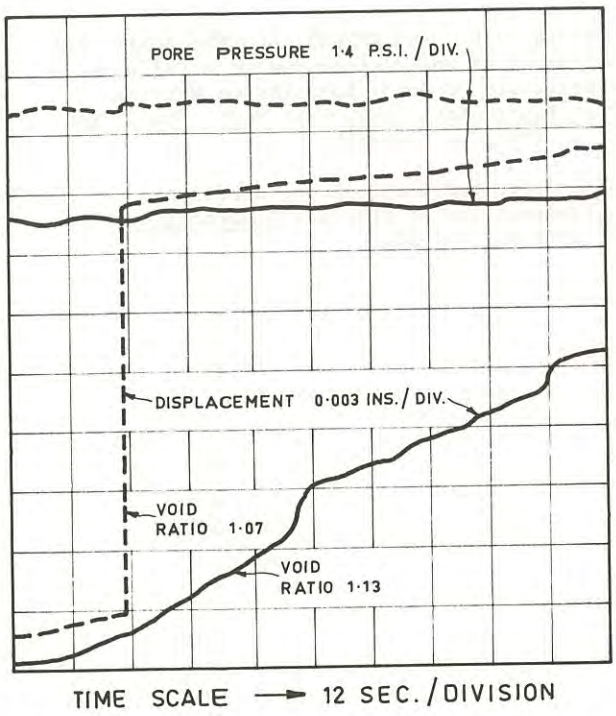

Fig. 8 Typical Collapse Patterns

mplantable blood pressure transducer. The ransducer, which consists of four semiconductor train gauges bonded to the interior surface of a .5 mm. diameter pressure sensing diaphragm, has a ressure range 0 to 8 lb/in^2. The diaphragm was nclosed in a small permeable case so that pore air ressures only would be measured.

Two typical results for tests on the white sand are shown in Fig. 8. In some tests the collapse occurred suddenly, in others it occurred gradually. The cause of the difference in the rates of collapse was not satisfactorily identified although it appeared to be related to the occurrence or non-occurrence of a sudden compression of the sand during loading. In all tests the change in pore air pressure during saturation was either negligible or barely detectable.

VIII.- SHEARING RESISTANCE BEFORE AND AFTER SATURATION

In order to obtain a measure of the influence of saturation upon the angle of contact friction ϕ_u, a series of drained direct shear tests was carried out on the white and Earlston sands. Horn and Deere (Ref. 7) have shown that the frictional resistance that can be developed between smooth surfaces of quartz increases as the surface moisture increases. However, this anti lubricating action of water was found to diminish rapidly as the surface roughness increased. The particle surfaces of the two sands which were examined under low magnification could not be described as smooth. The conclusions of Horn and Deere were therefore considered to be inapplicable.

A typical set of results is shown in Fig. 9. The shear strength of the moist sand exceeded that of the saturated sand over the entire range of void ratios tested, the strength difference increasing as the void ratio increased. This finding confirms that, in terms of total stresses, the shearing resistance of the moist sand is decreased by saturation. The volume change behaviour of the moist sand during shearing which is shown in Fig. 10 possesses marked similarities with the volume change behaviour following saturation as shown in Fig. 5. The processes of saturation and shearing of the moist sand produce similar decreases in volume. The collapse or volume decrease following saturation becomes very small as the void ratio approaches the critical void ratio, which is the void ratio at which the sample exhibits no volume change following shearing.

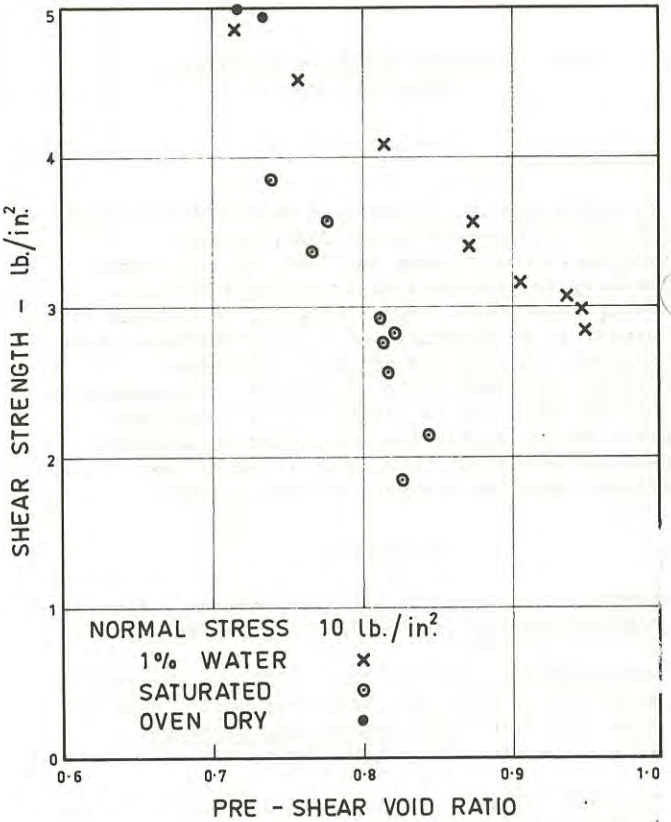

Fig. 9 Shear Strength of Earlston Sand

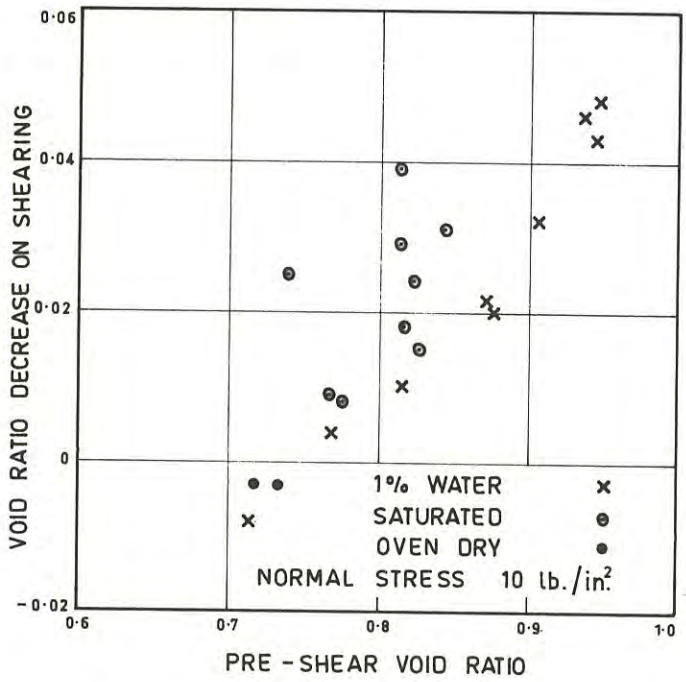

Fig. 10 Volume Change on Shearing for Earlston Sand

IX.-CONCLUSIONS

From the results of tests on two sands the major reason for collapse or volume decrease upon saturation of moist sands was found to be contact instability related to a shear strength decrease following saturation. Pore air pressure changes do not appear to be a factor influencing collapse since the increase in pore air pressure following saturation was found to be negligible. Reductions in the normal force due to dissipation of capillary stresses may be a contributing factor in collapse at shallow depths but it appears to be of less importance than the changes in shear strength.

REFERENCES

1. BISHOP, A.W., The principle of effective stress, Teknisk Ukeblad, Vol 39 1959, pp 859-863.

2. MASSACHUSETTS INST. OF TECHNOLOGY, Engineering Behaviour of Partially Saturated Soils, Research Report R 63-26, Soil Engineering Division, Publication No. 134, 1963, 68 pp.

3. JENNINGS, J.E.B., and BURLAND, J.B., Limitations to the Use of Effective Stresses in Partly Saturated Soils, Geotechnique, Vol. 12, 1962 pp. 125-144.

4. MOORE, P.J., An Oedometer for Static and Dynamic Loading, Proc. Fifth Aust.-N.Z. Conf. Soil Mech. and Found Eng., 1967 pp. 170-174.

5. ADAM, N.K., The Physics and Chemistry of Surfaces, 3rd ed. Oxford Univ. Press, 1941, 436pp.

6. JENNINGS, J.E., and KNIGHT, K., The Additional Settlement of Foundations due to a Collapse of Structure of Sandy Subsoils on Wetting, Proc. Fourth Int. Conf. Soil Mech. Found. Eng. Vol 1, 1957, pp. 316-319.

7. HORN, H.M., and DEERE, D.V., Frictional Characteristics of Minerals Geotechnique, Vol. 12, 1962 pp. 319-335.

Stresses Induced by Mining Operations at Mount Charlotte

By

W. E. Bamford, B.E., A.M.Aus.I.M.M.

(Senior Lecturer in Rock Mechanics, University of Melbourne)

SUMMARY.- Mount Charlotte is a mechanized underground mine, extracting low-grade gold ore, at Kalgoorlie, Western Australia. Following a "bump", or partial brittle failure of a rib pillar, a quick series of rough calculations, utilising published elastic theory stress concentration factors, was carried out to determine whether the overstressing of this pillar could have been predicted, and, if successful, whether this rock mechanics approach could be used to suggest modifications to the mining methods. The previously-measured high horizontal stress field was assumed to be consistent with Hast's measurements, and calculations showed that the stress induced in the rib pillar after partial removal of the crown pillar was of the same order as the rock mass strength, so rendering it logical that failure would ensue. Another rib pillar was shown to be in a slightly less highly stressed state, and a prediction that it would be safe until its planned extraction was proved to be correct. A more refined recalculation is in progress.

I.- INTRODUCTION

Gold Mines of Kalgoorlie Ltd.(GMK) operates a large underground mine at Mount Charlotte, on the edge of the town of Kalgoorlie, Western Australia. The orebody is almost vertical, about 700 feet long (azimuth 142°True), varying in plan width from 100 to 200 feet. The host rock is a massive quartz dolerite greenstone of Archaean age, and the gold ore occurs associated with pyrite mineralization and quartz veins. The ore grade is approx. 3 penny-weights per ton (approx. 4.5 grams per metric ton).

The mining method adopted in A Block (0 to 500 feet below the surface) was cut and fill, with transverse support pillars. This method was designed with the aid of the Snowy Mountains Hydro-Electric Authority (S.M.A.), in 1963 (Ref.1,2). In B Block (500 to 900 feet below the surface) the mining method is sub-level open stoping, with open stopes 300 feet high, 100 to 180 feet wide and 80 to 180 feet long, separated by rib pillars 80 to 90 feet thick (in plan). Open stopes are filled with broken ore by blasting adjoining rib- and crown-pillars. As the broken ore is drawn off at the 860 ft. and 900 ft. levels, a plug of dry fill from A Block, continuously replenished by dumping into an old open-cut at the outcrop, moves down on top of the subsiding ore.

Fuller descriptions are given in Refs.3 and 4.

II.- FAILURE OF RIB PILLAR B2

At 5.23 a.m. on 1st April 1970 a seismic event was recorded on the Kalgoorlie seismograph of the Bureau of Mineral Resources. Gregson (Ref.5) states that this event had relative amplitude 15 (= approx. Richter magnitude 0.7) and strain release 18×10^6 (ergs). The "bump" was heard by many persons over a wide area of the Kalgoorlie-Boulder district. Later that morning mining engineer R.A.Tastula carried out inspections and noted (Ref.6):

(a) On the 600 level cracking and scaling were evident in the P.B.2 Rib Pillar cross cut and in the west wall of the stripping drive Approx. 10-15 tons of rock had fallen in this area. The rails had been moved 6 inches off line.

(b) On the 700 level similar cracking had occurred and about 20 tons had fallen.

(c) On the 800 level cracking had occurred in several places along the P.B.2 Rib Pillar cross-cut and also on the N.E. and S.W. corners of the pillar.

(d) On the 900 level major scaling had taken place along the walls of eastern millholes in P.B.2 and S.B.2. On the western side, only the most southern millholes, No.5, had shown signs of movement.

From these observations he concluded that the pillar had been subjected to excessive stress from the walls towards the centre.

Later that month the author was invited to make an inspection. The pattern of cracking and fracturing within Rib Pillar B2 was strongly suggestive of failure due to compression along the East-West axis of the pillar. In the central pillar axis drives the walls typically showed cracking and slabbing parallel to the side walls, with some vertical tensile cracking in the roofs. This could indicate that the major stresses were either vertical or East-West. However, in transverse (North-South) drives, slabbing and spalling parallel to the roof and vertical tensile cracking normal to the walls indicated that the major stress was acting in an East-West direction. (See Fig.1)

A survey pin in the centre of the pillar on the 800 level was re-surveyed, to give an indication

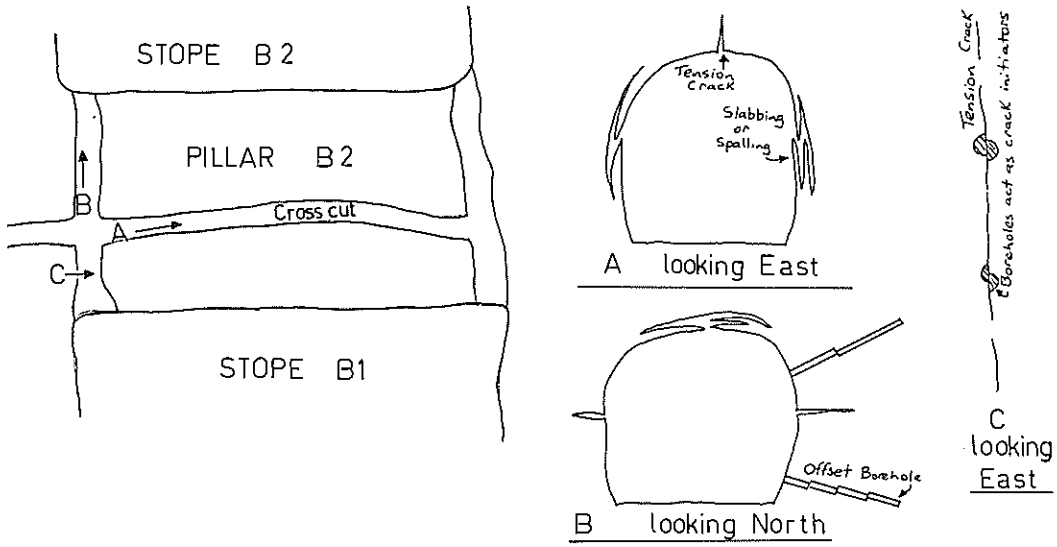

FIG.1. SKETCHES OF TYPICAL FAILURE PHENOMENA IN RIB PILIAR B.2

of the movements.

December 1969	9274.80N	R.L.=408.05
24th April 1970	9274.68N	R.L.=408.07
Movement =	0.12foot North	0.02 foot up

This movement is more consistent with a horizontal East-West compression, causing slight lateral (Northwards and upwards) buckling than with a vertical compression.

III.- ESTIMATION OF VIRGIN FIELD STRESSES

The virgin rock stresses measured by the SMA (Ref.1) on the 300 and 500 levels were of the order of 2500 lb/in,^{2}(p.s.i.) along the long axis of the orebody (henceforth referred to as North), 1500 p.s.i. across the orebody (henceforth referred to as East), and 1500 p.s.i. vertical. The sum of the horizontal stresses is consistent with the relationship postulated by Hast (Ref.7)

$\sigma 1 + \sigma 2 = 191 + 0.99\ H$ kgf/cm^2 (with H in meters) or
$\sigma 1 + \sigma 2 = 2716 + 4.36\ H$ p.s.i. (with H in feet).

At a depth of 400 feet Hast's equation indicates that the sum of principal stresses is approx.4,400 p.s.i., compared with the measured 4,000 p.s.i. (if the 300 and 500 level results, which show no increasing or decreasing trend with depth, are averaged and assumed to be valid for a depth of 400 feet). Stresses at any other depth were inferred as shown in Fig.2, with the ratio of σN to σE assumed constant at 5:3, and σV increasing as γH.

The deduction of stresses concentrated by the large excavations presented a formidable problem. No three-dimensional method was feasible within the limitations of cost and the short time within which results were required. The earlier photoelastic studies by the SMA (Ref.2) had been limited to boundary stresses of the A Block stope, with no results that could be confidently extrapolated to B Block. The finite element method of computer analysis showed promise, but, paradoxically, was thought would probably take longer to obtain an answer (albeit possibly more correct) from, because of "debugging" and time use limitations, than a deductive or analytical method. Also, the data available on material properties and excavation shapes were not very voluminous or reliable, rendering exact methods of solution less appropriate. So, it was decided to study the two-dimensional stress concentrations around each stage of excavation, superimposing and sythesising, to arrive at the overall picture.

IV.- ESTIMATION OF STRESS CONCENTRATIONS

Following the comments of personnel who had tested rock specimens from Mt.Charlotte at the S.M.A Cooma, and the Australian National University, Canberra, and personal observations on the rock mass the assumption of perfectly elastic behaviour of the rock can be made with only slight error. Simplified versions of the shapes of the excavations were

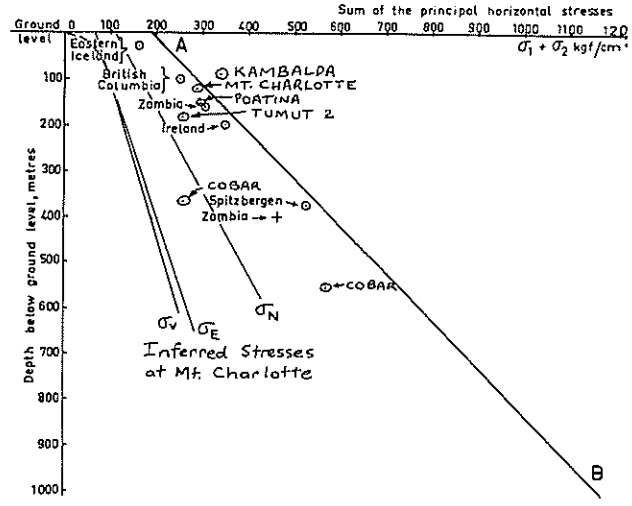

Fig.2. Principal Stress sums, after Hast and others Inferred principal stresses at Mt.Charlotte.

assumed, and stress concentrations calculated by Savin (Ref.8) were followed.

The effect of the mined-out A Block notch, open to the surface, was approximated by taking the stress concentrations due to the lower half of a rectangular hole. Although this is obviously not the same model, a quick comparison of notch stresses (Ref.9) with hole stresses (Ref.8) indicated that they were reasonably similar, in magnitude and distribution pattern. So, an East-West cross-section through A Block, generalized as being 500 feet deep and 150 feet wide, was simulated by the lower half of a rectangle with rounded corners, 1000 feet high and 150 feet wide. (See Fig.3)

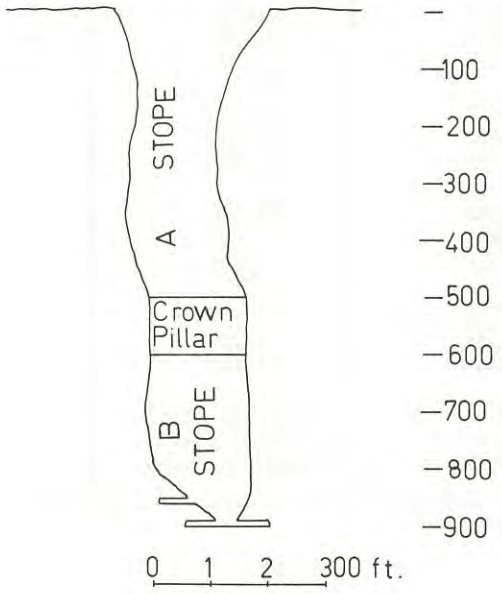

Fig. 3 Typical West-East Cross-section

In a similar fashion, in a North-South longitudinal section the effect of a notch 540 feet long and 500 feet deep on the North-South field stresses was evaluated. (See Fig.4).

Table 1 shows the calculated average stresses existing in the orebody after removal of A Block.

TABLE I

CONCENTRATED STRESSES BELOW A BLOCK

Depth	S_E	S_N	S_V(lbs/sq.in.)
500 ft.	15,200	10,500	0
550	12,500	7,400	400
600	9,200	4,900	1,300
650	5,300	4,700	1,800
700	4,700	4,700	2,100
750	3,800	4,700	2,100
800	3,200	4,700	1,800
850	3,200	4,800	1,900
900	3,200	4,900	2,100

(Note: S_E = Concentrated stress in East direction,
N = North,
V = Vertical

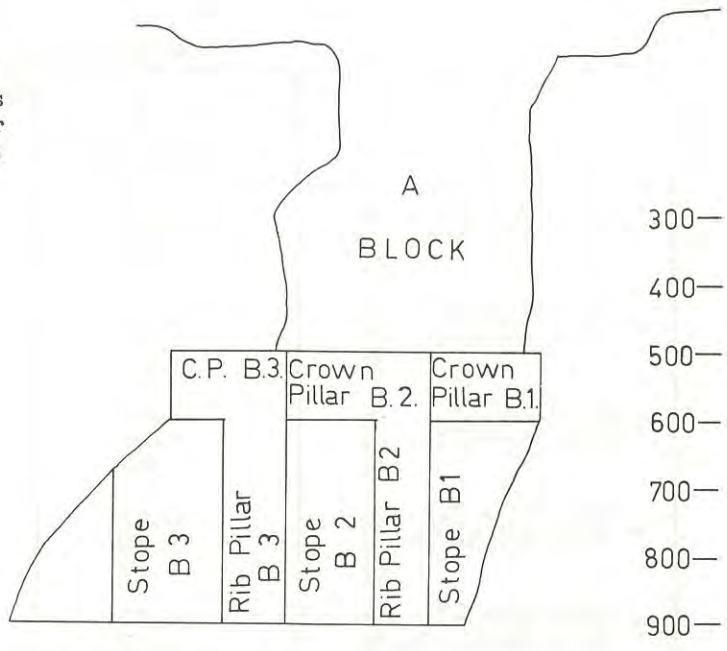

Fig.4 Typical North-South Cross-section

The next phase of excavation simulated was the opening of the stopes in B Block, from 600 to 900 feet below the surface. The effect on the average stresses in the crown pillar is shown in Table 2.

TABLE II
CONCENTRATED STRESSES IN CROWN PILLAR ABOVE B STOPES

Depth	S_E	S_N	S_V (lbs/sq.in.)
500 ft.	15,600	10,600	0
550 ft.	13,500	7,600	-1900
600 ft.	13,400	5,500	0

The next model was the plan outline of the stopes generalized as rectangles with rounded corners (See Fig.5). The stress concentration factors, in a horizontal plane, about each stope could then be calculated, and multiplied by the concentrated stresses due to the proximity of the A Block notch, to give the doubly-concentrated stresses around the B Block stopes. By the principle of superposition the stresses in the Rib Pillars could then be estimated. It was realized that while the two-dimensional model of stress concentrations across the long axis of the excavation would be valid in the central portion, near the ends the stresses would be changing. It was assumed that the zone of uniform concentrated stresses would extend to within a distance of one stope width (i.e. 120 to 160 feet) of the end of the excavation viewed in the North-South longitudinal section, and that the stresses would then undergo a transition, returning to their undisturbed value at a distance of two stope widths from the end of the excavation (c.f. St.Venant's principle).

A similar rectangle model was applied to the concentrated stresses in the crown pillar, to study the effect of the removal of Crown Pillar B.1 in December 1969, an event which was followed within 4 months by the "bump" in the adjoining pillar. The

TABLE III

DEDUCED AVERAGE STRESSES IN PILLARS (lbs/in.^{2})

		Stage of Mining			
		A After Removal of A Block	B After Opening of B Block Stopes	C After Firing of Crown Pillar B.1	D After Firing of Crown Pillar B.2
1. Crown Pillar B.1 Depth 500-600ft.	S_E	10,200	11,700	-	-
	S_N	6,700	6,900	-	-
	S_V	600	-100	-	-
2. Rib Pillar B.2 Depth 600-800ft.	S_E	4,800	10,100	17,700	-
	S_N	4,700	1,000	1,000	
	S_V	1,900	3,700	4,600	-
3. Rib Pillar B.2 Depth 500-600 ft.	S_E	12,800	12,800	18,000	-
	S_N	7,600	7,600	2,700	-
	S_V	300	300	20	-
4. Crown Pillar B.2 Depth 500-600 ft.	S_E	12,800	14,300	15,200	-
	S_N	7,600	7,900	5,600	-
	S_V	300	-600	-600	-
5. Rib Pillar B.3 Depth 600-800 ft.	S_E	4,200	11,300	16,700	14,900
	S_N	4,400	1,600	2,000	2,100
	S_V	1,900	3,700	4,700	4,700
6. Rib Pillar B.3 Depth 500-600 ft.	S_E	10,100	10,100	13,300	16,700
	S_N	6,700	6,700	6,900	3,000
	S_V	600	600	600	400
7. Crown Pillar B.3 Depth 500-600 ft.	S_E	3,800	4,200	Probably little changed from previous stage	10,700
	S_N	3,300	3,900		5,000
	S_V	1,400	1,200		1,200

variation of stresses with height in the rib pillars after the removal of A Block was plotted, the average stress in the crown pillar at this stage compared with that after the removal of Crown Pillar B.1 to indicate a further proportional increase, and the stress concentration factors at various depths within the pillar similarly proportionately adjusted, to give an indication of the rib pillar stresses after the partial removal of the crown pillar.

The effect of further removal of Crown Pillar B.2 was also modelled, to attempt to predict whether its removal, in July 1970, would be followed by catastrophic failure, or whether the adjoining Pillar 2 would remain intact until the scheduled firing in December 1970.

The final results of much manipulation and calculation, the deduced progressive changes in stresses during mining, are shown in Table 3. Each stress quoted is the average over the specified portion of a pillar. The apparent differences in stresses between contiguous blocks of rock do not reflect sudden stepwise changes, but rather gradual variations over tens of feet.

V.- ESTIMATION OF ROCK MASS STRENGTH

It is of interest to observe in Table III that the stresses in Units 4 and 3 (Crown Pillar B.2 and Rib Pillar B.2 from 500 to 600 feet) at Stage C (after firing of Crown Pillar B.1) are somewhat higher than those acting on any other Unit at any stage. As the "bump" took place within Units 4 and 3 at Stage C,

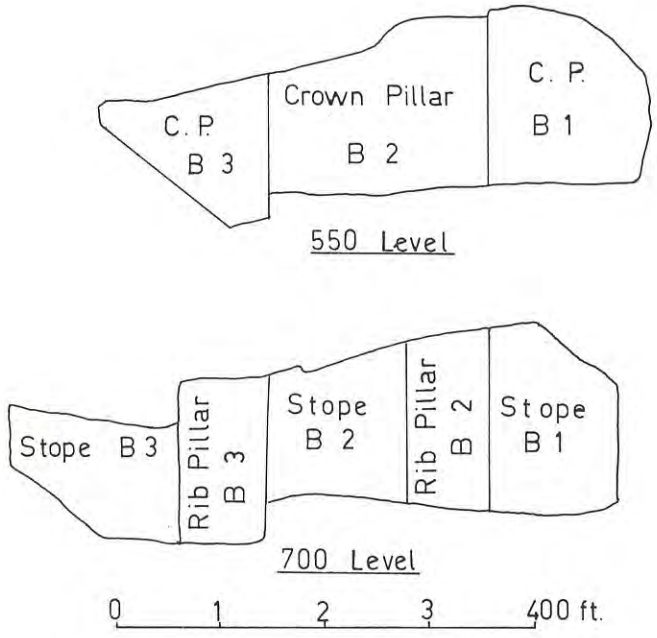

Fig.5 Typical Plan Outlines.

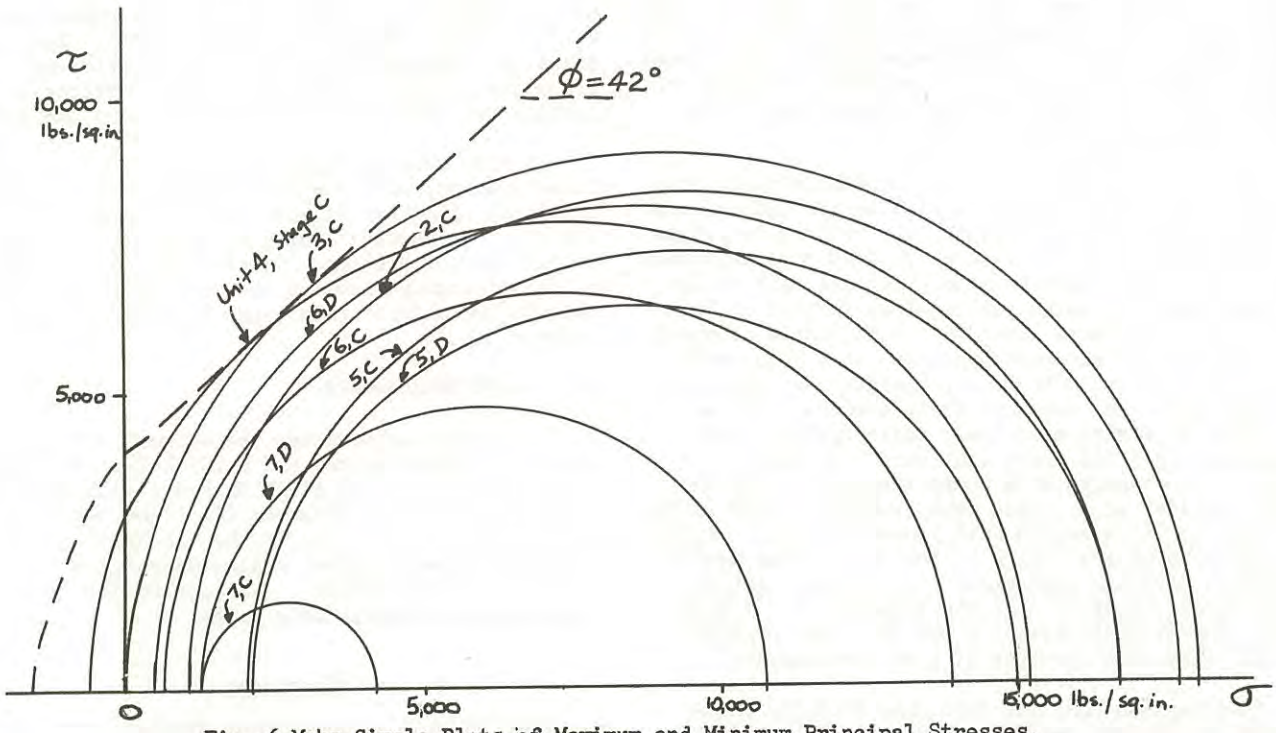

Fig. 6 Mohr Circle Plots of Maximum and Minimum Principal Stresses.

this can be regarded as a large-scale in-situ compression test to failure, and the inferred strength used as a guide in checking stability of other parts of the mine.

Mohr circle plots of the maximum and minimum stresses for Units 4 and 3 at failure (15,200 and -600; 18,000 and 20 lbs/sq.in. respectively) indicate that a straight line with apparent cohesion =4,000 lbs/sq.in., apparent angle of shearing resistance ϕ = 42° can be drawn tangent to them, and this can be taken as indicating an in-situ failure criterion for the rock mass (See Fig.6). Mohr circles for the worst stress conditions in each of the other Units can be drawn, and the apparent factors of safety deduced.

TABLE IV

APPARENT FACTORS OF SAFETY

Unit	Stage C	Stage D (Terminology as in Table III)
2	1.19	
3	1.00	
4	1.00	
5	1.47	1.36
6	1.30	1.11
7	4.9	1.82

With these figures available, it becomes quite apparent that when Units 3 and 4 failed, the next most highly stressed Unit, 2 (Factor of Safety 1.19) should be the most likely Unit to fail as load was shed onto it by the partially failed Units, so leading to failure of Units 2, 3 and 4 - the entire Pillar B.2. It is also reasonable that Unit 6, the most highly-stressed portion of Pillar B3, with a factor of safety of 1.30 should stand safely, without danger of failure, for a few more months, from the April prediction until the July firing of Pillar B2, as in fact happened.

When Stage D was reached, in July 1970, the likelihood of a catastrophic failure of Pillar B3 before it was due to be fired in December was of interest to the mine management. Although other commitments delayed the analysis, the author was able to give the opinion in August that if a factor of safety safety of 1.00 implied failure 3½ months after loading, a factor of safety of 1.11 (for Unit 6) should allow the required 5 months' standing time before failure. An additional strengthening factor appeared to be the fact that the contiguous Unit 5 had a substantially higher factor of safety. No failure had been observed before Pillar B3 was successfully blasted, in December 1970.

Another interesting sidelight to the above analysis was provided by the blasting of an undercut to Pillar B3, from the 860 to the 900 feet level, several weeks before the main pillar blast, to improve fragmentation and throw into the adjacent open stopes. As long as it was thought that the pillars transmitted mainly vertical stresses it was unthinkable to undercut them without introducing the likelihood of total collapse. When the implications of the above analysis were pointed out, that the pillars were mainly transmitting horizontal (East-West) stresses, it became evident than an undercut would not greatly affect their stability. In the event, the undercut was successfully accomplished, and the fragmentation of Pillar B3 was much better than that of Pillar B2.

VI.- LABORATORY PREDICTION OF ROCK MASS STRENGTH

Before uncritically accepting the results of an in-situ strength test, they should be compared with any available laboratory test results. As part of the 1963 investigations (Refs.1 and 2) the S.M.A.

carried out unconfined compressive and tensile strength tests on BX rock core samples supplied by G.M.K. from Mt.Charlotte. The mean compressive strength was found to be 26,800 lbs/sq.in., with a standard deviation of 6,200 p.s.i.. The mean tensile strength was 2,130, with a standard deviation of 800 p.s.i.

Before the results of tests on cylindrical pieces of rock 1 5/8 inch diameter by 1.9 to 3.8 inches long can be applied to the strength of a rectangular prism of rock 400 feet by 150 feet by 90 feet some allowance for scale factors must be made. Several authors in the past have suggested scaling-down factors as high as 100 i.e. rock mass strength = 0.01 sample strength. More recently it has been suggested that such scale factors may be valid for soft, yielding, or intensely jointed rocks, but for hard brittle rocks, such as quartzite or norite much lower scale factors apply. Bieniawski (Ref.10) shows that hard rock samples decrease in strength with increasing size until they reach the size of a 5 inch cube, whereupon they suffer no reduction in strength with increasing size. Applying his results for norite to the case of the Mount Charlotte dolerite greenstone (a somewhat similar rock) it can be shown that the strength of a 5 inch cube - and by implication, a 100 foot cube - should be 0.77 times the strength of a BX core sample.

This implies that the rock mass strength parameters are: Unconfined compressive strength =20,800, Standard Deviation = 4,800 p.s.i.; Tensile strength = 1640, Standard Deviation = 620 p.s.i. The observations, shown on Fig.6, are of an unconfined compressive strength of about 18,000 p.s.i. If this is regarded as the result of a precise computation of stresses, it implies that failure took place at a stress 0.58 standard deviations below the mean strength, which in its turn implies a 28% chance of failure, and renders the eventual failure quite logical. On the other hand, the computations were in fact not precise, and for the actual stresses to be within 10 to 20% of the computed stresses is all that could reasonably be expected of them.

The predicted tensile strength is -1640 p.s.i., while the maximum tensile stress predicted, in Crown Pillar B2, was of the order of -600 p.s.i.. It appears logical then that the pillar should have suffered compressive failure in Stage B rather than tensile failure in Stage C.

VII.- CONCLUSIONS

The rock mechanics approach to determining the stability of mine structures is :(a) deduce virgin stress field, (b) determine stress concentration factors around excavation shapes, (c) predict concentrated stress magnitudes, (d) compare these with rock mass strength to determine factors of safety. The validity of this approach was demonstrated satisfactorily at Mt.Charlotte, by being able, by back analysis, to explain a pillar failure, and by forward prediction, to predict that another pillar would not fail.

It is now being used to study and modify the mining method planned for extracting the deeper C Block (from 900 to 1150 feet below the surface). A preliminary suggestion is that it may be almost impossible to avoid overstressing pillars of economic size in the higher stress field conditions prevailing at the greater depths, and that the orebody may be more easily mined as one large open stope, with de-stressing of critical parts of the barren wall rock to reduce risk of catastrophic failures. This approach has to be modified because of the vagaries of ore grade distribution, resulting in the desirability of leaving one pillar of very low grade ore unmined.

A more detailed (and hopefully, more precise) investigation, with the aid of finite element programs developed by Mr.A.G.Bennet, a Ph.D. candidate in the Melbourne University Mining Department, is underway at the time of writing. Comparisons of the results of this investigation and the more elementary study forming the bulk of this paper will be presented when appropriate.

VIII.- ACKNOWLEDGMENTS

I wish to acknowledge the support and encouragemen ment of Mr.Clive Annear and Mr.Dick Tastula (respectively Manager and Assistant Manager, Mt.Charlotte Project), Mr.Gordon Anderson (Resident Manager, Gold Mines of Kalgoorlie) and Mr. Bob Nichols (Senior Mining Engineer, Western Mining Corporation). I am grateful to Gold Mines Kalgoorlie Ltd. for permission to publish this paper.

REFERENCES

1. BOWLING, A.J. - Rock Stress Measurements in the Mt. Charlotte Mine Kalgoorlie, Western Australia. Snowy Mountains Hydro-Electric Authority, Scientific Services Division, Engineering Physics Rept. No. S.E. 56, August 1963.

2. BOWLING, A.J. - A Photoelastic Investigation For The Design Of The Mt. Charlotte Stope, Kalgoorlie, Western Australia. Snowy Mountains Hydro-Electric Authority, Scientific Services Division, Engineering Physics Report No. S.E. 57, November 1963.

3. SIMPSON, R.C. - Operations at Mt. Charlotte. Eighth Commonwealth Mining and Metallurgical Congress, 1965 - Paper 125.

4. ANON. - Mt. Charlotte. An open cut gold mine underground. Australian Miner October 20, 1969.

5. GREGSON, P.J. - Letter from Mundaring Geophysical Observatory, W.A., to the Resident Manager, G.M.K. 10th April 1970.

6. TASTULA, R.A. - Report to the Manager, Mt. Charlotte Project. 2nd April 1970.

7. HAST, N. - The State of Stress In The Upper Part Of The Eerth's Crust. Tectonophysics, Vol. 8, 1969, p. 169-211.

8. SAVIN, G.N. - Stress Concentration Around Holes New York, Pergamon, 1961.

9. STURGUL, J.R. and SCHEIDEGGER, A.E. - Tectonic Stresses in the Vicinity of a Wall. Felsmechanik Vol. V, No. 2-3, 1967, p. 137-149.

10. BIENIAWSKI, Z.T. - The Compressive Strength of Hard Rock. Tydskrif vir Natuurwetenskappe, Vol. 8 No. 3, Sept. 1968, p. 163-182.

A Rock Mechanics Survey and its Use in an Underground Stability Analysis at Kambalda, W.A.

By

L. A. Dyson, Dip.C.E., B.E. (Mining)

(Project Mining Engineer, Hamersley Iron Pty. Ltd., formerly M.Eng.Sc. Research Student, Mining Department, University of Melbourne)

SUMMARY.- A basic rock mechanics survey at the Kambalda Nickel Mines in Western Australia was carried out and the resulting data was used in a structural mine design example.

The survey consisted of - a structural geological investigation,
the determination of the virgin rock stress field at the Durkin Mine,
and the ascertainment of the physical engineering parameters of some Kambalda rocks.

These results were combined into a mathematical model, and using the "finite element" technique, a study was made of the variation in ground movement occurring near the Durkin shafts, caused by different mining methods and mining sequences.

A residual rock stress field with high horizontal stresses and a vertical stress greater than a gravity induced stress, was measured at a shallow depth in the Durkin Mine. This stress field, when simulated in conjunction with the rock mass material properties, in the finite element model, gave several significant results. The roof or back of most underground openings was naturally prestressed, indicating probable stable roof conditions. Very little stress change occured in stope pillars and the rock surrounding the Durkin shafts when different mining methods were simulated.

I.-INTRODUCTION

Prior to any engineering structural design, four basic quantities must be defined:-

(a) The geometry of the proposed structure

(b) The nature of, and the relationships between the component physical parts of the structure

(c) The physical engineering properties of all component parts

(d) The loads acting on the structure and thus the stresses induced in its component parts

The combination of these quantities defines the mathematical model of the structure.

"Rock mechanics is the theoretical and applied science of the mechanical behaviour of rock; it is that branch of mechanics concerned with the response of the rock to the force fields of its physical environment."*

In mining design, the science of rock mechanics is used in conjunction with conventional engineering mechanics because rocks are the physical components of the engineering structure.

The role of geology in rock mechanics is of paramount importance. The materials involved are rock masses that either exist in, or have been extracted from a geological environment. The characteristics of the rock masses are a function of their mode of origin and of the subsequent geological processes that have acted upon them. These events, combined during the geological history of a given area, lead to a particular lithology or rock type, to a particular set of geological structures and to a particular insitu state of stress (Ref. 1).

---

*Definition by the Committee on Rock Mechanics, National Academy of Sciences, in "Rock-Mechanics Research", Natl. Acad.Sci.-Natl. Res. Council, Washington, D.C., 1966.

The work reported in this paper was aimed at introducing the subject of rock mechanics to people responsible for applied mining design. Being in a new mining environment, the Kambalda Nickel Mines of Western Australia were used to furnish actual data obtained by a rock-mechanics survey, with the object of fabricating a mathematical model of the physical geological environment in which future mining operations would be undertaken. More specifically the results were used to simulate ground movement around the Durkin Shafts when different stoping methods and sequences were analysed.

II.-INSITU ROCK STRESS DETERMINATION

Using the United States Bureau of Mines (U.S.B.M.) 3-component Borehole Deformation Gauge, (Ref.2), underground rock stress determinations were carried out from the 3-level plat of the Durkin Haulage Shaft. A total of 15 independent diametral deformations was recorded after overcoring 3 diamond drill holes oriented in 3 mutually different directions.

To calculate the complete state of stress at a point requires the measurement of six independent deformations from at least 3 non-parallel boreholes (Ref. 3). Using the statistical method proposed by Panek (Ref.4) more than 6 sets of deformation equations were combined to calculate the least squares estimate of the rock stress field. Starting with 15 sets of equations, a computer was used to remove, in turn, the statistically most unacceptable equation and then calculate the stress field. In Fig. 1 the change in principal stress magnitudes with decreasing number of equations emphasises the need for

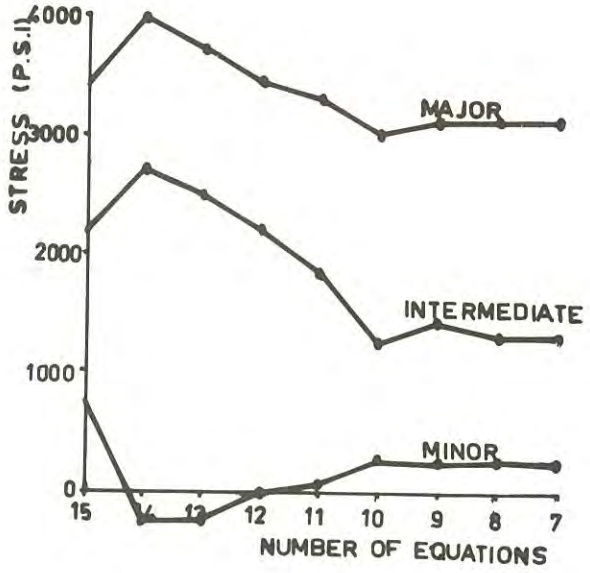

Fig. 1 Variation in Principal Stress Magnitude with Number of Reduction Equations

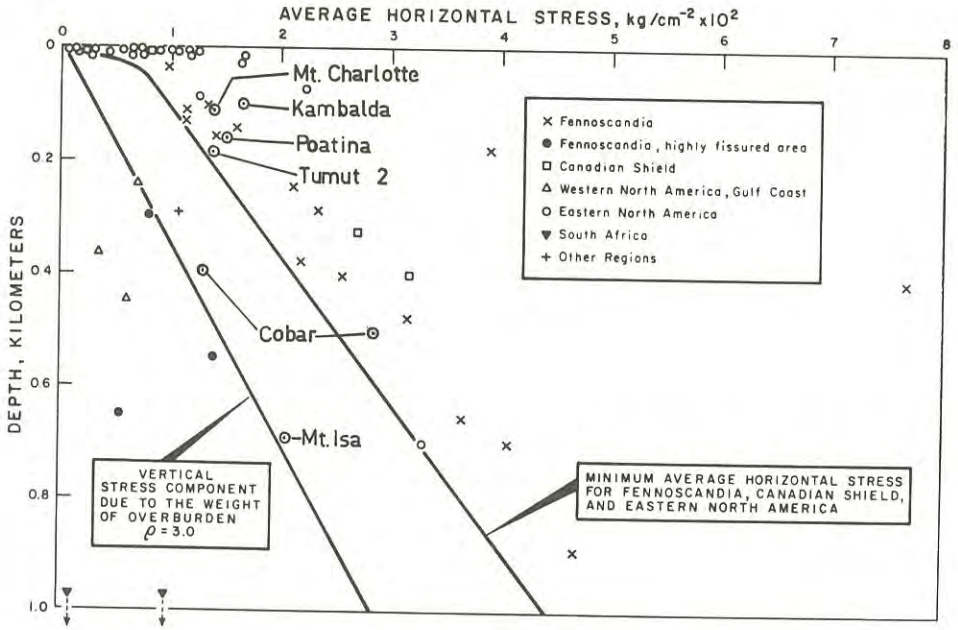

Fig. 2 World Wide Stress Field Results (After Hast Ref. 6)

enough deformation measurements to be made to allow a statistical analysis to be performed to produce the final answers. This condition most probably applies to a mathematical determination of any property of the geological environment.

The virgin rock stress at the Durkin mine was altered when the plat opening was mined thus the "as measured" stress is actually the altered virgin stress.

Using the "finite element" method (Ref.5) both vertical and horizontal sections of the plat were simulated and analyses gave the unconcentrated virgin rock stress that should have been acting prior to excavation of the plat opening.

The rock stress acting approx. 300 ft. below surface in the Durkin Mine was calculated to be

3600 psi – horizontal east-west
1200 psi – horizontal north-south
1080 psi – vertical

These results were particularly significant considering the shallow depth at which they were measured. Fig. 2 is a plot of rock stresses measured world wide by Hast (Ref. 6) and Kambalda results with other Australian measurements are superimposed.

III.-STRUCTURAL GEOLOGICAL INVESTIGATION

The Kambalda Nickel deposits occur on the flanks of a small stratigraphic dome in an ultramafic (serpentinitic) sill like body lying conformably between two meta-basalt formations (Ref. 7).

Most of the detailed structural investigation was carried out on the Durkin shoot. This is generally a tabular ore body dipping approximately 30° to the north and striking approximately east-west with a 10° plunge to the east.

Survey work consisted of:

(a) Inspection and logging of exploration drill core to ascertain general joint frequencies and positions and inter-relationships of the various Kambalda rock types.

(b) Detailed underground structural mapping in all available openings in the Durkin shoot area. Using the "random line" logging technique, joints and discontinuities were recorded then plotted and contoured on equal area stereographic projections, by computer. Fig. 3 gives a typical stereojoint pattern drafted from the computer output.

(c) Recording physical characteristics of predominant joint types, then triple tube core-barrel sampling of them for shear testing.

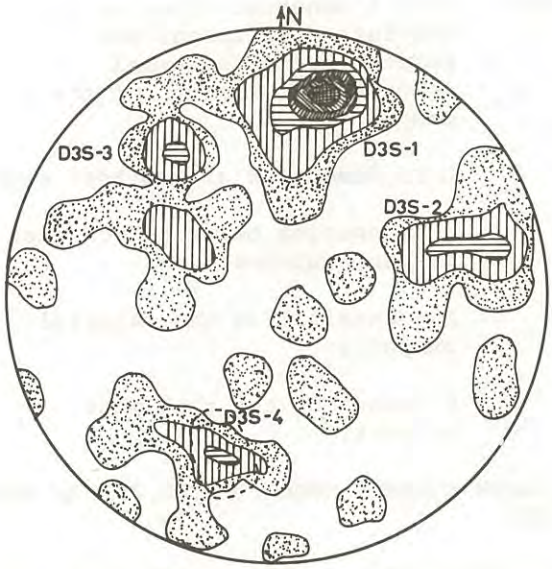

Fig. 3 Joint Contour Diagram

IV.-LABORATORY PHYSICAL ROCK PROPERTY TESTS

A series of laboratory tests was undertaken to determine physical properties of the Kambalda rock types. The various tests carried out were:

(a) Unconfined compression tests

(b) Triaxial compression tests

(c) Tensile (Brazilian) tests

(d) Joint shear tests using the recently designed and built University of Melbourne shear box (Refer to Paper by E.P. Waghorne to be presented at this conference, for shear box details).

V.-ROCK MASS PHYSICAL PROPERTIES

The method of Protodyakonov (Ref. 9) was used to reduce laboratory test values to those of the rock mass. As the work by Deshwar (Ref. 9) gave accurate predictions of ground movement using Protodyakonov's

technique this method was employed at Kambalda.

The rock structural discontinuity statistics were combined with the laboratory test results in equation (1) to predict the rock mass properties.

$$\frac{P\ (material)}{P\ (mass)} = 1 + \frac{b\ (m-1)}{b + L} \qquad (1)$$

where : m is a constant known as mass fracture coefficient and is related to the uniaxial compressive strength of the sample

L is dimension of the test sample

b is spacing between rock mass discontinuities

P (material) is the material property

P (mass) is the rock mass property

VI.-FINITE ELEMENT MODEL OF THE DURKIN SHAFT AREA

A two dimensional computer analysis was made on a vertical east-west section passing through the Durkin shafts. The mining methods and sequences considered were :

(a) Open slot stoping to two different shaft pillar sizes (ore pillar width = ½ stope width).

(b) Uncemented or cemented hydraulic sand fill placed in the stopes and then the ore pillars removed.

(c) Longwall open stoping, retreating towards the shafts.

Stope and pillar layouts on the analysis section are presented in Fig. 4.

The finite element grid is shown in Fig. 5 and extends approximately 400 feet either east or west of the shaft. The model consisted of 399 three or four sided elements connected by 351 nodal points. The element density is greatest around the orebody and shafts as most structural changes occurred in these areas. Also computational procedure becomes more accurate with increasing element density.

The model loading system consisted of a vertical and horizontal tectonic stress field superimposed on a gravity loaded stress field. Model boundary pressures were adjusted until the stresses at the simulated stress measuring site were the same as the predicted insitu field stresses.

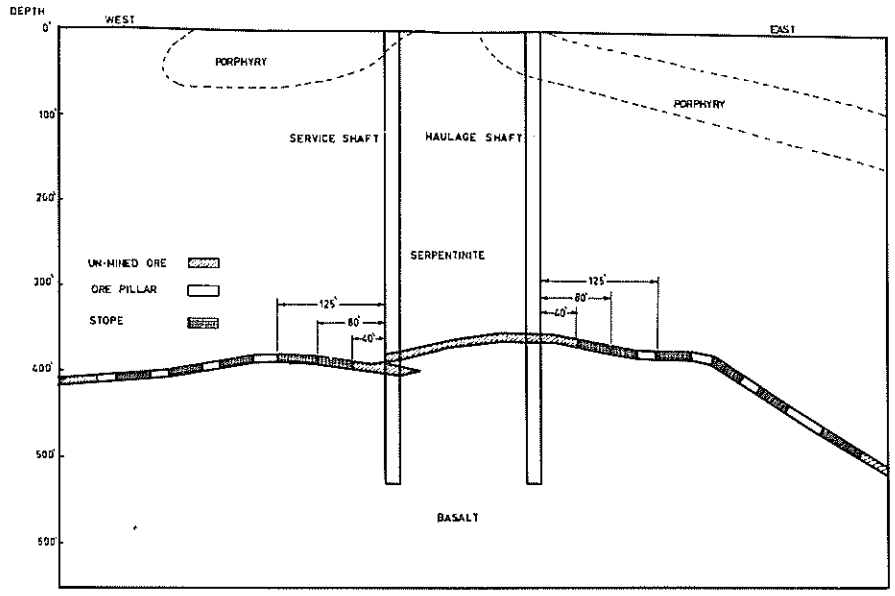

Fig. 4 Stope & Pillar Mining Layouts (E-W Section)

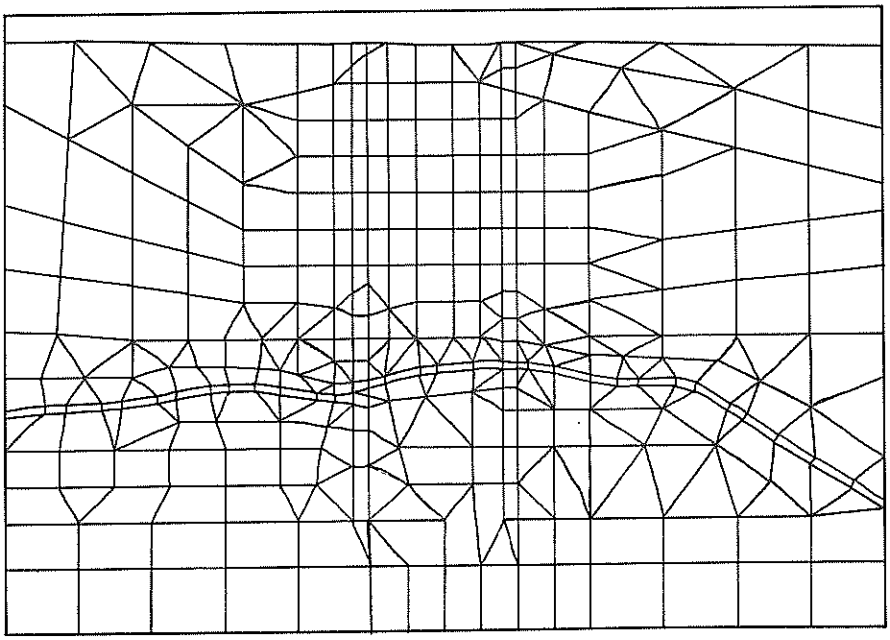

Fig. 5 E-W Section Through Durkin Shafts - Finite Element Grid

VII.-RESULTS OF MINING SIMULATIONS

Results of each analysis of the various mining alternatives were contour plotted by computer. The plots obtained for each test were :

(a) Major principal stress (psi)

(b) Minor principal stress (psi)

(c) Vertical displacement (subsidence)

(d) Horizontal displacement

A typical vertical subsidence plot is given in Fig. 6.

From an assessment of all simulations it was obvious that hydraulic fill played very little part in ground control. In reality, it is known that once the rock has failed the fill does control ground movement. The finite element procedure however did not consider inelastic failure and thus caving of rock. This is a limitation in studies of total ground movement. However, prior to failure the fill appeared to provide negligible support.

Wide openings appeared to remain stable probably due to the 'prestressing' horizontal compression of the stope 'backs'.

Stresses within the shaft pillars changed very little in all the simulations thus concrete shaft linings would probably remain relatively low stressed.

Decreasing the shaft pillar radius by mining closer to the shaft brought the subsidence trough (high subsidence gradient) closer towards the shafts. In this case the location of fault or weakness zones would be expected to control any shaft movements.

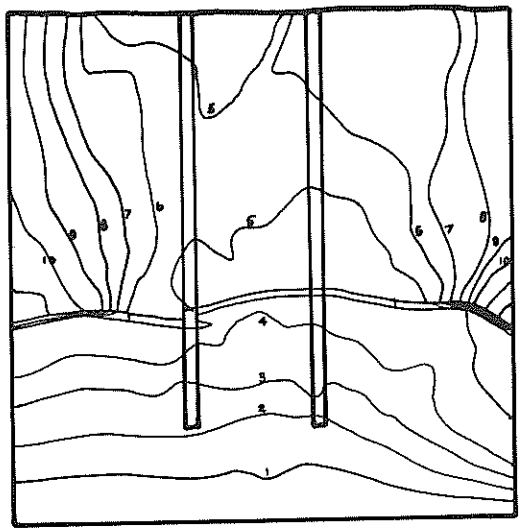

Fig. 6 Vertical Subsidence Plot

Ground movement monitoring stations would thus be required in these regions.

VIII.-CONCLUSIONS & DISCUSSION

The work described above was carried out with the aim of introducing to practising mining engineers the basic requirement of a rock mechanics investigation and to show the use of the data obtained in a structural mine investigation.

The results of the finite element analysis although probably not quantitatively realistic show the relative effects of different mining strategies or sequences.

With continual updating of the mathematical model as more detailed information becomes available the predicted results should quantitatively approach the actual measured values. Only with this constant updating will the method become a major decision making tool for use in long term planning and design.

IX.-ACKNOWLEDGEMENT

The author wishes to thank the management and staff of Kambalda Nickel Operations, Western Mining Corporation Pty. Ltd., for the opportunity to use their facilities at Kambalda during the course of his University Research work and for permission to publish this paper.

He is also indebted to Mr. W. E. Bamford of the University of Melbourne Mining Department for suggesting and supervising the project.

In addition he would like to thank Mr. A. G. Bennet, Ph. D. research student, Dept. of Mining, University of Melbourne, without whose assistance and computer programming all finite element analyses could not have been undertaken.

REFERENCES

1. DEERE, D.V., 1968 - Rock Mechanics in Engineering Practice (ed. Stag and Zienkiewicz : Wiley and Sons : London), Ch. 1.

2. MERRILL, R.H., 1967 - Three component borehole deformation gauge for determining stress in rock, U.S. Bur. Mines, Rept. Inv., No. 7015.

3. GRAY, W.M., and TOEWS, N.A., 1967 - Analysis of accuracy in determination of ground stress tensor by means of a borehole device, 9th Rock Mech. Symp.Colorado School of Mines.

4. PANEK, L.A., 1966 - Calculation of the ground stress components from measurements of the diametral deformation of a drill hole, Testing Techniques for Rock Mechanics A.S.T.M. STP.402.

5. ZIENKIEWICZ, O.C., and CHEUNG, Y.K.,1967- The Finite Element method in Structural and Continuum Mechanics (McGraw Hill : London).

6. HAST, N., 1969 - The state of stress in the upper part of the earth's crust. Tectonophysics Vol. 8 : 169-211.

7. WOODALL, R., and TRAVIS, G.A., 1969 - The Kambalda nickel deposits, Western Australia, 9th C'wlth. Min. Metall. Cong. London.

8. PROTODYAKONOV, M.M., 1965 - Methods of evaluating the cracked state and strength of rock insitu. 4th Int. Conf. Strata Control & Rock Mech., New York.

9. DESHWAR, K.H.S., 1970 - Determining insitu rock strength, Engineering and Mining Journal, May, 84-5.

Horizontal Pillar Extraction at Mt. Isa Mines Limited –Some Rock Mechanics Aspects

By

D. B. Edwards, B.Sc., Ph.D. (Dunelm), C.Eng., M.Aus.I.M.M.

(Senior Rock Mechanics Engineer, Mount Isa Mines Limited)

SUMMARY AND ABSTRACT.- Sublevel caving in rib pillars in the 650 Copper orebody allowed excessive dilution of ore. For horizontal pillar extraction after encouraging photoelastic analysis a series of cut and fill stopes 12 ft wide using ringblasting and cemented fill, and leaving temporary transverse pillars proved successful. Subsequently the temporary pillars up to 42 ft wide were extracted. Crown pillars 10 ft thick (and sometimes 20 ft) provided safety from filled stopes above. Stability measurements of levelling and convergence and with borehole extensometers indicated high stress values, but the deterioration which occurred did not lead to collapse.

In preparation for sublevel stoping of pillars above old cut and fill stopes in the 8, 9 and 10 lead orebodies, finite element and photoelastic two dimensional analyses were made, and indicated extremely high stress concentrations. To overcome limitations of two dimensional analyses a three dimensional physical model, highly instrumented, was tested and indicated less extreme conditions. Subsequent extraction bore out the practicability of sublevel stoping beneath the narrow wedge of ore forming the crown pillar. Fracturing was observed, but no serious instability resulted, but due to fill breakthroughs from above 30 percent of drawpoints were abandoned prematurely. Extensometers and stress meters monitored the initial slotcutting and subsequent stoping and showed greatest ground adjustments on shotfiring. Some correlation was found between these measurements and the prior finite element analyses, although both analytical methods indicated stress much higher than experienced in practice. Lack of detail in the physical model apparently gave higher strength and prevented some crown pillar failures which occurred in practice.

I.- INTRODUCTION

Remnant pillar extraction has always been one of the more interesting activities in mining due to the higher than normal stress levels encountered. Adequate planning involves ensuring that pillar extraction design must be part of the overall mining design in an area if recovery is to be optimised. Two examples of pillar extractions will be given which were not integrated into the initial planning stage but, which having proved successful, can now be used on a repetitive basis.

II.- HORIZONTAL PILLAR EXTRACTION 'A' 10 LEVEL COPPER STOPES, 650 OREBODY

(a) Extraction Method

Sublevel caving had been used to extract vertical rib pillars and a section of the 10 level floor pillar, but the degree of recovery of the broken ore was found to be severely dependent upon the distribution of copper slag in the dry fill used to fill the original void. This fine material filtered through very quickly after firing causing unacceptable dilution. Most of the remaining 10 level floor pillar had slag immediately overlying it, so another method of extraction was designed for this section.

Transverse stopes were extracted in the pillar leaving a thin shell of ore intact to prevent dilution, with filling of these stopes with cemented fill immediately after mining (Ref. 1). The remainder of the pillar between the filled stopes could then be extracted by a method dependent upon the experience gained in the initial extraction.

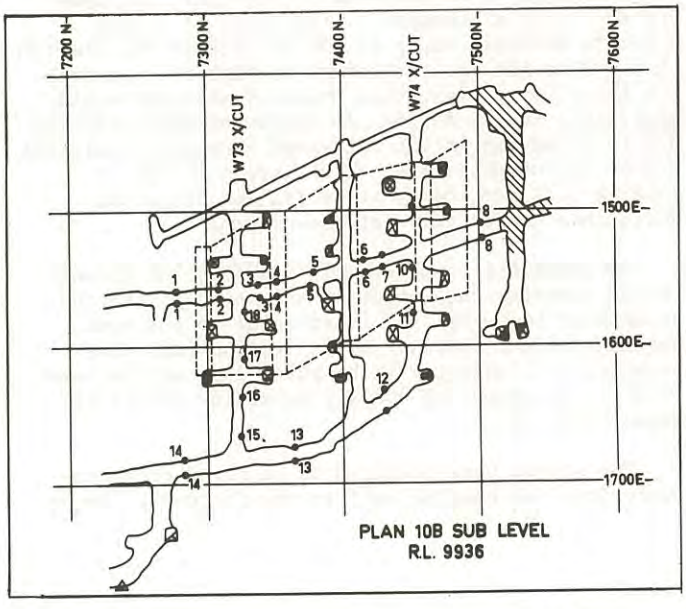

Fig. 1 Plan of 10B sublevel 650 copper orebody.

The pillar to be extracted was approximately 200 ft in strike length and between two vertical pillars. Stope No. 1 (Figs. 1 and 2) had its southern wall at the northern limit of the 7250N vertical pillar and stope No. 8 had its northern wall at the southern limit of the 7550N vertical pillar. The eight transverse stopes were 12 ft wide with a pillar of approximately 15 ft between each stope in the initial design but this was subsequently modified (see later).

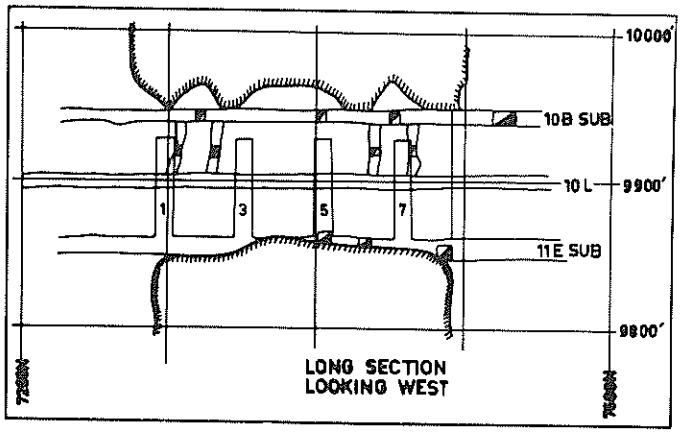

Fig. 2 Long section, looking west, of pillar extraction area.

A 10 ft thick (minimum) crown pillar was left below 10B sublevel as a support to prevent dilution to fill from the grizzlies of the stopes above. It was realised that at some stage of the extraction this crown pillar would be stressed well above the rock strength in an East-West direction. The laboratory uniaxial compressive strength of silica dolomite averaged about 21,000 psi and it was through that due to the massive nature of this rock comprising the floor pillar, this order of strength would be applicable in the field. It was hoped that cracking due to stressing in the East-West direction would not reduce the effectiveness of the crown pillar in holding fill vertically above it, and the crown would span effectively between stopes.

Cemented fill requirements included the potential of carrying the weight of the crown pillar and an arch of loose fill at least equal to the span between initial stopes. Stope heights (and thus cemented fill unsupported heights) were approximately 80 ft to in excess of 100 ft, depending on cut off grade (Fig. 3).

The stopes were designed to be fired progressively from the hanging wall to the footwall. Rings

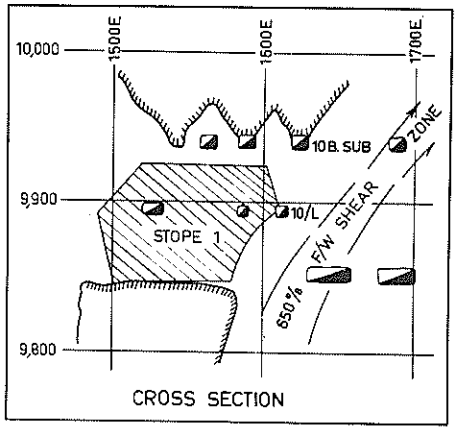

Fig. 3 Cross section on stope 1, 650 orebody.

drilled in north-south vertical planes were fired back until slashing rings drilled in east-west vertical planes could be fired. Slushers and LHD units were used to extract the fired ore on 11E sub.

(b) Model Work

A photoelastic examination was made of the area in an attempt to arrive at an optimum stoping sequence from the viewpoint of ground stresses. Two photoelastic models of various stope extraction sequences in plan were tested. The average east-west stress on the pillar was estimated to be 6500 psi, and the 'in situ' uniaxial compressive strength was taken to be 15000 psi with the tensile strength at 2500 psi. The models were cut from $\frac{1}{2}$ in. thick sheets of Columbia Resin No. 39, being $11\frac{1}{2}$ in. square and loaded uniaxially in a direction at about 20° to the long axis of the stopes.

Analysis of the first model was carried out in two stages.

First stage – stopes 1, 3, 5 and 7 out (Fig. 4)
Second stage– all stopes out.

In the second model, analysis was carried out in four stages.

First stage – stopes 4 and 5 out.
Second stage – stopes 3, 4, 5 and 6 out.
Third stage – stopes 2, 3, 4, 5, 6 and 7 out.
Fourth stage – all stopes out.

The models were each loaded to two 'fringes' and stress concentration factors calculated at the

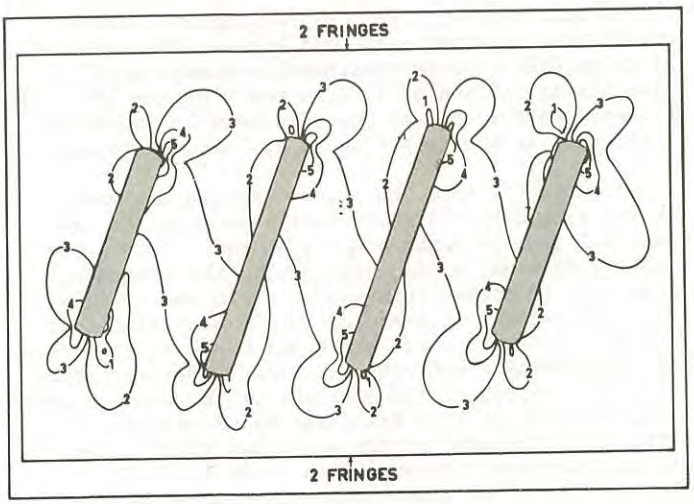

Fig. 4 Photoelastic fringe pattern, first stage of first model.

mid span of the pillars together with the maximum and minimum stress concentration factors. The maximum values were usually at the NW-SE corners and the minimum values on the opposite diagonal.

Conclusions drawn from the photoelastic work were:-

(i) The extraction sequence in the first model produced lower stress concentrations for a greater part of the extraction sequence than that in the second model.

(ii) The north west and south east corners of the stopes would exhibit scaling effects and audible microseismic activity would take place at an early stage with each sequence. This was not noticeable in practice.

(iii) The rock tensile strength would be exceeded at the north east and south west corners of the stopes. This would cause vertical cracking roughly perpendicular to the bedding. Again this was not immediately apparent in practice but could have been hidden by cracking due to blasting.

(c) Movement Monitoring

It was recommended that no delay took place between emptying a stope and filling it with cemented fill. It was not anticipated that the wide zone of shearing to the footwall of the orebody would have much effect on the operation. Development cross sections were to be kept to a minimum and bolted in an attempt to reduce ground failure effects. In practice, some trouble was found in development on 11E sub in that the ground of the back of Z74-75 stope was very broken with flat dipping cracks at right angles to the general bedding plant dip predominating. As the crosscut development for 1, 2 and 3 stopes neared the hanging wall one of these partings was followed and used as the back of the crosscut. This increased the height of the drive but provided a more stable excavation. The lower parts of the pillars between the extraction crosscuts of Nos. 1 to 4 stopes were very broken near the hanging wall, while between 3 and 4 stopes an opening appeared in the wall due to development firings. There was no difficulty rockbolting the backs, but the broken walls could not be completely bolted. Further north the development was in more competent ground.

Movement measuring stations were set up on 10B sub in the crown pillar above the stopes (Fig. 1) and in the vertical pillars to the north and south on 10 level in order to monitor ground behavior. Extensometers and a self adjusting parallel plate level giving measuring accuracies of $\pm$ 0.01 inch were used.

Extraction of 1,3,5 and 7 stopes produced unusual levelling rises possibly due to tilting of blocks in the two crosscuts (Figs. 5a and 6a). Measurements in the crosscuts were not possible after these initial stope extractions due to difficulty of access. Generally east-west compressions were measured with the extensometer due to this extraction the order of movement being quite low (Figs. 5b and 6b) but in excess of what would be expected from a purely elastic situation. Stress increases of approximately 40,000 psi could be calculated using a rock modulus of 10^7 psi.

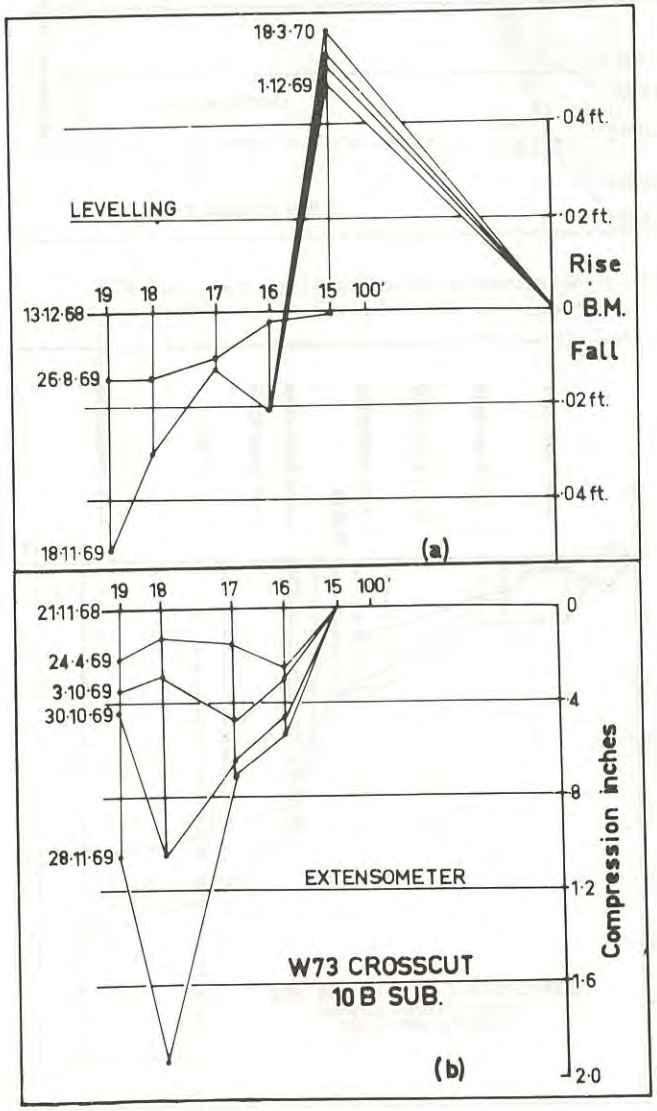

Fig. 5 Extensometer and levelling results, W73 crosscut, 10B sublevel.

Visible cracking occurred between stations 17 and 18 after the extraction of stope 3 but not after the extraction of stope 1. This cracking was comparable to that described previously as being in the back of the stopes below 10 level, that is, flatly dipping to the east and roughly perpendicular to the general bedding direction. Thus the capacity of the crown pillar to span north-south was not affected.

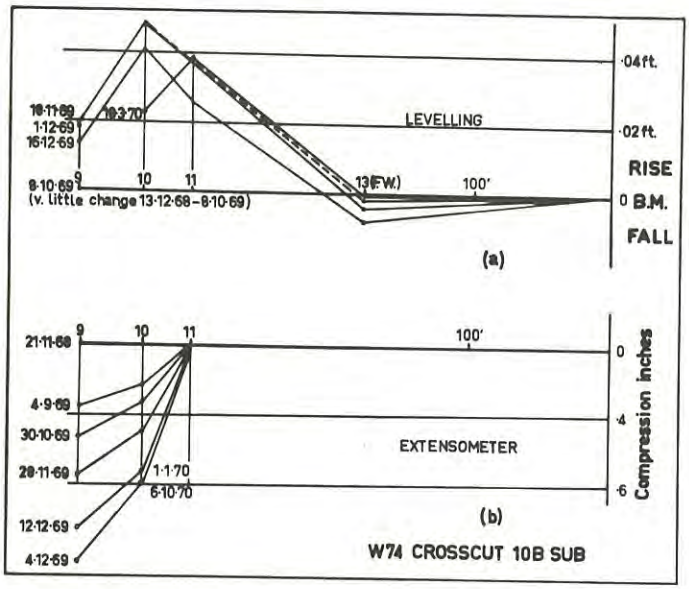

Fig. 6 Extensometer and levelling results, W74 crosscut, 10B sublevel.

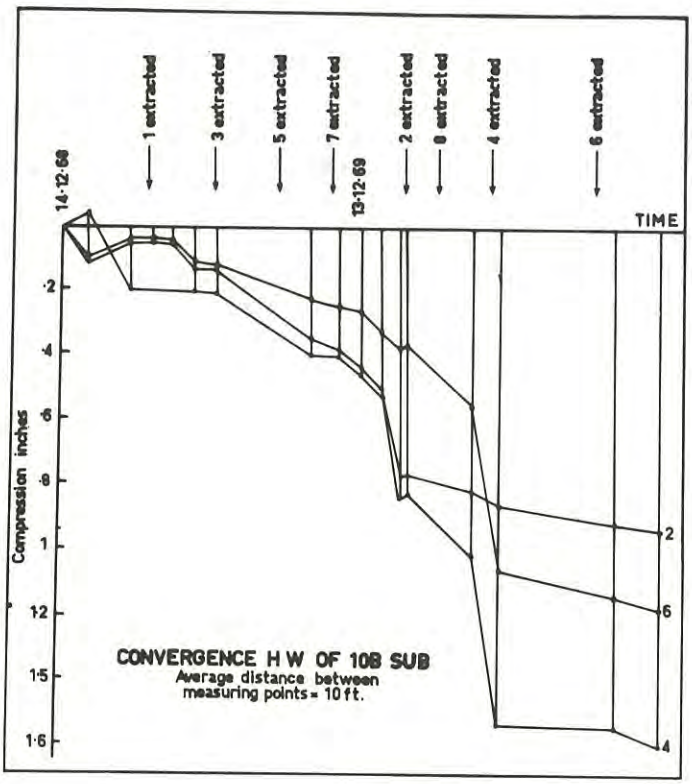

Fig. 7 Extensometer convergence measurements – hanging wall drive 10B sublevel.

It will be noted that the hanging wall drive convergence, measured east-west between the sides of the drive did not show considerable change until after the extraction of 1, 3, 5 and 7 stopes (Fig. 7). This was probably due to the considerably increased strike span of the remaining 2, 4, 6 and 8 stopes.

A variation from the initial design was made for the secondary stopes in that a proposal to extract all the ore between 1 and 3 stopes leaving cemented fill walls was made, giving the subsequent stope a 42 ft north-south width. This was successfully carried out in practice but it was noted that when the east-west stope width was 80-90 ft considerable microseismic activity and visible deterioration suddenly occurred on 10B sublevel in the hanging wall area. Because of this No. 4 and No. 6 stopes, although of the same strike width had their crown pillar thickness increased from 10 ft to 20 ft minimum dimension. These were also successfully extracted but again with signs of increased deterioration at stope widths of 80-90 ft. No. 8 stope design was not altered and gave little trouble since it was abutting onto a vertical pillar.

The increase in east-west stress necessary to produce the observed deformation in the hanging wall drive was estimated to be about 40,000 psi assuming a field elastic modulus of 10^7 psi. Some spalling of the roof occurred in this drive to a depth of about 1 ft but no cracking of the sides was observed.

(d) Conclusions

Although fractured near its hanging wall side after the primary stope extractions the crown pillar successfully prevented fine fill from entering subsequent open stopes spanning 42 ft by 100 ft area. Monitoring of ground movements indicated that most deterioration occurred during the extraction of the secondary stopes. Stress increases in the crown pillar were equivalent to 30,000-40,000 psi if a rock modulus of 10^7 was assumed.

III.- HORIZONTAL PILLAR EXTRACTION 'B' 8, 9 AND 10 LEAD OREBODIES, 9 LEVEL

(a) Extraction Method

Upper limits for cut and fill mining were reached in Nos. 8 and 9 hanging wall lead orebodies at about 75 ft below 9 level due to localised ground falls resulting from high stressing. This occurred earlier than anticipated probably because of an under-estimation of the stress level which was based on the weight of superincumbent rock. Calculation showed that a 50% recovery of pillar ore in all orebodies would be equivalent to a new orebody.

The sublevel stoping method proposed to recover the horizontal pillar is shown in Fig. 8.

Transverse cut off slots were to be developed at about 80 ft intervals along strike. The remaining ore would be fired to expand into the slots. A vital requirement was that a narrow wedge of ore immediately below the hydraulic fill in the stopes above 9 level remained intact and prevented dilution from this fill. Due to the attractive economics of the method, in that all metal above that extracted for cut off slots was clear profit, and the potential repeatability of the operation in other orebodies, additional investigation programmes were pursued.

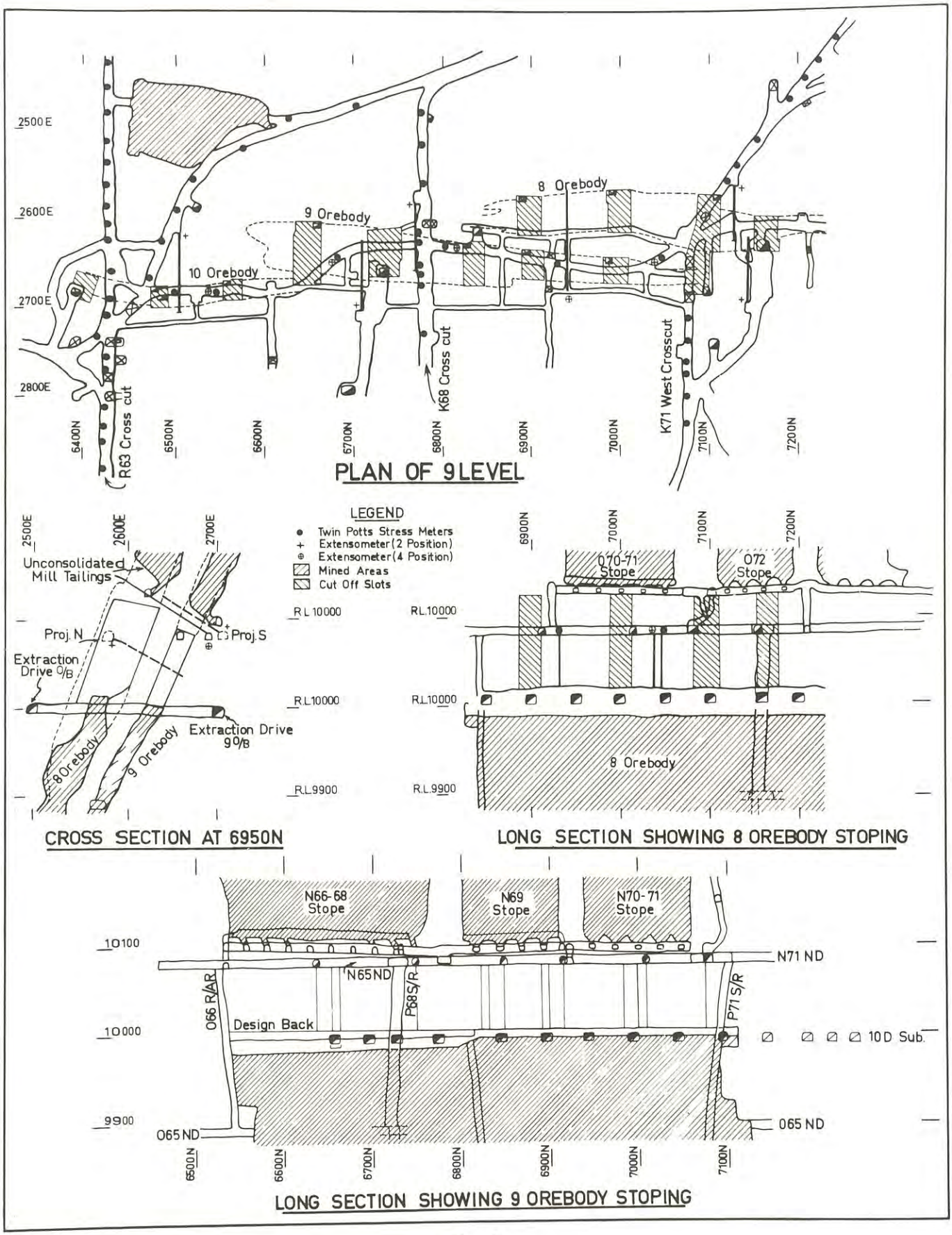
2500E
2600E
2700E
2800E
9 Orebody
8 Orebody
10 Orebody
K68 Cross cut
K71 West Crosscut
R63 Cross cut
6400N
6500N
6600N
6700N
6800N
6900N
7000N
7100N
7200N
PLAN OF 9 LEVEL
LEGEND
Twin Potts Stress Meters
Extensometer (2 Position)
Extensometer (4 Position)
Mined Areas
Cut Off Slots
Unconsolidated Mill Tailings
Proj. N
Proj. S
Extraction Drive 9/B
Extraction Drive 9/B
8 Orebody
9 Orebody
R.L 10000
R.L 9900
CROSS SECTION AT 6950N
070-71 Stope
072 Stope
8 Orebody
LONG SECTION SHOWING 8 OREBODY STOPING
N66-68 Stope
N69 Stope
N70-71 Stope
10100
10000
9900
N71 ND
N65 ND
066 R/AR
P68S/R
P71S/R
Design Back
10D Sub.
065 ND
065 ND
LONG SECTION SHOWING 9 OREBODY STOPING

Fig. 8.

(b) Model Tests

Three models of the area were made of the extraction to investigate stability. Firstly, a two dimensional finite element model was constructed with loading perpendicular to the bedding about 1.4 times that down the bedding. The effect of extracting the pillar upon stresses and displacements in an isotropic elastic medium defined by a modulus of 10^7 psi and Poissons ratio 0.25 was determined. Compressive stresses of over 40,000 psi for an applied stress perpendicular to the bedding of 2500 psi were found on the immediate underside of the wedge so that plastic flow or failure was expected here. It was realised however that this two dimensional model did not take into account the finite strike length of the orebodies or the effects of vertical pillars in 8 and 9 orebody stopes above 9 level (see also comparison between actual and calculated displacements on 9 level in section on monitoring). A photoelastic model, also in two dimensions, was made to investigate stresses due to pillar extraction with comparable results but even higher stress concentrations on the wedge.

A physical model was also constructed by the Australian Coal Industry Research Laboratories (ACIRL) to determine the feasibility of design and the stress distributions as the respective orebodies were mined. The model scale was 1 in 148 with stresses applied being 2500 psi normal to bedding, 1400 psi down bedding and 1900 psi horizontally along bedding. A full report of the model test is given in Ref. 2. The main conclusions drawn were:-

(i) The formation of expansion slots for the mass firing was a feasible procedure. The stability of the openings and the pillars surrounding them was excellent and no troubles were likely to accur at this stage. This was borne out in practice.

(ii) Longitudinal separation parallel to the bedding coupled with a transverse break on the 8 orebody side occurred in the footwall of 9 orebody at 7200N in the model. Some fracturing of the diaphragm between 8 and 9 was noted in practice but little damage occurred at 7200N.

(iii) Most of the 50 strain gauges incorporated in the model indicated stresses well below 20,000 psi which was the maximum recorded. The general impression gained from the model was that high stressing would not occur and this was borne out in practice except that the northern abutment of the area gave some audible microseismic effects for one week after the firing.

(iv) The planned wedge dimensions seemed more than adequate in the model but possibly fill arching took place in the model which did not occur in practice since a fill breakthrough actually occurred immediately after firing in the widest part of the extraction at 6600N. Seven of the twenty three drawpoints had to be abandoned prematurely. In the model, fill was exposed in places but did not run.

(v) An important factor in wedge stability would be jointing but this unfortunately could not be incorporated in the model.

Overall, the model gave a reasonable assessment of the situation as found but probably over-estimated wedge stability by omitting the finer structural features.

(c) Monitoring of Ground Movements and Stresses

Devices installed to detect strain changes as a result of slot cutting were as follows:-

(i) Two position extensometer installations to monitor change in strain across the pillar.

(ii) Four position extensometer to monitor changes in strain down dip in the pillar.

(iii) Twin 'Potts' stressmeter installations between each slot with blades located on strike and at 90°.

The latter showed little change and the majority were damaged before and during slot cutting. The extensometers showed movements of $\frac{1}{2}$ in. compression across the pillar due to slot cutting and are thought to be of little significance and so are not reported here.

Of more interest were the levelling and extensometer measurements taken in R63, K68 and K71 on 9 level (see Figs. 9 and 10).

The results in R63 and K71 crosscuts are shown in Fig. 9 and give the difference between immediately before the firing and immediately after the firing. These crosscuts were in the south and north abutments respectively and appear to indicate different behavior vertically as R63 hanging wall area rises but K71 falls while R63 footwall rises close to the extraction area while K71 has a pronounced fall. Horizontal movement trends are similar however with the larger extraction width at K71 possibly causing the larger order of movement at this location.

K68 crosscut, being approximately on the centre line of the extraction might allow a comparison with the movements calculated from the finite element model. Such a comparison is made in Fig. 10. Some correlation was achieved in that the same directional trends of movement were observed on the hanging and footwalls as were indicated by the model.

(d) Conclusions

The stresses estimated by finite element and photoelastic models seemed to be too high, possibly because of the three dimensional nature of the problem involving incorporation of vertical pillars. The lower deformations than obtained in practice of the finite element model may be due to too high a modulus being assumed.

The physical model could be deemed a fair assesment of reality but by not incorporating the finer structures in the shale the wedge stability was over-estimated.

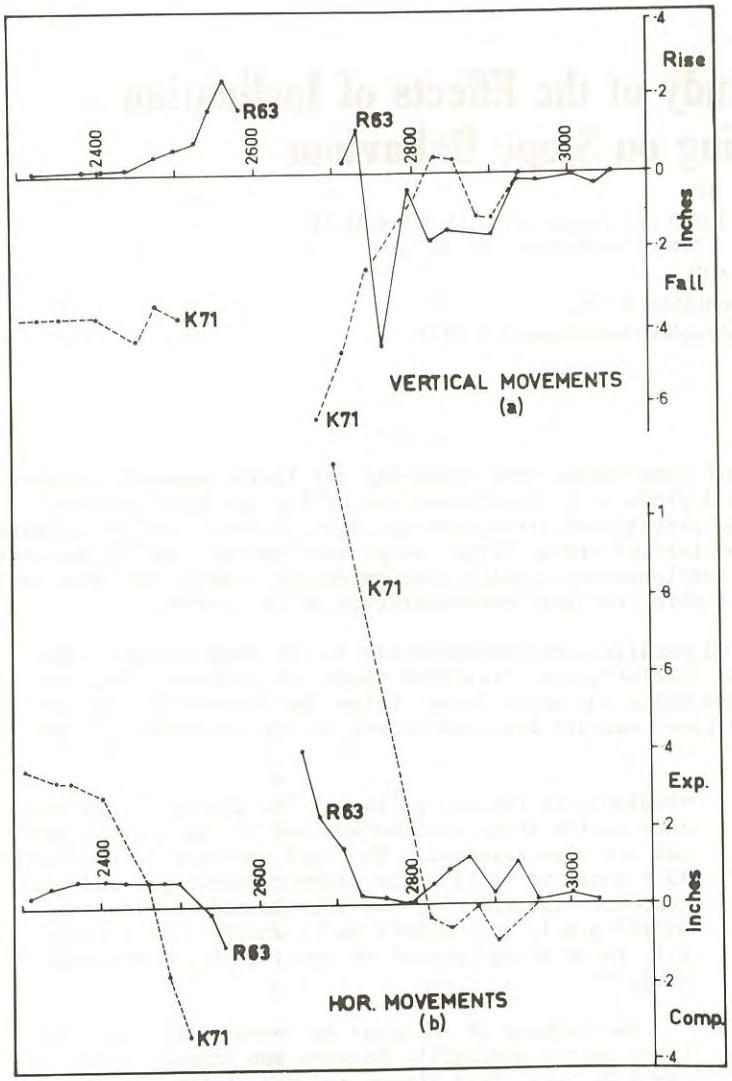

Fig. 9 Levelling and extensometer results, R63 and K71 crosscuts, 9 level.

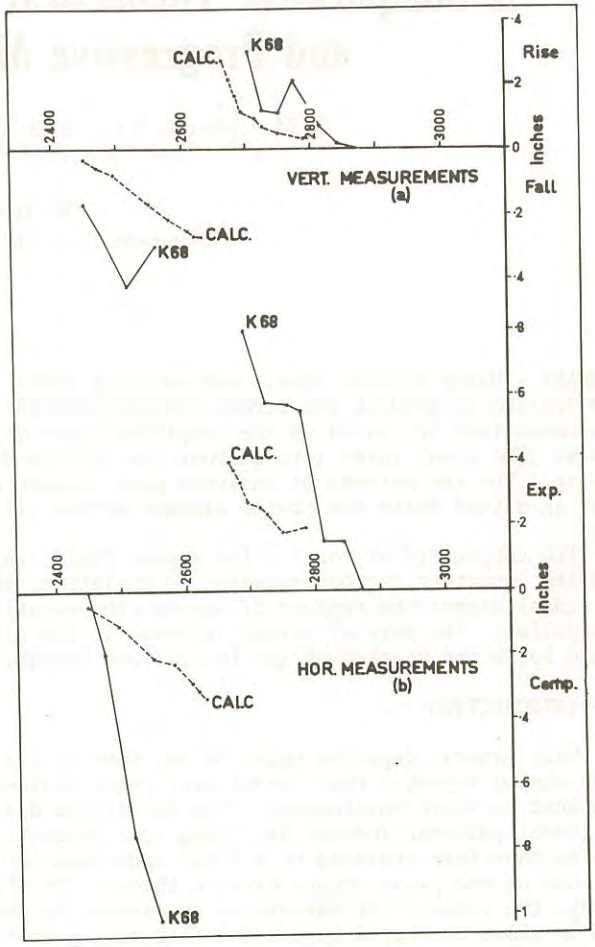

Fig. 10 Extensometer and levelling results K68 crosscut and comparison with finite element calculated movements.

IV.- ACKNOWLEDGMENTS

The author wishes to thank the management of Mount Isa Mines Limited for permission to publish this paper.

REFERENCES

1. JONES, T.O. - Pillar recovery in a Section of the 650 Orebody Floor Pillar using Cemented Fill. Proc. Regional Conference Aus.I.M.M. Tennant Creek, May 1970.

2. A.C.I.R.L. - Report on Model Test to Examine the Extraction of 8 and 9 Orebodies of the Racecourse Lead Orebodies to Mount Isa Mines Limited, July 1969.

A Comparative Theoretical Study of the Effects of Inclination and Progressive Mining on Stope Behaviour

By

C. M. Gerrard, B.E., M.Eng.Sc., Ph.D., M.I.E.Aust., A.M.Aus.I.M.M.
(Senior Research Scientist, Division of Applied Geomechanics, C.S.I.R.O.)

AND

W. Jill Harrison, M.Sc.
(Experimental Officer, Division of Applied Geomechanics, C.S.I.R.O.)

SUMMARY.- Using elastic theory and assuming plane strain conditions, both crack-tip and finite element analyses are applied to predict the stress and displacement field produced by the excavation of two co-linear stopes. The conditions are based on the simplified geometry and provisional stress modulus data of the C.S.A. Mine Cobar, N.S.W. The study takes into account the effects of the initial stress field, stope inclination, and progressive mining. The two methods of analyses give similar and complementary results; the crack-tip results are more general in nature while the finite element method allows a more realistic representation of the geometry.

The components of the initial stress field, resolved parallel and perpendicular to the stope orientation, are the important factors relating to variations in the initial stress field and stope inclination. For two co-linear stopes the regions of stress concentration are above the upper stope, below the lower stope and in the pillar. The rate of stress increase in the pillar rises rapidly when the length of the ore pillar is reduced below one quarter of the final stope height.

I.- INTRODUCTION

Many mineral deposits occur in the form of flat lens-shaped deposits that extend over great distances compared to their thicknesses. The stress and displacement patterns induced by mining such deposits can be therefore analysed to a first approximation by the use of the plane strain elastic theory. In this study, the geometry of the stopes considered is modelled on those developed by cut and fill mining at the Cornish, Scottish, Australian (C.S.A.) Mine, Cobar, New South Wales, Australia. Here, the ore bodies are in a number of parallel zones of lenticular shape, striking north-south and dipping east at approximately 75° (Ref. 1, 2). The ore bodies are approximately 40 ft wide and several thousand feet deep. The planned mining procedure is to commence stopes at every 600 ft (183 m) of this depth. Two such levels, 1200 ft (366 m) and 1800 ft (549 m), are currently being worked by mining upwards.

The analysis presented is concerned only with a single ore body and with the development of two adjacent stopes corresponding to the above levels (Fig.1). While being based on conditions at Cobar, this analysis is sufficiently general for application to other similar mining operations. The initial stress magnitudes used, and their variation with depth, are shown in Fig. 2 and are based on the measurements of Stephenson (Ref. 3). His results confirm the assumption that one of the principal stress directions is almost parallel to the strike. From Fig. 2 it can be seen that the variation of vertical, direct stresses approximately agrees with the rule of thumb of 1 p.s.i. per foot depth (22,290 Nm^{-2} per metre), and this was found by the U.S.B.M. to have widespread application (Ref. 4).

The aim of these studies is to predict the effect of progressive stope development on the stresses and displacements developed in the surrounding rock, particularly in the ore pillars. The effects of variations in the stope inclination and in the initial stresses are also examined. The rock surrounding the stopes is assumed to be linearly elastic, isotropic and homogeneous. The value of the elastic modulus was taken as 10^7 p.s.i. (6.9×10^{10} Nm^{-2}) and Poisson's ratio 0.2, these being typical of rocks in the Cobar area (Ref. 5).

Two methods of analyses are used. The first is based on the similarity between the stress fields surrounding long, thin stopes and the stress fields surrounding Griffith cracks (Ref. 6, 7). The stress and displacement fields surrounding cracks are given by simple, crack-tip expressions from which the role of the various parameters can be readily seen. In the second method, the geometry of the stopes is represented more accurately by the use of finite element meshes, and the displacement and stress fields are computed. However, because of its numerical nature this method does not lead to any simple expressions indicating the effect of the various parameters on stresses and displacements.

For a single stope of a width less than 5 per cent of a stope length, Ryder and Officer (Ref. 6) have obtained a good correlation between the displacement field surrounding a Griffith crack and the rock movement measured *in situ*. For stopes of a larger width to length ratio (1:3), Nair and Udd (Ref. 8) have calculated the principal stresses for a two-stope situation by combining photo-elastic techniques and a finite difference procedure.

II.- NOTATIONS

x, z	cartesian co-ordinates in horizontal and vertical directions.
α, β	cartesian co-ordinates parallel to and perpendicular to the stope orientation (see Fig. 1).

r, θ	cylindrical co-ordinates with origin at the crack-tip (see Fig. 1).
a	half length of stope or crack.
$\widehat{xx}$, $\widehat{zz}$, $\widehat{xz}$	components of stress referred to the x, z co-ordinates.
$\widehat{xx}_o$, $\widehat{zz}_o$, $\widehat{xz}_o$	components of initial stress referred to the x, z co-ordinates.
$\widehat{\alpha\alpha}$, $\widehat{\beta\beta}$, $\widehat{\alpha\beta}$	components of stress referred to the α, β co-ordinates.
$\widehat{\alpha\alpha}_o$, $\widehat{\beta\beta}_o$, $\widehat{\alpha\beta}_o$	components of initial stress referred to the α, β co-ordinates.
u_α, u_β	displacements referred to the α, β co-ordinates.
$\widehat{aa}$, $\widehat{bb}$	principal stresses.
E, ν	elastic modulus and Poisson's ratio of the rock mass.
S	elasticity tensor of the rock mass.
K_I, K_{II}	stress intensity factors for Mode I and Mode II respectively.
g_I, g_{II}, h_I, h_{II}	functions of S and θ for Mode I and II respectively.

III.- METHODS OF ANALYSIS

(a) Crack-Tip Analysis

A single stope may be considered as a long, thin opening surrounded by elastic material. The surfaces of the opening are stress-free and have a dominating influence on the distribution of stresses in the regions surrounding the ends of the opening, while the intensity of the stress field depends only on the loading conditions on remote boundaries. As suggested by Jaeger and Cook (Ref. 7), an idealization of a long, thin opening is a Griffith crack, the limiting case of a slender ellipse. This method makes use of the fact that the stress field near the end of a long, thin opening is very similar to the stress field in the vicinity of a crack in a body outside of a circle centred on the tip of the crack and of a radius of the same order of magnitude as the width of the opening.

General stress fields near crack tips can be obtained by a linear superposition of the stress fields due to several distinct modes of cracking. For plane strain conditions with no initial, longitudinal shear stress, the two relevant modes are the compressive or tensile mode (Mode I), where the crack surfaces move directly towards one another or apart, and the forward shear mode (Mode II), where the crack surfaces move with respect to one another in a direction parallel to the crack orientation, i.e. direction α in Fig. 1. Paris and Sih (Ref. 9) have presented closed-form results for the stresses and displacements produced by these two modes. In the region relatively close to the end of a crack, i.e. $r < a$, their formulae can be summarized as:

Mode I

$$\widehat{\alpha\alpha},\ \widehat{\beta\beta},\ \widehat{\alpha\beta} = K_I \cdot r^{-\frac{1}{2}} \cdot g_I(S,\theta) \qquad \ldots(1a)$$

$$u_\alpha,\ u_\beta = K_I \cdot r^{\frac{1}{2}} \cdot h_I(S,\theta) \qquad \ldots(1b)$$

Mode II

$$\widehat{\alpha\alpha},\ \widehat{\beta\beta},\ \widehat{\alpha\beta} = K_{II} \cdot r^{-\frac{1}{2}} \cdot g_{II}(S,\theta) \qquad \ldots(2a)$$

$$u_\alpha,\ u_\beta = K_{II} \cdot r^{\frac{1}{2}} \cdot h_{II}(S,\theta) \qquad \ldots(2b)$$

These equations hold for the general case of multiple co-linear stopes, non-uniform, initial stress fields and anisotropic material properties.

The stresses and displacements are products of three quantities. The first of these, either K_I or K_{II}, are known as the stress intensity factors appropriate to Modes I and II. These are functions only of the initial stress field and the crack geometry, and are very useful in comparing different situations. The second quantity is a function of the radial co-ordinate of the point being considered (r), $r^{-\frac{1}{2}}$ for stresses, and $r^{\frac{1}{2}}$ for displacements. The last quantity is a function of both the material properties and the angular co-ordinate of the point being considered θ. For the simple case of a single crack surrounded by isotropic material in a uniform initial stress field the following results apply:

$$K_I = \widehat{\beta\beta}_o \cdot a^{\frac{1}{2}};\quad g_I(S,\theta) = fn(\theta);$$
$$h_I(S,\theta) = \frac{1+2\nu}{E} \cdot fn(\theta) \qquad \ldots(3a)$$

$$K_{II} = \widehat{\alpha\beta}_o \cdot a^{\frac{1}{2}};\quad g_{II}(S,\theta) = fn(\theta);$$
$$h_{II}(S,\theta) = \frac{1+2\nu}{E} \cdot fn(\theta) \qquad \ldots(3b)$$

(b) Finite Element Analysis

The ore body and surrounding country rock were considered to be in a state of plane strain. Accordingly, a two-dimensional mesh of triangles was used to represent the stope geometry.

The finite element program is very similar to that described by Zienkiewicz and Cheung (Ref. 9), and is based on the assumption that, within any triangle, stresses and strains are constant and the displacements vary linearly.

The boundary conditions used to apply the assumed state before mining commenced were as follows. The outer boundaries of the mesh were fixed in position, and inward and shear forces were applied to the edges of the stopes to simulate the effect of removing material previously supporting the initial stress field. The stresses and displacements were calculated by the finite element program and, finally, the initial stress field was added to produce resultant stresses of zero on the stope surfaces. In a trial series of runs, it was found that the outer grid boundary had to be placed a large distance away from the stope walls in order to minimize the effect on displacements and stresses.

IV.- RESULTS OF ANALYSIS

The results of the crack-tip and finite element analyses are jointly used to illustrate several points of practical importance. Firstly, consideration is given to the general conditions at the end of a long, thin opening, and to the important features of a system of two co-linear stopes. This is followed by discussion of the effect of initial stress pattern, the influence of stope inclination, and the stope behaviour associated with the progressive development of both a single stope and two co-linear stopes.

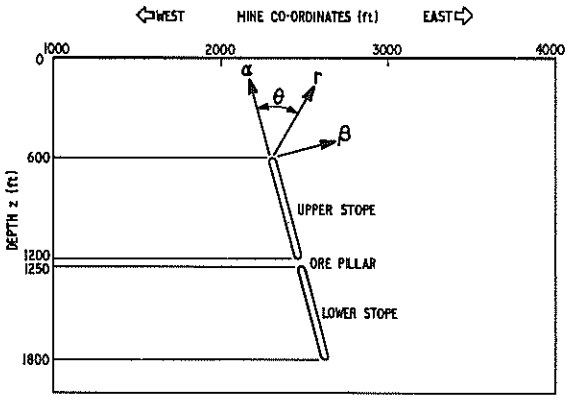

Fig. 1.- Cross-section of model stopes.

(a) Conditions at the End of a Long, Thin Opening

The crack-tip solutions indicate that the stresses and displacements at the end of a long, thin opening have the following characteristics.

(i) The stress concentration produced at the tip diminishes with the distance from the tip, and is proportional to $r^{-\frac{1}{2}}$ for a given angle θ (r, θ are defined in Fig. 1). The displacements are proportional to $r^{\frac{1}{2}}$ for a given angle θ.

(ii) The stresses and displacements increase with the applied, initial stress, $\hat{\beta}\hat{\beta}_0$ and $\hat{\alpha}\hat{\beta}_0$, the longitudinal, initial stress $\hat{\alpha}\hat{\alpha}_0$ having no effect.

(iii) For single cracks in uniform or linear, initial stress fields, stresses and displacements are proportional to the square root of crack length.

(iv) For an isotropic material the stress field is independent of the elastic modulus while the displacements are inversely proportional.

(v) Any two-dimensional, initial stress state can be considered by the superposition of the required proportions of the compressive or tensile mode (Mode I), and the forward shear mode (Mode II). For a single, vertical crack between the depths of 600 ft and 1200 ft the stress field produced at its upper tip by the initial stress $\hat{x}\hat{x}_0$ (see Fig. 2) is shown in Fig. 3a; the stress field produced by the initial stress $\hat{z}\hat{z}_0$ (see Fig. 2) is shown in Fig. 3b. For Mode I cracking, for the case where crack surfaces move directly towards one another, the stress field is symmetric about the line of the crack, and no tensile stresses occur. For Mode II cracking, where crack surfaces slide relative to one another, the stress parallel to the crack changes from a high, compressive value on one side of the crack to a high, tensile stress on the opposite side.

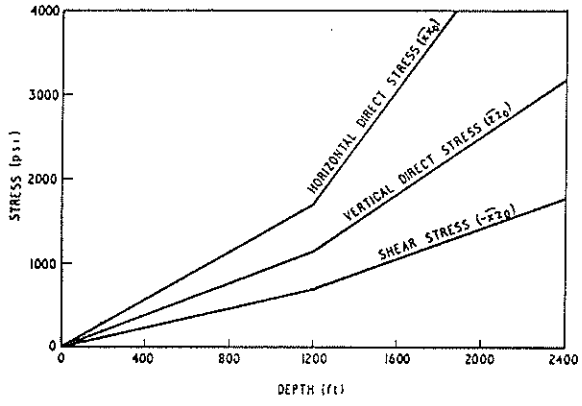

Fig. 2.- Initial stress field.

(vi) The displacements on the surface of the crack for Mode I are perpendicular to the plane of the crack, while for Mode II the surface displacements are parallel to the plane of the crack. Hence the ratio of the parallel to perpendicular components of displacement depends on the ratio of initial shear stress $\hat{x}\hat{z}_0$ to initial compressive stress $\hat{x}\hat{x}_0$. The general pattern of stresses given by the crack-tip analysis is very similar to that obtained from the finite element analysis. For a single stope between the depths of 600 ft and 1200 ft under the action of the initial stresses ($\hat{x}\hat{x}_0$, $\hat{z}\hat{z}_0$, and $\hat{x}\hat{z}_0$) shown in Fig. 2, the crack-tip solution is shown in Fig. 4a, and the analogous, finite element solution at the top of a 35 ft (11 m) wide stope is shown in Fig. 4b.

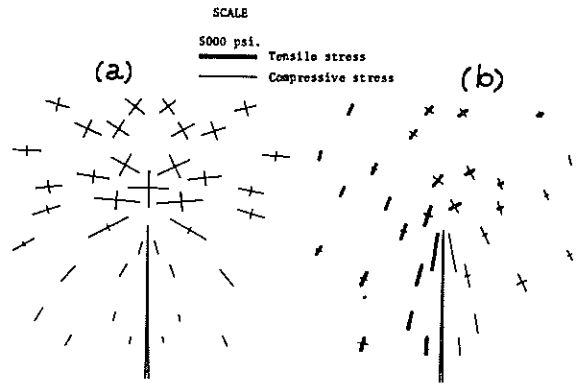

Fig. 3.- Crack-tip stress fields:
(a) Compressive mode (Mode I);
(b) Forward shear mode (Mode II).

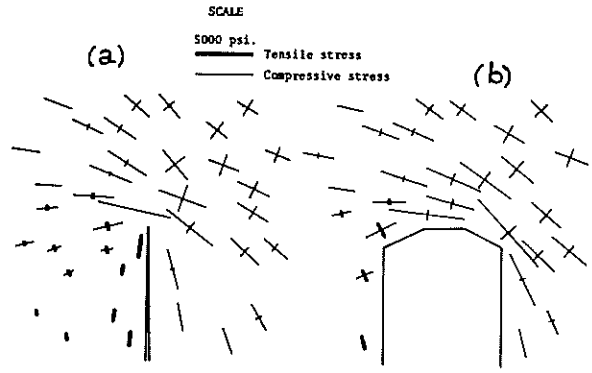

Fig. 4.- Combined stress fields:
(a) Crack-tip analysis;
(b) Finite element analysis.

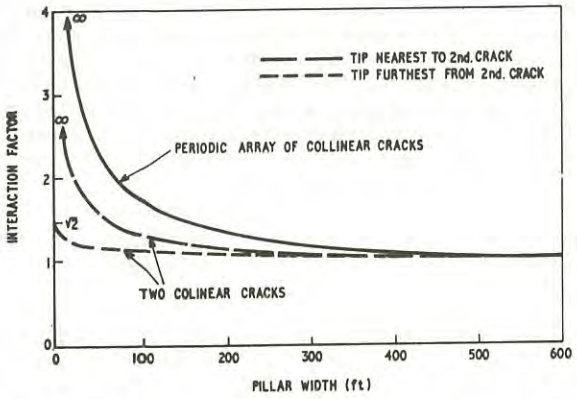

Fig. 5.- Interaction factor for different pillar widths.

The crack-tip solutions predict an infinite stress at the top of the crack. In the finite element analysis, for a stope of finite width, this does not occur. However, the stresses at points very close to the ends of a stope decrease as the stope width increases. At points outside the immediate vicinity of the end of a stope i.e. $a > r >$ stope width, the geometry at the end of the stope is of secondary importance in determining the stress field. The finite element solution was approximately proportional to $r^{-\frac{1}{2}}$ for a given angle θ, as predicted by the crack-tip solution.

(b) Features of a System of Two Co-linear Stopes

The intensity of the stress field near a crack-tip is altered by the presence of a second co-linear crack, but the pattern of stresses and displacements remains very similar to that near the tip of a single crack (Ref. 9). Thus the effect of the interaction of two co-linear cracks of equal length can be simply illustrated by calculating interaction factors, these being the ratio of the stress intensity factor at crack-tips in the two-stope system to the stress intensity factor in a system where the second stope is absent. These factors apply to any combination of Modes I and II. Fig. 5 shows plots of interaction factors versus pillar width for the two tips of a crack in a two-crack system, the cracks being spaced at 600 ft centres. As expected the tip nearest the second crack is influenced the most, because of a rapid increase in interaction factor as the pillar width is decreased below 100 ft (30.5 m). For the tip furthest from the second crack, the interaction factor tends to a limit of $2^{\frac{1}{2}}$ as the pillar width tends to zero. Also shown on Fig. 5 are interaction factors for the tips of a periodic array of co-linear cracks spaced at 600 ft. These are significantly greater than the ratios for two co-linear cracks, particularly when the pillar width is less than 100 ft.

A typical finite element result for two co-linear stopes is shown in Fig. 11d in the form of a plot of the principal stresses and resultant displacements. The stopes dip at 75°E, which corresponds to the general dip of the ore bodies at the C.S.A. Mine at Cobar. The initial stresses applied are those shown in Fig. 2.

The predominant features of the stress fields are the three stress concentrations which occur in the pillar between the stopes, below the lower stope and above the upper stope, these being in order of magnitude. Along lines radiating from the ends of the stopes in these regions, the magnitude of the principal stresses reaches a maximum value very close to or at the end of the stope, and then falls off gradually to the initial stress field. With the angle of these radial lines, the sign and magnitude of the principal stresses vary considerably from high, compressive stresses on the eastern side above the stope to tensile stresses on the western side. Below the stopes, these signs are reversed.

The stresses are independent of the elastic modulus of the rock, while the displacements are inversely proportional to it. The magnitude of the displacements decreases very slowly with distance from the stope, but this is, to some extent, due to the assumption of plane strain. For example, near the centre of the upper stope (Fig. 11d), the displacements at a point 500 ft (152 m) from the stope wall have only fallen to 50 per cent of the value at the stope wall.

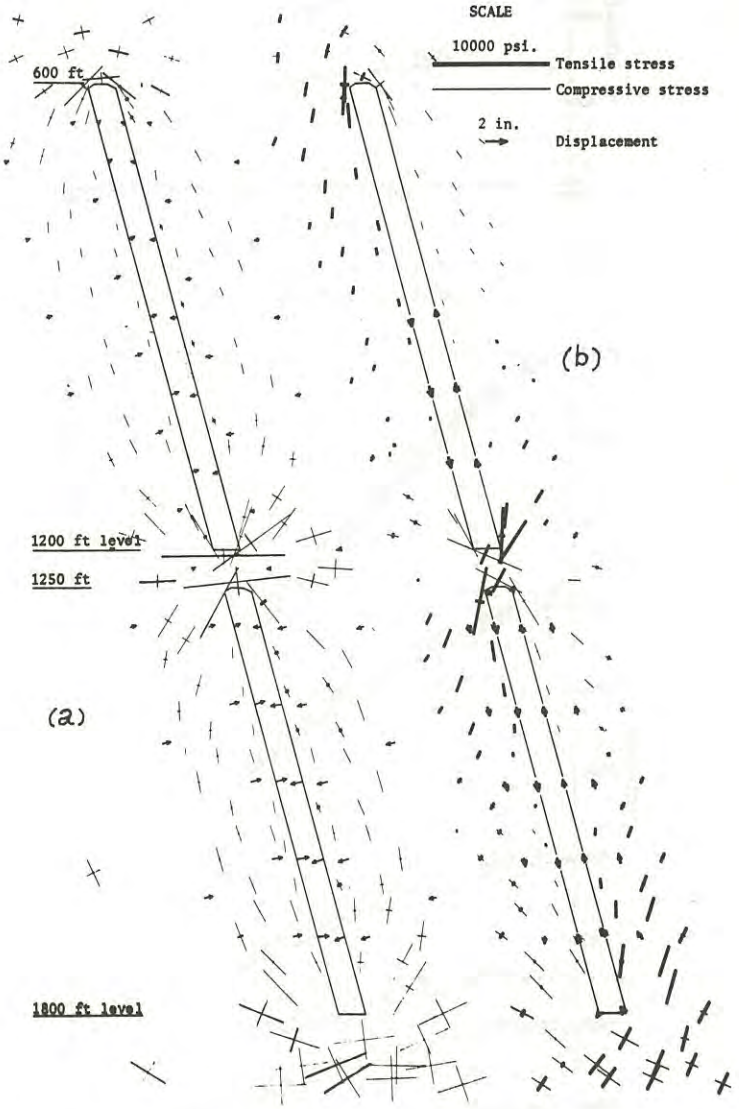

Fig. 6.- Effect of initial stresses on a two-stope system
Stope width = 35 ft, stope dip = 75°E,
$E = 10^7$ p.s.i., $\nu = 0.2$
(a) "Compressive" component only.
(b) "Shear" component only.

The displacements in the lower stope are significantly higher than in the upper stope. At a given depth the displacements on one wall are approximately equal in magnitude but of opposite signs to the displacements on the opposite wall. Displacements at points down a stope wall are approximately parallel to one another.

(c) Effect of Initial Stress Field

Any initial stress field can be divided into two components. The first contains only direct stresses that are either parallel or perpendicular to the stope; this corresponds to Mode I in the crack-tip analysis. The second component contains only shear stresses acting on planes parallel and perpendicular to the direction of the stope; this corresponds to Mode II of the crack-tip analysis. The relative effect of the two components can be seen from the crack-tip analysis as shown in Fig. 3a and 3b. It is evident that significant tensile stresses are only developed when the shear stress component of the initial stresses is applied. Corresponding finite element results for two stopes dipping at 75°E are shown in Fig. 6a and 6b.

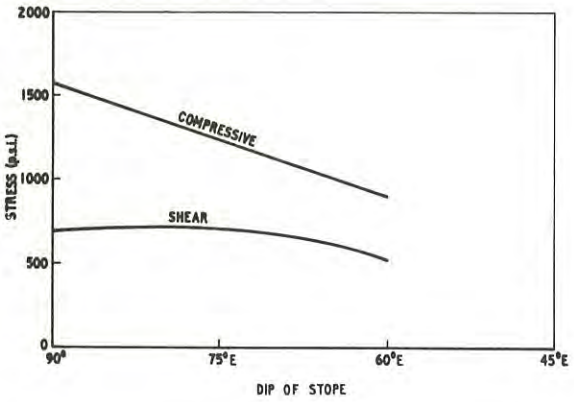

Fig. 7(a).- Effects of stope inclination: initial stress component.

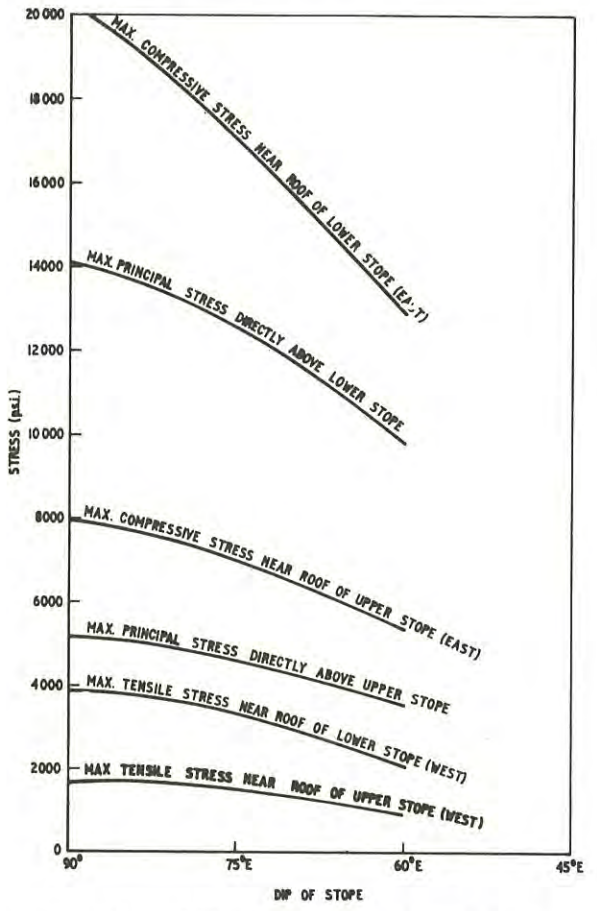

Fig. 7(b).- Effects of stope inclination: stresses developed around stopes.

The initial stresses shown in Fig. 2 were used. The results in Fig. 6a are based on the 'comprehensive' component and Fig. 6b on the 'shear' component. The finite element results are complementary to the crack-tip analysis showing that significant tensile stresses are only developed when the 'shear' component of the initial stresses is applied. These tensile stresses chiefly occur on the western side of the stope roofs with compressive stresses on the eastern side. The signs are reversed at the bottom of the stopes.

(d) Effect of Stope Inclination

The effect of a change in stope inclination is closely related to the initial stress considerations discussed. For a given orientation of the principal axes of the initial stress field, changes in the dip of the stope cause changes in the components of the initial stress resolved in co-ordinates parallel and perpendicular to the stope. For example, in Fig. 7a the initial stress field at the 1200 ft level (Fig. 2) is resolved into the 'compressive' components and 'shear' components for dips of stope between 60°E and 90°. The 'compressive' component decreases monotonically with decreasing dip angle, while the 'shear' component is relatively flat between 90° and 75°E but decreases from 75°E to 60°E. It follows from the crack-tip analysis (eq. 1 to 4) that for a given stope geometry the stress intensity factors would change in direct proportion with their corresponding components of the initial stress field. The stresses and displacements for a dip of 60°E would, therefore, be less than for dip of 90°. The results of the finite element analysis (Fig. 7b) show similar results of decreasing stresses with decreasing dip angles. In general, the compressive stresses directly above the stopes (Fig. 7b) are generated by the 'compressive' component of the initial stresses, while the tensile stresses are generated by the 'shear' component of the initial stresses. The variations of these compressive and tensile stresses (Fig. 7b) are consistent with the variations of the components of initial stress shown in Fig. 7a. If the 'compressive' component of the initial stress field is sufficiently greater than the 'shear' component then tensile stresses are practically eliminated.

(e) Progressive Mining of a Single Stope

A stope is started at a certain depth and developed upwards in near-vertical ore bodies. The crack-tip analysis was applied to the development of a single stope from the 1200 ft (366 m) level to the 600 ft (183 m) level. A separate single stope developed from the 1800 ft (549 m) level to the 1250 ft (381 m) level was also considered. In both cases the stopes dip at 75°E, and the initial stresses shown in Fig. 2 were applied. The variation of stresses and displacements

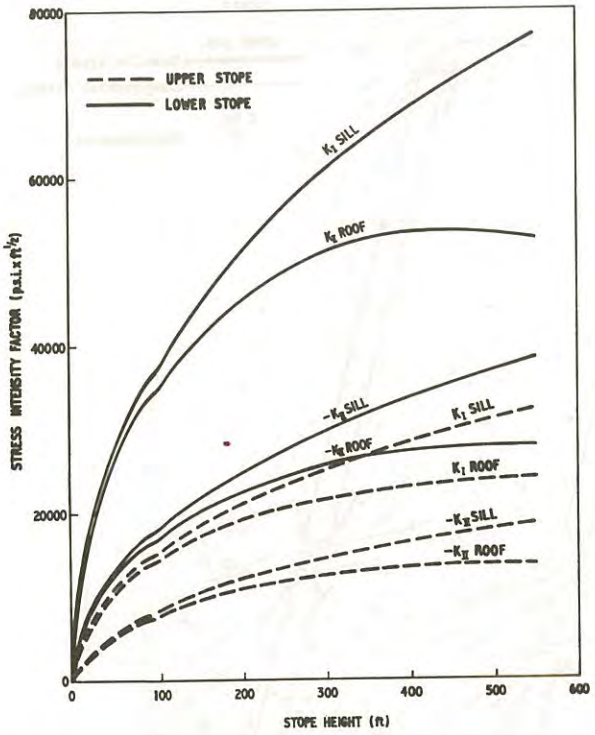

Fig. 8.- Stress intensity factors for single stopes.

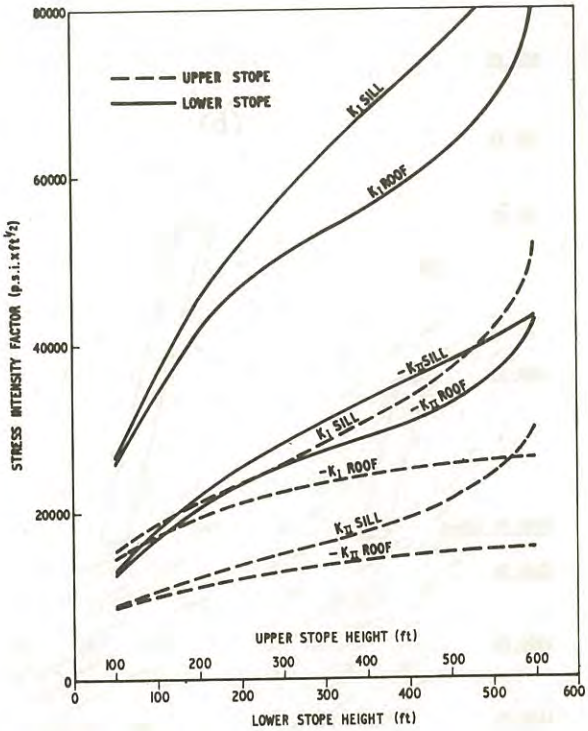

Fig. 10.- Stress intensity factors for two co-linear stopes.

with stope development can be gauged from the plots of stress intensity factors shown in Fig. 8. As a result of the higher initial stresses involved the stress intensity factors for the lower stope are generally much higher. In the stope roofs the stress intensity factors rise steeply initially and then flatten out for stope heights greater than 300 ft (91 m). This behaviour is due to two conflicting influences. Firstly, increased stope height leads to increased stresses in proportion to $a^{\frac{1}{2}}$ (see eq. 1 and 2). Counteracting this is the fact that as the roof of the stope rises it is acted upon by continually decreasing initial stresses (see Fig. 2 and eq. 3 and 4). For the stresses in the sill of the stope the predominant factor is crack length (stope height) and accordingly they increase monotonically with stope height.

For stopes of the same orientation and within the same stress field the finite element analysis showed similar trends to those indicated from the crack-tip analysis. The stresses induced in the roof of a stope developed from the 1200 ft (366 m) level to the 600 ft (183 m) level are shown in Fig. 9a, while the displacements at several points below the stope roof are shown in Fig. 9b. The counteracting influences of increasing stope height and decreasing initial stresses are clearly shown in the stress plots (Fig. 9a) and the displacements at points close to the stope roof (Fig. 9b).

Other features of the finite element results are as follows.

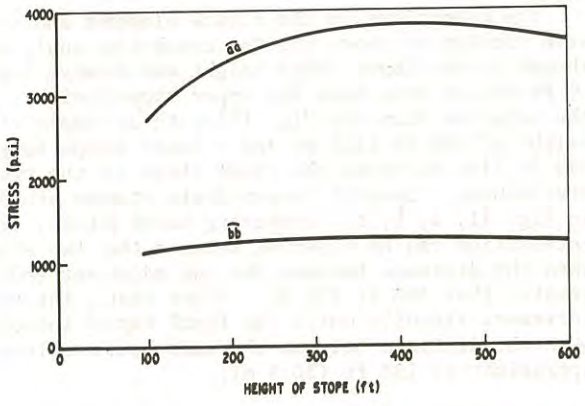

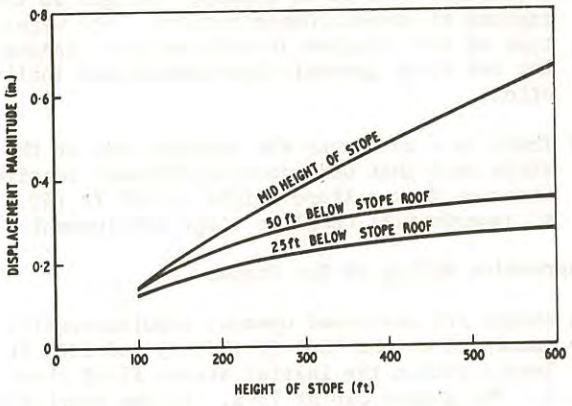

Fig. 9.- Single stope development - stresses and displacements.

(a) Stresses directly above stope:
Stope width = 35 ft, stope dip = 75°E,
E = 10^7 p.s.i., ν = 0.2

(b) Displacements
Stope width = 35 ft, stope dip = 75°E,
E = 10^7 p.s.i., ν = 0.2

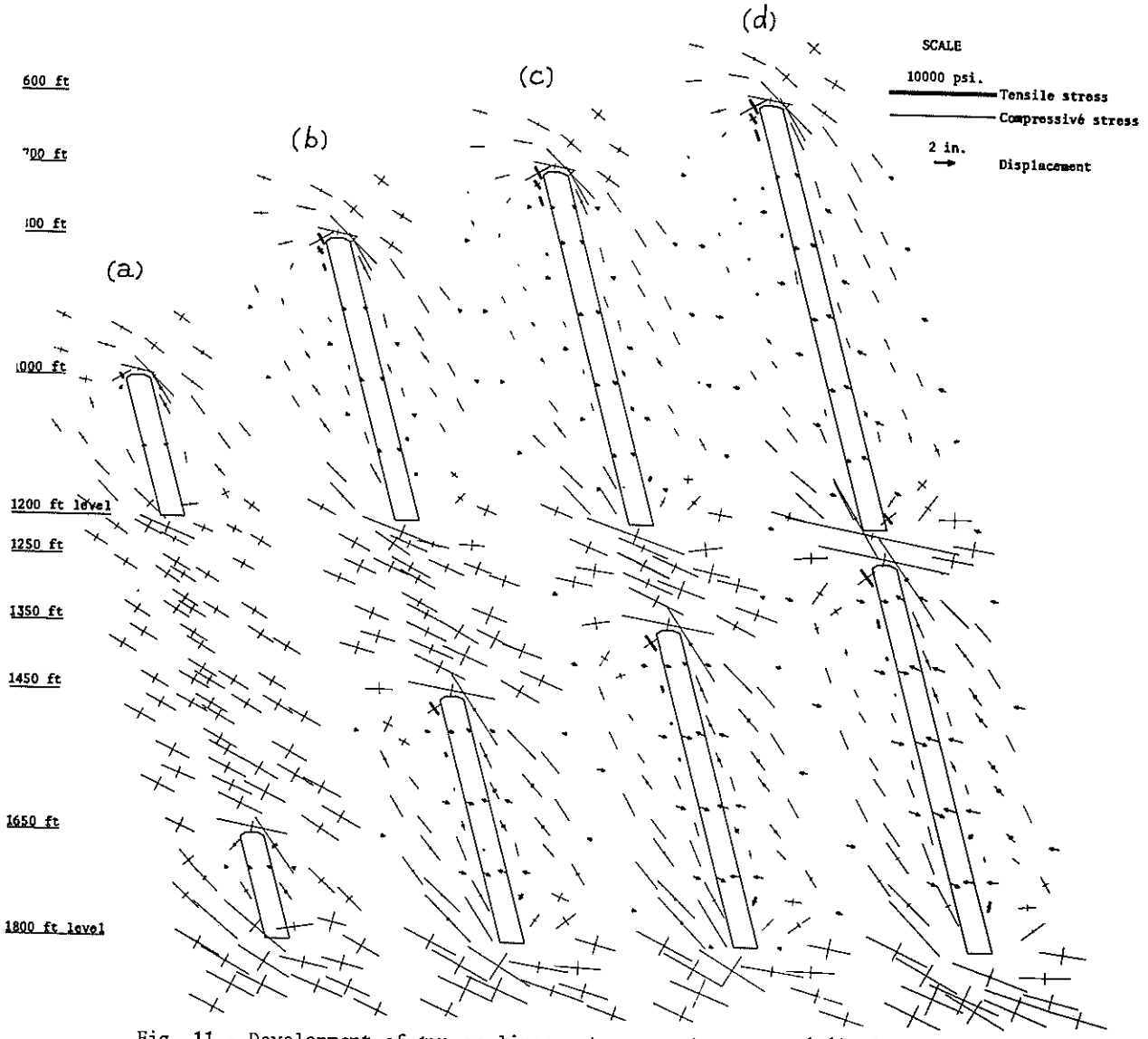

Fig. 11.- Development of two co-linear stopes - stresses and displacements:
stope width = 35 ft, stope dip = 75°E,
$E = 10^7$ p.s.i., $\nu = 0.2$

(i) For stopes of height greater than 200 ft (61 m), a distinct pattern of stresses emerges in the regions of stress concentrations. The magnitude of the stresses in this pattern changes, but not their general distribution and inclination.

(ii) There is a zone near the western side of the stope roof that undergoes significant tensile stresses from a stope height of 100 ft (30.5 m) onwards till complete stope development.

(f) Progressive Mining of Two Stopes

Two stopes are developed upwards simultaneously, and are commenced at the 1800 ft (549 m) and 1200 ft (366 m) levels within the initial stress field shown in Fig. 2. The stopes dip at 75°E. In the crack-tip analysis, the appropriate interaction factors (Fig. 5) are applied to the single stope stress intensity factors (Fig. 8), to obtain the double stope stress intensity factors (Fig. 10). The effect of the interaction factor is to cause a marked increase in pillar stresses for pillar widths less than 100 ft (30.5 m).

The conditions in the finite element analysis were similar to those for the crack-tip analysis, although in the lower stope height was always kept at 50 ft (15 m) less than the upper stope height. Hence the solution shown in Fig. 11d with an upper stope height of 600 ft (183 m) and a lower stope height of 550 ft (168 m) forms the final stage of the progressive mining. Several intermediate stages are shown in Fig. 11, a, b, c. Comparing these plots, little interaction can be observed between the two stopes when the distance between the two adjacent ends is greater than 300 ft (91 m). After that, interaction increases steadily until the final rapid increase when the distance between the ends becomes less than approximately 100 ft (30.5 m).

V.- CONCLUSIONS

The crack-tip analysis provides closed-form solutions based on simple geometry and material properties. These are particularly valuable in establish-

ing general trends of behaviour. The finite element method allows consideration of particular combinations of geometry and material properties, the generality of the solution being forfeited. The two methods are therefore complementary.

The results of the analyses show three regions of stress concentration in the stress field for a system of two co-linear stopes, i.e. (i) above the upper stope, (ii) in the pillar, and (iii) below the lower stope. In these regions the stress field is similar to the stress field surrounding a crack-tip for regions (i) and (iii), and is similar to the stress field between two co-linear cracks in region (ii).

The magnitude of the stresses in these regions depends on the length of the stopes, and the magnitude and inclination of the initial principal stresses in the rock, in particular the component of direct stress perpendicular to the stope walls and the component of shear stress in the plane of the stope walls along the whole length of the stope. The former causes a compressive, induced stress field symmetric about the line of the stopes. The latter causes an anti-symmetric field with tensile stresses on the western side* near the stope roof, and compressive stresses on the eastern side. At the sill of the stopes, the signs of the induced stresses are reversed.

The stope length to width ratio of about 15, used in the authors' analysis, was compared with that of Nair and Udd (Ref. 8) who have studied two co-linear stopes each having a ratio of 3. Most of their results regarding the effect of initial stresses and interaction between stopes can be predicted by the crack-tip results. However, the effect of the increased stope width was to introduce regions of tensile stress under the compressive mode (Mode I) conditions.

The effect of different stope inclinations depends largely on changes in the components of the initial stress field as resolved into a direct stress perpendicular to the stope walls and a shear stress parallel to the stope walls. For the initial stress field, generally assumed in this analysis (Fig. 2), a change in orientation from the vertical position to one dipping 60°E decreases the magnitude of these two stress components along the length of the stope, and consequently the stress field surrounding the stopes is decreased. However, it should be realized that for a different initial stress field, quite different results would be obtained.

For the progressive development of a single stope of 600 ft (183 m) height, the results show that both the sill stresses and the wall displacements at mid-height of the stope increase monotonically with stope height. The roof stresses, and the wall displacements just below the roof, initially increase with stope height. However, for stope heights above 300 ft (91 m) these stresses and displacements are approximately constant with further increases in stope height.

During the progressive development of two co-linear stopes each of about 600 ft (183 m) height the following features are observed.

(i) The conditions at the sill of the lower stope and the roof of the upper stope are little different to those produced by a single stope, although for very narrow pillar widths there is an intensification of up to 40 per cent.

(ii) As the development proceeds, the sill of the upper stope and the roof of the lower stope define an ore pillar. The conditions in this sill and this roof are very similar to those predicted by single stope development until the ore pillar is less than 150 ft (46 m) wide. At this stage important interaction effects start to develop leading to a sharp rise in stresses.

(iii) For stopes of height 300 ft (91 m) or more, the patterns of stresses above and below the stopes are very similar, and the change is only in the magnitude of the stresses and displacements.

This paper has considered the stress and deformation patterns that develop in a two-stope system. The stability of any part of the system depends not only on these but also on the strength and structure of the rock mass.

* For the initial shear stress field shown in Fig. 2.

VI.- ACKNOWLEDGEMENT

This investigation forms part of a research program being carried out under the financial sponsorship of the Australian Mineral Industries Research Association.

The assistance of Mr. G. Bonner with computer programming is gratefully acknowledged.

REFERENCES

1. BRADY, J.T., OWERS, N.F. and ANNEAR, C.H. - Ore Breaking and Handling at the C.S.A. Mine, Cobar. Proc. Aust. Inst. Min. Met. No. 229, March 1969.

2. KAPELLE, K. and ASHCROFT, J.F. - Stope Control at the C.S.A. Mine, Cobar. Proc. Aust. Inst. Min. Met. No. 229, March 1969.

3. STEPHENSON, B.R. - Stresses and Joint Directions Correlated at Cobar Mines Pty. Ltd. Rock Mechanics Symp. Sydney, 1969.

4. OBERT, L. - Private communication (1970).

5. STEPHENSON, B.R. - The Results of the Core Testing Programme for Cobar Mines Pty. Ltd. Proc. Aust. Inst. Min. Met., No. 229, March, 1969.

6. RYDER, J.A. and OFFICER, N.C. - An Elastic Analysis of Strata Movement Observed in the Vicinity of Inclined Excavations. J. of the South African Inst. Mining and Metallurgy, 1964, Vol. 64, p. 219.

7. JAEGER, J.C. and COOK, N.G.W. - Fundamentals of Rock Mechanics. Methuen, 1969.

8. NAIR, O.B. and UDD, J.D. - Determination of the Principal Stresses in Pillars Using an Iterative Method. Symp. on Rock Mechanics, Rolla, Missouri, 1964.

9. PARIS, P.C. and SIH, G.C. - Fracture Toughness Testing and its Applications. A.S.T.M., Spec. Tech. Publ. No. 381. Stress Analysis of Cracks, 1964.

10. ZIENKIEWICZ, O.C. and CHEUNG, Y.K. - The Finite Element Method in Structural and Continuum Mechanics. McGraw Hill, 1967.

The Gravity Flow of Material in the Sub-Level Caving Mining System

By

G. D. Just, B.E., Ph.D., A.M.Aus.I.M.M.

(Lecturer in Mining Engineering, University of Queensland)

AND

G. D. Free, B.E., M.Eng.Sc.

(Postgraduate Research Student, University of Queensland)

SUMMARY.- The exploitation of lower grade ore deposits has required a reduction in unit extraction costs. This is being achieved by mechanisation and an increased scale of operations. The design of such large mining systems, by the trial and error methods used in the past, is not economically justified. Unfortunately the use of more sophisticated design techniques is restricted by the lack of data concerning the relationships between the design variables. This paper describes part of a research project which involves the investigation of design parameters for the sub-level caving mining method. The gravity flow of material, which is one of the most important factors in sub-level caving design, is discussed in some detail. Two-dimensional model tests are described and a statistical analysis of results is presented.

The project is being carried out in the Department of Mining and Metallurgical Engineering at the University of Queensland. Assistance for the work has been obtained from a number of Australian mining companies through the Australian Mineral Industries Research Association.

I.- INTRODUCTION

The depletion of high grade ore deposits and the rapid increase in metal requirements are major factors which have influenced the unit costs of metal production. The mining industry has prevented a proportionate increase in costs by the development of large scale low cost mechanised mining methods. These techniques have been applied to a number of mining systems with varying degrees of success.

The sub-level caving mining method, can be completely mechanised to give high production rates in almost any type of material. These factors in addition to the safety of the method have led to the wide use of this technique of underground mineral extraction in large ore-bodies.

In the design of a sub-level caving system there are a large number of variables to be considered and little knowledge exists of the fundamental factors involved. This lack of knowledge has required the use of trial and error methods to design mining systems.

There are considerable economic incentives to develop a systematic approach to the design of sub-level caving systems based on detailed information of the many variables involved. These incentives are due to the fact that each sub-level layout must be integrated with the sub-level above and below. If the original design is changed during operations ore recovery is lowered and development costs are increased. This causes a corresponding increase in the overall unit costs of metal production from the ore-deposit.

A considerable amount of basic research into sub-level caving has been carried out in Sweden where the method is used in the mining of high grade iron ore deposits. The results of this research cannot be applied directly to the mining of base metal deposits where the ore is usually very similar to the waste rock. Methods of draw control based on visual observation of dilution are not effective in this material. Flow characteristics are also different from those applying to sub-level caving in iron ore and the necessity for accurate design methods is increased by the absence of effective operating controls.

A research programme to investigate the fundamental factors involved in sub-level caving design was commenced in the Department of Mining and Metallurgical Engineering at the University of Queensland in 1966. The work completed to date has included a study of the flow of material in two-dimensional models and a statistical analysis of results to determine the draw shape for a range of different conditions. This paper describes the methods used in this study of draw shapes and some of the results obtained. This work is only one section of the overall programme of research so far completed. It has provided information for use in the development of a two-dimensional sub-level caving mathematical model. This has made it possible to use mathematical techniques to simulate design parameters on the digital computer and to prepare a series of graphs for use in sub-level caving mine design.

II.- DESCRIPTION OF SUB-LEVEL CAVING METHOD

The sub-level caving mining method consists of mining consecutive slices of ore (sublevels) from the top of the orebody, and allowing the overlying rock (waste overburden) to cave into the opening formed by the extraction of broken ore. Fans of holes (rings) are drilled from a number of parallel extraction headings driven under each slice, and are fired individually. All of the recoverable ore from each ring is extracted by loading units prior to firing

the next ring. This process is repeated with every ring, in all the extraction headings throughout the sublevels, until the orebody is completely worked from top to bottom. This system is illustrated schematically in Fig. 1.

As the extraction of ore from a fired ring is bounded by the solid wall of the adjacent ring on one side and the caved waste on all the other sides, the problems of recovery and dilution are greater than in any other mining method. The success of the whole operation depends upon the maximisation of ore recovery and the minimisation of waste dilution. As an inverse relationship exists between recovery and dilution effective draw control is essential to obtain optimum recovery and dilution ratios. Therefore, a complete knowledge of the theory of gravity flow of granular materials, and in particular flow of ore in sub-level caving, is required to effectively design for and control optimum draw.

III.- GRAVITY FLOW OF GRANULAR MATERIALS

Flow characteristics of the broken material (both ore and waste) are important since the shape of the draw volume affects the overall recovery and dilution. Although results of research into the flow of granular and coarse materials in bunkers can be used for approximate analyses, their use is limited by the differences between the flow of materials in bunkers and in sub-level caving systems.

These differences include the following:

(i) Draw heights in relation to draw widths are lower in sub-level caving than in bunker flow;

(ii) Overburden pressures can be very much higher in sub-level caving;

(iii) Blasting of the ore to be drawn in sub-level caving causes variations in the density of the waste and ore; and

(iv) The solid face of unbroken ore affects the draw shape.

Although these differences exist it is possible to apply many of the principles of bunker flow to sub-level caving.

(a) Determination of the Shape of Draw

An indication of the state of knowledge in this field is given by Coates (1967, p. 5-9) in the following statement:

> Little theoretical information exists on the subject of drawing caved ore or other granular materials. This is a serious deficiency in the science of rock mechanics. Consequently, any information that is to be used for the rational solution of drawing problems must be obtained from models or from experience in full-scale drawing operations.

Considering this statement and the proportionate lack of technical papers, it can be concluded that theoretical contributions towards the determination of the shape of draw or draw pattern of granular material in bunkers are extremely limited.

Of all the technical papers reviewed, not one applied a mathematical approach to the actual determination of the shape of draw. Qualitative observations of the draw patterns of granular materials under various conditions are discussed, for example, by Janelid and Kvapil (1966), Deutsch and Clyde (1967), Woehlbier and Reisner (1962), Brown and Richards (1959), Kvapil (1965) and Coates (1967).

Two of the various theories that have been developed to date by researchers, generally working independently of each other, are discussed to enable a comparison of the similarities of these different theories. From these selected similarities the shape of draw applicable to the sub-level caving mining system is postulated to enable the design of experiments to determine the actual draw shape.

(i) Janelid and Kvapil (1966)

A certain zone of the bunker is set in motion and is called the active zone. The remaining part of the bunker contents is immobile and forms a passive zone (Fig. 2).

The movement of particles in the active zone is affected by gravity and is therefore called the gravity flow zone of granular material or limit ellipsoid. This movement is caused by the extraction of a much smaller ellipsoidal volume, the ellipsoid of motion.

(ii) Deutsch and Clyde (1967)

Four characteristic zones have been observed to occur. These are illustrated in Fig. 3. The theory is simply explained by a description of these zones:

Dead zone —— The material within this zone does not move.

Plug flow zone —— This is the region above the influence of the bunker outlet in which the material moves as a solid mass and is in a non-failure state. As soon as the pipe breaks through to the surface, this zone no longer exists.

Pipe feed zone —— Material entering this zone receives a radial velocity component towards the centre of the bunker, thus feeding the pipe.

Pipe zone —— All material leaves the bunker via the pipe zone which is directly affected by gravity.

A study of these two gravity flow theories reveals the following similarities:

(a) The actual material drawn flows from the ellipsoid of motion —— shown dotted in Figs. 2 and 3.

(b) There will always be some undisturbed material which remains stationary —— shown cross-hatched in Figs. 2 and 3.

(c) The ellipsoid of motion disturbs a larger zone of material which feeds the material displaced from the ellipsoid of motion in

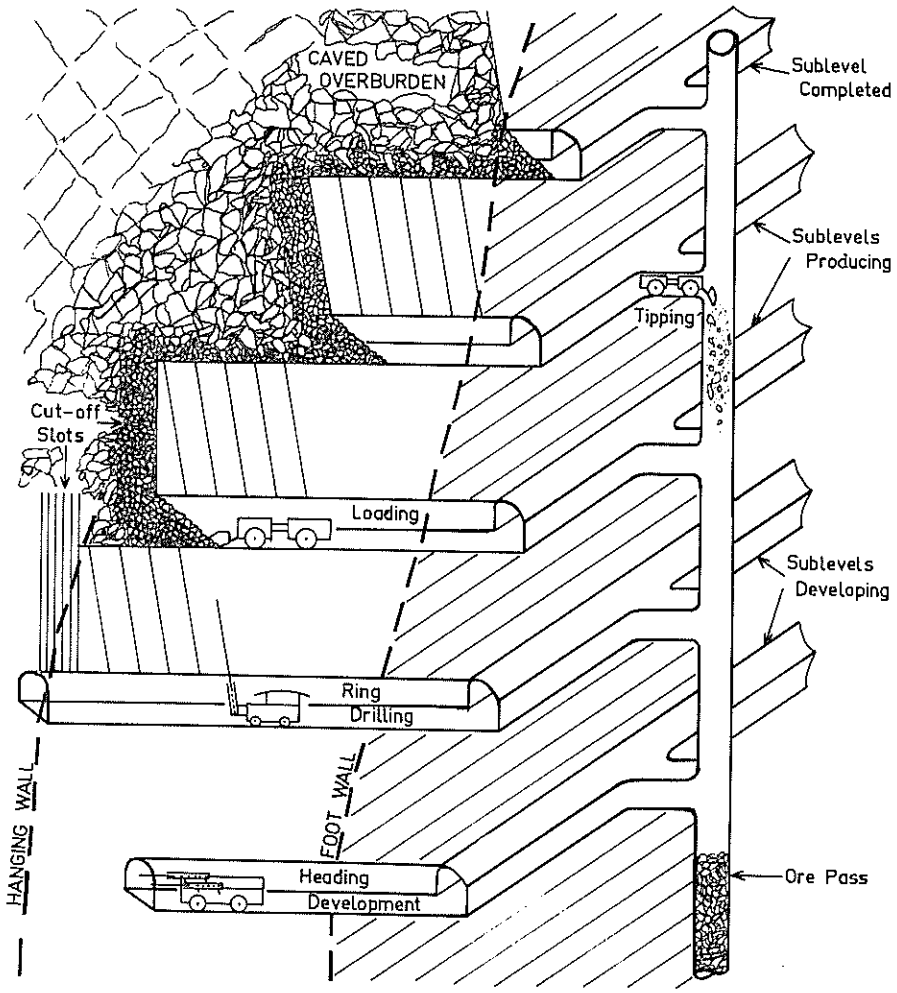

Figure 1. Schematic representation of the sub-level caving mining method.

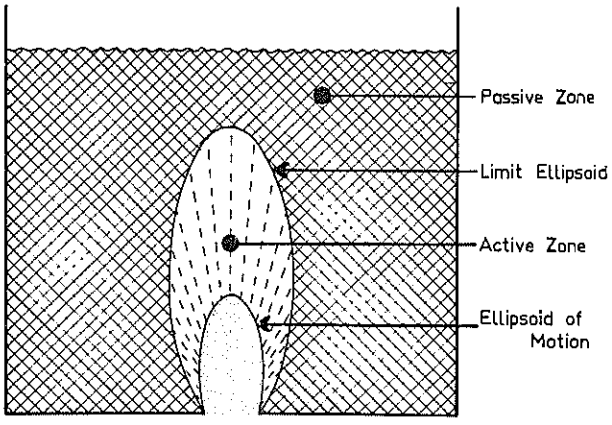

Figure 2. Flow theory according to Janelid and Kvapil (1966).

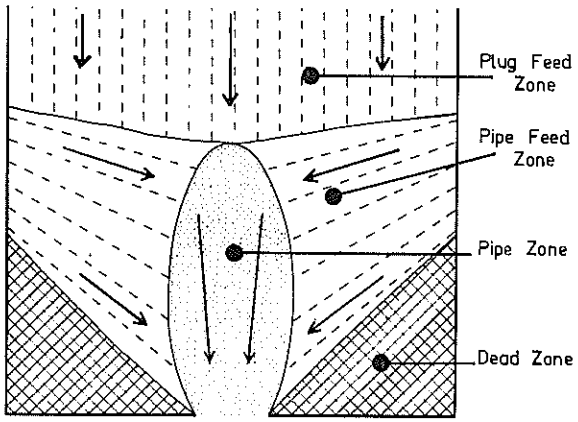

Figure 3. Flow theory according to Deutsch and Clyde (1967).

each theory. It can be concluded that the material drawn may not have the precise shape of an ellipsoid, but resembles it so closely that for the resolution of a simple mathematical expression, the shape of draw may be taken as a vertical, rotary, elongate ellipsoid.

(b) Principles of Material Flow in Sub-level Caving

By making the above assumption regarding draw shape it is possible to list certain principles regarding the movement of particles under the influence of gravity. Some of these principles are discussed below:

(i) The shape of the vertical, rotary, elongate ellipsoid is defined uniquely by its eccentricity,

$$\varepsilon = \frac{1}{a}\sqrt{a^2 - b^2}$$

where a = semi-major axis of ellipsoid.
b = semi-minor axis of ellipsoid.

(ii) It has been observed that the width of the ellipsoid of motion, c, increases as a greater amount of material is drawn through the draw-point. Consequently, the use of any one particular ellipsoid (possibly based on model experiments) to predict the amount of material that will be drawn from any draw-point, and particularly the lateral extent of the draw pattern, c, could be erroneous. It is therefore necessary to analyse any model data in such a way as to have the shape of the ellipsoid a function of the volume of draw. Hence the following relation has been deduced:

$$\varepsilon = \sqrt{\frac{3w^2}{4h^2} - \frac{6V_e}{\pi h^3} + 1} \qquad (1)$$

where w = width of extraction opening or drawpoint
h = height of draw
V_e = volume of material drawn, that is, volume of the ellipsoid of motion.

The variables and parameters used in equation 1 are shown in Fig. 4. The lateral extent of the draw, c, can likewise be calculated from the volume of draw:

$$c = \sqrt{\frac{7.6934\ V_e\ h\ (1 - \varepsilon^2)}{(w^2 + 4h^2(1 - \varepsilon^2))}} \qquad (2)$$

If the following approximation is assumed,

$$h = 2a$$

then equation 2 is reduced to the following form:

$$c = \sqrt{\frac{1.910\ V_e}{h}}$$

(iii) As the material is drawn from the ellipsoid of motion, all the material within the limit ellipsoid is influenced. The broken material within this limit ellipsoid is therefore in motion, and has a lower bulk density than the broken material adjacent to this ellipsoid. This difference in the bulk densities of the broken material is defined by the loosening factor, S_1.

$$S_1 = \frac{\gamma_o}{\gamma_e}$$

where γ_o = bulk density of the broken material outside the limit ellipsoid

γ_e = bulk density of the broken material within the limit ellipsoid; that is, the bulk density of the extracted material.

According to Just (unpublished data, 1967), in the general case the volume of the limit ellipsoid, V_1, is given as follows:

$$V_1 = V_e\left(1 + \frac{1}{S_1} + \frac{1}{S_1}2 + \frac{1}{S_1}3 + \ldots\right) \qquad (3)$$

Considering the sum of an infinite series, equation 3 reduces to:

$$V_1 = V_3\left(\frac{S_1}{(S_1 - 1)}\right) \qquad (4)$$

Some published values of the loosening factor for unconsolidated broken material lie within the range 1.066 to 1.100 (Janelid et al, 1966, p.135). If these figures are substituted for S_1 in equation 4, volumes of the limit ellipsoid between 11 to 16 times the volume of the ellipsoid of motion are obtained. This indicates that, in general, the height of the limit ellipsoid is two to three times greater than the height of the ellipsoid of motion.

In the actual design of a sub-level caving system there are many other principles to be considered. However those factors mentioned above are the most significant in the study and analysis of draw shapes which is the main subject of this paper.

IV.- MODEL TESTING - TRANSVERSE SECTION

A simple, two-dimensional model that would allow the profile of the gravity flow of material to be determined was designed and constructed. This model effectively consisted of a transverse section of an extraction heading and ring, Fig. 5.

The model design had to include the following intrinsic prerequisites:

(i) An approximately constant extraction volume for each draw.

(ii) A method of loading material into the model without disturbing previously loaded material and markers.

(iii) Some system of depositing markers in predetermined positions.

(iv) The capability to visually observe the displacements of the markers on drawing.

The model, pictured in Fig. 6, effectively resembles a two-dimensional, transverse section of a ring with the extraction outlet at the centre of the base of the model. To achieve an approximately

constant extraction volume for each draw, the extraction outlet system contains a trap arrangement incorporating two metal slides and a hand-operated wooden piston. This trap arrangement was constructed within the bases of the model.

Five separate bases were constructed, each having a different extraction outlet width; the range of outlet widths being from two to six inches in intervals of one inch. The front and back of the model consisted of two glass panels, while the sides were fabricated from perspex strips. One side incorporated a vertical slide (pictured on the right side of the model in Fig. 6) enabling the model to be loaded from the side rather than the top.

(a) Technique of Testing

Two basically dissimilar types of material were tested in the models:

(i) spherical glass beads

(ii) finely crushed rock

The spherical glass beads are commercial beads that are primarily manufactured for use in laboratory condensers. Three sizes of these beads were used in the model testing, three, five and eight millimetres.

The crushed rock consisted of marble and shale chips. Four grades of crushed rock were used, ranging from 1/16 to 5/16 inch chips.

Markers were loaded into the two-dimensional model at predetermined intersections on a grid system. The grid system incorporated one inch horizontal intervals and two inch vertical intervals. The markers used were coloured, eight millimetre glass beads each of which were individually numbered.

The test material was loaded into the model on a thin, wooden board from a funnel-shaped, metal feeder. The markers could be deposited in their exact position by employing a thin, glass tube attached to a suction pump.

The material was removed from the model in approximately equal sized draws through the trap arrangement at the base of the model.

The test material (including any markers) for each draw was then weighed on an electronic balance. Following this, the markers were identified and removed from the weighing pan and recorded together with the weight and draw number. These measurements enabled the calculation of eccentricity values for the different conditions of draw.

In addition, by knowing the predetermined positions of each respective marker, it was possible to sketch the draw ellipses onto a sheet of graph paper, to represent the actual "area" extracted. A typical sketched set of draw ellipses is illustrated in Fig. 7.

(b) Analysis of Test Results

A large number of tests were carried out using the two-dimensional models. These tests mainly involved the measurement of eccentricity values for different conditions of draw. The most significant results are summarised in the discussion of test results. One feature of this work was the development of a method of analysis to statistically determine the accuracy of the assumed ellipsoidal shape of draw. Previous workers have made qualitative observations of the geometry of this shape. The following analysis determines the level of confidence associated with the assumption that this shape is ellipsoidal.

The draw "ellipses", an example of which is illustrated in Fig. 7, were sketched by linear interpolation of the drawn markers and therefore represent the actual draw shape. These draw shapes have only been presumed to be elliptical because they closely resemble ellipses. Therefore, the degree of error in the presumed draw may be determined by superimposing an actual elliptical shape over the draw shape obtained from one complete extraction.

To determine a measure of the error associated with the above assumption, the elliptical equation was initially converted to polar co-ordinates, a curve fitting program consequently applied to the polar co-ordinate data, and finally, an estimate of the statistical significance deduced.

The geometrical equation with the origin of the cartesian co-ordinate system at the centre of the extraction outlet is of the following form:

$$\frac{x^2}{b^2} + \frac{(y - h + a)^2}{a^2} = 1 \qquad (5)$$

Converting to polar co-ordinates, with the pole in the identical position to that of the origin, and the initial line parallel to the positive X axis, the variable transformations are as follows:

$$x = r \cos \theta$$

$$y = r \sin \theta$$

Subsequently, applying these variable transformations to equation 5, the following polar co-ordinate equation is obtained:

$$r^2 \left(\frac{\cos^2 \theta}{b^2} + \frac{\sin^2 \theta}{a^2}\right) + 2 r \sin \theta \frac{a-h}{a^2}$$

$$+ \frac{h^2 - 2ha}{a^2} = 0 \qquad (6)$$

This relationship was the mathematical model that was employed in the curve fitting program. Any draw shape could be sketched onto graph paper by linear interpolation between the outline of the drawn and undrawn markers, as illustrated in Fig. 7. Consequently, from a pole positioned at the centre of the extraction outlet, polar chords could be superimposed onto the draw shape. The angle of each chord from the initial line, and the radius from the pole to the intersection with the draw shape were recorded. These observed angles and radii were inserted into the curve fitting program; subsequently predicting the parameters a, b and h of equation 6.

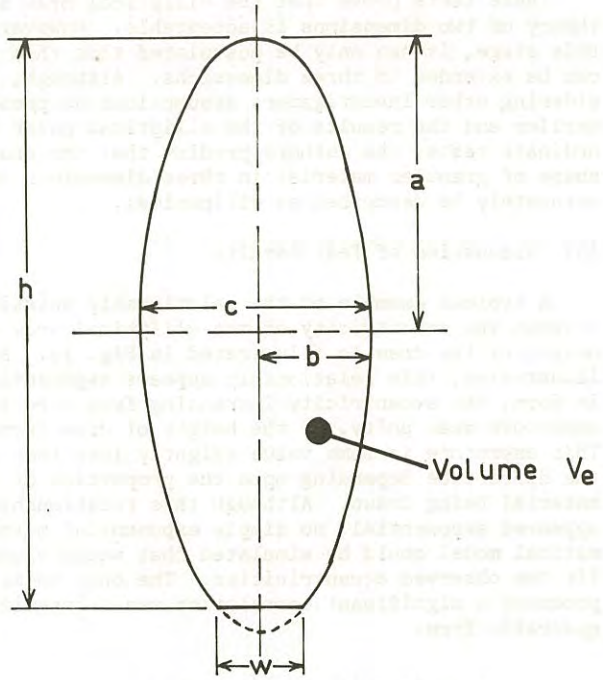

Figure 4. Schematic representation of variables and parameters involved in the definition of eccentricity of ellipsoid.

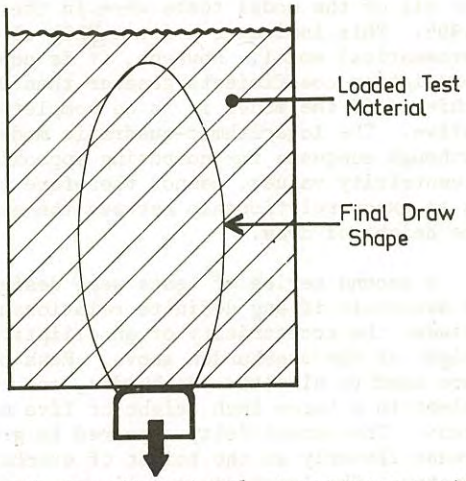

Figure 5. Schematic two-dimensional, transverse section of a ring.

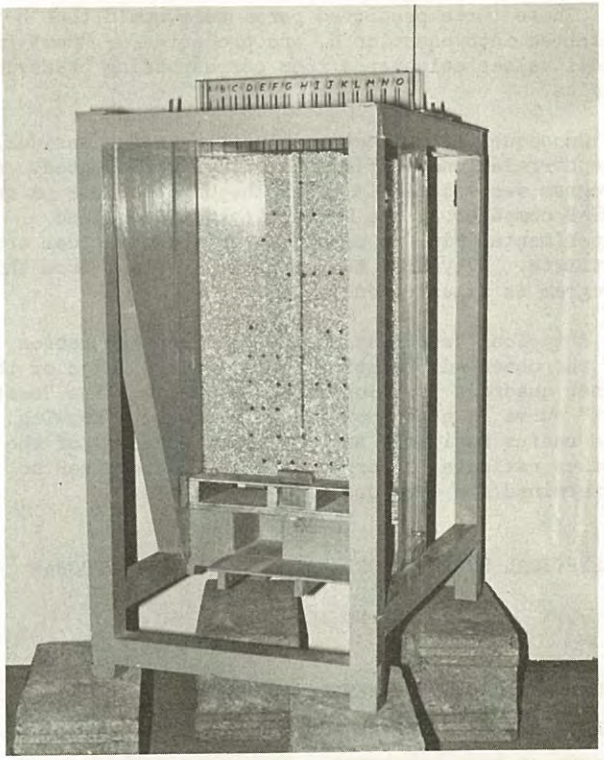

Figure 6.

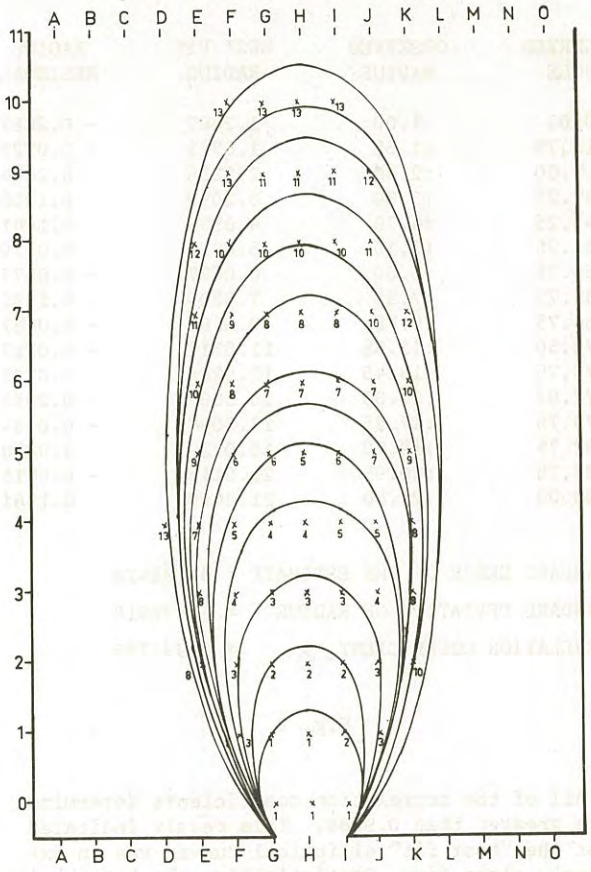

Figure 7. Typical sketched draw ellipses from a test in the transverse sectional model.

These three predicted parameters could then be inserted into equation 6, and predicted or "best fit" radii values calculated from corresponding observed angles.

Consequently, by determining the radius residuals, the correlation coefficient could be calculated. A program was written in FOCAL language for use on the PDP-8 computer at the University of Queensland Experimental Mine to calculate this statistical error estimate. A typical set of printed output from this program is illustrated in Fig. 8.

A typical cartesian co-ordinate representation of the observed elliptical polar co-ordinates of the first quadrant is illustrated in Fig. 9. The "best fit" curve is also shown in this Figure. knowing the radius residuals and the standard error of the radius estimate, a correlation coefficient can be determined for each quadrant considered.

ELLIPTICAL POLAR CO-ORDINATE CORRELATION PROGRAM

TEST NO :C:2::1Q

SEMI-MAJOR AXIS PARAMETER :10.91725

SEMI-MINOR AXIS PARAMETER :3.90364

HEIGHT OF DRAW PARAMETER :21.24187

NUMBER OF OBSERVATIONS :16

OBSERVED ANGLE	OBSERVED RADIUS	BEST FIT RADIUS	RADIUS RESIDUAL
:0.00	:1.00	1.2687	- 0.2687
:13.75	:1.65	1.6723	- 0.0223
:24.00	:2.40	2.1356	0.2644
:37.25	:3.30	3.1092	0.1908
:45.25	:4.20	4.0559	0.1441
:51.25	:5.10	5.0621	0.0379
:55.75	:6.00	6.0577	- 0.0577
:61.75	:7.95	7.8305	0.1195
:66.75	:9.75	9.8183	- 0.0683
:70.50	:11.65	11.6717	- 0.0217
:73.75	:13.45	13.5285	- 0.0785
:77.00	:15.35	15.5585	- 0.2085
:79.75	:17.25	17.3084	- 0.0584
:82.75	:19.10	19.0722	0.0278
:87.75	:20.95	21.0115	- 0.0615
:90.00	:21.40	21.2419	0.1581

STANDARD ERROR OF THE ESTIMATE = 0.138420

STANDARD DEVIATION OF RADIUS = 6.890910

CORRELATION COEFFICIENT, R = 0.999798

Fig. 8

All of the correlation coefficients determined were greater than 0.9988. This result indicated that the "best fit" elliptical curve, was an extremely close fit. Statistically, the hypothesis of assuming the draw shape to be elliptical can therefore be accepted with greater than 99.5 percent confidence.

These tests prove that the elliptical draw shape theory of two dimensions is acceptable. However, at this stage, it can only be postulated that this theory can be extended to three dimensions. Although, considering other investigators assumptions as presented earlier and the results of the elliptical polar co-ordinate tests, the authors predict that the draw shape of granular material in three dimensions should accurately be described as ellipsoidal.

(c) Discussion of Test Results

A typical example of the relationship existing between the eccentricity of the elliptical draw and height of the draw is illustrated in Fig. 10. As illustrated, this relationship appears exponential in form, the eccentricity increasing from zero to an asymptote near unity, as the height of draw increases. This asymptote is some value slightly less than unity, the difference depending upon the properties of the material being drawn. Although this relationship appeared exponential, no simple exponential mathematical model could be simulated that would closely fit the observed eccentricities. The only model that produced a significant correlation was a logarithmic-quadratic form:

$$\log_e (1 - \varepsilon) = a\,h^2 + b\,h + c$$

a, b, and c being coefficients.

Typical values of these coefficients are as follows:

$$a = +0.00549 \pm 0.00037$$

$$b = -0.23805 \pm 0.00819$$

$$c = -0.06400 \pm 0.03529$$

In general, the correlation coefficients obtained for all of the model tests were in the range 0.970 to 0.995. This indicates a reasonably close fitting mathematical model. However, it is considered that correlation coefficients greater than 0.995 should be achieved if the model is to be completely representative. The logarithmic-quadratic model selected, although adequate for computing approximate eccentricity values, cannot therefore be considered as an exact relationship between the eccentricity and the height of draw.

A second series of tests were designed principally to ascertain if any definite relationship existed between the eccentricity of an elliptical draw and the height of the overburden above. Rows of lead sinkers were used to simulate overburden, one row being equivalent to a three inch height of five millimetre glass beads. The eccentricity appeared to gradually increase linearly as the height of overburden became greater. The least squares linear regression line is given by the following relationship:

$$\varepsilon = 0.9206 + 0.0003\,h_o$$

where h_o = height of overburden (inches)

The correlation coefficient associated with this regression is 0.8341. As this statistic is relatively low, this series of tests exhibits only a trend rather than a definite model relationship. A qualitative observation of the quasi forces involved in the

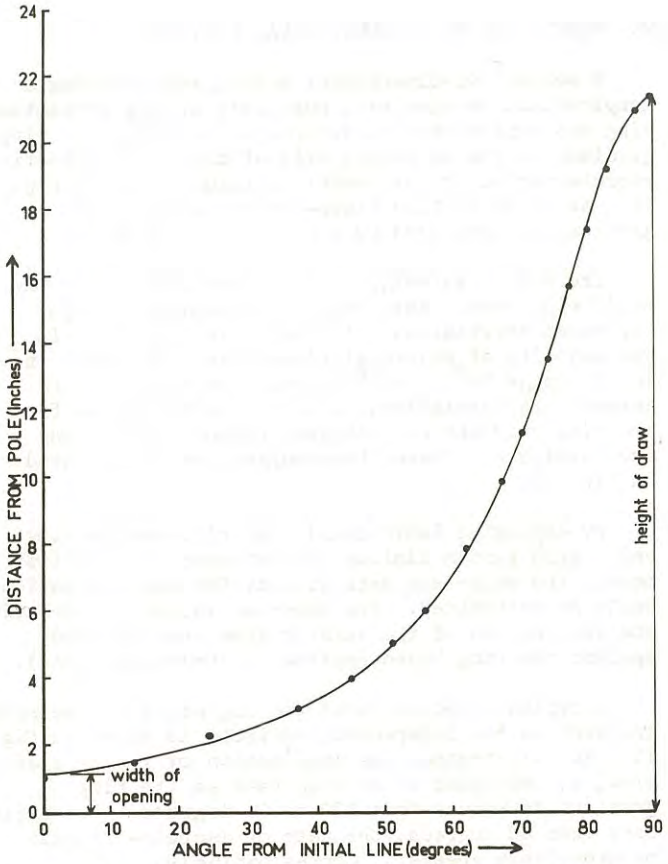

Figure 9. Example of the cartesian co-ordinate representation of the first quadrant elliptical polar co-ordinates.

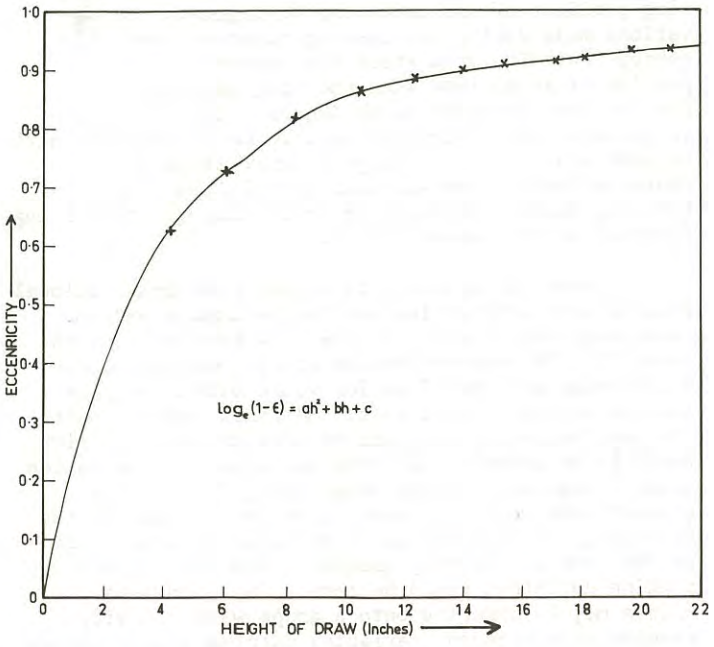

Figure 10. Graph of eccentricity versus height of draw.

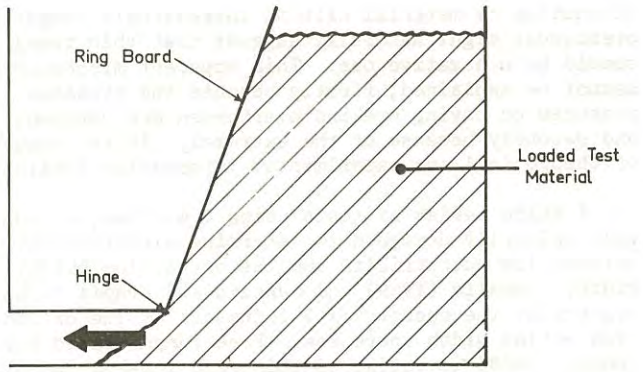

Figure 11. Schematic two-dimensional, longitudinal section of a ring.

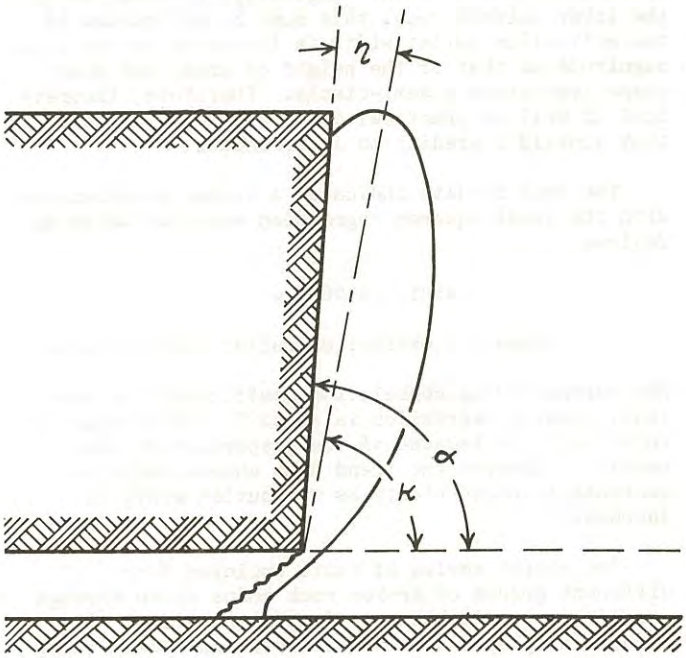

Figure 12. Schematic representation of the definitions of the ring gradient, α, and the deviation, η, and inclination, κ, of the axis of draw.

extraction of material with an increasingly large overburden might naturally suggest that this trend should be a negative one. This apparent misconception cannot be explained, firstly because the stresses produced on caving ore and overburden are unknown, and secondly because of the extremely limited amount of theoretical and experimental information available.

A third series of tests using 5 millimetre beads were primarily designed to determine a relationship between the eccentricity and the extraction outlet width. Janelid (1964) and Janelid and Kvapil (1966) state that the eccentricity increases as the extraction outlet width increases. Free (unpublished B.E. thesis, 1968) investigated this relationship in 1968 and discovered contradictory results to those of Janelid's and Kvapil's. This series of tests confirmed that for a constant height of draw, the eccentricity definitely decreases with an increasing extraction outlet width. Logically, by considering the lower extreme case, this must be so because if the extraction outlet width is increased to the same magnitude as that of the height of draw, the draw shape approaches a semi-circle. Therefore, theoretical as well as practical considerations indicate that Janelid's prediction is erroneous.

The test results indicated a linear relationship with the least squares regression equation being as follows

$$\varepsilon = 0.9501 - 0.0024\ w$$

where w = extraction outlet width (inches).

The corresponding correlation coefficient for this least squares regression is -0.8377. This value is relatively low because of the dispersion of the results. However the trend does show a definite decrease in eccentricity as the outlet width is increased.

The fourth series of tests employed four different grades of broken rock chips drawn through a constant two inch extraction outlet width. The results displayed a marked decrease in eccentricity as the average size of the particles increased. This relation was predicted by Janelid (1964). The least squares regression equation to this relationship is expressed below:

$$\varepsilon = 0.9708 - 0.0092\ d_r$$

where d_r = average diameter of particles (inches)

The correlation coefficient for this equation is -0.9100.

It should be realized that the relationships determined apply only to the specific type of material extracted from the specific test model, and cannot be used to quantitatively analyse any other prototype or practical extraction system. However the relationships do serve as guidelines, indicating definite trends that will occur in any caving extraction system.

V.- MODEL TESTING - LONGITUDINAL SECTION

A second two-dimensional model, representing a longitudinal section of a sub-level caving extraction ring was constructed to ascertain the affect of ring gradient on the shape and axis of draw. A schematic representation of this model is illustrated in Fig. 11. As shown in this figure, the varying ring gradient is simulated by a pivoting ring board.

The ring gradient, α, is the inclination of the solid ring face. This angle is measured through the caved material as illustrated in Fig. 12. In the majority of practical situations this angle is in the range 60° to 100° in order to minimise ore losses. The deviation, η, of the axis of draw from the ring gradient will largely depend on the ring inclination κ. These three angles are illustrated in Fig. 12.

By employing individually identifiable markers and a grid system similar to that used in the first model, the shape and axis of draw for each situation could be determined. The observed values of deviation and inclination of the axis of draw were plotted against the ring board inclination (ring gradient).

A typical plot of these two angles, with the ring gradient as the independent variable is given in Fig. 13. As illustrated, the inclination of the axis of draw, κ, decreases at an even rate as the ring gradient decreases from 120 to 80 degrees. For angles less than 80 degrees, the rate of decrease becomes progressively greater. Correspondingly, the deviation of the axis of drawn, η, decreases evenly to a ring gradient of approximately 80 degrees subsequently passes through a minimum and then increases slightly.

This change of rate phenomenon was thought to occur due to a sudden change in the draw shape for a ring gradient of approximately 80 degrees. Observations made during the testing substantiated this conception. The draw shape was observed to be a portion of an ellipse when the ring gradient was greater than or equal to 80 degrees, but the draw shape below this value appeared to be rectangular with rounded ends. This rectangular draw shape is characterised by the granular material rilling down the ring board, the depth of this rilling action being dictated by the run-off width.

In order to explain this change from gravitational flow to a rilling action two theoretically extreme cases were considered. If the ring gradient was extended to 180 degrees then in effect no ring board would exist and the situation would effectively be similar to that simulated by the first model. Hence, the inclination of the axis of draw at this position would be 90 degrees, with the corresponding deviation also 90 degrees. On the other hand, if the ring gradient was reduced almost to the rill angle of the material, the inclination of the axis of draw would be the same as the ring gradient, and the corresponding deviation would be zero. These extreme points may be inserted onto a graph with the ring gradient (independent variable) varying from 0 to 180

degrees. If the lines connecting the observed points are extrapolated in either direction they intersect these extreme points. This indicates that the observed results are consistent with the two extreme points. This is illustrated in Fig. 14, which in effect represents the deviation and inclination of the axis of draw over the complete range of possible ring gradients. The average ring gradient that produced zero deviation (that is, exactly half of an elliptical draw) was 79.5 for the glass beads and 83.0 degrees for the rock chips.

VI.- CONCLUSIONS

In order to optimise the design of a sub-level caving system of mineral extraction it is essential to understand the factors influencing the gravity flow of material. The shape of the draw pattern is one of the most important parameters. Statistical analysis of the results of two-dimensional model tests have shown that this shape can be uniquely described by an eccentricity value. This has been shown to increase as the height of draw and height of overburden increases; and the average rock size decreases. Conversely the eccentricity decreases as the extraction heading width increases.

The results of this research have led to the development of mathematical models to describe the sub-level caving system. This has enabled the development of computer programmes to assist in the design of such systems. The work has also indicated other factors which require more detailed analysis and measurement. This particularly applies to the need for full scale insitu tests. The detailed planning of such tests has been made possible as a result of the model work that has been developed at the University of Queensland within the Department of Mining and Metallurgical Engineering.

VII.- ACKNOWLEDGEMENTS

The Australian Mineral Industries Research Association (AMIRA) sponsored the project which made it possible for one of the authors to conduct a one year study at the University of Queensland. Sincere appreciation is expressed to AMIRA.

VIII.- REFERENCES

1. BALSLEY, H.L. - Introduction to Statistical Method, Reprinted 1966, (Litterfield, Adams and Co., New Jersey).

2. BROWN, R.L. and RICHARDS, J.C. - Exploration study of the flow of granular materials through apertures, Trans. Instn. Chem. Engrs., Vol. 37, No. 2, 1959, p. 108.

3. BROWN, R.L. and RICHARDS, J.C. - Profile of flow of granules through aperatures, Trans. Instn. Chem. Engrs., Vol. 38, 1960, pp. 243-256.

4. CHASE, C.I. - Elementary Statistical Procedures, 1st ed., 1967, (McGraw-Hill Inc., U.S.).

5. COATES, D.F. - Rock Mechanics Principles, Canadian Mines Branch Monograph 874. Revised 1967.

6. DEUTSCH, G.P. and CLYDE, D.H. - Flow and pressure of granular materials in silos, J. Eng. Mech. Div., Pro. American Soc. Civil Engr., Dec. 1967, p. 103.

7. FREE, G.D. - Exploratory study of the flow of ore in sub-level caving, B.E. Thesis, (unpublished), University of Queensland.

8. JANELID, I. - Guide on sub-level caving, Swedish Mining Ass., B Series, No. 75, 1965.

9. JANELID, I. and KVAPIL, R. - Sub-level caving, Int. J. Rock. Mech. Min. Sc., Vol. 3, 1966, pp. 129-153.

10. KVAPIL, R. - Gravity flow of granular materials in hoppers and bins - Part I, Int. J. Rock. Mech. Min. Sc., Vol. 2, 1965, pp. 35-41.

11. WOEHLBIER, H. and REISNER, R. - Fundamental principles in bunkering of loose materials, Nov. 8, 1962, Lectures of the Westfaelische Berggewerkachaftskasse in Bockum, West. Germany.

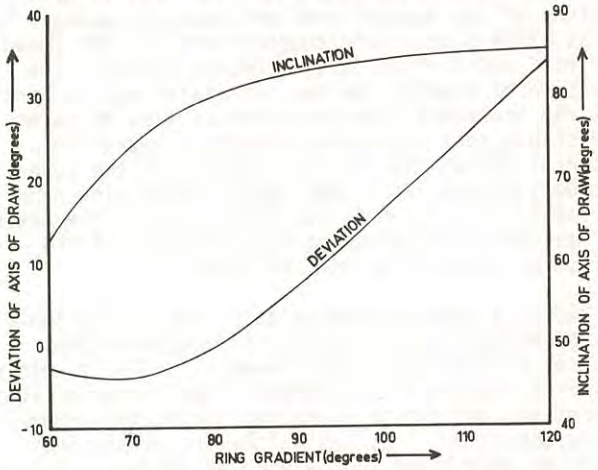

Figure 13. Example of a graph of the observed inclination and deviation of the axis of draw versus the ring gradient.

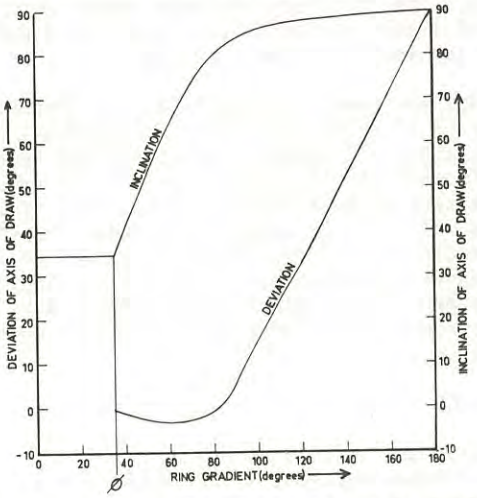

Figure 14. Example of a full range graph of the inclination and deviation of the axis of draw versus the ring gradient.

The Establishment of Optimized Design Parameters for a New Gypsum Mine

By

I. Weir-Jones, B.Sc., Ph.D.

(Assistant Professor, Department of Mineral Engineering, University of British Columbia)

SUMMARY.- Reliable values for some of the mechanical properties of gypsum are determined and these are used as a basis for establishing the optimum working dimensions for a new mine.

I.- INTRODUCTION

Many stratified orebodies are mined by means of partial extraction methods. In this type of mining, portions of the deposit are left between roadways to act as pillars providing support both for the immediate roof and for the superincumbent strata. The provision of support for the immediate roof is particularly important from the point of view of safety - an unstable roof obviously presents a hazard to personnel below. The overall support of the superincumbent strata has a less immediate bearing upon the safety of personnel, but there may well be pressing reasons for maintaining the stability of the surface or intervening mineral deposits.

Hence, a company contemplating the initiation of partial extraction operations is faced with two mutually contradictory requirements. Firstly, mining economics require that, within a given area, as much mineral as possible be extracted during the primary mining operation, i.e., as little ore as possible should be sterilized in the form of pillars. Secondly, however, it is essential that safe working conditions be maintained; this means that a stable roof is most desirable. Furthermore, there is often the need to provide general support for the superincumbent strata. The corollary of these requirements is an array of stable pillars, i.e., ones which may contain a considerable amount of ore.

The engineer seeking to optimize the dimensions and extent of an array of pillars and roadways must, therefore, achieve a compromise between the necessity to maintain safe working conditions and the requirement to extract as much mineral as possible from a given area. It will be shown that, providing the material making up the deposit lends itself to reliable mechanical testing, and if the prevailing conditions can be defined with reasonable accuracy, then a close approach may be made to the optimum working dimensions.

II.- NOTATION

σ_t	ultimate tensile strength, p.s.i.
σ_c	ultimate compressive strength, p.s.i.
τ	shear strength, p.s.i.
E_p	secant modulus of pillar, p.s.i.
E_r	secant modulus of roof, p.s.i.
E_s	secant modulus of solid, p.s.i.
ν	Poisson's ratio
V	specimen volume, ins^3
H	specimen or pillar height, ins.
D	specimen or pillar width or diameter, ins.
M	moment, lbs. ft.
C	pillar constant
k	coefficient of permeability, m/sec.
$F(\varsigma)$	probability coefficient

III.- APPRECIATION OF CONDITIONS AT THE MINING SITE.

The new mine is situated below the extensive post-glacial plains which cover a large area of northeastern Yorkshire. These plains extend inland from the coast for a distance of about 15 miles and are an extremely prosperous farming area. The deposit of gypsum dates from Permian times and it is considered to have been associated with the western-most edges of the ancient Zechstein Sea which was also responsible for the formation of the extensive evaporite deposits lying north-east of this area. The gypsum, which is usually 16ft. thick, is extremely pure and it is found at comparatively shallow depths; at the mine site area, the overburden is only 120ft. thick.

The shallowness of the deposit, however, tends to give a somewhat false idea of the magnitude of the problems associated with its extraction. These problems are partly natural and partly dependent on the existence of conflicting interests in the vicinity of the mine. They do, however, all stem from the nature of the overlying strata. As has already been mentioned, the surface deposits are post-glacial, consisting of an extremely large number of thin layers of varved clays, fine silts, and sands extending down from the surface to a depth of approximately 75 ft. From the bottom of the lacustrian deposit to the seam, a distance of approximately 45ft., the strata consists of a succession of marls, weak sandstones and siltstones which, although they are inherently incompetent materials in the mining sense, are appreciably stronger than the surface material which, to all intents and purposes, may be considered to have negligible strength.

Despite the fact that the presence of the large amounts of clay in the surface deposits renders them almost completely impervious to the vertical movement of water, there are two continuous beds of fine sand at 25ft. and 60ft. which readily permit its lateral movement.

It is the presence of these sand beds which presents one of the natural problems. Any disturbance of the beds causes them to become fluid and in this condition they present an extremely serious hazard to any unprotected excavation to which they have access. The potential hazards associated with the sand beds necessitated the imposition of certain legal restrictions upon the mine design. These restrictions will be discussed later.

The gypsum seam itself was by far the strongest material encountered during the development of the mine. Physically, the gypsum, in excess of 98% pure, occurs as a fine-grained massive pink material with a few minor faults and some thin bands of satinspar; fairly thin fragments are clearly translucent and even at the interface with the overlying marls there is no deterioration in quality. Petrographic examination of exploratory cores confirmed that almost no impurities were present - it also indicated that the bulk of the gypsum was very fine-grained with the maximum crystal size being less than 2.0mm. Additional petrofabric analysis revealed no sign of any post-depositional deformations having taken place, and provided further confirmation of the extremely homogeneous composition of the gypsum.

Below the gypsum lay a thick deposit of competent dolomite. In most places this was in intimate contact with the gypsum, but in a few areas from 6 - 9 in. of marl occurred between the two evaporites.

The majority of the problems which exist at the new mine can be related to the nature of the overlying material and the ability of the upper and lower sand beds to flow, given the least opportunity to do so. Knowledge of this unstable structure caused the Inspector of Mines to impose certain arbitrary restrictions on the workings within the seam. These included:

(1) Bord and pillar workings should be used, i.e., the workings would consist of two sets of mutually perpendicular drifts forming an array of square or rectangular pillars.

(2) 6ft. of gypsum should be left between the roof of the workings and the gypsum/marl contact.

(3) The pillars should have a safety factor of 8 to 1.

Further restrictions were imposed upon the mine owners by the local Planning Authority. Before granting planning permission for the mine, the Authority required an assurance that there would be no detectable ground movement at the surface. The reason for the imposition of this condition was again connected with the nature of the upper strata. The lacustrian material at the surface covers a large area and this plain is valuable farming land. Because of its extent, an extremely complex system of artificial drainage ditches has been constructed to facilitate the removal of excess ground water. The Planning Authority feared that if mining caused the surface to subside, there would be an immediate tendency for the subsidence basin to flood. In addition to this, should there be drainage ditches passing through the affected area, the water flow in them would be either impeded or reversed, with extremely deletrious effects on the overall drainage pattern.

In view of these conditions, it was decided that whatever layout of bord and pillar mining was employed, the overlying strata should be disturbed as little as possible so that there would be negligible vertical movement at the surface. Therefore, even before development work commenced at the mine, and before the results of laboratory testing became available, certain conditions relating to the design of the workings became apparent.

Preliminary boreholes which had passed through the seam and penetrated the underlying dolomite had indicated that below this lay an aquifer with an artesian head of approximately 170ft. However, as the dolomite had a minimum proven thickness of 15ft., the presence of this aquifer was not felt to present any hazard.

Thus, the initial conclusions were that the mine workings would be situated in the lower two-thirds of the gypsum seam, there would be a 6ft. thick roof layer and, whatever working dimensions were chosen, there should be no detectable subsidence at the surface. Furthermore, the mine workings would have to be stable on a long-term basis.

As the deposit lay at a depth of 120ft., it was assumed that the gypsum would be subjected to a mean inherent vertical stress of 120 p.s.i. This meant that, even with an extraction rate of 80%, the mean vertical pillar stress would only be 600 p.s.i. Therefore, it appeared that the load bearing capacity of the individual mine pillars was probably not going to be the most important factor in the design of the mining layout.

With the conclusion concerning the strength of the pillars in mind, attention was turned to a preliminary examination of the other basic structural component in the proposed layout, i.e., the roof span. The most probable limitations on the final working dimensions would be those imposed by the maximum tensile stress induced in the roof.

An additional limitation on the overall design could be imposed by the magnitude of the shear stresses which would be induced in the roof adjacent to the edges of the mining panel. It was felt desirable to examine these, together with the tensile stresses due to overall panel roof deflections, in order to establish overall working dimensions.

The mechanical properties of the gypsum which would play important parts in the former limitations would probably be:

(1) The ultimate tensile strength of the gypsum - this would effectively limit the maximum tensile stresses which might be induced in the roof

(2) The shear strength - shear stresses would be induced at the panel edges.

(3) Young's Modulus and Poisson's Ratio - pillar deformation would control overall roof deformation and, hence, the magnitude of the tensile stresses

(4) Time dependent deformation properties - long term pillar stability was of paramount importance

(5) The permeability characteristics of the gypsum would have a bearing upon the build-up of hydro-

-static pressure above the roof layer.

In addition, a testing programme was initiated to establish relevant values for the uniaxial and triaxial compressive strength of the gypsum.

IV.- LABORATORY INVESTIGATIONS.

The high degree of homogeneity and the continuous nature of the gypsum, revealed by the preliminary study of numerous cores, has already been commented upon. The exploratory holes provided approximately 220ft. of 4in. diameter gypsum core, taken perpendicular to the plane of the deposit. In addition, large quantities of material became available when the exploratory shaft was completed. This gypsum took the form of either blocks, weighing up to 2500lb. cut from the face of the development heading, or very large amounts of BX core from horizontal holes within the seam.

Thus, at the start of the laboratory phase, the following samples were available:-

(1) 220ft. of 4in. diameter core - vertical

(2) large amounts of BX core - horizontal

(3) massive blocks up to 36in. x 36in. x 24in.

It was apparent that, since the pillars would be formed in the lower part of the seam, there was little point in carrying out extensive tensile strength determinations in this region. Similarly, there appeared to be no reason to carry out innumerable uniaxial compressive strength determinations in the roof horizon, other than for obtaining data concerning the homogeneity of the gypsum. However, it was decided that it would be instructive to establish whether or not there was a variation in tensile strength along the vertical section. The results of these tests showed that, with the exception of a 2ft. thick portion at the top of the deposit, where some leaching may have taken place, there was no significant variation in tensile strength down the vertical section.

(a) Tensile Strength Determination.

Because of the large quantities of core available, the most convenient method of obtaining tensile strength data was by means of the Brazilian Disc Test. However, it was appreciated that the '4-Point Loading Test' would more closely approach the loading conditions that the gypsum would be subjected to in the mine. Correspondingly, prismatic specimens were cut from some of the large core and tested. The results of these '4-Point Loading Tests' were compared to the results obtained from testing adjacent material by means of the Brazilian Disc Test. Two facts immediately became apparent; firstly, the results from the prisms were consistently higher than those from the discs, and secondly, as the length of the constant tensile stress region between the two loading points increased, there was a reduction in the calculated tensile strength. However, this decrease did not continue indefinitely. There appeared to be a critical length for the constant stress zone above which there was little further reduction in tensile strength. This critical length was 3.0in., i.e., approximately 35 times the maximum grain dimension in the specimen. The higher strength obtained from what is frequently described as a flexural test agrees with the results of other tests made with different materials (1). Specifically, the mean tensile strength of the supercritical prismatic specimens was greater than the mean strength of the disc specimens by a factor of 2.2.

Additional testing gave values for the indirect tensile strength of the gypsum which agreed closely with the results of the initial disc tests and had a comparatively small standard deviation. The results from two typical groups of disc specimens taken from BX cores are given below -

Group 17(ii) 77 discs		
	Mean indirect tensile strength	434 p.s.i.
	Standard deviation	±44 p.s.i.
Group 9(iv) 64 discs		
	Mean indirect tensile strength	453 p.s.i.
	Standard deviation	±53 p.s.i.

These results compare favourably with the disc results obtained initially from one of the vertical boreholes -

Boreholes 1/51 89 discs		
	Mean indirect tensile strength	441 p.s.i.
	Standard deviation	±47 p.s.i.

Although no evidence of anisotropy was found, great care was taken to ensure that the plane of tensile failure in the discs cut from the horizontal boreholes was parallel to that of the perpendicular boreholes, and that both these lay in the same plane as the anticipated tensile stresses in the roof.

As a result of testing 669 discs, it was felt that a reliable value for the indirect tensile strength of the gypsum had been obtained, i.e., 457 p.s.i., ±66 p.s.i. Furthermore, the results of the preliminary flexural testing suggested that the indirect tensile strength was equal to 0.46 x the flexural tensile strength. Hence, a preliminary value for the tensile strength of the gypsum was obtained, 992 p.s.i. - the standard deviation, ±66 p.s.i.

(b) Shear Strength Determination.

The shear strength of the gypsum was taken as the value of the Mohr's envelope intercept on the shear axis; this value was 1230 p.s.i. Thirty specimens with a D/H ratio of 0.5 and a diameter of 3in. were tested in a triaxial cell capable of exerting a maximum radial stress of 10,000 p.s.i. at a maximum axial stress of 150,000 p.s.i. The shape of the envelope suggested that, at the confining pressures used, the gypsum behaved as a brittle material.

(c) Young's Modulus and Poisson's Ratio Determination.

The modulus of the pillars would influence both the deformation of the roof between the pillars and the overall deformation across the entire width of the panel. It was apparent that the modulus which would be most relevant would be the secant modulus between 120 p.s.i. and 800 p.s.i., i.e., between the probable inherent vertical stress level and a stress equal to the mean pillar stress at 85% extraction. Correspondingly, the secant moduli of a large number of gypsum specimens were established between these stress levels. Two facts became apparent; firstly, there was the customary increase in modulus as the

specimens were cycled - the fifth and subsequent cycles displayed no increase - and secondly, as the specimen volume increased, the D/H ratio remaining constant at 0.5, there was a decrease in secant modulus. However, in specimens with a volume of more than about 70 cu.in., there was no further decrease - hence, the secant modulus of the gypsum was taken to be this limiting value, 2.1 x 10^6 p.s.i. Concurrent measurements of Poisson's Ratio gave a value of 0.28.

(d) Creep Testing.

This was carried out on both cylindrical and prismatic gypsum specimens. Although the material displayed time dependent deformation characteristics, these only became apparent when the compressive stress exceeded 4000 p.s.i. At a stress of 2500 p.s.i. at 90% humidity, and with an ambient temperature of 70°F, negligible deformation occurred during 300 day creep tests. In view of this, it would appear that there is little liklihood of time dependent deformations occurring in this mine.

(e) Permeability Testing.

It was possible that the development of a hydrostatic head above the roof would depend upon the permeability of the gypsum. Although the absolute value was thought to be quite low, no leaching having extended more than 2ft. below the top of the seam, a series of permeability tests were carried out. Cylindrical specimens 4.1cm. in diameter and 5.0cm. long were bonded inside steel cylinders and these assembled cells were used for testing. The apparatus consisted of a small positive displacement pump connected to these cells and was designed to permit the application of pressures of up to 2000 p.s.i. The results of this work showed quite conclusively that the permeability of the gypsum was very low, i.e., k = 6.13 x 10^{-10} m/sec.

(f) Compressive Testing.

This programme was designed to provide data relating to the probable strength of the gypsum pillars within the mine. Since it is an established fact that the compressive strength of rock specimens varies with both volume and D/H ratio, the testing programme had to fulfil two functions:

(1) it was necessary to establish a relationship between mean specimen strength and specimen volume over as wide a range of volumes as possible

(2) the influence of variations in the D/H ratio upon the compressive strength of the specimens had to be determined.

Very briefly, the first part of the programme consisted of testing 419 specimens of D/H ratio 0.5. Ten different diameters of specimens were tested, ranging from 0.75in. to 6.0in. and, as was expected, there was a marked reduction in the ultimate compressive strength as the specimen volume increased. The mean strength fell from an initial value of approximately 7400 p.s.i., to a constant value of 5100.

After processing these results, the following expression was obtained relating ultimate compressive strength to specimen volume when the D/H ratio was 0.5 -

$$\sigma_c = 6662\ V^{-.059} \qquad (1)$$

The second part of the compressive testing programme involved the determination of the strength of 570 gypsum specimens divided into groups whose diameters varied from 1 to 8 in. and whose D/H ratios ranged from 0.4 to 3.7. In accordance with the results obtained by many other workers, there was found to be a marked increase in the compressive strength as the D/H ratio increased. This was primarily due to radial constraint on the central core inducing triaxial loading conditions. This phenomenon is responsible for the situations where mine pillars support loads considerably in excess of their mean uniaxial compressive strength (2).

Analysis of the results obtained during this phase permitted the derivation of the following expression:-

$$\sigma_c = 8340\ D^{0.27}\ H^{-0.36} \qquad (2)$$

(i) Conclusions drawn from the compressive testing.

It should be remembered that expression (1) only applies to specimens with a D/H ratio of 0.5 and that, therefore, it does not take into account the effect of triaxial loading on the central portion of the specimen. However, expression (2) caters for variations in both diameter and height and, hence, it takes into account the effect of constraint and the consequential increase in the specimens apparent mean compressive strength.

The primary function of the testing of specimens with a constant D/H ratio but variable volume was to determine the magnitude of the "size" or "scale effect" for gypsum (3) (4) (5), i.e., to establish the relationship between uniaxial strength and specimen volume. The results of this programme indicated that, although there was a fairly rapid reduction in strength as the volume increased, a limiting value was reached quite quickly. This critical volume appeared to be slightly in excess of 60cu.in. and it represented a reduction in compressive strength of approximately 40%. When the results of this constant D/H ratio testing are viewed in the light of the work of Bieniawski, it would appear justifiable to treat the gypsum as a 'hard' rock in the sense that it is fine-grained, homogeneous, and free from any discontinuities. On the basis of Bieniawski's work, it would appear that the 'in situ' compressive strength of a material is closely approximated by the strength of specimens whose minimum dimension is greater than 25 times the maximum grain or particle size (3). Applying this criterion, it would appear that a specimen of the gypsum with a minimum dimension of more than 2in. would have a compressive strength close to the limiting value. However, an examination of the graphic presentation of the compressive strength vs. specimen diameter curve for D/H ratio 0.5, Fig.1, indicates that the limiting strength is reached when the minimum dimension of the specimen exceeds 3.2in., i.e., about 40 times the maximum grain size.

However, even if the critical specimen dimension is slightly greater than 3in., this is still well within the capabilities of laboratory testing and it is suggested that it is reasonable to use expression (2) as a basis for the design of the support pillars.

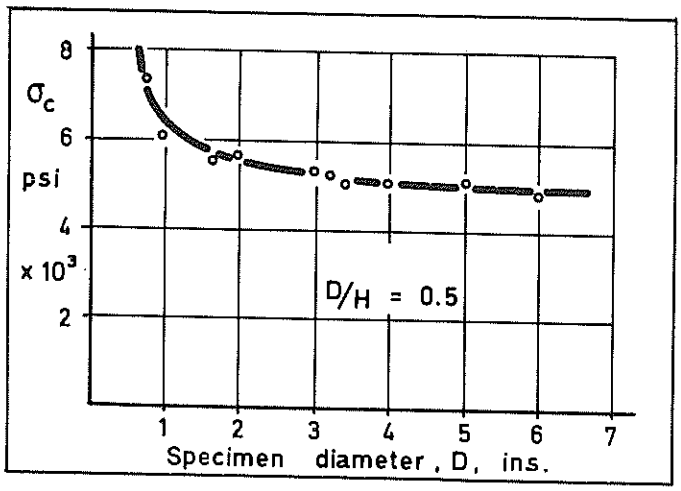

Fig.1. Relationship between σ_c and specimen volume.

The laboratory testing yielded values for all the relevant mechanical properties. The data from the testing, dealing with the 'size effect' for this gypsum, would appear to indicate that, in this case, the laboratory results may be used as the basis for design work. The relevant values are -

Ultimate tensile strength	992 p.s.i.	±66 p.s.i.
Shear strength	1230 p.s.i.	
Secant modulus	120 - 800 p.s.i.	2.1×10^6 p.s.i.
Poisson's ratio	0.28	

Ultimate compressive strength $8340\ D^{0.27}\ H^{-0.36}$ p.s.i.

V.- THE ESTABLISHMENT OF WORKING DIMENSIONS.

It has already been noted that the tensile strength of the roof material will probably be the property which limits the working dimensions. In discussions with the mine operators, it had been decided that the probability of the roof failing under tension at any intersection should be maintained at less than 1%. As the results obtained during tensile testing displayed normal distribution, the value for $F(\zeta)$ required to give a confidence coefficient of 99% could be derived from statistical tables (6). Thus, the value for the ultimate tensile strength which, it was suggested, would result in less than 1% of the intersection roofs failing was 836 p.s.i.

(a) The Pillar Dimensions.

Before calculating the permissible span, it was necessary to establish what the maximum percentage extraction might be, given the required safety factor of 8 and the compressive strength of the gypsum from expression (2). The nomogram - Fig.2 - has been constructed to permit the dimensions of acceptable pillars to be established for any given extraction rate. A series of pillar and span widths may then be evaluated for tensile stability by the technique referred to below. The nomogram may, therefore, be used to determine one of two things: either whether the pillar formed at a particular extraction rate with a specific span width is stable, or to establish minimum limits for the span necessary to maintain a specified extraction with pillars which fulfil the stability requirements.

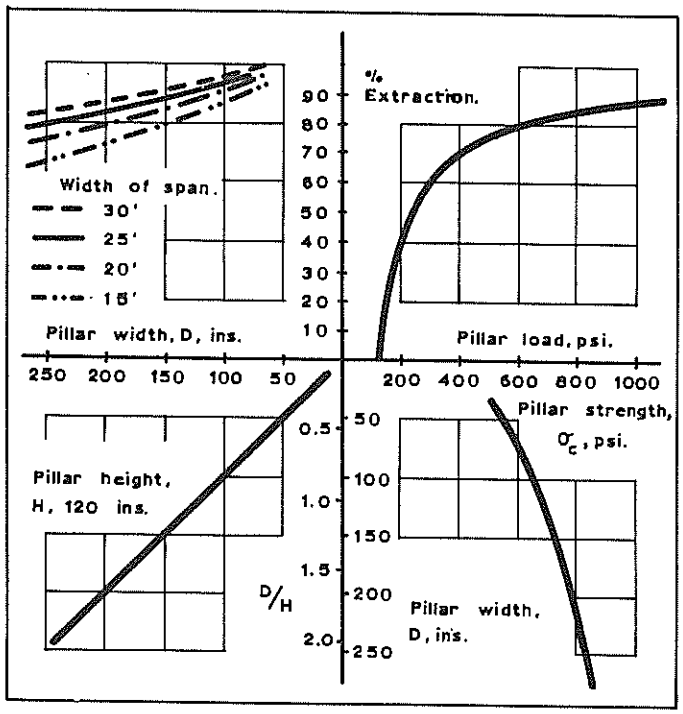

Fig.2. Relationship between percentage extraction and working dimensions.

As an example, the nomogram will be used to determine whether the pillar necessary to maintain an 80% extraction rate, with 20ft. wide rooms, will meet the stability requirements. The 80% extraction intercept on the 20ft. room width curve gives a pillar width of 15ft. on the horizontal axis. The pillar will be 10ft. high, hence the D/H ratio on the vertical axis is seen to be 1.5. The permissible load on a 15ft. wide pillar is 755 p.s.i., a value lying well to the right of the theoretical load and, therefore, the pillar is deemed to be stable.

(b) The Width of the Roadways.

Various procedures exist for calculating the magnitude of the tensile stresses induced in the roof. In all of them, certain limiting assumptions are made in order to reduce the problem to one of manageable proportions. The most satisfactory technique appears to be the one described by Wright, Ratti and Wang (7), in which they assume that the roof behaves as an elastic plate upon elastic supports. Briefly, the assumptions which are made are that the roof is elastic, and only subjected to forces acting normal to its plane. Furthermore, the roof is assumed to be thin, uniform, and only slightly deflected. Finally, the entire layout is presumed to be symmetrical. It is felt that these assumptions are valid in this situation, where the roof and pillars form a regular and elastic system. Based upon these assumptions, the techniques described in Wright's paper (7) are used to establish values for the maximum tensile stresses induced in roofs of various widths. In this way, the maximum roadway width may be determined using previously established or specified data.

Wright et. al. introduced the concept of the Pillar Constant, C, a measure of the rigidity of the

mining layout, which influences the size of the bending moments in the roof. The Pillar Constant, the distributed load on the roof, and the factor a, the sum of the half-widths of the rooms and pillars, together determine the magnitude of the bending moments. Hence, if a value may be obtained for the distributed load, and for various combinations of pillar and room half-widths, it is possible to calculate the magnitude of the tensile stresses in the roof. Fig.2 is designed to give a range of possible pillar and room widths for specific extraction rates and, from these, using a value for the distributed load, the maximum tensile stresses can be obtained.

At this mine, where the rigidity of the overlying strata was greater than that of the gypsum roof, the overlying material was not expected to contribute to its loading. However, due to the nature of the sediments and to the very low permeability of the gypsum, it was anticipated that the full hydrostatic head would be developed at the gypsum/sediment contact. The value of this was taken to be 52 p.s.i., i.e., 120ft., and thus the total distributed load on the 6ft. thick roof was 58 p.s.i.

Based on the figure of 58 p.s.i. for the distributed load on the roof, and using the data from Fig.2, the following dimensions are suggested as being those which will ensure maximum extraction and yet meet the stability requirements for the pillars and roof:-

Pillar width	17ft.
Roadway width	25.5ft.
Extraction	84%

(c) Panel Width.

Tincelin and Sinou (8) and Höfer and Menzel (9) describe methods which may be used to calculate the tensile and shear stresses induced in the strata above the working horizon. These stresses are induced by the deformation of the strata due to the general lack of rigidity of the workings, rather than to the inter-pillar deformations affecting the immediate roof. Unfortunately, these techniques require an accurate knowledge of the mechanical properties of the overlying beds to give reliable results. In the case of this mine, assumptions had to be made about these properties, and this gave rise to inaccuracies in the calculated values of the maximum shear and tensile stresses. Assuming that the pillars supporting the roof act as a uniform elastic medium with a modulus equal to one-fifth of the solid seam, and that the gypsum roof and overlying sediments behave as separate layers, the following data concerning the magnitude and location of the stresses were calculated.

The tensile stress induced in a gypsum roof rose as the panel width was increased. A maximum of 140 p.s.i. occurred when the panel was approximately 160 ft. wide, then stress decreased to a steady value of 110 p.s.i. when the panel width exceeded 220 ft. If the width was less than 220ft., the position of the maximum tensile stress was displaced toward the centre of the panel, but once the width exceeded this figure, the maximum stress was found to be consistently 70ft. from the ribside. It was apparent that the high rate of extraction was responsible for this fairly high tensile stress.

The maximum shear stress always occurred directly above the ribside and once again it was noted that the magnitude of the stress increased rapidly as the panel was opened up - reaching a maximum at about 160 ft. width and then reducing slightly to a steady value of 2100 p.s.i. when the panel width exceeded 200ft. As with the tensile stresses, the high percentage extraction envisaged was responsible for the large shear stress. It was quite apparent that the economic requirement of maintaining a high percentage extraction, and the structural requirement of lowering the induced shear stress to about 1200 p.s.i. were mutually exclusive.

VI.- CONCLUSIONS.

It is suggested that the working dimensions have been established so that the conditions which were imposed for reasons of operator safety have been satisfactorily met. Furthermore, the suggested percentage extraction will enable the mine to operate as a highly profitable unit.

The question of the optimum panel width cannot be dealt with as satisfactorily. The induced tensile stresses do not present too much of a problem as they will occur above the pillars, away from the tensile stress concentrations which occur above the pillar corners. However, the predicted shear stress clearly exceeds the experimentally determined shear strength of the gypsum, and, for practical panel widths, it is difficult to see how the possibility of shear failure above the ribside may be eliminated. A possibility in a static system would be the formation of a zone of intermediate rigidity between the main production area and the solid rib. In a dynamic system, where the extension of the mined region is an economic necessity, there are always going to be boundaries between mined and unmined regions where high shear stresses will be set up. It is possible that, in the future, a mining method will be developed which will permit the shear stresses to be maintained at a sufficiently low level, but in the absence of this, the possibility of shear failure in the roof along the panel edge will have to be accepted.

As a check upon the validity of the assumptions made regarding the modulus of the gypsum making up the pillars, and as a means of monitoring surface subsidence, borehole extensometers were used. Anchors were installed in boreholes which passed through the portions of the seam which would form pillars. Normally, four anchors would be placed in each hole, one situated about 12ft. below the proposed pillar in the underlying limestone, one at the base of the pillar, one at the top, and one 12-15ft. above the gypsum/sediment contact, the purpose of the last anchor being to establish whether or not bed separation occurred. All movements were measured relative to the bottom anchor, which was assumed to be stable, using a constant tension extensometer. The deformation predicted for the pillars in the centre of the panel was .039in. However, the average measured deformation was .027in. As the extensometer used was known to be accurate to within ±.002in., two possible reasons for the discrepancy are suggested. One, the mining had not developed to a point where the pillars were fully loaded, and thus undergone maximum deformation. Two, variations in the moisture content of the surface deposits could have caused slight heaving of the instrument stations and, thus, an apparent reduction in the amount of deformation detected. The former explanation is more likely and additional evidence in its favour was the fact that, at the last

examination, the gradients of the anchor displacement curves had not become zero.

It is not suggested that this approach to the problem of establishing optimum mining dimensions may be generally employed. Previous workers have shown that the minerals found in many stratified deposits do not lend themselves to the laboratory determination of the mechanical properties. In view of this, alternative methods of dimension determination have been developed (10) (11). However, if preliminary investigations indicate that the mineral to be mined is homogeneous, isotropic and does not display extensive discontinuities, it is suggested that the type of techniques discussed here will give rise to considerable increases in the profitability of the mining operation.

VII.- ACKNOWLEDGEMENTS.

The laboratory programmes on which this paper was based were carried out at the Department of Mining Engineering, University of Newcastle upon Tyne. The author wishes to thank the Head of Department, Professor E.L.J. Potts, for his invaluable assistance. He would also like to thank the United Kingdom Science Research Council, who were his sponsors.

REFERENCES

1. AKAZAWA, T. - Tension Test Method for Concrete. Union of Testing and Research for Materials and Structures, No. 16, 1953.

2. OBERT and DUVALL - Rock Mechanics and the Design of Structures in Rock, J. Wiley, New York, 1967, pp. 289-290.

3. BIENIAWSKI, Z.T. - The Effect of Specimen Size on Compressive Strength of Coal. Int. J. Rock Mech. Min. Sci., Vol. 5, No. 4, 1968.

4. PROTODYAKANOV, M.M. and KOIFMAN, M.I. - The Size Effect in Investigations of Rock and Coal. Proc. 5th Conf. of Int. Bureau for Rock Mech. Leipzig, Nov. 1963. Pub. Berlin, 1964.

5. DENKHAUS, H.G. - Strength of Rock Materials and Rock Systems. Int. J. Rock Mech. Min. Sci., Vol. 2, No. 2, 1965.

6. WEATHERBURN, C.E. - Mathematical Statistics. Cambridge University Press, London, 1957.

7. WRIGHT, F.D., RATTI, G. and WANG, F.D. - Stresses in Mine Roof Slabs Over Rectangular, Elastic Pillars. 4th Int. Conf. Strata Control and Rock Mech., New York, 1964.

8. TINCELIN, E and SINOU, P. - Collapse of Areas Worked by the Small Pillar Method. Paper G.C. 3rd Int. Conf. Strata Control, Paris, 1960.

9. HOFER, K-H. and MENZEL, W. - Comparative Study of Pillar Loads in Potash Mines. Int. J. Rock Mech. Min. Sci., Vol. 1, No. 2, March, 1964.

10. SALAMON, M.D.G. and MUNRO, A.H. - A Study of the Strength of Coal Pillars. Transvaal and O.F.S. Chamber of Mines, Research Organization. Research Report No. 71/66.

11. SALAMON, M.D.G. - A Method of Designing Bord and Pillar Workings. Transvaal and O.F.S. Chamber of Mines, Research Organization. Research Report No. 72/66.

Non-Linear Consolidation and the Effect of Layer Depth

By

E. H. Davis, B.Sc. (Eng.), F.I.E.Aust.

(Professor of Civil Engineering (Soil Mechanics), University of Sydney)

SUMMARY.- This paper generalises the previous theory published by Davis and Raymond which only dealt with a relatively thin layer and showed that, although the rate of pore pressure dissipation is slower than that of the classical Terzaghi linear theory, the degree of settlement is the same. This theory and its generalisation are based on the assumption that the coefficient of consolidation is constant but that the coefficients of volume decrease and of permeability are not.

The generalisation of the original theory takes into account the effects of non-linear behaviour on the rate of consolidation of deep layers. For such situations it is shown that the rate of pore pressure dissipation may be faster or slower than that of the classical Terzaghi linear theory depending on the ratio of the initial to the final effective stress at the top of the layer and on the ratio of the initial effective stress at the top to that at the bottom of the layer. The rate of settlement on the other hand is virtually always faster than that given by the classical theory and in the case of very deep layers subject to small consolidation pressuresthe increase in rate may have practical significance.

I.- INTRODUCTION

In the classical consolidation theory of Terzaghi it is assumed that the coefficient of volume decrease m_v and the coefficient of permeability k are individually constant both with time and throughout the depth of the consolidating layer, that is the theory is a linear one. For real soils both m_v and k decrease with decrease in void ratio so that in problems where the consolidation pressure is high enough to eventually cause a significant change in void ratio, or where the soil layer is deep enough for the void ratio at the top to be significantly higher than at the bottom, it may be necessary to take the non-linear behaviour of the soil into account.

The effect of variation of m_v and k with depth but not with time has been studied by Schiffman and Gibson (Ref.1). Davis and Raymond (Ref. 2) on the other hand developed a theory which allowed for the variation of m_v and k with time but not with depth and was therefore only applicable to oedometer tests and to relatively thin layers in the field. A similar approach was developed independently by Mikasa (Ref.3).

Non-linear effects are likely to be most often of practical importance in considering the settlements produced by sand reclamation filling on deep beds of soft normally consolidated clay. For such problems the depth of the clay is likely to be a significant factor in the divergence of the consolidation behaviour from that of the classical linear theory. It is therefore the purpose of this paper to extend the theory given in Ref.2 to include the depth effect. The earlier theory will then appear as a special limiting case of the more general theory.

II.- FORMULATION OF THEORY

The analysis is restricted to vertical one-dimensional strain conditions with pore pressure dissipation occurring only in the vertical direction. It is assumed that the relation between void ratio e and vertical effective pressure p_e follows the usually accepted logarithmic relation:

$$e = e_1 - C_c \text{ Log } p_e \qquad (1)$$

where C_c is the Compression Index, a constant, and e_1 is the void ratio corresponding to $p_e = 1$.

It follows that:

$$m_v = -(de/dp_e)/(1+e) = 0.434C_c/(1+e)p_e \qquad (2)$$

Since (1+e) varies, both throughout the soil mass and with time, much less than p_e, m_v may be taken to be inversely proportioned to p_e, and the resulting mathematical analysis is rendered much easier. Thus it is assumed that:

$$m_v = A/p_e \qquad (3)$$

where $A = 0.434C_c/(1+e) = \text{constant}$.

Typical tests results showing the reasonable nature of this assumption are given in Fig.1.

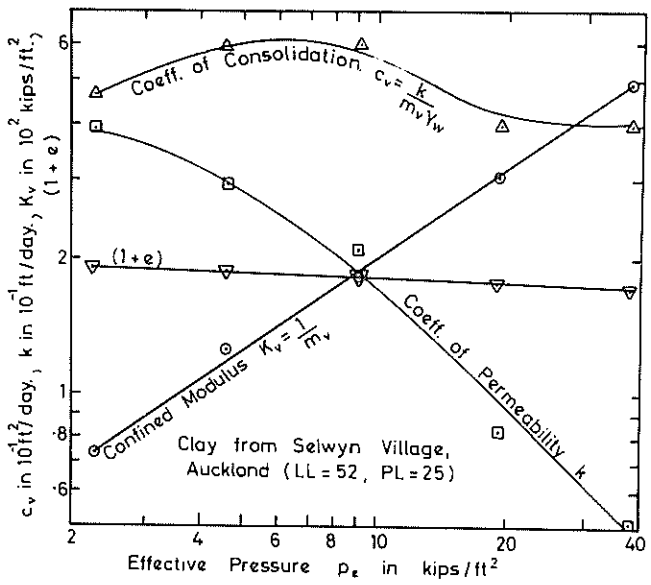

Fig.1 Typical Oedometer Results on Normally Consol. Clay

It is found with most normally consolidated clays that the coefficient of consolidation ($c_v = k/m_v\gamma_w$ where k is the coefficient of permeability) varies much less with p_e than either m_v or k. As the void ratio decreases, the consequent decrease in the coefficient of permeability is approximately proportional to the decrease in the coefficient of volume decrease. For the purposes of the present theory it is assumed that c_v is actually constant. The reasonable nature of this assumption is also illustrated in Fig.1. It therefore follows that:

$$k = c_v\gamma_w\, m_v = c_v\gamma_w A/p_e \qquad (4)$$

Assuming that the soil is saturated, that the pore water and soil particles are incompressible relative to the soil skeleton and that the movement of water obeys Darcy's Law, the rate of water loss from an elemental layer may be equated to the rate of volume decrease:

$$\partial(k\partial u/\partial z)/\partial z = c_v\gamma_w(\partial e/\partial T)/(1+e) \qquad (5)$$

where u = excess pore pressure,
zD = depth below top of consolidating stratum of total depth D,
$T = c_v t/D^2$,
and t = time from start of consolidation.
If T_v is the Time Factor as normally defined in one-dimensional consolidation theory, $T_v = T$ for one way drainage and $T_v = 4T$ for two way drainage.

Using eqs. (1) and (4) eq.(5) becomes:

$$-\partial p_e/\partial T = \partial^2 u/\partial z^2 - (\partial p_e/\partial z)(\partial u/\partial z)/p_e \qquad (6)$$

If the stress causing consolidation remains constant during the consolidation process, eq. (6) can be written as:

$$\partial u/\partial T = \partial^2 u/\partial z^2 - (\partial p_e/\partial z)(\partial u/\partial z)/p_e \qquad (7)$$

Without the second term on the right-hand-side, eq. (7) reduces to the usual equation of Terzaghi's linear theory of consolidation in which m_v and k are both constant. This term is therefore a modifying term which introduces the effects of non-linear behaviour of soil into the theory.

In passing, it can be remarked that, if (1+e) in eq. (2) is not regarded as constant, the equation corresponding to eq. (7) is:

$$\partial u/\partial T = \partial^2 u/\partial z^2 - (1-A)(\partial p_e/\partial z)(\partial u/\partial z)/p_e \qquad (8)$$

The only difference between this equation and eq. (7) is the factor (1-A). Although this factor changes during the consolidation process, for the majority of clays and situations it is greater than about 0.90 and is always less than one. In view of the fact that the second term on the right-hand-side of eq. (7)& (8) is only a modifying term, it can be seen that the use of the simpler eq. (7) should not introduce serious errors.

In order to facilitate comparison between the linear and non-linear theories, the boundary conditions selected in this analysis correspond to those of the Terzaghi linear theory.

Throughout, it is assumed that the total stress causing consolidation remains constant during the consolidation process. The conditions and their code letters are set out in Table 1.

Thus for conditions A_1 and A_2:

$$p_e = p_{eo} + \gamma_s Dz + q - u \qquad (9)$$

and for conditions B_1 and B_2

$$p_e = p_{eo} + \gamma_s Dz + q(1-z) - u \qquad (10)$$

where γ_s = the average submerged density of the soil.

Introducing the dimensionless parameters:

$$\beta = p_{eo}/\gamma_s D \qquad (11)$$

$$\alpha = (p_{eo}+q)/p_{eo} \qquad (12)$$

and changing the definition of u so that the actual excess pore pressure is uq, substitution of eq. (9) or (10) into the general eq. (7) gives:

$$\partial u/\partial T = \partial^2 u/\partial z^2 + (\partial u/\partial z)(b\partial u/\partial z - a)/(1+az-bu) \qquad (13)$$

where $b = (\alpha-1)/\alpha$
and $a = 1/\alpha\beta$ for conditions A_1 and A_2
or $a = (1+\beta-\alpha\beta)/\alpha\beta$ for conditions B_1 and B_2.

TABLE 1

BOUNDARY CONDITIONS

	Condition	Code
Original effective stresses	top, D, bottom; Peo; $p_{eo}+\gamma_s D$	A_1, A_2, B_1 & B_2
Final effective stresses	Original plus q	A_1 & A_2
	Original plus q	B_1 & B_2
Drainage at boundaries	permeable; D=H; $T_v = \frac{c_v t}{H^2} = T$; impermeable	A_1 & B_1
	permeable; D=2H; $T_v = \frac{c_v t}{H^2} = 4T$; permeable	A_2 & B_2

By making the substitution $-w = \ell n(1+az-bu)$, a form of eq. (13) which has some computational advantages may be obtained:

$$\partial w/\partial T = \partial^2 w/\partial z^2 + a \exp.(w)\, \partial w/\partial z \qquad (14)$$

From eq. (1) it can be shown that:

$$\text{Log}\alpha = (e_{ot}-e_{ft})/C_c \qquad (15)$$

and $$\text{Log}((\beta+1)/\beta) = (e_{ot}-e_{ob})/C_c \qquad (16)$$

where the suffixes o, f, t and b to the void ratios e indicate original, final, top and bottom respectively.

In determiining the values of α and β appropriate to particular field problems it is probably more reliable to substitute the directly measured values of e_{ot} and e_{ob} and the calculated value of e_{ft} into eqs. (15) and (16) than to use eqs. (11) and (12).

III.- LIMITING CASE I

For shallow strata and for the oedometer test, the original effective stress at the bottom is negligibly higher than that at the top so that the parameter $\beta \to \infty$. This is referred to as limiting case I. For conditions A_1 and A_2, a = 0 and eq. (13) becomes:

$$\partial u/\partial T = \partial^2 u/\partial z^2 + (\partial u/\partial z)^2 b/(1-bu) \qquad (17)$$

and eq. (14) becomes:

$$\partial w/\partial T = \partial^2 w/\partial z^2 \qquad (18)$$

It was shown in Ref. 2 that, because eq. (18) is identical with the Terzaghi equation except for the substitution of w for u, and because the boundary conditions for w are similar to those for u in Terzaghi's theory, the degree of settlement U_s for limiting case I (for conditions A_1 and A_2) is exactly equal to that given by the Terzaghi theory. However the pore pressures of the non-linear theory are only equal to those of the Terzaghi theory when $\alpha = 1$. As α increases the pore pressures of the non-linear theory became increasingly greater than the Terzaghi values. The pore pressures of the non-linear theory are given by:

$$u = \alpha(1-\alpha^{-u^*})/(\alpha-1) \qquad (19)$$

where u^* = pore pressure given by Terzaghi linear theory with $u_o = 1$. The distributions of pore pressure with depth given by eq. (19) at three values of T_v are plotted in Fig. 2

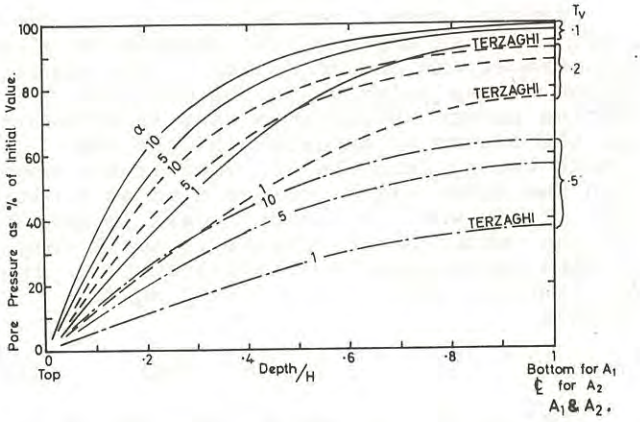

Fig. 2 Pore Pressures, Case I

It can easily be shown that, provided c_v is constant, the conclusion, that U_s is the same as for the classical linear theory, still holds whatever the relation between stress and strain, not only when it is that implied by eq. (1). It is also clear that, in contrast to the linear theory, the degree of settlement U_s in any non-linear theory is not identical with the average degree of pore pressure dissipation $\bar{U}_p$.

It was shown in Ref. 2 that oedometer tests on three normally consolidated clays with one-way drainage and pore pressure measurement at the impermeable boundary gave satisfactory confirmation of eq. (19), at least in the later stages of pore pressure dissipation. A summary of this experimental evidence is given in Fig. 3. Experimental confirmation has also been reported by Barden (Ref. 4) and Burland and Roscoe (Ref. 5). Further evidence is shown in Fig. 7 for hydrostatic triaxial tests on a Kaolin with axial drainage for which the same analysis should hold.

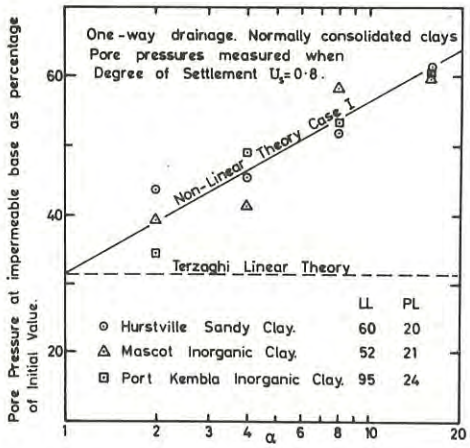

Fig.3 Experimental Confirmation of Case I (Ref.2)

IV.- LIMITING CASE II

Limiting case I can be regarded as the limit when the depth of the stratum is of no importance, and the magnitude of the consolidation stress relative to the original effective stress is all important in determining the extent of departure of the non-linear theory from the Terzaghi linear theory. Then the other limit, referred to as limiting case II, is when the depth is all important and the consolidation stress is small compared with the original effective stress. Thus for limiting case II $\alpha = 1$, and eq.(13) becomes:

$$\partial u/\partial T = \partial^2 u/\partial z^2 - (\partial u/\partial z)/(\beta+z) \qquad (20)$$

From eq.(20) it can be seen that as $\beta \to \infty$ Case II tends to the classical linear theory. Equation (20) can be solved analytically to give:

$$u = \sum_{n=1}^{\infty} a_n x\, \Psi_1(\lambda_n x)\, \exp.(-\lambda_n^2 T) \qquad (21)$$

where $x = \beta + z$,

$$\Psi_m(\lambda_n x) = J_m(\lambda_n x) + b_n Y_m(\lambda_n x),$$

and J and Y are Bessel Functions of the 1st and 2nd kind respectively.

The values of a_n, b_n and λ_n are given by equations determined by the boundary conditions. Thus λ_n and b_n are given by the following:

For one-way drainage (conditions A_1 and B_1):

$$\left.\begin{aligned} &u = 0 \text{ when } z = 0 \text{ and hence } \Psi_1(\lambda_n \beta)=0 \\ &\partial u/\partial z = 0 \text{ when } z=1 \text{ and hence } \Psi_0(\lambda_n(\beta+1))=0 \end{aligned}\right\} (22)$$

For two-way drainage, (conditions A_2 and B_2):

$$\left.\begin{aligned} &u = 0 \text{ when } z = 0 \text{ and hence } \Psi_1(\lambda_n \beta)=0 \\ &u = 0 \text{ when } z = 0 \text{ and hence } \Psi_1(\lambda_n(\beta+1))=0 \end{aligned}\right\} (23)$$

The values of a_n are then determined by the distribution of the initial excess pore pressure with depth.

For conditions A_1 and A_2

$$a_n = -2\left[\Psi_0(\lambda_n x)\right]_{\beta}^{\beta+1} \Big/ \lambda_n\left[x^2\Psi_0^2(\lambda_n x) + x^2\Psi_1^2(\lambda_n x)\right]_{\beta}^{\beta+1} \qquad (24)$$

For conditions B_1 and B_2

$$a_n = -2\left[(1+\beta)\Psi_0(\lambda_n x) + 0.5\pi \times \Psi_1(\lambda_n x)H_0(\lambda_n x) - 0.5\pi \times \Psi_0(\lambda_n x)H_1(\lambda_n x)\right]_{\beta}^{\beta+1} \Big/ \lambda_n\left[x^2\Psi_0^2(\lambda_n x) + x^2\Psi_1^2(\lambda_n x)\right]_{\beta}^{\beta+1} \qquad (25)$$

where H is Struve's Function.

Distributions of pore pressure calculated from eq.(21) at three values of T_v are shown in Fig.4 for condition A_2. From this figure it can be seen that, when the pore pressures of case II are significantly different from those of the Terzaghi linear theory, they are smaller than the Terzaghi values. This is the reverse of case I. The discrepancy can be seen to increase as β decreases, that is as the depth of the stratum increases. The same trend was found to be even more marked for the conditions A_1. This can be seen from the vertical axis values in Fig.7. Similar general trends were found for the conditions B_1 and B_2 although for B_1, the non-linear theory gave somewhat higher pore pressures at the impermeable base than the Terzaghi values during the earlier stages of consolidation.

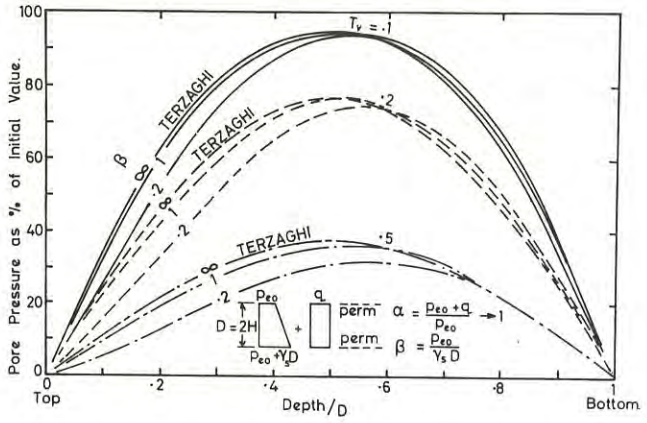

Fig.4 Pore Pressures, Case II, Condition A_2

The degree of settlement U_s is given by the following:

For conditions A_1 and A_2

$$U_s = \int_0^1 m_v(1-u)dz \Big/ \int_0^1 m_v dz \qquad (26)$$

and for conditions B_1 and B_2

$$U_s = \int_0^1 m_v(1-z-u)dz \Big/ \int_0^1 m_v(1-z)dz \qquad (27)$$

After some manipulation eqs. (26) and (27) give:

$$(1-U_s)\, L = \sum_{n=1}^{\infty} G_n \qquad (28)$$

$$\left.\begin{aligned} &\text{where } G_n = \frac{-a_n}{\lambda_n}\left[\Psi_o(\lambda_n x)\right]_{\beta}^{\beta+1} \exp.(-\lambda_n{}^2 T) \\ &\text{for all conditions } A_1,\ A_2,\ B_1 \text{ and } B_2 \\ &\text{and } L = \ln((\beta+1)/\beta) \text{ for conditions } A_1 \text{ and } A_2 \\ &\text{or } \quad L = (1+\beta)\ln((\beta+1)/\beta) - 1 \\ &\qquad \text{for conditions } B_1 \text{ and } B_2 \end{aligned}\right\} (29)$$

The relationship between U_s and T_v has been determined from eq. (28) and for condition A_1 is plotted for the range $\beta = 0.1$ to ∞ in Fig.5. From this figure it can be seen that settlement proceeds significantly faster as β decreases. There is also some change in the general shape of the settlement/log time curve with change in β.

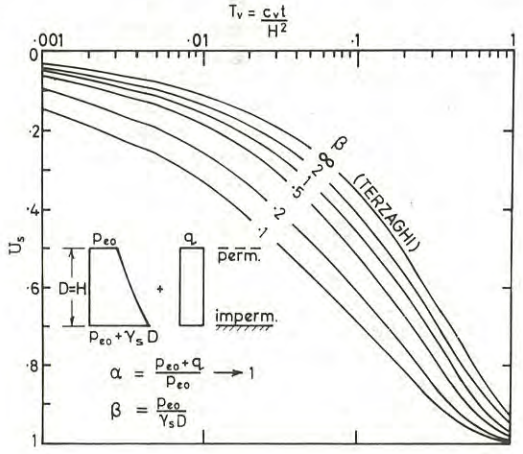

Fig.5 Rate of Settlement, Case II, Condition A_1

A similar change in shape of the settlement/log time curve was found for the other conditions A_2, B_1 and B_2 but again the most significant feature of the results was the increase in general rate of settlement as β decreased. This is clearly shown in Fig.6 in terms of the value of T_v for 50% settlement. The effect is more marked for one-way than for two-way drainage.

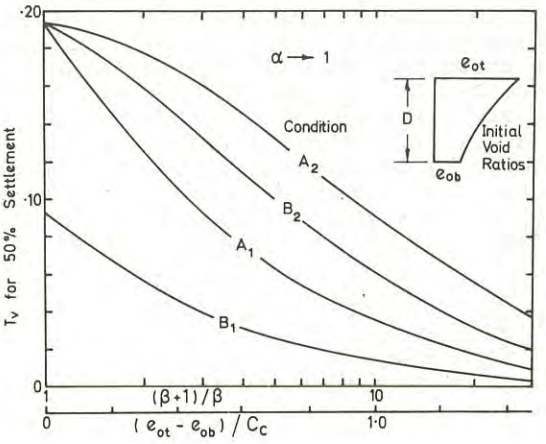

Fig.6 Case II, T_v Values for $U_s = 0.5$

V.- GENERAL SOLUTION

The general solution of the differential eqs. (13) or (14) to give the distribution of excess pore pressure at all times, and from this the relation between U_s and T_v, for cases when neither $\alpha = 1$ nor $\beta = \infty$, does not appear to be feasible by analytical methods. Solutions covering this general field between limiting cases I and II have however been obtained by numerical computer methods.

A selection of the numerical results for pore pressure are presented in Fig.7 for the condition A_1. This figure demonstrates the transition from Limiting Case I ($\beta \rightarrow \infty$), which always gives pore pressures higher than the linear theory, to Limiting Case II ($\alpha \rightarrow 1$), which normally gives pore pressures lower than the linear theory.

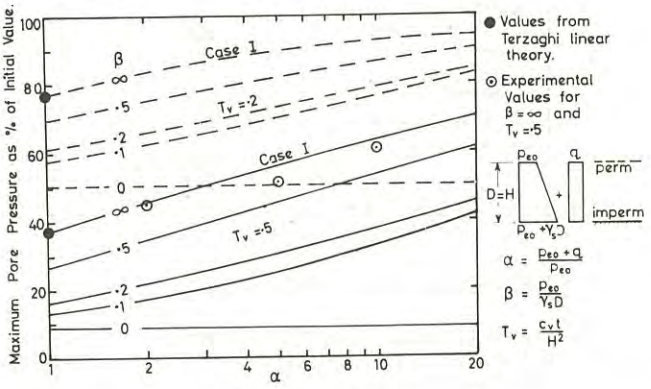

Fig.7 Maximum (Base) Pore Pressures, Condition A_1

For $\beta = 0.1$ and Condition A_1, the relationship between U_s and T_v is shown in Fig.8 from which it can be seen that the accelerated rate of settlement produced by a small value of β with case II ($\alpha \rightarrow 1$) is counterbalanced by the effect of having values of $\alpha > 1$ until the linear Terzaghi answer is once again approached as $\alpha \rightarrow \infty$. A similar trend was found for condition A_2. For conditions B_1 and B_2, al-

though increasing α while keeping β constant slowed the rate of settlement, the linear solution no longer provided the limit as α→∞. Fig.9 shows the general effects for all conditions A_1, A_2, B_1, and B_2 in terms of the value of T_v for $U_s = 0.5$ and for β = 0.1. For values of β other than 0.1 and for α > 1 it should be possible to obtain for practical purposes a sufficiently accurate estimate of the U_s/T_v relationship from the information provided by Figs.5,6,8 and 9.

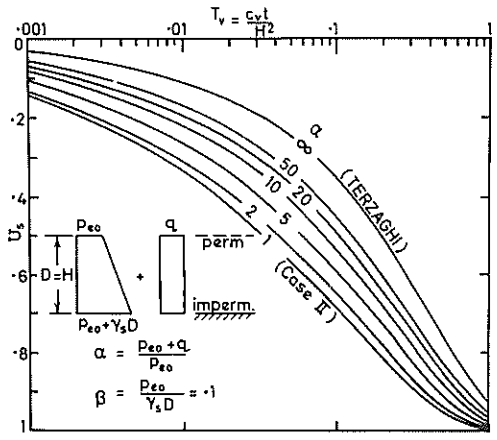

Fig.8 Rate of Settlement, Condition A_1, Varying α

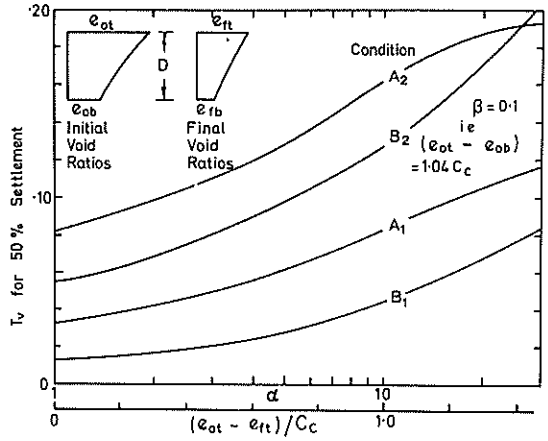

Fig.9 T_v Values for $U_s = 0.5$, β = 0.1, Varying α

VI. - DISCUSSION AND CONCLUSIONS

The non-linear theory developed in this paper shows that the pore pressures, at intermediate stages of consolidation of a deep bed of soft clay subject to relatively minor consolidation pressure, may be considerably less than those predicted by classical linear theory. On the other hand, reducing the thickness of the clay layer and increasing the consolidation pressure both have the effect of, in general, increasing the pore pressure at a given T_v and relative depth, so that, with thin layers and high consolidation pressures, the pore pressures may be considerably higher than those predicted by classical theory. Unless these effects are taken into account, the use of piezometers to monitor the progress of consolidation in reclamation and similar work may lead to an inaccurate interpretation of the field measurements. In this connection it is worth recording that a reformulation of the non-linear theory for the axi-symmetric conditions applicable to sand drains can be readily done and was successfully employed in interpreting piezometer readings for reclamation work with sand drains in W.Australia. When drainage is only radial, it is easily shown that for Limiting Case I, as with the one-dimensional vertical problem of this paper, the degree of settlement U_s (averaged over the inner to outer radii) is identical to that calculated from linear theor but that the pore pressures are higher as given by eq.(19). u^* must now be obtained from standard sand drain theory, see Barron (Ref.6) and earlier references.

The non-linear theory developed in this paper also shows that, although for relatively thin beds of clay the rate of settlement should be given sufficiently accurately by classical linear theory no matter how high the consolidation pressure, the rate for deep beds with low consolidation pressures may be considerably faster than that indicated by the classical theory.

It will be clear from its formulation that the theory presented in this paper is a small strain theory. This may appear to be an anomaly since the theory attempts to allow for relatively large changes in void ratio. However, the use of the average of the initial and final thicknesses of the clay layer in calculating the real time from the time factor T_v should remove the effects of the anomaly to a large extent and the experimental evidence from several sources supports this. For extreme values of the governing parameters it may be advisable to resort to finite strain theory, see Gibson et al. (Ref. 7). Further work to obtain guides, such as that the small strain theory is sufficiently accurate for practical purposes as long as the final settlement is no more than 10 or 20% of the total thickness, is desirable.

Although the non-linear theory presented in this paper is only one-dimensional, it seems reasonable to use it in approximate fashion to obtain a correction factor to the rate of settlement for three dimensional situations given by linear theory such as that in Refs.8 and 9. The solutions for the conditions B_1 and B_2 in which the consolidation pressure decreases with depth may be of assistance for this purpose. These solutions are of course also directly applicable to one-dimensional problems in which a steady vertical flow of water is either the initial or final equilibrium state.

VII.- ACKNOWLEDGMENTS

This paper forms part of a general programme of research into the settlement behaviour of foundations being undertaken at the University of Sydney with the support of the

Australian Research Grants Committee. The assistance of Mr. C-S.G.Kwei in performing many of the numerical computations is gratefully acknowledged.

REFERENCES

1. SCHIFFMAN, R.L. and GIBSON, R.E. - Consolidation of Non-Homogeneous Clay Layers. J.Soil Mech.Fndn.Divn.ASCE, Vol.90, SM5, 1964, pp.1-30.

2. DAVIS, E.H. and RAYMOND, G.P. - A Non-Linear Theory of Consolidation. Geotechnique. Vol.15, 1965, p.161.

3. MIKASA, M. - The Consolidation of Soft Clay. Civil Engineering in Japan, Japan Soc.C.E., 1965, pp.21-26.

4. BARDEN, L. - Consolidation of Clay with Non-Linear Viscosity. Geotechnique, Vol. 15, 1965, p.345.

5. BURLAND, J.B. and ROSCOE, K.H. - Local Strains and Pore Pressures in a Normally Consolidated Clay Layer During One-Dimensional Consolidation, Geotechnique Vol.19, 1969, pp.335-356.

6. BARRON, R.A. - Consolidation of Fine-Grained Soils by Drain Wells. Trans.ASCE, Vol.113, 1948, p.718.

7. GIBSON, R.E., ENGLAND, G.L. and HUSEY, M.J.L. - The Theory of One-Dimensional Consolidation of Saturated Clays. I. Finite Non-Linear Consolidation of Thin Homogeneous Layers. Geotechnique. Vol.17, 1967, pp.261-273.

8. GIBSON, R.E. and McNAMEE, J. - The Consolidation Settlement of a Load Uniformly Distributed over a Rectangular Area. Proc.4th Int.Conf.Soil Mech.F.E., Vol.1, 1957, p.297.

9. DAVIS, E.H. and POULOS, H.G. - Rate of Settlement under Three-Dimensional Considitions. To be published. 1971.

Recompression Characteristics of Perth Overconsolidated Clays

By
R. J. Frost
(Tippetts-Abbot-McCarthy-Stratton, Tarbela Dam Project, West Pakistan)
L. K. Walker, Ph.D. (Cantab.), M.Eng.Sc., M.I.E.Aust.
(Maunsell and Partners Pty. Ltd., Melbourne)
AND
I. K. Nixon
(Director, Soil Mechanics Ltd., Melbourne)

SUMMARY. - The recompression properties of Perth overconsolidated clays are discussed in detail, with reference being made to laboratory tests on samples from a number of sites in the City area. Recommendations are made which should enable the accuracy of future settlement estimates to be improved. An analysis of the limited field records available offers some support for the approach presented.

I. - INTRODUCTION

The City Centre of Perth is located on a series of interbedded sands and clays of alluvial and aeolian origin. The general geology of the area has been summarized by Andrews (1970), and consists of a surface layer of aeolian sand often about 25 ft. thick, overlaying an interbedded clay/sand alluvium of some 80ft. thickness, with bedrock being the Tertiary King's Park shale. The clay/sand alluvium generally contains an upper 35ft. of stiff clay and a lower layer of sand with some clay lenses. Geological history of the area suggests that a preconsolidation effect has been caused by the past erosion of a significant thickness of overburden soil.

Of the larger buildings in the City Centre, most have been provided with basements and a raft foundation to reduce average bearing pressures. Although allowable bearing pressures in the clay often exceed 2.5 ton per sq. foot, and field stresses are usually well below the preconsolidation pressure, calculated settlements often have a major effect on an analysis of the raft/soil system. However, present experience, both published and unpublished, suggests that consolidation settlement estimates are commonly higher than those observed by a factor of 2 or more, and hence unnecessarily expensive foundation designs may be in use.

The purpose of this Paper is to present data from tests on samples of the stiff clay layer at a number of sites in Perth, to discuss the likely behaviour of the material in the field, and to assess the limited field evidence which has been published to date. Specific recommendations are made in an attempt to improve current settlement estimate techniques.

II. - NOTATION

C_α	Coeff. of secondary compression
$C_R (C_S)$	Recompression (swelling) index
c_v	Coefficient of consolidation
e	Void ratio
e_o	Field void ratio
e_s	Void ratio at swelling pressure
I_P	Plasticity Index
I_L	Liquidity Index
m_v	Modulus of volume change
p	Normal pressure (laboratory)
p_c	Preconsolidation pressure
p_o	Existing effective overburden stress
Δp	Applied pressure increment
t	Time
w	Moisture content
w_L	Liquid limit
w_P	Plastic limit

III. - SOURCES OF DATA

(a) Laboratory Data

Laboratory tests have been performed on 24 clay samples from 7 different sites in the Perth City area. The stiff clay layer under study varies in thickness and properties between the sites, and hence certain simplifications are necessary to enable comparisons to be made between different samples; determinations of Atterberg limits and field moisture contents prove useful in this regard. The majority of laboratory consolidation data were obtained from conventional oedometer tests of either 3 inch or 2 inch diameter obtained from 4 inch or $2\frac{1}{2}$ inch diameter undisturbed samples.

The "undisturbed" samples used in the testing programme were undoubtedly disturbed to varying degrees for different samples. Disturbance can result during the sampling operation, during transportation, extrusion in the laboratory and during trimming and setting up in the test apparatus. The effect of sample disturbance on consolidation test results can be described by reference to Figure 1, which

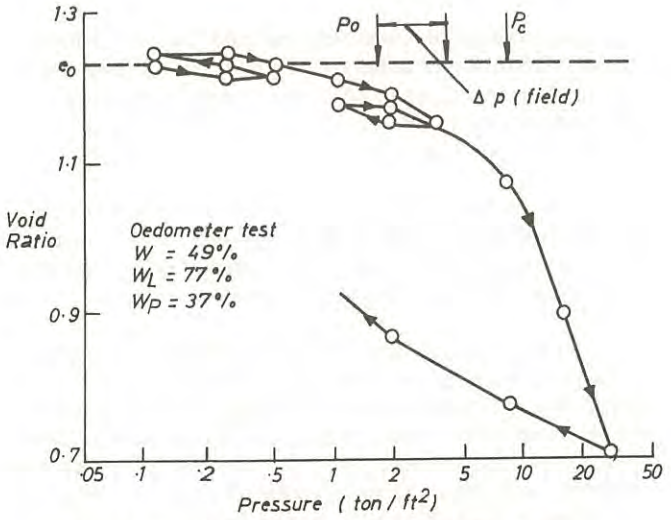

Figure 1. Typical Oedometer Test Data

represents an e vs. log p curve obtained from a typical oedometer test on the stiff clay, with several rebound/recompression cycles being introduced into the test. The effective overburden stress (p_o) and pre-consolidation pressure (p_c) are shown on Figure 1 and indicate an approximate over-consolidation ratio of 4. For such overconsolidated clays, disturbance generally decreases the estimated void ratio in the field (e_o) and increases the slope of the e - log p curve in the recompression region (Rutledge 1944). For any field pressure increment from p_o which results in a final pressure less than p_c, predicted settlements from laboratory tests will be too high by an amount directly related to the degree of disturbance.

(b) Field Performance

The settlement of buildings in Perth was discussed in detail at a recent Symposium on Foundations on Interbedded Sands held in Perth in October, 1970. Three case records were presented which will be discussed in detail in a later section. Settlement measurements were presented by Glick and Gosbell, while Wood discussed the soil/structure problems involved in a particular raft design. Sufficient soils data were given in the first two papers to enable comparisions to be made between predicted and estimated settlements.

Total estimated settlements in the stiff clay vary between the three sites, being related to the thickness of sand overlying the clay, and to the area of raft and average bearing pressure. In the first two references, there are suggestions that settlement predictions were considerably in excess of those observed. Discussion at the Symposium suggested that this conclusion was applicable to a number of other sites for which results have not been published.

(c) Scope of the Study.

The laboratory testing programme has enabled the variation in stiff clay properties to be defined, and the basic consolidation parameters to be determined. The presence of significant sample disturbance requires that unconventional methods for estimating settlements be adopted, and these are briefly outlined. Available field data are analysed to support the approach recommended.

IV. - TOTAL SETTLEMENT ESTIMATES

(a) General

Total settlements are conventionally calculated from the e vs. log p curve by estimating a value of the co-efficient of compressibility (m_v) or recompression index (C_R) relevant to the stress increment applied in the field. With this in mind, e vs. log p curves were obtained for all of the samples involved in this study; in some of the tests (such as that shown in Figure 1), swell-back and recompression loops were inserted to assess the recompression characteristics of the clay at a number of different pressures. A pressure increment ratio of one was adopted throughout, with average curves being drawn through the points obtained.

For each sample, appropriate values of p_o were calculated and estimates of p_c made using Casagrande's method (Casagrande 1936). The accuracy of this determination is significantly reduced by sample disturbance, however a general trend was noted by which p_c decreased with decreasing liquidity index for a given field water content. Average values of p_o and p_c of 1.8 ton per sq. ft. and 5.6 ton per sq. ft. were obtained, although individual values varied with depth of the sample and its exact classification. Nevertheless, the overconsolidated nature of the deposit was well established.

(b) Determination of a Recompression Index

The determination of a realistic recompression index for total settlement prediction is extremely difficult if the effects of sample disturbance are accepted. A value of C_R could be extracted from the laboratory e vs. log p curve by determining the average slope over the pressure range p_o to $(p_o+\Delta p)$, Δp being the applied pressure increment in the field. Almost certainly this value of C_R will lead to an overestimate of field settlements.

An alternative method of estimating C_R requires a laboratory study of the recompression index at various pressures. A sample is cyclically loaded as shown in Figure 1, with a typical hysteresis loop being formed from which either a swelling or recompression index (C_S or C_R) can be estimated. For relatively small pressure changes ($\Delta p/p \leq 2$) the hysteresis loop is almost closed and C_S and C_R are closely equal. From a detailed analysis of results,

a value of C_R appropriate to the stress range in the field can be derived. It is suggested that this value should reasonable approximate the recompression behaviour of the undisturbed soil in-situ. This assumption is more likely to be valid where $p_o + \Delta p$ significantly less than p_c, and truly elastic (recoverable) behaviour can be expected in the field.

The use of cyclic load oedometer test data can be illustrated by reference to Figure 1, on which values of p_c and Δp are shown. A conventional recompression index of 0.13 would be obtained for this pressure increment by using the first-loading curve. It is noted that a similar value would apply if the swelling index (C_s) were calculated from rebound at the end of the oedometer test, and used as an approximation to the recompression index. However, by using the cyclic load curve which is applicable to the applied stress increment, a recompression index of 0.04 is obtained.

Settlements estimated conventionally would thus be over three times those obtained from using cyclic load data. As predicted settlements in Perth clays are reported to exceed those observed by factors of two or more, it appears that the proposed technique for obtaining a recompression index should find direct application.

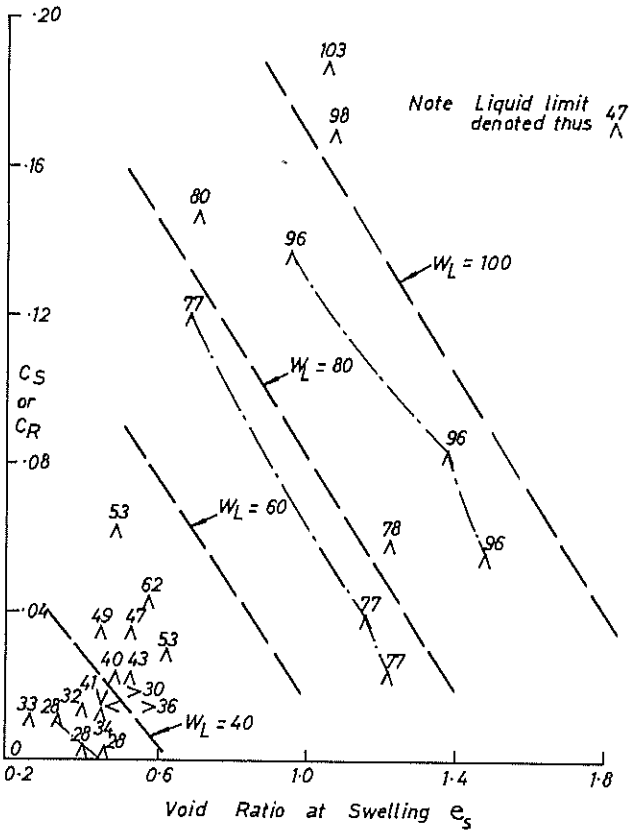

Figure 2. Correlations for Recompression Index.

(c) Laboratory Correlations

Recompression/swelling indices for the Perth clay have been estimated from all cyclic loops (two shown in Figure 1) or unloading curves obtained after completing each test (swelling from 32 ton per sq. ft. shown in Figure 1).

Points obtained from the latter source predominate for the range of samples tested. For complete cycles, a single index has been computed by averaging the slope of the hysteresis loop.

The test results have been presented in Figure 2. The recompression or swelling index is plotted against the calculated void ratio (e_s) at which swelling occurred in the laboratory. At each plotted point, the value of liquid limit (W_L) for the sample has been indicated, and approximate lines of constant W_L have been drawn. Liquid limits range from 28 to 103 and indicate the wide variability which can be found at different sites in the City area, and at different depths in the soil profile.

The data of Figure 2 show that for a soil of given W_L in the field, the value of C_R (or C_S) decreases almost linearly with increasing void ratio. Increasing values of W_L result in higher recompression indices. The constant W_L lines shown on Figure 2 are in broad agreement with a similar correlation indicated in the Navdocks DM-7 Design Manual (1961), although an exact correspondence of individual lines is not achieved.

Figure 2 is, of course, strictly applicable only to the Perth clays under discussion. However the similarity with U.S. data suggests that the empirical curves may be of considerable practical value, particularly in cases where detailed consolidation testing has not been performed.

V. - RATES OF SETTLEMENT

(a) General

It is well appreciated that laboratory rates of settlement are significantly influenced by pressure increment ratio (Leonards and Altschaeffl 1964). A ratio of one was used in all oedometer tests reported below, hence the data presented will not be representative of all field situations.

Rates of settlement of the Perth clays have been considered by separating primary and secondary consolidation, this being most simply done by referring to the settlement log-time curve. Primary consolidation is usually represented by the standard reverse S - shaped curve associated with Terzaghi's consolidation theory. Secondary consolidation is generally recognized by the linear tail to the curve, which is formed after pore water pressures have essentially dissipated. The test data presented below summarize the range in consolidation paramet-

ers which can be obtained from samples at different sites in the Perth City area.

(b) Primary Consolidation

An analysis of settlement/log time curves for all samples tested showed that 96% of all curves were of the standard reverse S shape, and c_v for primary consolidation could be computed using Terzaghi theory. Some 9% of all curves were so shaped that c_v could be estimated from the square root time/settlement plot, while the remainder were such that c_v could not be calculated. The range of parameters obtained is presented in Figures 3 and 4.

In Figure 3, tests on four samples with varied properties have been selected, and c_v values plotted against pressure ratio, defined as the ratio of consolidation pressure to the preconsolidation pressure estimated for the sample. As a general rule c_v was observed to decrease with increasing pressure ratio, the effect being most marked for samples with high liquid limits. A similar reduction in c_v with increasing pressure has previously been predicted by Raymond (1966).

The variation of c_v between samples is summarized in Figure 4, where liquid limit has been plotted against the value of c_v determined at a pressure ratio p/p_c equal to 0.5. This would approximate the pressure ratio applicable to many field problems. A decrease in c_v with increasing liquid limit is noted, with a factor of about 100 between extreme values. This trend is consistent with the lower permeabilities to be expected in samples with higher liquid limits (and larger clay fractions).

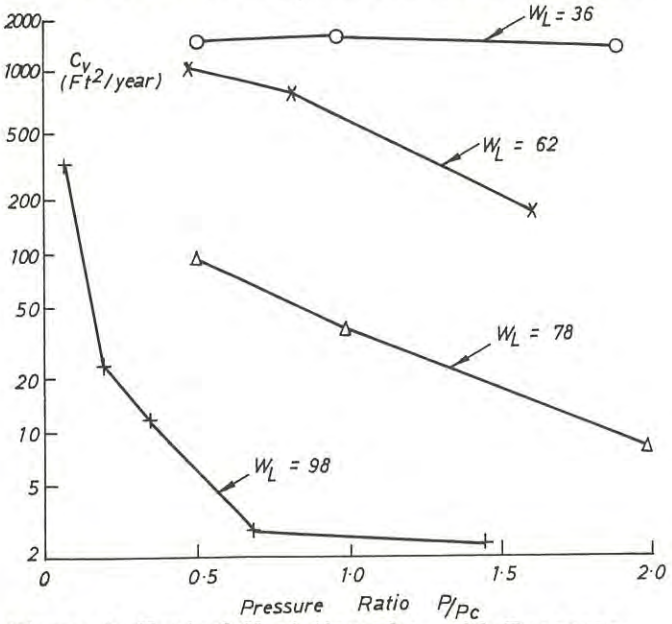

Figure 3. Typical Variation of c_v with Pressure.

The primary consolidation data summarized in Figures 3 and 4 give an indication of average properties for the Perth clays, with some measure of consistency being achieved between tests on various samples. However the usefulness of the parameter c_v is likely to depend on details of the particular problem being considered. Rowe (1968) has discussed the effect of sand pockets or seams in clay deposits and the extent to which drainage is accelerated in the field when compared with laboratory estimates. In addition the effect of small pressure increment ratios in the field is such that results from standard oedometer tests may be inapplicable and a more accurate duplication of field stresses may be necessary.

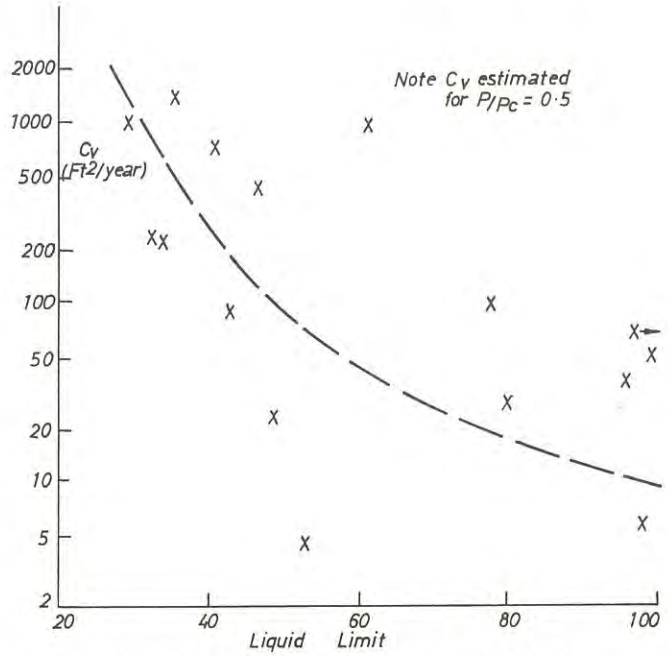

Figure 4. Variation with Liquid Limit of c_v (at P/P_c =0.5)

(c) Secondary Consolidation

Rates of secondary consolidation can conveniently be defined by the slope of the final linear portion of the settlement/log time curve expressed as a proportion of sample thickness. The resulting parameter (C_α) has been estimated wherever possible on a variety of the Perth clays, although accuracy is limited in many cases where only a short period of secondary compression occurred. The secondary consolidation data have been summarized in Figures 5 and 6.

In Figure 5 data from the four tests selected for Figure 3 have been reproduced in a plot of C_α vs pressure ratio. The rate of secondary consolidation is seen to increase with pressure ratio, with a flattening off above a ratio of one. This type of behaviour has been illustrated in many previous publications (e.g. Jonas 1964).

Figure 6 summarizes all of the data (in a similar way to Figure 4) by plotting liquid limit against the estimated C_α value at a pressure ratio of 0.5. A

general increase in $C_{\alpha\varepsilon}$ with increasing liquid limit is noted, this again being consistent with previously published data.

Figures 5 and 6 illustrate that quite high $C_{\alpha\varepsilon}$ values are possible for Perth clays of high liquid limit if pressures close to p_c are applied. Secondary

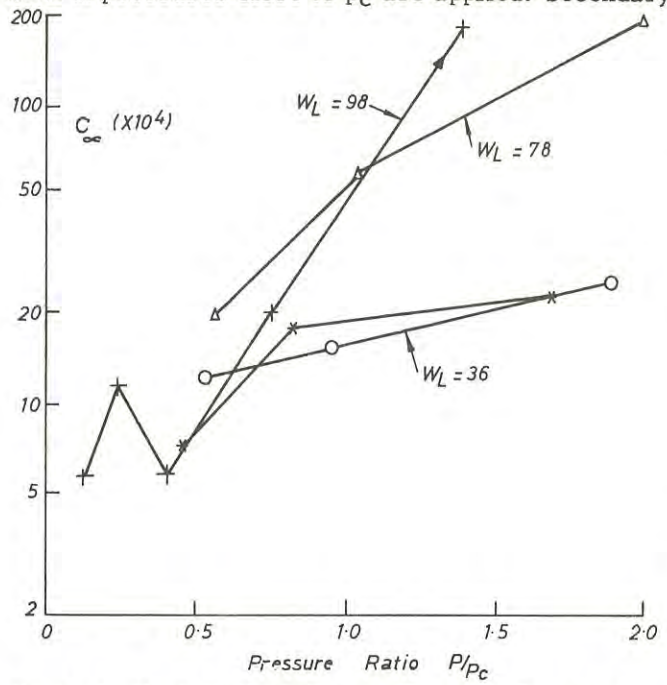

Figure 5. Typical Variation of $C_{\alpha\varepsilon}$ with Pressure Ratio.

consolidation in the field is therefore likely to be a factor of some significance when any assessment of field settlement records is made.

VI. - ASSESSMENT OF FIELD DATA

In analysing field data from various sites in Perth, immediate (undrained) settlements have not been considered, and must be added to the consolidation settlements being discussed. Load application

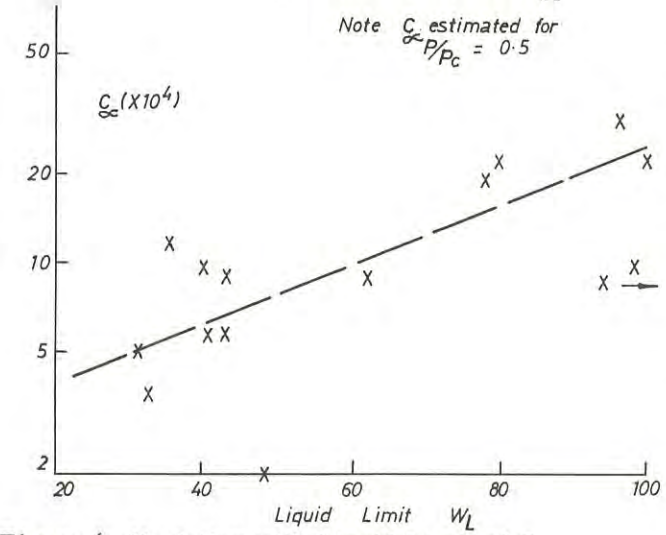

Figure 6. Variation with Liquid Limit of $C_{\alpha\varepsilon}$ (at P/P_c =0.5)

in most cases is such that one-dimensional conditions are closely satisfied in the field, and hence normal settlement estimate techniques might be expected to apply.

(a) Main Roads Department Building - Glick (1970)

At this site 55 ft. of sand overlies about 60ft. of stiff clay, with the effective overburden stress on the clay estimated at about $2\frac{1}{4}$ ton per sq. ft. For the clay, W_L varied from 30 to 50 and W_P from 10 to 20, with c_v estimated at 150 sq. ft. per year. The combination of raft and spread footings described in the paper result in a pressure increment on the clay which can be estimated at about 0.4 ton per sq. ft. i.e., a pressure increment ratio of about 1/5, or less with increasing depth. Conventional settlement estimates in the clay were about 3/4 inch or 0.065 ft. with a time to 90% consolidation estimated at 5 years.

The observed settlement-time data at six reference points are reproduced graphically in Figure 7, with curves being drawn in an attempt to separate sand and clay settlements. Construction activity ceased after about 10 months, at which time it appears that primary consolidation had been completed with a settlement in the clay of about 0.015 ft. This conclusion is based on assessing the rates of settlement occurring at the time of the last observation.

Sufficient soils data are available at this site to enable use to be made of the data presented in previous sections. In calculating total settlements, Glick assumed that only 15 ft. of clay contributed to settlements. This enables a settlement estimate to be made using Figure 2. For an average W_L of 40, and e_s of 0.4 (close to the plastic limit), a recompression index of 0.025 is obtained. This leads to an estimate clay settlement of 0.03 ft. i.e., half the conventional estimate but still twice the observed primary settlement.

Estimates of rates of primary settlement are of little value due to the small field pressure increment ratio, which leads to a predominance of secondary consolidation. This is borne out by Figure 7 which suggests that after 20 months, secondary settlements are already greater than inferred primary settlements, and should continue to increase gradually in the coming years. The data do however, enable a field $C_{\alpha\varepsilon}$ value to be estimated. An average secondary slope from Figure 7 is 0.057 ft. per log cycle of time, leading to a $C_{\alpha\varepsilon}$ value of 0.004 if the assumed clay thickness of 15 ft. is adopted. If an estimate of $C_{\alpha\varepsilon}$ were obtained by reference to the average properties in Figures 5 and 6, a value of about 0.001 would apply. The large discrepancy between these two values is considered to be due to the fact that more than 15 ft. of clay is contributing to creep settlements in the field. It would be anticipated that a reasonable correlation between laboratory and field $C_{\alpha\varepsilon}$ values should exist as has been shown for other clays (Walker 1969).

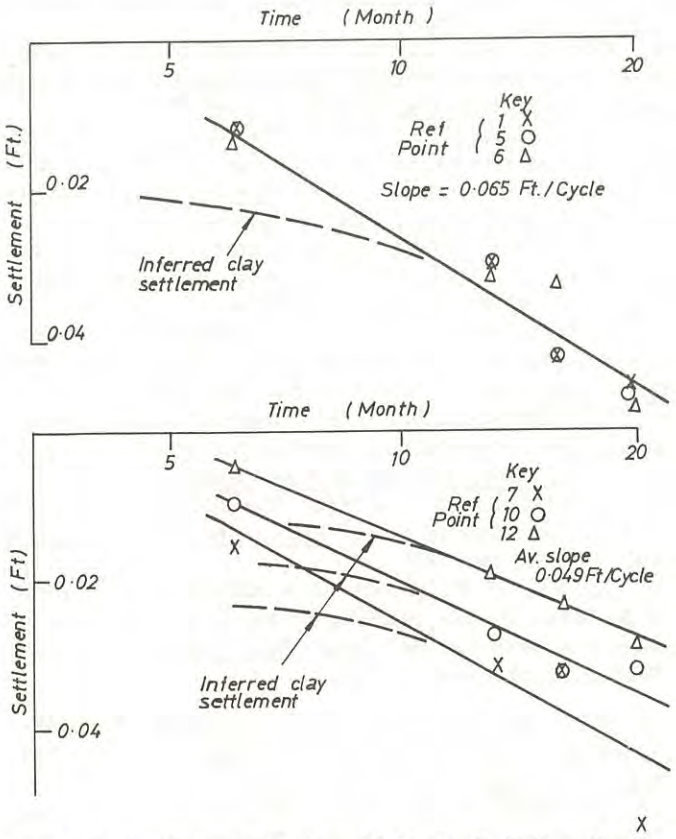

Figure 7. Settlement Data - M.R.D. Building Perth

(b) Commonwealth Offices Building - Gosbell (1970)

The profile at this site consisted of about 50 ft. of sand overlaying 30 to 40 ft. of stiff clay. Average soil properties were W_L = 60 to 100, W_P = 25 to 40, w = 22% to 40%, shear strength = 1.5 ton per sq. ft. and m_v from .004 to .008 sq. ft. per ton. Consolidation settlements of from 2-3½ inches were estimated, with the major part of this movement occurring during the construction period. Only three sets of settlement measurements were taken over the first 18 months, hence only the crudest analysis of field behaviour can be made. It is tentatively suggested from the data that a primary settlement in the clay of about 0.03 to 0.04 ft. has been completed, and that the secondary phase has been commenced. An assessment of C_α in the field is not considered reasonable from the limited data.

Data presented in the paper suggest that reasonable values of p_o = 2.5 ton per sq. ft., and a maximum Δp for the clay of about 0.7 ton per sq. ft. might be adopted. Classification tests on the clay indicate from Figure 2 that an average C_R value of 0.11 would apply. This leads to a consolidation settlement estimate of about 2¼ inches, i.e., within the range of the conventional estimate, but well above the inferred primary settlement in the field.

(c) National Bank Building - Wood (1970)

Despite the fact that no field data are available, this site is of particular interest as it provides a case in which the field pressure increment ratio is in excess of one. The profile consists of 27 ft. of sand overlying 29 ft. of stiff clay, then clayey sand and sand to bedrock. The value of p_o is about 1.2 ton per sq. ft., with the increase in pressure from the proposed raft being in excess of 1 ton per sq. ft. The soil properties are variable with W_L ranging from 30 to 60. Total settlements have been estimated using recompression indices obtained from cyclic loading in oedometer tests, and a maximum value of 1-1/4 inches obtained. The building is presently being constructed, with accurate field observations being undertaken.

(d) Summary

The case records discussed above are not sufficiently detailed for a thorough analysis, and considerable judgement has been exercised in their interpretation. It is immediately apparent, however, that significant variations in clay properties and in applied pressure increment can occur, hence laboratory test results must be applied with care. Total (primary) settlements calculated using Figure 2 can be less than half conventional estimates, but are still considerably larger than those observed. Rates of settlement are difficult to assess because of the influence of small load increment ratios. However it appears that the application of c_v values in such cases has little meaning due to the significance of secondary settlements.

The apparent discrepancy between observed settlements and thos predicted using correlations such as Figure 2 may be confused by the precise interpretation of the consolidation test. It can be argued that laboratory settlements include a significant proportion of secondary compression when small pressure increment ratios are involved, and a comparison with total (primary plus secondary) field settlements should be made. This point must be resolved by more detailed laboratory sudies in the future, in particular by using pressure increments reflecting field loading conditions more accurately. It is also apparent that a range of carefully documented case records is required before the full significance of laboratory procedures can be assessed.

VII. - CONCLUSIONS

Detailed consideration has been given to the problems of estimating settlements in the over-consolidated clays underlying the Perth City Centre. Analysis of laboratory tests on samples from a variety of sites has led to specific recommendations for estimating both total settlements and rates of settlement. The former requires a new approach to obtaining a representative recompression index using cyclic loading in the oedometer test. Rates of settlement

are dominated by secondary effects in many cases where small pressure increment ratios are applicable, and the determination of c_v values are of limited use. The determination of secondary settlements can be made by using the creep parameter C_α

Consideration has been given to the limited field data available in Perth, and some support for the suggested approach is observed. However, further study of the interaction of primary and secondary consolidation is probably required before an acceptable accuracy of prediction is obtained. The need for more detailed field records is also evident.

VIII. - ACKNOWLEDGEMENTS

The authors wish to acknowledge the various Perth organizations in the Government and private sector who initiated the various site investigations which provided the basis for the work reported. The laboratory results were obtained from tests performed in the Melbourne Laboratory of Soil Mechanics Ltd. for whom the first author was formerly Australian Manager.

REFERENCES

1. ANDREWS, D.C. (1970) "Soils of the Perth Area the City Centre", Symposium on Foundations on Interbedded Sands, Perth, August 1970.
2. CASAGRANDE, A (1936) "Determination of the Preconsolidation Load and its practical significance" Proc. 1st. Int. Conf. Soil Mech and Found. Eng., Vol. III
3. DAVIS, E.H. and POULOS, H.G. (1963) "Triaxial testing and three-dimensional settlement analysis" Proc. 4th Aust. - New Zealand Conf. Soil Mech. and Found. Eng., Adelaide.
4. GLICK, G.L. (1970) "Settlement Study of Main Road Department Building" Symposium on Foundations on Interbedded Sands, Perth, August 1970
5. GOSBELL, K.B. (1970)" The design, instrumtation and performance of the Perth Commonwealth Offices raft foundation". Symposium on Foundations on Interbedded Sands, Perth, August, 1970
6. JONAS, E (1964), "Surface stabilization of organic silty clay by recompression" Proc. Am.Soc. Civil Eng. Vol. 90 No. SM5 pp. 363-376.
7. LEONARDS, G.A. and ALTSCHAEFFL, A.G. (1964) "The compressibility of clay" Proc. Am. Soc. Civil Eng. Vol. 90 No. SM5 pp. 133-156
8. NAVDOCKS DM-7 (1961) Design Manual - Soil Mechanics, Foundations and Earth Structures, U.S. Depth. of Navy, Bureau of Yards and Docks.
9. RAYMOND, G.P. (1966) "Consolidation of slightly overconsolidated soils "Proc. Am.Soc. Civil Eng. Vol. 92 SM5 pp 1-20
10. ROWE, P.W. (1968) "The influence of geological features of clay deposits on the design and performance of sand drains" Proc. Inst. Civil Eng. Paper 70585, Supplementary Vol.
11. RUTLEDGE, P.C. (1944) "Relation of undisturbed sampling to laboratory testing". Trans, Am. Soc. Civil Eng. Vol. 109 pp. 1155-1183.
12. WALKER, L.K. (1969) "Secondary settlement in sensitive clays". Canadian Geotechnical Journal, Vol vi No.2 pp. 219-222
13. WOOD, A.B. (1970) "Design of multi-story building with flexibile raft on Perth sands" Symposium on Foundations on Interbedded Sands, Perth, August 1970

LL
28-62 ϕ 14 tests po av. 4 tsf Range 7.2 and close to grey silty clay (Andrews)

125 ϕ 7 tests po av. 9 tsf 6.2 ϕ 11 tsf. Police HQ lower clays (Andrews)

Aspects of the Consolidation of Morwell Brown Coal

By
D. C. Green, B.E. (Civil), M.I.E.Aust.
(Engineer, State Electricity Commission of Victoria)

SUMMARY.- A number of one-dimensional consolidation tests have been carried out on samples of brown coal in an attempt to quantify problems associated with ground movements arising from open cut mining operations. The effects of variations in test procedures are discussed (including the use of elevated temperature), and some observations are made from a large field load test on the coal.

I.- INTRODUCTION

The great majority of electrical energy for the State of Victoria is provided by thermal power stations which burn brown coal (lignite) from the extensive deposits of this material found in the Latrobe Valley. The principal mines are at Yallourn and Morwell, where the coal is won by open cut methods by the State Electricity Commission of Victoria.

The general geology of these areas has already been described elsewhere (Ref. 1). At Morwell, where the coal was sampled for the tests here reported quaternary alluvial sediments of about 25 ft to 75 ft thickness (9 to 28 m) overlie two principal brown coal seams of tertiary age, the Morwell No. 1 Seam (hereafter referred to as M1 coal) of about 450 ft thick and the Morwell No. 2 Seam (hereafter referred to as M2 coal) of about 150 ft thick. These two seams of coal are separated by a layer of sediments ranging from sands to clayey silts and organic clays, of thickness varying from 50 ft to about 75 ft.

In the course of mining operations at Morwell, where the Open Cut has now reached a depth of about 100 m below the natural surface, vertical and horizontal movements in the batters have occurred which have been attributed to several factors. These factors include pressure relief due to removal of overburden and coal, lowering of the groundwater table resulting from increased drainage from the batters as the cut is deepened, and dewatering of the aquifers which underlie the coal. An appraisal of these movements, which are broadly similar to those described elsewhere (Ref. 2), depends partly on a knowledge of the consolidation characteristics of the coal.

As part of the investigations into these problems, a range of one-dimensional consolidation tests has been carried out on samples of brown coal taken from bore holes up to 700 ft (213 m) deep. The programme of tests has not been carried out as a fundamental study of material behaviour, but rather to give guidelines for technical decisions which need to be made in the short term, and some of the conclusions suggested by the laboratory tests and certain field tests are given below.

II.- NOTATION

C_c = Compression index

e = Void ratio

E = Young's modulus

h = Thickness of layer considered in settlement calculation

m_v = Coefficient of volume decrease

P = Applied vertical pressure

P_o = Preconsolidation pressure (maximum past pressure)

$\frac{\Delta P}{P}$ = Load increment ratio in consolidation test

S = Total settlement

σx, σy = Lateral (horizontal) stresses

σz = Vertical stress

μ = Poisson's ratio

III.- SAMPLING AND TESTING PROCEDURE

(a) Sampling

By means of a rotary drill rig, samples have been obtained from a number of bores using triple tube clay coring barrels. The inner tubes used to retain the samples have been of thin steel. Two diameters have been used, namely, 4-1/8 in (10.48 cm) and 5-11/16 in (15.08 cm), and all tubes have been 5 ft long (1.52 m). Both solid tubes and split tubes have been used. Solid tubes were sealed for transport using rubber rings sandwiched between perspex discs designed to effect a good seal when the discs were clamped together by a screw. The cores were cut into shorter lengths by means of a bandsaw, the ends of tubes being

re-sealed using wax for longer term storage and the rubber sealing rings for shorter term storage ("tube" samples). Cores removed from split tubes were cut or broken into shorter lengths, surrounded by a gauze bandage and completely covered in wax until required for testing ("bandaged" samples).

(b) Sample Preparation

The very brittle nature of the coal and its proneness to cracking on drying made it very difficult to prepare the disc-shaped specimens used for testing. About two-thirds of the samples were of sufficiently good quality to be turned in a powered lathe using a slow-cutting speed, while the remainder were prepared on a hand-trimming lathe. Most samples were taken from solid tubes, but about one-third were "bandaged" samples of the type referred to above.

(c) Apparatus and Range of Loads

Consolidometers used were of the Clockhouse fixed ring type, wherein pressures were applied by dead loads delivered to the specimens by a lever loading device. All specimens were of 2.45 in diameter (6.22 cm) and approximately 3/4 in thick (1.90 cm). The apparatus provided for two-way drainage, and applied pressures ranged up to 746 psi (52.5 kg/cm^2).

(d) Reduction of Test Data

Basic calculations on the test data, including plotting of e - log P curves, have been carried out by computer, by the void ratio method, using a value of specific gravity of 1.50, a figure based on previous laboratory determinations using ethylene glycol as the immersion liquid. The calculated degree of saturation using this figure for specific gravity of the solid coal particles was always within a few per cent of 100 per cent.

IV.- ESTIMATION OF PRECONSOLIDATION PRESSURE

(a) General

As the pit is deepened and the underlying artesian and sub-artesian aquifers are dewatered to avoid failure of the bottom of the pit by heaving due to hydrostatic uplift, the implication has been made that effective stress is increased, and the coal and interseam sediments are being subjected to progressively increasing consolidation pressures despite removal of overlying material by excavation to great depth. For the coal itself, this effect of dewatering is quite unusually marked, because the natural density in the absence of a free water table is only about 72 lb/ft^3 (1.15 g/cm^3). There is therefore a tenfold increase in effective consolidation pressure per foot depth for complete removal of a previously existing water table as the effective density changes from the buoyant to the bulk density. A similar effect, though not so marked, occurs in the interseam sediments, which have considerably higher bulk densities.

From previous experience, including geological evidence of regional erosion of several hundreds of feet of both coal and non-coal materials, the coal measures are known to be over-consolidated. It has become necessary with continued extension of the mine in depth to obtain reasonably accurate estimates of the preconsolidation pressures in order that a limit of depth of excavation may be set (assuming continued dewatering) at which increasing subsidence due to the onset of virgin consolidation can be expected. Then, with the additional estimate of how great these movements might be, decisions can be made as to the future development of the mine, or alternatively allowance for such movements may be incorporated in the design of structures and engineering services likely to be affected by them.

(b) Estimated values of P_o

Estimates of preconsolidation pressure have been made for all specimens tested using Casagrande's method (Ref. 3) applied to the curve of void ratio versus logarithum of consolidation pressure. Both the M1 and M2 coal gave results which were mostly very consistent for specimens taken from immediately adjacent locations, and even for specimens cut from locations within a few feet of each other. This has been taken as evidence of the lack of sensitivity of the coal to sample disturbance, an inference which is reinforced by the lack of any marked or consistent differences in the estimated preconsolidation pressure between the "tube" samples and the "bandaged" samples, and further reinforced by the observed shape of the e - log P curves. These curves in general tend to be quite flat in slope initially, with a relatively pronounced downturn of short radius near the estimated preconsolidation pressure, a feature which according to Schmertmann is a mark of relatively undisturbed material (Ref. 4).

The low buoyant density of the coal indicates that the preconsolidation pressure could not be expected to vary greatly within either seam, considering the great thickness of each seam. Specimens tested from the M1 seam have covered so far a range of in situ elevation of about 460 ft (140 m) while those from the M2 seam have covered a range of 97 ft (30 m). The ranges of estimated preconsolidation pressures for the two seams are about 148 psi (10.4 kg/cm^2) and 68 psi (4.8 kg/cm^2) respectively, these differences being partly accounted for by variations in thickness of overlying coal and non-coal sediments between locations at which samples were taken. Typically, the following values of preconsolidation pressure P_o have been assigned to the two seams for the vicinity of the Open Cut:

Morwell No. 1 Seam (M1) 340 psi (23.8 kg/cm^2)

Morwell No. 2 Seam (M2) 420 psi (29.5 kg/cm^2)

These figures are substantially higher than those of 150 psi and 200 psi which had been obtained for samples of M1 coal cut from the working face of the mine some years previously and reported by Trollope, Rosengren and Brown (Ref. 5).

(c) Changes in Test Procedure

The value of the estimated P_o appears to be insensitive for practical purposes to sample disturbance, but it also seems that it is virtually insensitive to most types of changes in the test procedure. For example, for clays it has been recognised that changes in the load increment ratio, $\frac{\Delta P}{P}$ have appreciable effect on the result, a smaller $\frac{\Delta P}{P}$ leading in general to a higher P_o estimate (Ref. 6). However, this effect has been sought without success in the brown coal of both the M1 and M2 seams, there being apparently no significant difference between the results for $\frac{\Delta P}{P}$ = 0.33, 0.50 and 1.0. This observation has provided the justification for departing slightly from the commonly used load increment ratio of 1.0, by inserting one or two additional loads in order to give a better definition of the e - log P curve in critical regions.

The time interval between loads also may be expected to have some effect on the e - log P curve and hence possibly also on the estimated preconsolidation pressure. It has been reported that use of a shorter time interval results in a greater P_o value (Ref. 6). Both M1 and M2 coal specimens have been subjected to time intervals between loads ranging from 3 minutes to 24 hours, with intervals of 72 hours being used in a few cases, without any significant change in the estimated P_o value having been observed. The majority of tests have used a "standard" interval of 24 hours between loads, however, rather than shorter intervals, because investigations have been concerned with other matters besides preconsolidation pressure.

(d) Temperature Effects

Subterranean temperatures on free water at Morwell are high, the maximum observed temperature being 60°C (140°F). In order to simulate field conditions more accurately, a number of consolidation tests have been performed on brown coal at elevated temperature, behaviour being compared with that of companion samples (generally contiguous or very nearly so) tested at room temperature.

The apparatus for the elevated temperature tests consisted of the normal consolidometer in which the consolidation cell was surrounded by a thermostatically-controlled water bath. Two types of bath have been used, one with an electrically-powered agitator and one using a simple immersion coil without agitation. Both have been equally effective in maintaining the water surrounding the specimen at the required temperature, which to date has been either 60°C or 45°C.

Relatively little work appears to have been done on the effects of temperature on soil properties, and no other work is known to the author of such work for brown coal. It has been suggested, however, that the consolidation void ratio curves for re-moulded clays are not particularly affected by temperature up to 80°F (Ref. 7). Subsequent work, however, also on clays, suggests that this holds true only for tests carried out at a constant elevated temperature, whereas changes in temperature at constant pressure are likely to produce volume changes. In particular, decreases in temperature yield volume increases, while increases in temperature cause volume decreases. This phenomenon has been explained in terms of irreversible physico-chemical structural adjustments between the solid and liquid phases at the pore water-soil interface (Refs. 8, 9, 10). Interestingly, the work of Campanella and Mitchell (Ref. 9) involved tests at temperatures up to 60°C, the same limit as that applied for the tests carried out under the author's supervision on brown coal.

Fig. 1 illustrates for illite the phenomenon of a decrease in volume for an increase in temperature, then a displacement to the right of the void ratio-pressure curve when load is increased after re-cooling, as reported by Plum and Esrig (Ref. 10).

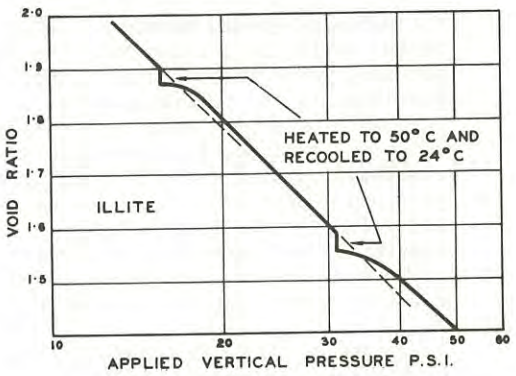

Fig. 1

Effect on stress-strain behaviour in consolidometer of heating and cooling illite. (After Plum and Esrig.)

Some evidence of this phenomenon has been gained in the laboratory for Morwell brown coal, but as yet the data is too limited to make general conclusions. Nevertheless, it

does appear that high temperatures up to 60°C held constant for the duration of a consolidation test have an insignificant effect on the P_o value estimated from the e - log P curves.

The implication of the work referred to on clays, and especially the phenomenon of Fig. 1, is that a temperature increase cycle may be equivalent to overconsolidation, i.e. "there may be a complete analogy between temperature-induced volume changes and stress-induced volume changes" (Ref. 9). If the phenomenon of Fig. 1 is confirmed in subsequent tests for brown coal, and if it be postulated that the coal has been subjected to in situ heating and cooling cycles during its geological history, the implication may be taken that laboratory testing may tend to over-estimate the maximum past pressure to which the coal has been subjected. The grounds for this are that part of the estimated P_o may have been due to temperature effects during deposition, rather than to pressure from superimposed load. The amount of such an over-estimate would depend on the total history of temperature fluctuations, which is indeterminate, but at present there are no grounds for considering that this effect, if it exists, is a large one. If Plum and Esrig's conclusion (for illite) that this effect of volume change resulting from temperature cycling is considerably less important for overconsolidated soil than for normally consolidated soil (Ref. 10) holds good for brown coal, then the effect would be small for the coal, which is highly overconsolidated.

V.- COMPRESSIBILITY

(a) Compression Index

Estimates of ground movements resulting from mining activities, especially the dewatering process, have required some quantitative knowledge of the compressibility of the coal, particularly in the virgin consolidation range. Trollope, Rosengren and Brown had concluded earlier (Ref. 5) that for practical purposes there was a unique curve of e versus log P for all the Latrobe Valley coals. This conclusion was based on the behaviour of a number of samples taken from several different coal seams, and not only at Morwell.

In recent tests by the State Electricity Commission of Victoria, the virgin e - log P curves for M1 coal have been found to be typically very close to the mean curve reported by Trollope et al for Morwell coal (Ref. 5), the compression index, C_c, having a mean value of about 1.5. For M2 coal, however, which is not reported in Ref. 5, C_c values had a mean of about 0.7, though this figure probably significantly underestimated the true virgin C_c, due to inadequate definition of the virgin curve arising from the limit of 52.5 kg/cm^2 used in the loading cycles being too low. Fig. 2 shows typical e - log P curves for samples from each of the two coal seams.

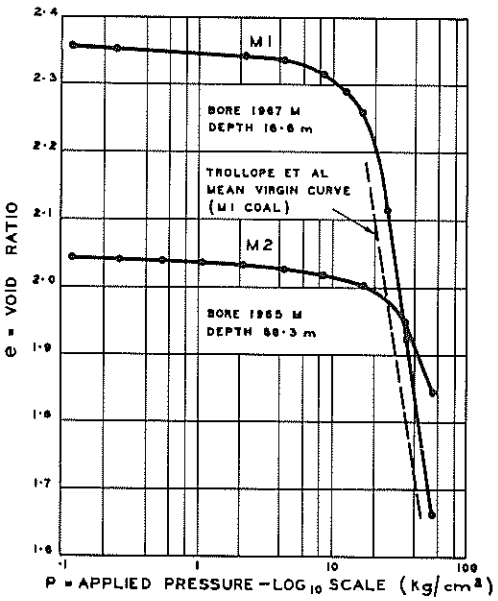

Fig. 2

Typical e - log P curves for M1 and M2 coal.

Even allowing for the inadequate definition of the virgin curve, the mean virgin curve for M2 coal appears to be somewhat further to the right of the mean curve reported by Trollope et al. Nevertheless, this curve does not lie very far outside the range of such curves which these authors reported, and hence their observation that virgin e - log P curves lie in a very narrow band for all Latrobe Valley brown coals has not been sensibly altered.

(b) Coefficient of Volume Decrease

For many engineering purposes, the coefficient of volume decrease, m_v, has been considered a more useful index of compressibility than the compression index, C_c. For brown coal this is especially so, because of the wide scatter found to occur in in situ void ratios (e.g. from 1.7 to 3.2 at Morwell). Furthermore, the calculation of void ratio requires the determination of specific gravity of the solid particles of coal, and since this does not appear to vary much from a figure of 1.5, and since the inferred degree of saturation is always very close to unity, moisture content may be considered as a substitute variable for void ratio. In this context the coefficient of volume decrease has been seen to depend not only on the consolidation pressure but also on the initial moisture content. The trend of this relationship for M1 coal is shown in Fig. 3.

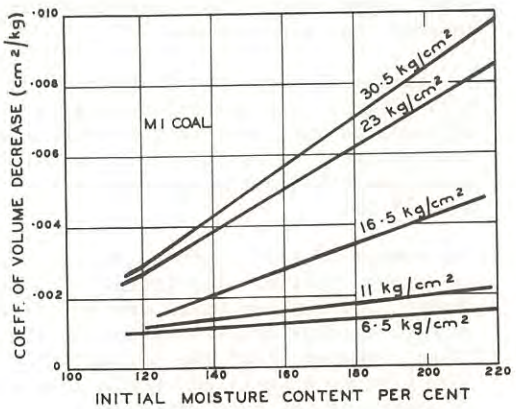

Fig. 3

Trend of effect of moisture content on coefficient of volume decrease for various consolidation pressures (M1 coal) - derived from m_v versus P curves.

This figure shows a trend only, and the scatter is not shown for purposes of clarity. A similar type of trend appears to exist for M2 coal, but to date a much narrower range of initial moisture contents has applied in tests on this material.

Fig. 4 shows typical plots of m_v versus mean consolidation pressure for samples from each seam.

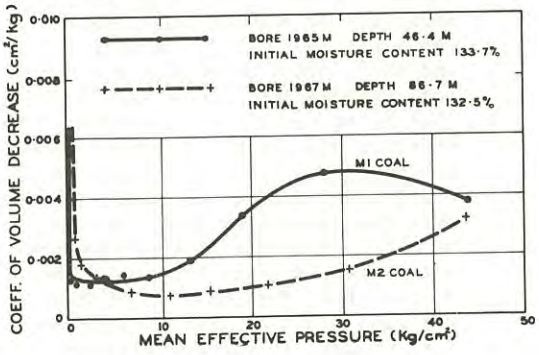

Fig. 4

Typical plots of coefficient of volume decrease.

The scatter about the m_v curve for M1 coal is substantial, whereas a much narrower scatter has appeared for M2 coal. Again, the narrower scatter for M2 coal is mostly explained by the much narrower range of moisture contents which have applied so far in tests on that material.

(c) Temperature Effects

In the tests carried out at elevated temperature, no significant change in compressibility has been observed compared with tests carried out at room temperature. For clays prepared in a slurry condition, it has been reported that at low pressures the compression index at high temperatures (50°C) exceeded that for lower temperature (24°C), whereas at high pressures this index was independent of temperature (Ref. 10). No significant effect of this nature has been observed so far with brown coal, though it must be admitted that the number of high temperature tests carried out in this material (three in M1 coal and two in M2 coal at the time of writing) makes the drawing of any conclusions only tentative. Fig. 5 shows a comparison between tests on companion samples of coal carried out at room temperature (20°C) and elevated temperature (60°C).

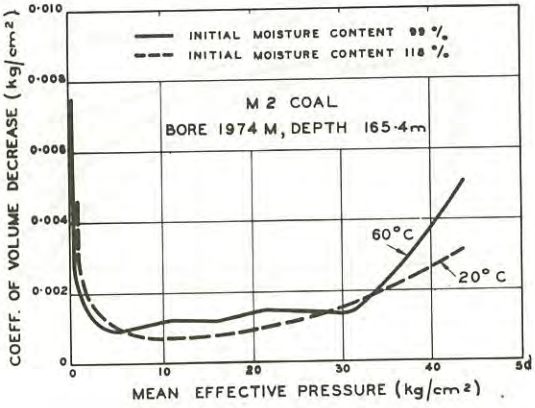

Fig. 5

Coefficient of volume decrease for companion specimens at room and elevated temperatures.

The major difficulty in determining the effect of temperature is in separating out the effect of moisture content of the samples to give an estimate of the effects due to temperature alone. The wide variation in initial moisture content between samples, coupled with the quite significant effect of moisture content itself on compressibility (see Fig. 3) makes it very difficult to extract any reliable conclusions as to the effect of temperature on compressibility from the small number of tests carried out so far. To date, it appears that there probably is some increase in compressibility at a constant temperature of 60°C as compared with compressibility at room temperature, but that this increase is relatively small, a few per cent only. In one test, however, in which the specimen was subjected to a heating and cooling cycle at different points in the loading cycle, it has been seen that with constant load, if heating from 20°C to 60°C is carried out

after consolidation at 20°C has been sensibly completed, compression may increase by a further ten to sixty per cent of that achieved under the load before heating began. As noted in the previous section, therefore, temperature fluctuations may yield more significant effects than the mere existence of high temperature.

However, this observation is subject to some qualification. The time rates of compression do appear to be affected significantly at least in a limited range of pressures, for tests at constant high temperature.

For clays, consolidation versus log time curves have been put into three categories by Lo, according to their shape in the secondary compression stage, as shown in Fig. 6 (Ref. 13).

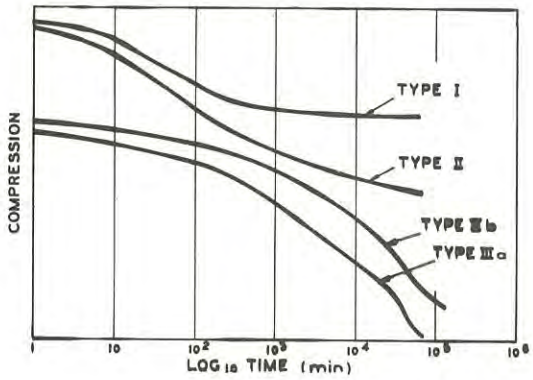

Fig. 6

Types of compression curves (after Lo)

At room temperature, the curves obtained for brown coal have generally been similar to Lo's type I, which is characterised by a relatively small and decelerating secondary compression, the majority of the curve being concave when viewed from the top right. At high temperature, however (45°C and 60°C), each of the five specimens so far tested showed a transformation to Type III curve for the range of pressure 19 psi to 50 psi (13 to 35 kg/cm^2), this transformation occurring within the same pressure range for both M1 and M2 coal.

The inference taken at this stage is that the use of load durations in excess of 24 hours may produce somewhat greater compressions than have been experienced at room temperature. If this is so, then two major conclusions would follow. Firstly, if the compression at high temperature is allowed to run its course under loads of this magnitude (19 to 50 psi), then it may be that compressibility is sensibly greater than that occurring at 20°C. Secondly, even if this is so, the time taken to achieve a given compression may be considerably greater at high temperature in this pressure range than at lower temperatures; hence predicted ground movements may occur more slowly than would otherwise be anticipated, even though their magnitude may be greater than anticipated.

It remains obscure at this stage what the mechanism of this phenomenon may be. Any explanation must take into account the observed re-transformation to type I compression-time behaviour at pressures greater than 50 psi.

The number of tests carried out is too small to warrant further speculation for the moment, but further tests are under way to attempt to clarify this matter. It seems clear, however, that the mechanism is not likely to be associated with a change in viscosity of the pore water due to the use of elevated temperature.

VI.- FIELD LOAD TEST

(a) General

In March, 1964, a test embankment was constructed not far from the Morwell Open Cut with the aim of simulating a power station loading of 1 ton/ft^2 (1.09 kg/cm^2), so as to study the settlement behaviour of brown coal.

The site was chosen because of the relatively shallow depth of material overlying the brown coal. The embankment covered a square area of side 200 ft (61 m) and had sides battered at about 1 : 1 to a total height of approximately 20 ft (6.1 m). The average bulk density of the embankment material was approximately 110 lb/ft^3 (1.77 g/cm^3). Investigation of the subsurface conditions carried out by both percussion and rotary drilling, and a knowledge of the area geology, showed that there was about 13 to 21 ft (4 to 6.4 m) of silty and sandy clays overlying the Morwell M1 coal seam which is about 375 ft thick (114 m) at the site. A marked layer of inferior coal 2 to 6 ft thick (0.6 to 1.8 m) was found to exist at the top of the coal seam, and since it was much more compressible than the clean coal, it was considered to make a significant contribution to total settlement, despite its small thickness. At the time, the location of the embankment was some 2,000 ft (610 m) west of the Open Cut, though the Cut has advanced a considerable distance westward since then.

Seven hydrostatic settlement cells were located at the natural surface level beneath the bank, three of the cells being connected by means of steel pipes to concrete plugs embedded in the clean coal about 30 ft (9 m) below natural surface. The average material overlying these observation points consisted of about 15 ft of overburden (silty and sandy clays), 5 ft of wet inferior coal and 10 ft of clean coal. In addition, twenty settlement markers were located around the test embankment, all within about 250 ft (76 m) of the toes. A survey pin about

600 ft west of the centre of the embankment was used as the datum for level measurements.

Graphs of observed settlement versus time are given in Fig. 7 for one of the surface cells, S_2, and one of the underground cells, U_3, both of these being near the centre of the embankment area in plan.

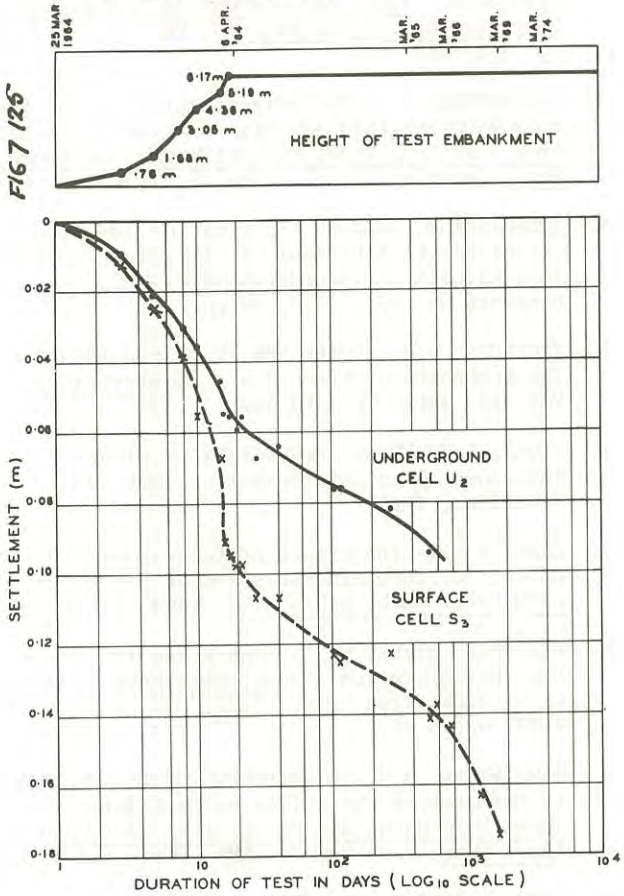

Fig. 7

Observed rate of settlement beneath centre of test embankment.

Periodic survey data showed that the level datum pin settled during the test, this movement being attributed to earth movements due to Open Cut operations. However, the conclusion was reached from examination of the data that only perhaps ten per cent of the settlements recorded beneath the centre of the test bank should be attributed to this source rather than to the test bank itself.

All three underground cells (including U_3) showed accelerated settlement after August, 1965. One of these cells, on being exposed for examination, was found to be still in contact with the steel pipe connecting it to the coal seam, but the pipe was found to be badly corroded and was fractured in three places. The other underground cells were not exposed, but since their behaviour was similar to that of the exposed one, the same explanation for the accelerated settlement in those locations was assumed to have applied. A study of the settlement-time plots led to the conclusion that about 70 to 80 per cent of the ultimate settlement due to the test load had occurred when these cells became ineffective.

(b) Computations

The last reliable results for the underground cells (i.e. those for August, 1965) were used in calculations made to compare theoretical with observed settlements. Two approaches to computation were used, namely, conventional one-dimensional consolidation theory and three-dimensional consolidation theory (Ref. 12). Vertical stress (σ_z) and horizontal stresses (σ_x and σ_y) beneath the test load were computed to a depth of 300 ft using Newmark influence charts. Calculations of horizontal stress assumed that Poisson's ratio $\mu = 0.35$, this value being taken from triaxial test data.

In theory, the three-dimensional approach should yeild more accurate results than the one-dimensional approach because the former takes into account lateral strains. The major drawback of the former method, however, is that calculation of settlement (S) must employ values of Poisson's Ratio and Young's Modulus E), as follows:

$$S = \Sigma \frac{1}{E} [\delta\sigma_z - \mu \ (\delta\sigma_x + \delta\sigma_y) \ ] \ \delta h \ - - - \ (1)$$

By contrast, the corresponding equation for one-dimensional compression is as follows, assuming that a suitable average value of the coefficient of volume decrease (m_v) can be found for the stratum affected.

$$S = m_v \ \Sigma\delta\sigma_z \delta h \ - - - - - - - - - - - - - - \ (2)$$

Thus, using equation (2), the shape of the calculated settlement profile is independent of the value of m_v. However, the shape of the settlement profile calculated by equation (1) depends on the values chosen for both E and μ. Settlement profiles calculated by the three-dimensional approach for various values of E showed essentially the same shape as profiles calculated by the one-dimensional approach. Consequently, in view of the observed very wide scatter in values of E and μ obtained experimentally (from triaxial tests), it was considered there was no advantage to be gained by using the three-dimensional approach.

For settlement beneath the centre of the test embankment, assuming that 70 per cent of consolidation had occurred when the underground cells became ineffective, the average value of m_v which fitted measured settlements to the one-dimensional theory was found to be 0.0027 cm^2/kg. This result was considered to be consistent with results of laboratory tests on the clean coal, after taking into account tests on the overburden and wet inferior coal, which showed m_v values which were approximately the same for

each of these strata, and about two to two and a half times as high as for the clean coal.

It was therefore considered that the one-dimensional consolidation test provides a useful means of predicting settlements due to full scale loads in the field, at least for loads of about the size likely to be applied by power station structures and ancillary works.

VII. - CONCLUSIONS

The behaviour of brown coal from the Morwell No. 1 and No. 2 seams in one-dimensional consolidation tests appears to be insensitive for practical purposes to a number of variations in test procedure. In particular, neither variation of the duration of the loads from 3 minutes to 24 hours, nor variation of the load increment ratio from 0.33 to 1.0 appears to have any significant effect on the value of the preconsolidation pressure estimated by Casagrande's method, nor do variations of this kind appear to have any significant effect on compressibility.

Data from a limited number of tests carried out at high temperature, however, suggested that while neither the estimated preconsolidation pressure nor the overall compressibility may be significantly affected by high temperature as long as that temperature is constant, both may be more significantly affected by temperature fluctuations. It is as yet too early to quantify these conclusions regarding temperature effects because of the small volume of test data, but qualitatively they are in line with conclusions reached by others in tests on clays.

The value of preconsolidation pressure has been estimated at about 340 psi for M1 coal, which is considerably higher than that reported earlier by other authors. The estimated value for M2 coal is about 420 psi.

The field settlement behaviour of M1 coal in a large load test has been found to be qualitatively and quantitatively consistent with behaviour inferred from one-dimensional consolidation tests.

VIII. - ACKNOWLEDGEMENTS

This paper is published with the permission of the Chief Civil Engineer of the State Electricity Commission of Victoria, Mr. R.L. Urie.

The laboratory tests were carried out in the Civil and Architectural Department of the SECV and the author wishes to acknowledge the co-operation of several members of that Department in analysing results of tests and in particular the diligent co-operation of Mr. J. Bodno in preparation of specimens and the monitoring of tests.

The analysis of the field load test was carried out by Dr. J.P. James of Civil and Architectural Department.

REFERENCES

1. GLOE, C.S. - The Geology of the Latrobe Valley Coalfields. Proc. Aust. Inst. Min. Met. No. 194, 1960, pp. 57-125

2. ROSENGREN, K.J. and KREHULA, F.J. - Earth Movements and Batter Stability in the Latrobe Valley Open Cuts. Proc. 8th Commonwealth Min. Met. Congress Aust. & New Zealand, Vol. 6, 1965, pp. 573-585.

3. CASAGRANDE, A. - The Determination of the Preconsolidation Load and its Practical Significance. Proc. 1st Int. Conf. on Soil Mech. and Found. Eng., Cambridge, Mass., Vol. 3, 1936, pp. 60-64.

4. SCHMERTMANN, JOHN H. - Estimating the True Consolidation Behaviour of Clay from Laboratory Test Results. Proceedings ASCE, Vol. 79, Separate No. 311, 1953, 26 pp.

5. TROLLOPE, D.H., ROSENGREN, K.J. and BROWN, E.T. - The Mechanics of Brown Coal. Geotechnique, Vol. 15, 1965, pp. 363-385.

6. YONG, RAYMOND N., and WARKENTIN, BENNO P. - Introduction to Soil Behaviour, New York, Macmillan, 1965.

7. FINN, F.M. - The Effect of Temperature on the Consolidation Characteristics of Re-molded Clay. ASTM Spec. Tech. Pub'n. 126, 1951, pp. 65-72.

8. PAASWELL, ROBERT E. - Temperature Effects on Clay Soil Consolidation. Jour. Soil Mech. and Found. Div., ASCE, Proc. Paper 5225, Vol. 93, No. SM3, 1967, pp. 9-22.

9. CAMPANELLA, R.G. and MITCHELL, J.K. - Influence of Temperature Variations on Soil Behaviour. Jour. Soil Mech. and Found. Div., ASCE, Proc. Paper 5958, Vol. 94, No. SM3, 1968, pp. 709-734.

10. PLUM, ROBERT L. and ESRIG, MELVIN I. - Some Temperature Effects on Soil Compressibility and Pore Water Pressure. Highway Research Board, Special Report No. 103, 1969 ("Effects of Temperature and Heat on Engineering Behaviour of Soils"), pp. 231-242.

11. STATE ELECTRICITY COMMISSION OF VICTORIA, Morwell Load Test Report. Design Division, Civil and Architectural Department Report, 1969. Not published.

12. DAVIS, E.H. and POULOS, H.G. - The Use of Elastic Theory for Settlement Prediction Under Three-Dimensional Conditions. Geotechnique, Vol. 18, 1968, pp. 67-91.

13. LO, K.Y. - Secondary Compression of Clays. Jour. Soil Mech. and Found. Div., ASCE, Proc. Paper 2885, Vol. 87, No. SM4, 1961, pp. 61-87

The Primary/Secondary Transition during the Consolidation of Clay

By
J. G. Hawley, M.A., Ph.D., B.E.
(Soil Engineer, Soil Bureau, D.S.I.R., New Zealand)

Pore pressure gradient affects rate of strain.

Steeper than primary

SUMMARY.- The question of a transition from the primary to the secondary stages of consolidation occurring at different times at different depths within a stratum is examined. The particular case of one-dimensional consolidation in saturated clay is considered in detail. The types of depth-time loci of transition implied by different theories and different primary/secondary criteria are discussed. The influence of stratum thickness on the transition, and in particular the limited relevance of the t/H^2 similarity rule, is emphasised.

I.- INTRODUCTION

Although it is common practice to assume that the transition from the primary to the secondary stage of the consolidation process takes place at the same instant throughout the depth of a stratum, it is evident that, whatever criterion is used to distinguish between primary and secondary processes, the transition must take place at the drainage surface(s) at $t = 0$ (the instant of application of an increment of load) and progress through the stratum towards the mid-plane as consolidation proceeds. Soil at a drainage surface is always in the secondary stage.

Although presented in the context of one-dimensional consolidation in saturated clays the ideas developed in this paper are not restricted to that particular case.

The adjective 'local' will be used in this paper to distinguish the value which a variable may have at a particular point within a stratum from the average value which the same variable may have when the stratum is considered as a whole. A simple instance occurs in connection with the variable 'strain'. Average strain within a stratum (at any instant) is closely related to 'settlement'. A consideration of local rather than average (or maximum) values of variables is the more rational procedure insofar as elements of soil need not then be assumed to 'know' where they lie in relation to a drainage face, and in particular whether they form parts of thin laboratory samples or thick field strata.

II.- NOTATION

e Voids ratio
e_o Voids ratio for an effective stress σ_o'
e_i Initial voids ratio
e_f Final voids ratio
σ' Effective stress
σ_i' Initial effective stress
σ_f' Final effective stress
u Excess pore pressure
z Length
a Length measured on an independent (fixed) reference space
H Maximum drainage path length
γ_w Density of water
k Permeability
t Time
T_v Dimensionless time factor $c_v t/H^2$
T_o " " " $c_F t/H^2$
c Constant
c_v Coefficient of consolidation
c_F Coefficient equal to $c_v (1+e_o)/(1+e)$
a_v Coefficient of compressibility
C_c Compression index

III.- THE TRANSITION LOCUS FOR AN IDEAL PRIMARY SOIL

In this section the behaviour of an ideal primary soil will be considered. Such a soil obeys a primary (e.g. Terzaghi, Ref. 1) theory by occupying at all times, states which correspond with points on a unique voids ratio (e) - effective stress (σ') curve. Strictly such a soil would approach the end of consolidation asymptotically but an end of the primary stage in finite time may be calculated according to a criterion such as either of the two following:

(A) the attainment by each element of soil within the stratum of a specified fraction X (say 0.99) of ultimate strain (as calculated from the unique $e - \sigma'$ relationship obeyed by this ideal soil).

(B) the reduction of excess pore pressure in each element within the stratum to a specified fraction x (say 0.01) of the load increment.

The loci in depth-time coordinates of the end of the primary stage have been plotted in Fig. 1 for each of the above two criteria. Three primary theories have been considered; those of Terzaghi (Ref. 1), Davis and Raymond (Ref. 2) and Gibson, England and Hussey (Ref. 3). In terms of voids ratio all three of these theories can be made to yield equations of the form

$$\frac{\partial e}{\partial t} = c \frac{\partial^2 e}{\partial z^2} \qquad 1$$

where z is a length term and t is time.

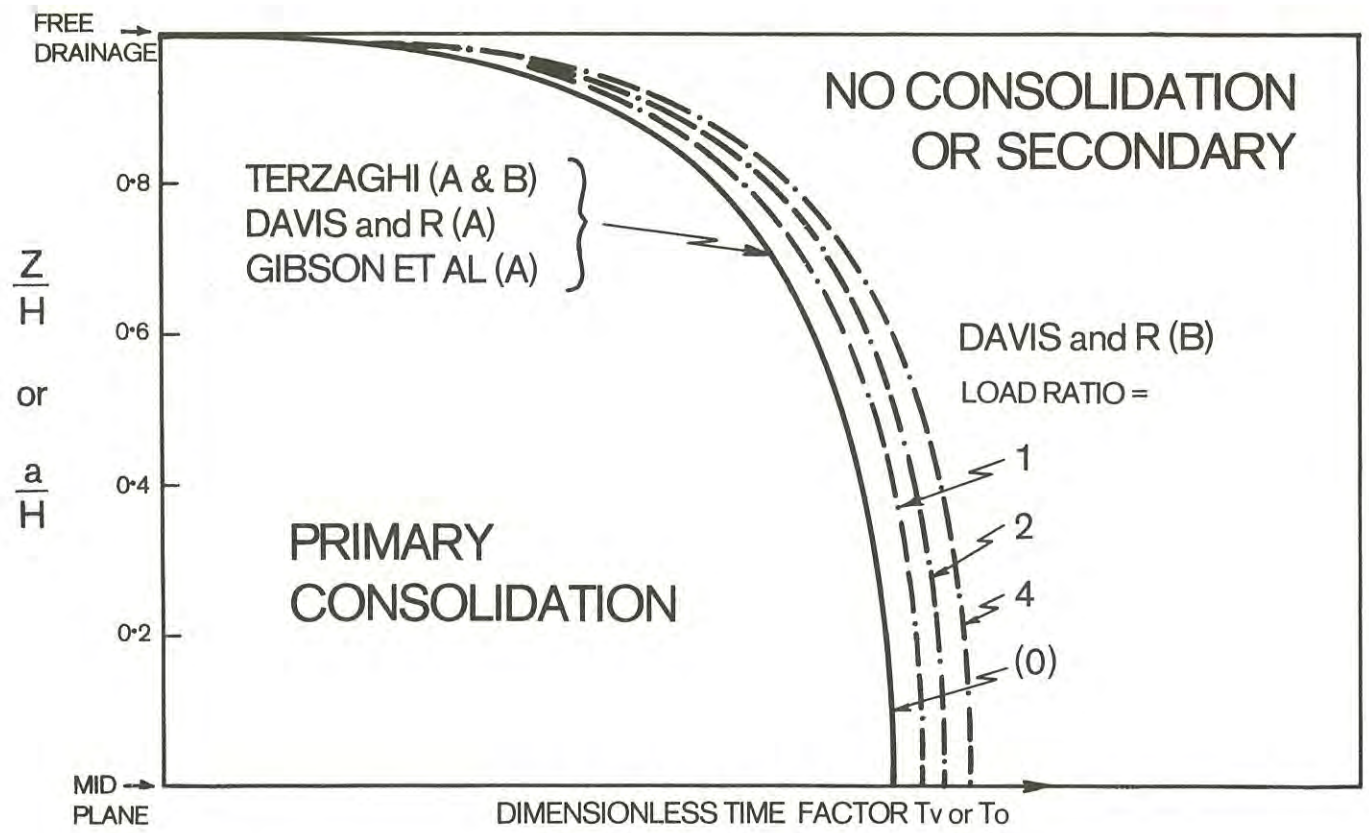

Fig. 1. Depth-Time Loci of the End of the Primary Stage for an Ideal 'Primary' Soil.

Terzaghi derives an equation of the form of equation 1 but in terms of excess pore pressure rather than voids ratio,

$$\text{i.e.} \qquad \frac{\partial u}{\partial t} = c_v \frac{\partial^2 u}{\partial z^2} \qquad 2$$

Equation 1 may be derived using only the equation of continuity, Darcy's law and the effective stress equation, if self weight effects (i.e. effects due to the difference between the densities of the soil particles and the pore water) are neglected and if the product $k\, d\sigma'/de$ is assumed constant. The derivation of equation 2 involves, in addition, a restriction to step-loading conditions and the assumptions that k and $\frac{d\sigma'}{de}$ are each constant for individual increments of load.

In the Terzaghi and the Davis and Raymond theories the constant c in equation 1 is the coefficient of consolidation c_v defined as

$$c_v = - \frac{k\,(1+e_o)}{\gamma_w} \frac{d\sigma'}{de} \qquad 3$$

where k is the permeability and
γ_w is the density of water.

In these two theories no distinction is made between lengths measured at time 0 and lengths measured on the (moving) soil skeleton at time t. These two theories are therefore small strain theories.

Gibson et al. following McNabb (Ref. 4) in this respect, have removed the limitation to small strains by making careful definition of length (and velocity) terms. They show that equation 1 may be written more precisely as

$$\frac{\partial e}{\partial t} = c_F \frac{\partial^2 e}{\partial a^2} \qquad 4$$

where lengths 'a' are measured at t = 0 (i.e. on an independent, fixed, reference space) and are not therefore functions of time. c_F is given by

$$c_F = - \frac{k\,(1+e_o)^2}{\gamma_w\,(1+e)} \frac{d\sigma'}{de} \qquad 5$$

The loci in Fig. 1 have been plotted in dimensionless form; the vertical axis in terms of z/H or a/H where H is the maximum drainage path length (at t = 0 in the case of a/H). The horizontal axis has been plotted in terms of the dimensionless time factor

$$T_v = c_v\, t/H^2 \qquad 6$$

for the first two theories

$$\text{or} \qquad T_o = c_F\, t/H^2 \qquad 7$$

for the Gibson et al. theory.

For the first two theories under conditions of step-loading, the local voids ratios are given by

$$e = e_f + \frac{4}{\pi}(e_i - e_f)\sum_{n=0}^{n=\infty}\frac{(-1)^n}{(2n+1)}\cos\left[\frac{(2n+1)\pi z}{2H}\right]\exp\left[\frac{-(2n+1)^2\pi^2 c_v t}{4H^2}\right] \quad 8$$

where e_i and e_f are the initial and final voids ratios corresponding to the initial and final values of total applied stress, and z = 0 has been taken as the mid-plane of the stratum. For the Gibson et al. theory the same expression for voids ratio applies, with the modification that the z term becomes an 'a' term and c_v becomes c_F.

For criterion (A) above, the end of the primary stage is given by

$$X = \frac{e_i - e}{e_i - e_f} \quad 9$$

and the depth-time locus for the end of the primary stage of consolidation has the same shape for all three theories. This has been plotted as the continuous curve in Fig. 1. The position of the curve relative to numbers which might be put on the time factor axis) depends on the value of X considered appropriate to signify the end of the primary stage.

For criterion (B) above, the end of the primary stage is given by

$$x = \frac{u}{\Delta\sigma} \quad 10$$

where u is the excess pore water pressure, and $\Delta\sigma$ is the applied increment of load.

Because equations 1 and 2 have the same form it is apparent that, for the Terzaghi theory, the same shape of transition locus is obtained for criterion (B) as was obtained for criterion (A). The same position of the locus is obtained if x = 1 - X. The continuous line in Fig. 1 represents therefore the locus of the end of the primary stage derived from Terzaghi theory for criterion (B).

The Terzaghi assumption (in the derivation of equation 2) that $\frac{d\sigma'}{de}$ is constant appears in the form

$$de = -a_v\, d\sigma' \quad 11$$

where a_v is assumed constant for individual increments of step loading. Davis and Raymond have shown that the assumptions of a constant coefficient of consolidation c_v and an e-σ' relationship of the form

$$e = e_o - C_c \log_{10}\left(\frac{\sigma'}{\sigma_o'}\right)$$

$$\text{i.e. } de = -.434\, C_c\, \frac{d\sigma'}{\sigma'} \quad 12$$

rather than the Terzaghi assumptions of constant permeability and the e-σ' relationship given as equation 11 above, lead to the expression for excess pore pressure

$$u = \sigma_f'\left[1 - \left(\frac{\sigma_i'}{\sigma_f'}\right)^B\right] \quad 13$$

where e_o is the voids ratio corresponding to an effective stress σ_o'

C_c is the compression index, assumed constant

σ_i' and σ_f' are the initial and final effective stresses, and B is given by

$$B = \frac{4}{\pi}\sum_{n=0}^{n=\infty}\frac{(-1)^n}{(2n+1)}\cos\left[\frac{(2n+1)\pi z}{2H}\right]\exp\left[\frac{-(2n+1)^2\pi^2 c_v t}{4H^2}\right] \quad 14$$

The transition locus implied by criterion (B) using the Davis and Raymond theory is therefore given by

$$x = \frac{u}{\Delta\sigma} = \frac{\sigma_f'}{\Delta\sigma}\left[1 - \left(\frac{\sigma_i'}{\sigma_f'}\right)^B\right] \quad 15$$

For any given value of x the position of this transition locus relative to the T_v axis is dependent on the load ratio $\frac{\sigma_f'}{\sigma_i'}$. The transition would occur later (at all values of z/H for a higher load ratio, see Fig. 1.

Because they do not derive a solution for excess pore pressure, Gibson et al. do not need to assume any particular e-σ' relationship. They do assume however (in their derivation of equation 4 above) that there exists some unique relationship between e and σ'. The position of the transition locus according to criterion (B) and Gibson et al. theory will be dependent upon the form of the e-σ' relationship used to extend their theory. If e-σ' relationships of the form given by equation 11 or 12 were assumed then the position of the transition locus would be respectively independent of or dependent on the load ratio in the manner already described for the Terzaghi and the Davis and Raymond theories.

IV.- THE TRANSITION LOCUS FOR A REAL SOIL

Common experience indicates that real soils exhibit secondary as well as primary consolidation behaviour. Attempts to derive transition loci based on primary (e.g. Terzaghi, Ref. 1) and secondary (e.g. Buisman, Ref. 5) equations are destined to be unsound because in order for a primary solution (such as equation 8) to be applicable, the whole stratum must obey the primary theory. Before a primary/secondary transition locus may be derived it is necessary that

(a) the terms 'primary' and 'secondary' be precisely defined, and

(b) the primary and secondary stages be united under the control of a single set of equations.

With regard to (a) the author (Ref. 6) has pointed out that elements of soil can have no knowledge of the origin for the measurement of the excess component of the local pore pressure at any instant. Rather it is the effective stress borne by, and the strain rate suffered by each element of soil, which determines the behaviour of (i.e. the path in e - σ' space followed by) that element of soil. Secondary consolidation is shown to be essentially "small strain rate" consolidation: primary consolidation is shown to be "that during which all elements of soil within a stratum follow the same path in e - σ' space, under conditions of high strain rate". Such primary consolidation is commonly observed in the early stages of routine laboratory tests in which thin

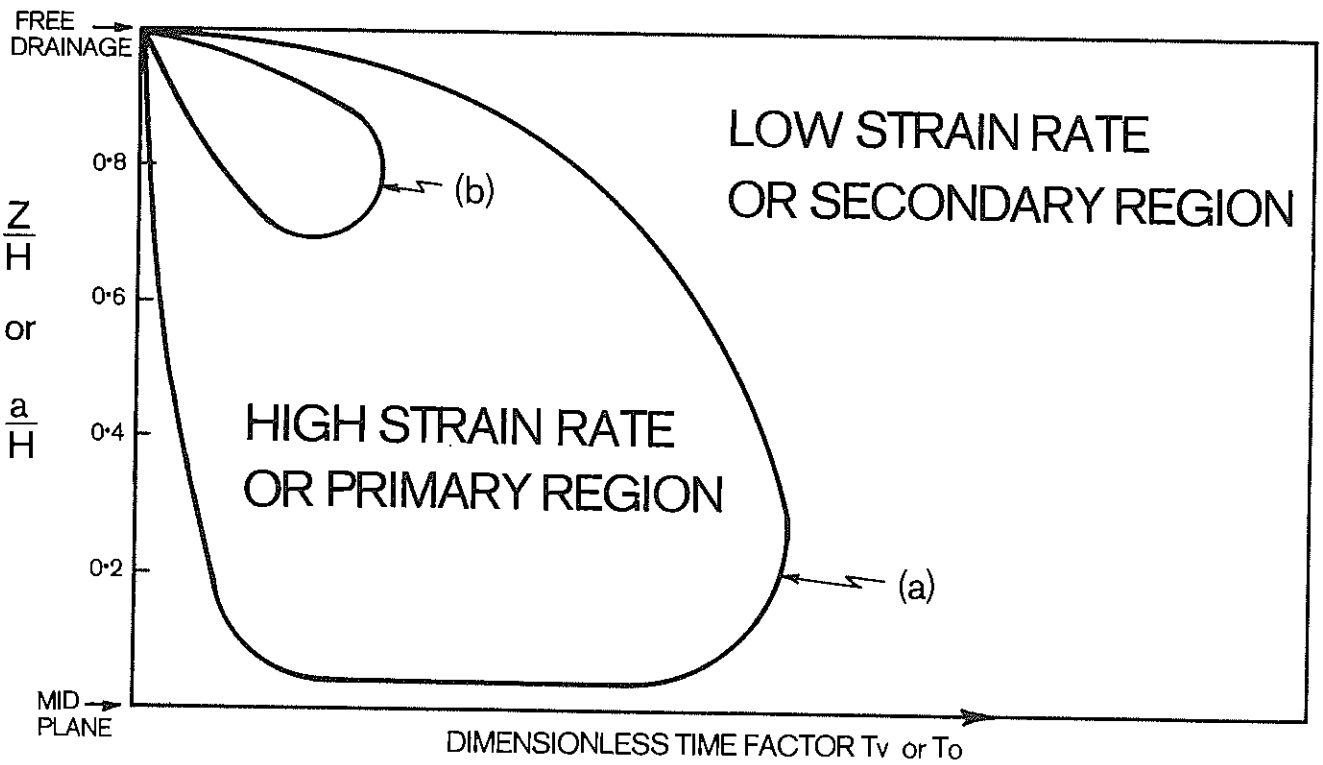

Fig. 2. Depth-Time Loci for the Primary/Secondary Transition for a 'Real' Soil, according to Strain Rate.

Curve (a) Typical locus for thin sample subjected to large load ratio.

" (b) " " " thicker stratum and/or smaller load ratio.

($H \simeq 1$ cm) samples are subjected to large (generally > 1.5) load ratios.

The high strain rate region in depth - time space lies within a 'bulb' such as is shown in Fig. 2. For thicker strata or smaller load ratios the high strain rate 'bulb' penetrates to a smaller fraction of the depth of the stratum. Under such conditions primary solutions for the whole stratum cannot be applied.

With regard to (b) it has been shown (Ref. 7) that by modifying primary theory to incorporate a unique $e - \sigma' - \frac{\partial e}{\partial t}$ relationship rather than a unique $e - \sigma'$ relationship, the laboratory primary and secondary stages may be united under the control of a single set of six equations, namely

i	Continuity
ii	Darcy's Law
iii	Stress equilibrium (self weight)
iv	The effective stress equation
v	A permeability - voids ratio (k-e) relationship
vi	An $e - \sigma' - \frac{\partial e}{\partial t}$ relationship.

This last equation constitutes the volumetric stress-strain-strain rate relationship for the soil. In general there will be no explicit solution to these six equations and the implicit solutions for particular problems must be calculated numerically. (Sensitivity and other physico-chemical effects, such as time-hardening which may be of importance over long times at low strain rates, are not included in this theory).

The well-known t/H^2 similarity rule follows from the form of equations such as equation 1. In a derivation of equation 1 it must be assumed that

(1) self-weight effects may be ignored (equation iii), and

(2) there exists some unique $e - \sigma'$ relationship - independent of $\frac{\partial e}{\partial t}$ (equation vi).

Furthermore if solutions to equation 1 are to be calculated it must be assumed that

(3) the coefficient c (c_v or c_F) is constant or a function of voids ratio alone.

This last condition is known to be violated in routine laboratory testing when, at large times after the application of increments of step loading, settlement is commonly observed to continue at sensibly constant effective stress. Under such conditions $\frac{de}{d\sigma'}$ tends to $-\infty$ and c_v (or c_F) tends to zero. In thick field strata all of these three conditions will commonly be violated. The t/H^2 similarity rule can not therefore be expected to hold for thick strata.

There is a need for more experimental investigation of the form of, and the constants in, both the $e - \sigma' - \frac{\partial e}{\partial t}$ and the k - e relationships for different soils. Only with the aid of such information and the acceptance (without modification for mathe-

matical expediency) of all of equations i to vi above, may the behaviour of thick strata be predicted from the results of tests on thin laboratory samples.

V.- CONCLUSIONS

The assumption of a transition from the primary to the secondary stages of consolidation occurring at the same instant of time throughout the depth of a stratum is unsound. A consideration of the values of variables at points within a stratum rather than average values for the stratum considered as a whole, reveals a need for a theory which unites the primary and secondary stages under a common set of equations. Only by means of such a theory may the results of laboratory tests on (thin) laboratory samples be used to predict the rate of consolidation of (thick) field strata. In general the t/H^2 similarity rule can not be expected to hold for thick strata.

VI.- ACKNOWLEDGMENTS

The ideas presented in this paper were developed by the author while a research student at Cambridge University under the supervision of the late Professor K. H. Roscoe and Dr J. B. Burland. Some further development of the ideas and their preparation for publication has been done at Soil Bureau, D.S.I.R., New Zealand. The author is grateful to Dr R. D. Northey for many helpful discussions.

REFERENCES

1. TERZAGHI, K. - Erdbaumechanik auf bodenphysikalischer Grundlage. Vienna, Deuticke, 1925.

2. DAVIS, E. H. and RAYMOND, G.P., 1965 - A non-linear theory of consolidation. Geotechnique, Vol.15, No. 2, 1965, pp. 161-173.

3. GIBSON, R.E., ENGLAND, G.L. and HUSSEY, M.J.L. - The theory of one-dimensional consolidation of saturated clays. I. Finite non-linear consolidation of thin homogeneous layers. Geotechnique, Vol. 17, No. 3, 1967, pp. 261-273.

4. McNABB, A. - A mathematical treatment of one-dimensional soil consolidation. Quarterly of Applied Mathematics, Vol.17, No. 4, Jan. 1960, pp. 337-347.

5. BUISMAN, A.S.K. - Results of long duration settlement tests. Proc. 1st Int. Conf. Soil Mech. and Found. Engg., Cambridge, Mass. Vol.I, 1936, pp. 103-106.

6. HAWLEY, J.G. - A Unified Theory for the One-Dimensional Consolidation of Saturated Clays. Thesis (Ph.D.), Cambridge University, 1970.

7. HAWLEY, J.G. and BORIN, D.L. - The use of the Terms 'Primary' and 'Secondary' to Describe Stages of the Consolidation Process in Saturated Soils. (In preparation).

An Investigation of the Three-Dimensional Creep Properties of a Clay

By

P. L. Newland, B.Sc.

(Principal Research Scientist, Division of Applied Geomechanics, C.S.I.R.O.)

SUMMARY.- The strain-log time curve for an increment in deviator stress under undrained triaxial compression conditions is shown to be essentially a straight line over most of the range, the slope of which increases rapidly as the effective stress ratio q/p increases from the k_o condition to failure. If the increment is preceded by either secondary consolidation or a prolonged strain under a lower deviator stress, the strains and pore pressures in the early stages are considerably reduced and a 'delay' is introduced before the linear relationship is established. This behaviour is shown to be a function of previous strain rather than of time.

The effective stress ratio-strain curve is shown to be independent of loading procedure to a first approximation. Finally, a model is presented which attempts to take the observed properties into account.

I.- INTRODUCTION

It is being recognized to an increasing extent that more accurate estimates of the behaviour of building foundations, etc., will be obtained if design is based on the stress-deformation-time properties of the foundation soil. Recent methods, notably those of Skempton and Bjerrum (Ref. 1) and Davis and Poulos (Ref. 2), take account of an 'immediate' component of deformation due to increase in shear stress, and a long-term component due to consolidation. However, in thick deposits of clay, there is clearly a possibility of a long-term component associated with the increase in shear stress. The work described herein was undertaken to investigate this aspect.

The word 'creep' is used in reference to the process where any one of the quantities pore pressure, volumetric strain and shear strain changes with time in a manner which differs from that normally associated with primary consolidation where pore pressure gradients due to hydrodynamic lag are set up in the sample. Secondary consolidation refers to the specific case where volumetric and shear creep strains accompany each other.

II.- NOTATION

$q = (\sigma'_1 - \sigma'_3)$ = deviator stress.

$$p = \frac{\sigma'_1 + \sigma'_2 + \sigma'_3}{3} = \frac{1}{3} q + \sigma'_3$$

= mean normal effective stress.

q/p = effective stress ratio.

$\varepsilon = \varepsilon_1 - \frac{1}{3}v$ = shear strain.

ε_1 = axial strain

v = volume strain.

III.- EXPERIMENTAL DETAILS

The clay used was a kaolin (LL 112; PL35) in the form of cores with a water content of about 70 per cent and a degree of saturation of 100 per cent, prepared by extrusion from a vacuum extruder. Side drains and filter discs at each end of the sample were employed. Further details are given in Ref. 3. It was found that the experimental results were unaffected by end restraint.

Tests were conducted on normally consolidated samples in a standard triaxial compression apparatus. Pore pressures in undrained tests were measured at the base of the sample using a gauge of the type described by Davis and Poulos (Ref. 2). Consolidation under anisotropic stress conditions was carried out while q was maintained constant.

IV.- PRESENTATION OF RESULTS

(a) Time Behaviour

Fig. 1 compares the results of two tests in which the depicted undrained increment in deviator stress q was preceded by consolidation which was effected by increasing σ'_3 while maintaining q constant. In the test illustrated in Fig. 1(a), primary consolidation only was allowed, the increment Δq being applied as soon as this was judged to have occurred, while in Fig. 1(b) considerable

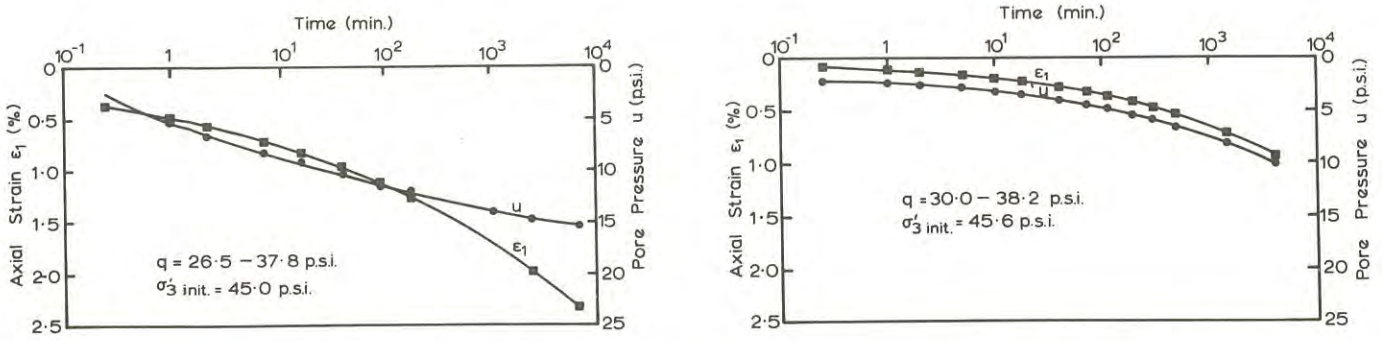

Fig. 1.- The effect of (a) zero and (b) 2-day secondary consolidation on the pore pressure and strain versus time behaviour for an undrained increment in deviator stress.

time was allowed for secondary consolidation to take place before applying Δq.

Referring first to Fig. 1(a), it will be seen that the pore pressure shows a steady increase with time, with some sign of tapering off toward the end of the test, while the axial strain curve is gently convex upwards on the long-time plot with a tendency to become linear at large times. It is clearly not possible to draw any distinction between 'primary' and 'secondary' phases in either of the two curves; in fact, the whole process from beginning to end resembles one of secondary creep with associated strain hardening. This observation contrasts with the results obtained by Walker (Ref. 4).

The degree of saturation of the pore water and the flexibility of the pore pressure measuring system in the tests described were such that the pore pressure rose to within 95 per cent of any increase in cell pressure in less than ½ min. An increment Δq increases the mean normal effective stress p by 1/3 Δq. Since undrained conditions prevail, the pore pressure may be expected to rise by at least this amount. It will be seen from Fig. 1(a) that the pore pressure did in fact rise to 1/3 Δq in about ½ min., and this rise was about 20 per cent of the total change in pore pressure. The axial strain occurring at the end of ½ min. might be termed the 'immediate' response to the application of Δq, which is somewhat less than 20 per cent of the total axial strain. It would seem that the effect of strain (or time) is to cause a change in the structure of the clay leading to a steady increase in pore pressure. It may be noted that the effective stress ratio q/p rises steadily as a result of this rise in pore pressure even though q is maintained constant.

Furning now to Fig. 1(b) which concerns an increment in q which was preceded by secondary consolidation for 2 days, both the pore pressure and the axial strain at a given time are considerably less than without secondary consolidation. For example, at 100 min., the change in pore pressure and the axial strain relative to the change in deviator stress are 0.58 and 0.045 respectively, whereas for the case with no previous secondary consolidation the corresponding values are 1.0 and 0.1, i.e. about twice as high.

The above results for incremental loading form the equivalent to those for the constant rate of strain case presented by Newland (Ref. 3).

Fig. 2 compares the results of two tests in which two undrained increments of deviator stress were applied consecutively. The first increment in each test was applied following primary consolidation as described with reference to Fig. 1(a). However, in one test, the second increment was applied after 75 min. (Fig. 2a), while in the other test the second increment was applied after 5 days. (Fig. 2b, in which the first increment is the same as that in Fig. 1a). Axial strains and pore pressures have been plotted relative to the beginning of the first increment for the sake of clarity in the diagram.

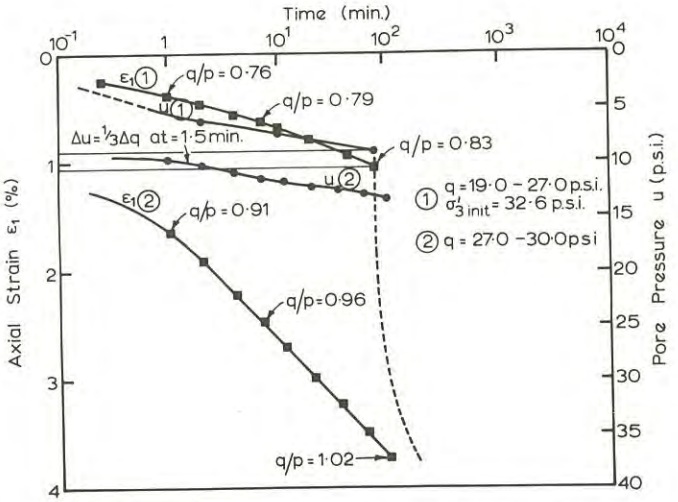

Fig. 2(a).- The effect of a short duration undrained deviator stress on the pore pressure and strain versus time behaviour of the succeeding undrained increment.

In Fig. 2a, it will be seen that, following the relatively short first increment, the axial strain in the second rapidly assumes a straight line when plotted against the logarithm of time, making the resemblance to 'secondary' creep very strong indeed. The 'immediate' strain occurring at the end of ½ min. is once again less than 20 per cent of the total axial strain at the expiration of 100 min. The effect of delaying application of the second increment for five days is illustrated in Fig. 2b. Here, very little axial strain occurs before about 100 min., (the 'immediate' strain is almost zero), after which there is a transition to a straight line in Fig. 2a. It is as if the additional strain occurring in the previous increment introduces a delay in the establishment of the linear portion of the axial strain-log time curve.

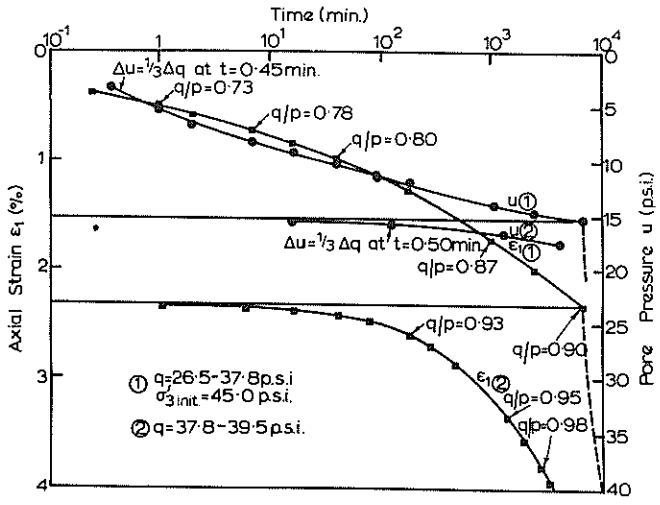

Fig. 2(b).- The effect of a long duration undrained deviator stress on the pore pressure and strain versus time behaviour of the succeeding undrained increment.

It was also found that the size of the increment affected this delay; the larger the increment the smaller the delay. This can be explained on the basis that the previous strain forms a smaller percentage of the strain in the current increment as that increment becomes larger.

A further point of interest is that the time for the change in pore pressure to reach 1/3 Δq is about 150 min. This suggests that there was a tendency for the clay to dilate when the second increment was applied as a result of the prolongation of the previous increment. This is similar to the effect reported by Richardson and Whitman (Ref. 5) where an actual decrease in pore pressure is recorded when the strain-rate is changed from a slow to a fast rate.

The second increment in both tests is also plotted (dashed curve) using a continuation of the time scale of the first increment. This curve is seen to descend very rapidly indeed towards the curve for the second increment with zero time at the beginning of this increment and would asymptote to the linear portion if the test were carried on long enough. There is a hint in this behaviour that either the increasing viscosity to which the strain hardening might be attributed is not simply a function of time, or the application of a further increment in q somehow causes a reduction in this viscosity. The latter explanation is difficult to accept since strain hardening eventually sets in during the later stages of the second increment.

To investigate the effect of time on the progress of undrained creep, an increment of deviator stress was applied for a period of 130 min. and then reduced to such a value that further axial strain was zero (about 3/4 of the elevated value) and this was maintained for a period of 1300 min. At this point, the deviator stress was returned to the elevated value. As Fig. 3 shows, the axial creep process continued almost as if there had been no interruption. Admittedly,

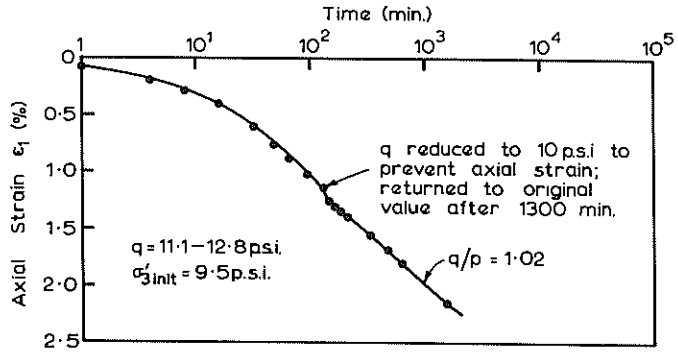

Fig. 3.- The effect of a time delay on the strain versus time curve.

the deviator stress level during the period of zero axial strain was lower than that at the beginning of the test before the final increment in q was added, although several increments had been added prior to this over a period of time. Nevertheless, the result gives support to the contention that the apparent increase in viscosity as creep proceeds is not a function of time. A better explanation would seen to be that, while the viscosity and shear stresses remain constant, the internal resistance to shear increases as a function of axial strain. This is similar to the second of the alternative models proposed by Walker (Ref. 4). However, the fact that the pore pressure rises beyond 1/3 Δq means that the normal effective stress, p, decreases as the axial strain proceeds. This in turn leads to a reduction in the resistance to shear, which must therefore be more than offset by the gain in resistance resulting from axial strain, since the net effect is one of strain hardening.

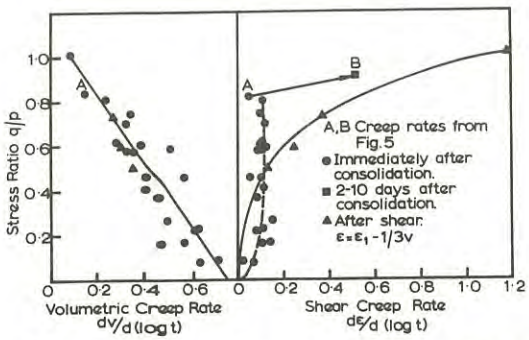

Fig. 4.- The variation of creep rates with effective stress ratio.

The linear relationship between axial strain and log time is a feature of the undrained behaviour following increase in q (Ref. 3, 4, 6), as it is of the secondary consolidation behaviour following increase in σ_3'. Walker (Ref. 4) suggested that the slope of the straight line sections be designated the creep rate. Results obtained by Newland (Ref. 3) are reproduced in Fig. 4. Referring to the plot of q/p against shear creep rate, it will be seen that the creep rate following an increase in q increases very rapidly for values of q/p beyond 0.5. On the other hand, for the case where the given stress ratio was reached by consolidation from a higher stress ratio as a result of increasing σ_3' while maintaining q constant, the shear creep rate remained constant over most of the range of stress ratio at a value equal to that for q/p = 0.5.following increase in q. This apparent anomaly has been resolved as will be seen by reference to Fig. 5. The strains occurring during the first 90 min. are largely due to conventional secondary consolidation. (The lack of a clear demarcation between primary and secondary consolidation is due to the small pressure increment ratio.) The points representing the creep rates obtained from the slopes of the straight line portions are plotted on Fig. 4 (letter A). It will be seen that they fit the original data reasonably well. Beyond 90 min. the drainage tap was closed and the creep continued as an undrained process, with pore pressures developing. It is of significance that after about a day the axial strain curve began to steepen, and after about 10 days it had clearly developed a linear section with a much steeper slope. The creep rate represented by this slope is also plotted on Fig. 4 (letter B). It will be seen to conform more closely to the curve for creep rates following increase in q. It seems that the process of consolidation introduces a similar delay in the establishment of the linear relationship between axial strain and log time as was observed earlier in the discussion of the creep behaviour where an increment in q was preceded by extended creep under a lower value of q. This phenomenon may be related to the surprising fact that shear strain ($= \varepsilon_1 - 1/3v$) occurs during consolidation as a result of an increase in all-round pressure while q is maintained constant (Ref. 3).

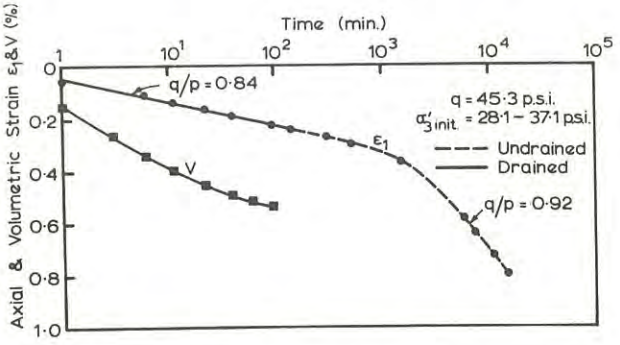

Fig. 5.- The change in rate of secondary consolition following consolidation with deviator stress maintained constant.

(b) The Effect of Loading Procedure on the Stress-Strain Properties

The results from the two-increment loading tests depicted in Fig. 2 are plotted in the form of stress ratio q/p against axial strain in Fig. 6. An arrow marks the end of the first increment in each case. Despite the large difference in the duration of the increments, the curves are very similar. The separation between them may, to some extent, reflect the difference in stress level in the two tests (Ref. 3). Also shown are the results of an incremental loading test with 2 sec. increment durations, and a constant rate of strain test with a rate of 0.016 per cent per min. These results also conform to the two curves to the extent that a unique stress-strain curve, which is essentially independent of loading procedure, may be said to exist for tests in which q is increased under undrained conditions provided the tests are commenced at the end of primary consolidation. Walker (Ref. 4) has already reported that the stress-strain curve from drained SSA tests is independent of increment duration.

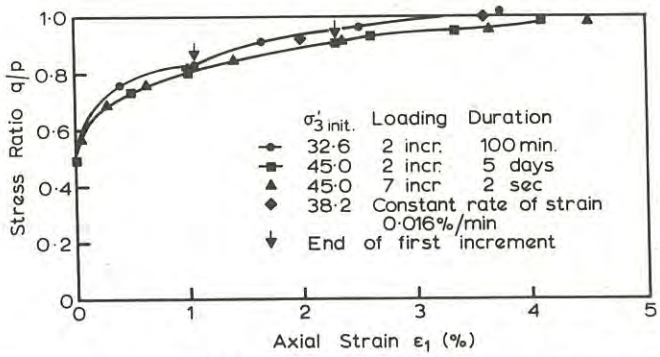

Fig. 6.- The effect of loading procedure on the stress-strain behaviour.

V.- MODEL FOR OBSERVED PROPERTIES

A possible model to account for the observed behaviour of the clay is illustrated in Fig. 7. It consists of spring-loaded oblique sliding contacts in parallel with each other and with a dashpot. At a given moment under a given stress, there are a certain number of 'activated' contacts while the remainder are 'lazy' contacts. The difference between the applied stress and the resistance mobilized in the activated contacts is equal to the stress in the dashpot, and this controls the rate of strain at the instant concerned. As strain proceeds, more of the 'lazy' contracts become activated to build up the resistance to strain. This is the strain hardening effect. At the same time, the stress carried by the dashpot is reduced so decreasing the rate of strain. This corresponds to the apparent increase in viscosity. Furthermore, the greater the total strain, the lower the residual stress in the dashpot, so that the initial rate of strain in a following increment is correspondingly reduced.

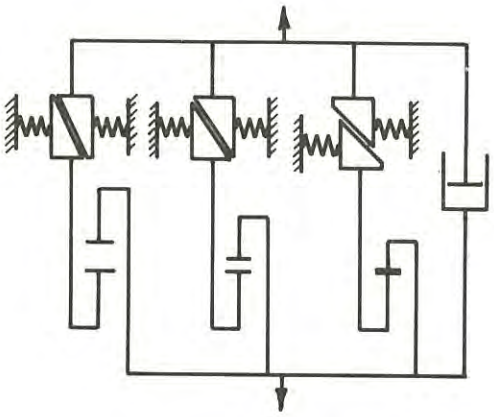

Fig. 7.- A rheological model to account for the observed stress-strain-time properties.

The spring-loaded oblique contacts represent the decrease in effective stress with increase in strain as a consequence of the increase in pore pressure. The rate of this decrease in effective stress must be more than offset by the rate at which the 'lazy' contacts are mobilized. However, the difference between them must decrease as the strain increases to account for the increase in creep rate with stress ratio. Ultimately, there are no further contacts to mobilize so that failure ensues. It is an interesting fact that the rate of strain at failure is extremely rapid, suggesting that the viscosity component represented by the dashpot is quite small.

Consolidation (with q = const.) increases the normal stress between contacts and restores the number of lazy contacts to the number appropriate to the particular stress ratio, and the shear behaviour may be repeated. If secondary consolidation is allowed, however, the strains and pore pressures are decreased at a given time in the following increment of deviator stress as if some of the lazy contacts had been mobilized during this process. There would appear to be an anomaly here.

It might be argued that there should be a spring in series with the above assembly to represent the immediate strain. However, this strain has been shown to be a function of previous strain and generally to be a small percentage of the total strain for all but the shortest duration increments. It would therefore seem to be better to incorporate this in the properties of the system as presented.

No doubt it is possible to represent the above model by a series of springs (probably non-linear) and dashpots, and this may be preferable from a mathematical viewpoint. The virtue of the present model is that the physical properties can be both easily portrayed and conceived.

VI.- CONCLUSION

The problem of determining the time behaviour of the vertical strains which result from the application of a shear stress to a clay seems to resolve itself into one of estimating the pore pressure as a function of time. From this knowledge, the effective stress-time relationship may be determined so that, by using the unique stress-strain curve, the strains can in turn be determined as a function of time. This problem is complicated by the fact that creep under previous stresses profoundly affects the time behaviour under current stresses.

Pore pressures are also a measure of the change in effective stress ratio which will occur when these pore pressures dissipate. It has already been shown (Ref. 3) that a unique relationship exists between change in stress ratio and volume strain during consolidation under constant q, and between volume strain and axial strain (with certain restrictions). Thus, the ultimate vertical strain arising from consolidation may be determined and from a knowledge of the coefficient of consolidation, the vertical strain-time behaviour may be estimated.

From the theoretical standpoint, prediction of the pore pressure behaviour may provide the key to the treatment of deviator stress and volume strain as uncoupled phenomena, and perhaps enable the handling of problems involving dilatant behaviour.

In the meantime, the problem of estimating the vertical strain-time behaviour in practical cases is complicated by the fact that pore pressures will be rising in some parts of the clay deposit as creep proceeds, while they will be dissipating in others as consolidation proceeds. The rates of strain associated with each process will in general be different. It is therefore important that tests simulate as closely as possible the conditions likely to prevail in the field.

VII.- ACKNOWLEDGEMENT

This work was undertaken while the author was on secondment to the Department of Civil Engineering, University of Sydney, and forms part of the research programme into the creep properties of clays under the general direction of Professor E.H. Davis.

REFERENCES

1. SKEMPTON, A.W. and BJERRUM, L. - A Contribution to the Settlement Analysis of Foundations on Clay. Geotéchnique, 1957, 7, pp.168–178.

2. DAVIS, E.H. and POULOS, H.G. - Triaxial Testing and Three-Dimensional Settlement Analysis. Proc. 4th A.N.Z. Conf.Soil Mech. & Found. Engng, Adelaide, 1963, pp.233-243.

3. NEWLAND, P.L. - An Experimental Study of the Stress-Strain Characteristics of a 'Wet' Clay and their Relevance to Settlement Analysis. CSIRO, Div. of Appl. Geomechanics, Techn.Rep. No.22, 1971.

4. WALKER, L.K. - Secondary Compression in the Shear of Clays. J. Soil Mech. & Found. Div., Proc. ASCE, Vol.95, No.SM1, 1969, pp.167-188.

5. RICHARDSON, A.M. and WHITMAN, R.V. - Effect of Strain-Rate upon Undrained Shear Resistance of a Saturated Remoulded Fat Clay. Geotéchnique, 1963, 13, pp.310-324.

6. WALKER, L.K. - Undrained Creep in a Sensitive Clay. Geotéchnique, 1969, 19 pp.515-529.

Application of Rate Analysis to Settlement Problems Involving Creep

By

A. K. Parkin, M.I.E.Aust.

(Lecturer in Civil Engineering, Monash University)

SUMMARY - Although creep in foundation strata is not usually a prime consideration, it can, in some specialized structures, be of quite considerable significance. Creep estimation from laboratory tests is not easy, and the analysis of field behaviour is often complicated by variable loading, and other error sources. The paper examines the characteristics of a creeping foundation and shows that rate analysis methods may be applied with advantage for the estimation of future settlement.

SYMBOLS -

a, b	coefficients
k	Boltzmann's constant
m, n	indices
t	time
Q	activation energy
T	absolute temperature
U	degree of primary consolidation at time t
ε	strain
σ	stress

I INTRODUCTION

In general terms, creep describes continuing deformations that are observed in materials under constant (effective) stress. Since the studies of creep in metal wires by Phillips (Reference 14), the phenomenon has been shown to occur in a wide range of materials (Murrell and Misra, Reference 12) that includes soils and rocks.

For settlement calculations in clays, methods based on the classical theory of consolidation are considered to be not greatly in error (Barden, Reference 2). The primary component of total settlement is usually substantial (although a function of pressure increment ratio, Leonards and Girault, Reference 10), but, in soft rocks, the situation can be quite different, primary compression often being rapid and allowing long term settlement to be dominated by creep.

The analysis of creep is often vague and ambiguous. Accommodation for creep can sometimes be provided by routine servicing, but this is unlikely to be practicable for major foundations. In the event of a reasonably accurate settlement estimation being required, there are certain problems, and significant departures from familiar consolidation behaviour, which make normal extrapolation dangerous, and which this paper seeks to evaluate.

II THE ORIGIN AND THEORY OF CREEP

The mechanisms causing creep apparently vary, and some differences in the kinetic characteristics are possible. Nevertheless, the similarity in creep behaviour between quite diverse materials is striking (Cottrell, Reference 5), such that useful inferences may be made from unrelated materials. With soil materials, such analogies are valuable, since it is not easy to determine, with confidence, the analytical form of the creep-time curve.

In rocks, creep is thought to result from micro-fissuring and recrystallization (Robertson, Reference 16). In clays, the primary and secondary compressions have been associated with "diffusion" and "viscous" processes (Walker, Reference 19; also see Barden and Poskitt Reference 3). However, for most materials, an essential feature appears to be the absence of an equilibrium condition, as for primary consolidation as $U \to 1$, and thus most postulated creep equations have no strain asymptote for large time ($t \to \infty$)*. Further, whereas the rate of consolidation settlement is uniquely specified by U**, no such relationship is possible for creep, and direct interpretation of settlement - time data is unlikely to be possible.

It has been established from the theory of absolute reaction rates (Glasstone, Laidler and Eyring, Reference 8) that steady state creep rates vary with temperature and stress according to equation 1.

$$\frac{\dot{\varepsilon}}{\dot{\varepsilon}_o} \propto \exp\left(\frac{Q}{kT}\right) \sinh\left(\frac{\sigma}{\sigma_o}\right) \qquad (1)$$

Transient creep, however, ($\dot{\varepsilon}$ variable with time) is normally described by empirical expressions only, although the logarithmic form (equation 3) can be derived from exhaustion theory (Wyatt, Reference 21).

In one of the earliest systematic studies of creep, Andrade (Reference 1) obtained the relation

$$\varepsilon = \varepsilon_o + at^{1/3} + bt \qquad (2)$$

---

* Notable exceptions are the Glanville equation for concrete (see Murrell and Misra, Reference 12), and expressions resulting from the Kelvin-Voigt and Burgers models (Robertson, Reference 16).

** For example, when $U < 0.5$, $\dot{U} \propto \frac{1}{U}$

A term in t^3 was added later (Graham and Walles, Reference 9), the terms in t then being associated with the divisions of primary (transient), steady and tertiary creep * (e.g. Cottrell, Reference 5; Murrell and Misra, Reference 12) (Figure 1). Other expressions in common use include:-

$$\varepsilon = \varepsilon_o + a \log (t - t_o) \qquad (3)$$

(e.g. Phillips, Reference 14) and (Crussard, Reference 7).

$$\varepsilon = \varepsilon_o + a (t - t_o)^n \qquad (4)$$

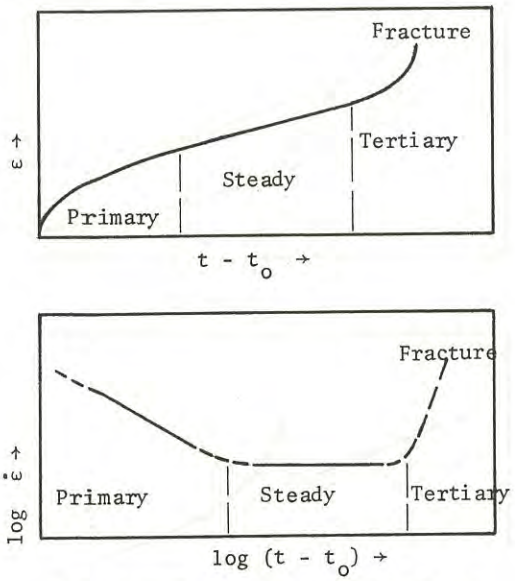

FIG. 1. GENERAL CHARACTERISTICS OF CREEP CURVES

Metals usually follow a third power low at high temperature, but show logarithmic behaviour at low temperatures. The situation is less clear for rocks, but logarithmic behaviour is often considered to apply (Robertson, Reference 16; Murrell and Misra, Reference 12). There is, however, no conflict in creep rates (equation 5) **

$$\dot{\varepsilon} = a (t - t_o)^{-m} \qquad (1 > m > 0) \qquad (5)$$

as shown by Crussard (Reference 7), and, by inference, the geometrical form of a creep equation, such as equation 3 and 4, is of little fundamental significance.

---

* Some writers report an initial, or incubation, stage (Wachtman and Maxwell, Reference 20).

** Singh and Mitchell (Reference 17) have experimentally established a similar equation for clays, viz,

$$\dot{\varepsilon} = Ae \left(\frac{t_1}{t}\right)^m \qquad (5a)$$

where $1 > m > 0.75$. It is supported by earlier theoretical work of Mitchell (Reference 11).

III COMPRESSION RATE ANALYSIS

Successful extrapolation of future behaviour depends on a reasonable determination of the analytical nature of the creep rate variation. This however, must be done on minimal data, since creep performance cannot be monitored at an accelerated rate, as in the case of laboratory consolidation testing.

Some of the problems in establishing functional identity are discussed by Crussard (Reference 7), who showed that approximate linearity in a given range does not exclude the existence of a better relationship. The most powerful analytical techniques are based on differencing (a standard mathematical procedure, e.g. Pipes, Reference 15), and creep rates necessarily show a simpler mathematical structure.

A further advantage of equation (5) over equations (3) and (4) is that the initial condition, ε_o, is eliminated, which is fortunate, since the point of initiation of creep is often obscure. The datum of time t_o, however, is similarly obscure, but cannot be eliminated from any equations. This precludes the determination of unique values of a and m, except in so far as they approach their true values for t large in relation to t_o. Techniques for the estimation of t_o do not appear to have been considered in literature.

Although equation 5 remains sensitive to t_o, an estimate, at least, of its value may be made by writing the equation as

$$(t - t_o)^m = \frac{a}{\dot{\varepsilon}} \qquad (6)$$

Since $m > 0$, a graph of t against $\frac{1}{\dot{\varepsilon}}$ must then indicate a value of t_o as the intercept where $\frac{1}{\dot{\varepsilon}}$ vanishes regardless of the values of a and m. A conventional graphical analysis will then yield values of a and m with minimum ambiguity (Figure 2).

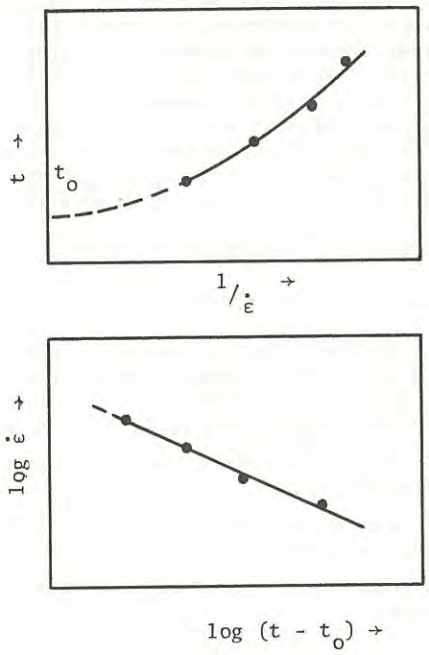

FIG. 2 CREEP RATE ANALYSIS (Diagrammatic)

IV SOME COMMENTS ON DIFFERENTIAL METHOD

The process of differentiation, on the derivation of a gradient function from a set of data, causes changes of character that are not easily visualized, particularly where the results are presented on logarithmic scales. Several points, therefore, will be noted.

Firstly, differentiation is a fully reversible process, without prejudice to the accuracy of the initial data, which may be recovered in toto by summation. It is merely a sorting process, and no new information is created.

Secondly, differentiation is a process which may be accompanied by diminished convergence. * In relation to a sequence of experimental data, differencing will amplify imperfections initially present, whereas summation will smooth and obscure any variations. The same imperfections, however, are present throughout.

Thirdly, because constant terms are eliminated in differentiation, short term factors (such as elastic strain), which may have a permanent effect on cumulative strain, have only a transient effect on strain rate. Thus, whereas a strain record does not readily permit differentiation between its various components, a strain rate record allows the creep component to be isolated, subject only to transient aberrations.

Such aberrations, which may interrupt or alter the basic creep pattern, are herein termed "secondary features", and arise due to environmental changes, such as variable loading. Some typical secondary features of creep are discussed below, as an understanding of these matters is pre-requisite to any reasonable assessment of creep behaviour.

Consolidation analysis is also subject to some secondary features, such as that resulting from the finite length of construction period, the subject of an empirical correction proposed by Gilboy (Taylor, Reference 18). The correction is possible because the effects of a loading sequence on cumulative strain are more or less additive. Whether this also applies for creep is not known, since there is no certainty that an equilibrium state exists. Only the creep rate shows any evidence of a limiting state.

V SOME SECONDARY FEATURES OF CREEP

(a) Effects of Stress Changes

It is unlikely that a foundation will not be subject to some stress changes during its early life, and these are likely to affect the deformation of a creep sensitive foundation in three ways, namely,

(i) An immediate effect, due to elastic compression

(ii) A short term effect, due to Terzaghi consolidation

(iii) A long term effect, due to a modified creep rate.

* For example, whilst a power series can always be integrated, there is no assurance that a derivative can be found (Pipes, Reference 15).

Often, it is not clear what stress changes have taken place, except by inference from their effect, which may show as a cusp on the settlement curve (Figure 3). If the curves are obtained as a sequence of experimental data, subject to reading error, it may be difficult to do other than draw a single smooth curve, which, of necessity, will over-estimate the creep rate and the deformation at large time.

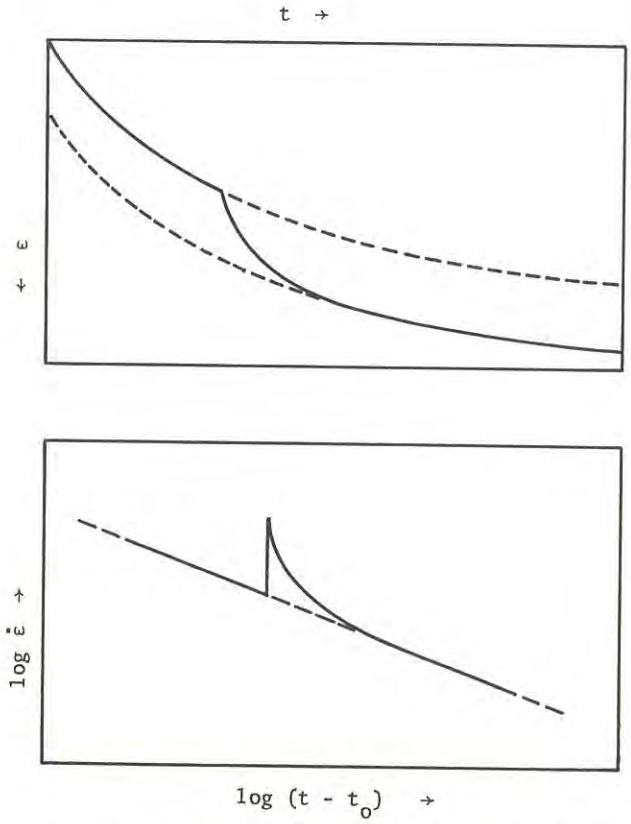

FIG. 3. SECONDARY FEATURE DUE TO CONSOLIDATION

Whether or not the creep mechanism remains operative through such interruptions is a matter of conjecture. By definition, creep is a component of strain at constant effective stress, and it is only studied under such conditions. However, the possibility of its continuance under varying effective stress is not excluded. In fact, Crawford (Reference 6) regards it as part of a continuous consolidation process, and Barden (Reference 2) acknowledges the probable initiation of creep during the primary compression stage. It is not unreasonable to assume, therefore, that creep acts continuously through any stress change and is only temporarily masked by other deformations. This being so, the two segments of a creep rate curve are likely to be approximately co-linear (Figure 3), and in practice this appears to be the case. Thus the creep rate curve has sufficient continuity to permit analysis whereas the creep curve has none.

In Figure 4, a secondary feature resulting from a temporary surcharge load is illustrated. Here, elastic recovery may cause the net strain rate to be temporarily arrested, prior to converging onto a parallel creep curve.

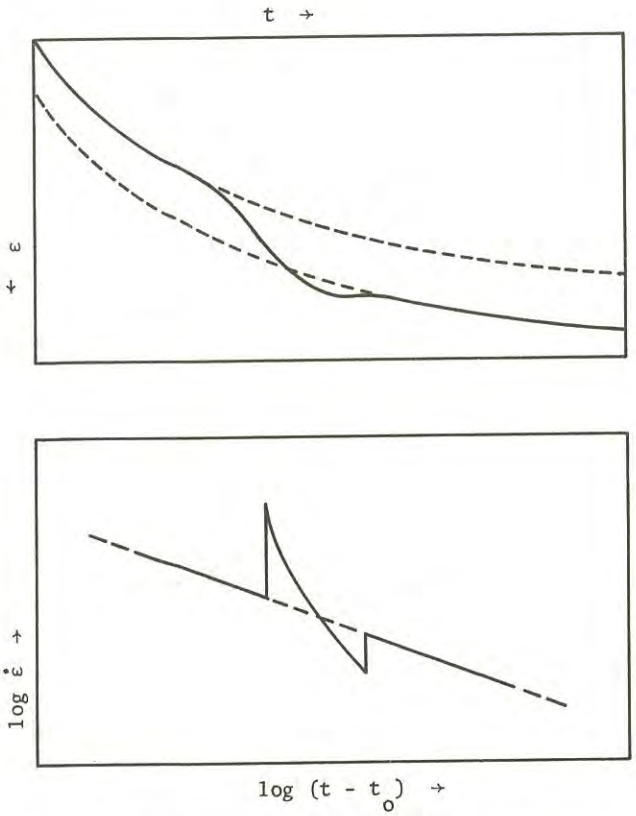

FIG. 4. DISTORTION DUE TO TEMPORARY SURCHARGE LOAD
Causing Elastic and Consolidation Settlement

(b) Effect of Stress Changes on Creep Rate

During small stress changes, some modification of the creep rate is possible. For steady state creep, stress dependence is usually expressed in the form*

$$\dot{\varepsilon} \propto \sigma^n \qquad (7)$$

The value of n varies considerably in rocks, from 1 at low stress up to 4 or 5 at elevated stress (e.g. Robertson, Reference 16), but the lower limit is more likely at engineering stress levels. Hence small changes in stress may be expected to produce relatively small changes in the steady state creep rate, and, in some instances, such as granodiorite and gabbro (Murrell and Misra, Reference 12), very little change.

Little is known of the stress dependence of primary creep, but the situation is unlikely to differ much from the preceeding. If, further, it is assumed that the time decay terms for transient creep are not stress dependent, then the effects of a stress increment would appear as a change of time scale, or, as a parallel displacement of creep rate curve on log-log scales (Figure 5). Once again, such behaviour is not readily discernible on a graph of creep strain, and any attempt to draw a single creep curve will result in an over-estimation of final strain.

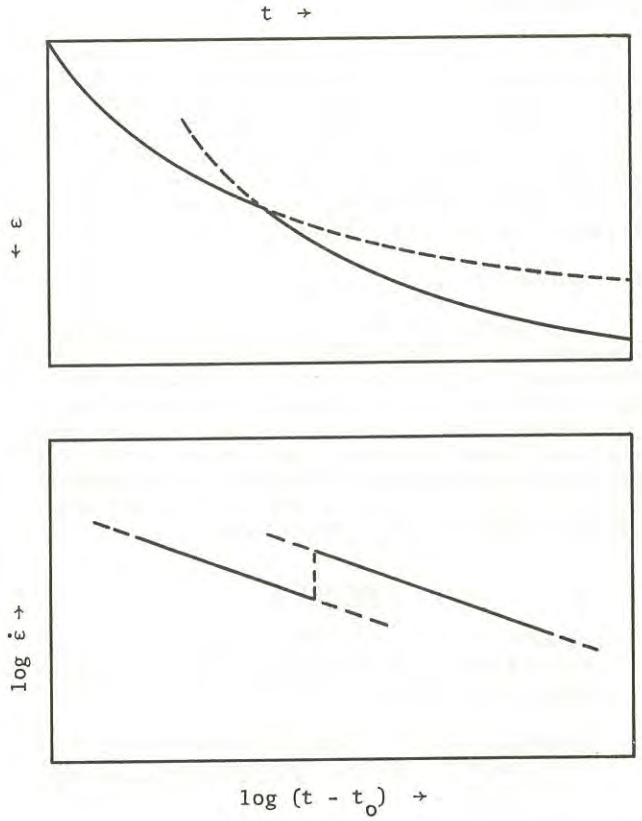

FIG. 5. EFFECT OF STRESS CHANGE ON CREEP RATE

The assumption above draws some support from the fact that it renders transient creep subject to the Boltzmann Superposition Principle, which is considered to apply for the non-constant loading of metals in steady state creep (e.g. Onaran and Findley, Reference 13). This states that, under various loads P_1, P_2.... applied at times t_1, t_2....previous to the final loading being considered, the final deformation can be computed by simple superposition of each of the loads acting independently. Evidently, the Principle operates best at lower stresses when n is close to 1.

(c) Effects of Fracture

Most structural foundations possess a high degree of rigidity in relation to the strata on which they are founded, and this results in stress concentrations at the periphery, in accordance with the effective rigidity factor (Borowicka, Reference 4). Although these are not normally of any consequence in plastic soils, the situation can be rather different in soft rock, with a brittle failure characteristic.

* Equation 7 is similar to the Ostwald Equation, on which Barden (Reference 2) has based his non-linear analysis of clay deformation. He indicates that n = 1 leads to Taylor's Consolidation Theory B. Equation 7 is evidently an approximation to Equation 1 for a restricted stress range.

It is not unlikely, therefore, that a foundation on creep sensitive rock may incur local peripheral fractures. Whilst there may still be a substantial factor of safety on general shear failure, local failures will result in a certain redistribution of stress, and may have a significant bearing on settlement behaviour.

The secondary features resulting from local shear failures will evidently be similar to those for stress changes, except in so far that their influence extends over a rather greater time. It is probable that fracture initiation involves a period of tertiary creep (Figure 1), which may be reflected in the overall deformation rate (Figure 6) during the period of fracture initiation.

VI CONCLUSION

Some aspects of the behaviour of a creeping foundation have been examined analytically, and, in particular, those factors which interrupt or obscure ideal behaviour. In each case, it is shown that a single interpolated curve on a strain v. time graph will significantly over-estimate future settlements. Such complications make the analysis of a creep-time graph virtually impossible, and any fruitful analysis should be made by way of creep rates.

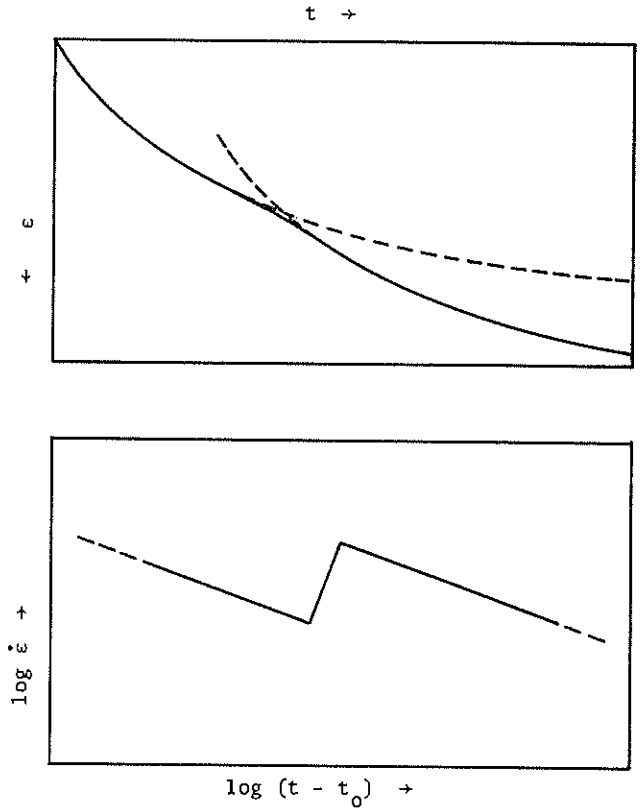

FIG. 6 SECONDARY FEATURE DUE TO FRACTURE

REFERENCES

1. ANDRADE, E.N. da C. (1910) - On the viscous flow of metals and allied phenomina. Proc. Royal Soc., London A, 84:1-12.

2. BARDEN,L. (1965) - Consolidation of clay with non-linear viscosity. Geotechnique, London, 15:4:345-362.

3. BARDEN,L. & POSKITT T.J. (1969) - Discussion, Proceedings, ASCE, 95:SM1:406-409.

4. BOROWICKA, H. (1936) - Influence of rigidity of a circular foundation slab on the distribution of pressures over the contact surface. Proceedings, Int. Conf. Soil Mechanics, Cambridge, Mass., 2:144-149.

5. COTTRELL, A.H. (1952) - The time laws of creep. Journal Mech. and Phys. of Solids, 1:1:53-63.

6. CRAWFORD, C.B. (1964) - Interpretation of the consolidation test. Proceedings, ASCE, 90:SM5:87-102.

7. CRUSSARD, C. (1963) - Transient creep of materials. Proceedings, ASME - ASTM - Inst. Mech. Engrs. Joint Int. Conf. on Creep, 2:123-129.

8. GLASSTONE, S., LAIDLER, K., & EYRING, H. (1941) The Theory of Rate Process. McGraw-Hill, New York.

9. GRAHAM, A. & WALLES, K.F.A. (1958) - Regularities in creep and hot fatigue data. Aeronautical Research Council, Papers CP379 and CP380, HMSO, London.

10. LEONARDS, G.A. & GIRAULT, P. (1961) - A Study of the one-dimensional consolidation test. Proceedings 5th Int. Conf. Soil Mechs. and Found. Eng., Paris, 1:213-218.

11. MITCHELL, J.K. (1964) - Shearing resistance of soils as a rate process Proceedings, ASCE, 90:SM1:29-61.

12. MURRELL, S.A.F. & MISRA, A.K. (1962) - Time dependent strain or creep in rocks and similar non-metallic materials. Transactions, Inst. Mining and Met., 71:7:352-378.

13. ONARAN, K. & FINDLEY, W.N. (1963) - Combined stress creep experiments on viscoelastic material with abrupt changes in state of stress. ASME - ASTM - Inst. Mech. Engrs. Joint Int. Conf. on Creep, 2:85.

14. PHILLIPS, P. (1905) - The slow stretch in indiarubber, glass and metal wires when subjected to a constant pull. Phil. Mag., 9:513-531.

15. PIPES, L.A. (1958) - Applied mathematics for engineers and physicists. 2nd Ed. McGraw-Hill, New York (723 pp).

16. ROBERTSON, E.C. (1963) - Viscoelasticity of rocks. Conf. on the State of Stress in the Earth's Crust, Santa Monica, California, 181-224, Elsevier, New York.

17. SINGH, A. & MITCHELL, J.K. (1968) - General Stress-strain-time function for soils. Proceedings, ASCE, 94:SM1:24-46.

18. TAYLOR, D.W. (1948) - Fundamentals of soil mechanics Wiley, New York, (700 pp).

19. Walker, L.K. (1969) - Discussion, Proceedings, ASCE, 95:SM1:409-415.

20. WACHTMAN, J.D. & MAXWELL, L.H. (1954) - Plastic deformation of ceramic-oxide single crystals. Journal Am. Ceramic Soc. 37:7:291-299.

21. WYATT, O.H. (1953) - Transient creep in pure metals. Proceedings Phys. Soc., London, B, 66:6:459-480.